Adaptation de la morphologie des plages au changement des vagues : une étude combinant expériences de laboratoire et observations de terrain

Ivana Maiten Mingo

THÈSE

En vue de l'obtention du

DOCTORAT DE L'UNIVERSITÉ DE TOULOUSE

Délivré par : *l'Université Toulouse 3 Paul Sabatier (UT3 Paul Sabatier)*

Présentée et soutenue le *10/07/2023* **par :**

Ivana Maitén MINGO

Beachface Adaptation to Waves Change: A Combined Study of Field Observations and Laboratory Experiments

---

JURY

Marissa YATES	CR LHSV Chatou	Rapporteur
Damien SOUS	MCF Université de Toulon	Rapporteur
Bruno CASTELLE	DR EPOC Bordeaux	Examinateur
Frédéric BOUCHETTE	PR Université de Montpellier	Examinateur
Laurent LACAZE	CR IMFT Toulouse	Directeur de thèse
Rafaël ALMAR	DR IRD Toulouse	Directeur de thèse

École doctorale et spécialité :
SDU2E : Océan, Atmosphère, Climat
Unité de Recherche :
IMFT (UMR 5502), LEGOS (UMR 5566)
Directeur de Thèse :
Laurent LACAZE, Rafaël ALMAR
Rapporteurs :
Marissa YATES et *Damien SOUS*

Résumé — Dans le contexte de la dynamique et des risques côtiers, la modélisation de l'évolution de la zone proche littorale et plus particulièrement du mouvement du trait de côte, qu'ils soient induits par des causes naturelle ou humaine, est devenue un enjeu majeur. Deux des principaux défis de cette modélisation sont : 1) la complexité du couplage entre l'hydrodynamique fortement non-linéaire et instationnaire associée à l'impact des vagues sur la plage et le transport des sédiments induit par ce forçage et 2) la nature fortement multi-échelle des processus physiques, à la fois temporellement et spatialement.

La zone de jet de rive, autour du trait de côte, est le lieu de transfert de sable entre la zone sèche et l'océan agissant sur le mouvement apparent du littoral. L'amélioration de la modélisation proche littorale doit donc passer par une meilleure compréhension et description de la dynamique hydro-sédimentaire dans cette zone. En se concentrant sur la zone de jet de rive, cette thèse propose de simplifier ces systèmes complexes hydro-sédimentaires grâce à une étude combinée d'expériences en laboratoire et d'analyses de données sur le terrain.

Ce travail se focalise sur la description de la zone proche littorale par une approche simplifiée, basée sur une analyse physique adimenisonelle qui caractérise le rôle de la zone de jet de rive dans les environnments de plages à terrasse. Ces dernières sont présentes dans différents environnements côtiers, tels que les récifs coralliens, les récifs rocheux et les plages de sable. Le travail se concentre plus particulièrement sur le Nombre de Dean (Ω) en tant que paramètre de contrôle de la dynamique de la zone de jet de rive, comme souvent fait pour décrire la morphologie globale des états de plage. L'étude analyse deux jeux de données de haute qualité provenant de deux environnements de plages à terrasse en utilisant une description simplifiée des systèms proches du littoral, révélant une corrélation significative entre le nombre de Dean (Ω) et la pente du haut plage (β). De plus, un dispositif de laboratoire à petite échelle a été développé pour quantifier la réponse de haut des plages aux variations des vagues dans des environnements de plage à terrasse. Par cette approche combinée, le projet s'articule autour de la notion d'équilibre de la zone de jet de rive dans le plan transverse au trait de côte pour un forçage hydrodynamique et un volume de sable donnés, et de la transition vers un nouvel état d'équilibre lorsque ces paramètres sont modifiés.

L'étude a conduit à une nouvelle classification et description de l'ajustement rapide de la pente de haut de plage dans des régimes de déficit sédimentaire, en établissant une nouvelle interprétation du Nombre de Dean comme une combinaison de la cambrure des vagues et du Nombre de Rouse. Cette nouvelle classification distingue les environnements de plages à terrasse en 1) plages dominées par la zone de jet de rive (swash-dominated) : où les valeurs d'ajustement rapide de la pente de haut de plage sont associées au forçage des vagues offshore et 2) plages dominées par la zone de surf (surf-dominated) : où les valeurs d'adjustement rapide de la pente de haut de plage sont fortement influencées par la dynamique de la zone de surf.

Finalement, la caractérisation des états de transition de la pente de haut de plage lors de sa migration vers son état d'équilibre a conduit au développement d'un dispositif qui tient compte des apports de sediments et étudie le système en excédent sédimentaire, laissé pour les travaux futurs. En conclusion, cette thèse apporte de nouvelles perspectives sur la compréhension du concept d'adjustement rapide et des états de transition des profils de plage dans les environnements de plages à terrasse, et pose les bases pour de futures recherches dans ce domaine.

Mots clés : Pente de haut de plage, transport sedimentaire, forçage hydrodynamique, zone de jet de rive, plages à terrasse, modèle de laboratoire, ombre de Dean.

Abstract — Within the context of coastal dynamics and coastal hazard, modeling the evolution of the nearshore zone is a major challenge, particularly the movement of coastlines associated to natural or human actions. Two of the main challenges in this modelling includes 1) complexity of coupling highly non-linear and unsteady hydrodynamics associated with the wave impact on the beach leading to sediment transport and 2) the highly scale-dependent nature of the physical processes both temporal and spatial.

The swash zone surrounding the coastline is the transfer zone of sand between the dry zone and the ocean affecting the apparent movement of beaches. Improving nearshore modeling requires a better understanding and description of the hydro-sedimentary dynamics, especially in the swash zone. By focusing on the role of the swash zone, this thesis proposes to simplify these complex coastal hydro-sedimentary systems through a combined study of laboratory experiments and field data analysis.

This research presents a framework based on dimensionless physical analysis to simplify nearshore dynamics and quantify the role of the swash zone on the low-tide terrace (LTT) systems found in a variety of coastal environments, including coral, rocky reefs, and sandy beaches. The work particularly focuses on the Dean number (Ω) as a control parameter of swash dynamics, as often used to describe the morphology of beach states. The study analyzed two high-quality field data sets from two LTT environments by applying the simplified approach of nearshore systems that revealed a significant correlation between the Dean number (Ω) and beachface slope (β). Additionally, a small-scale laboratory device was developed to quantify the response of beachface with a flat lower platform to changing waves. This device focused on the swash zone equilibrium and out of equilibrium states in the cross-shore direction for a given parameters such as hydrodynamic forcing and sediment volume, and the transition to a new equilibrium state when these parameters were varied.

The study led to a new classification and description of the beachface slope rapid adjustment under sediment-deficit regimes by deriving a new interpretation of the Dean number as a combination of wave steepness and Rouse number. The new classification distinguishes LTT environments into 1) swash-dominated: where rapid adjustment of the beachface slope are associated with offshore wave forcing and 2) surf-dominated: where rapid adjustment of the beachface slope are highly influenced by the dynamics of the surf zone.

Lastly, the quantification of beachface transitional states when migrating to its equilibrium state resulted in the development of a device that accounts for sediment inputs and studies the system under the influence of sediment nourishment, left for future works. In conclusion this thesis provides new insights into the concept of rapid adjustment and transitional states of beach profiles in LTT environments, laying the groundwork for future research in this area.

Keywords: Beachface slope, swash zone, low tide terrace, nearshore evolution, sediment transport, hydrodynamic forcing, laboratory model, Dean number.

Acknowledgements

After completing my university studies at the National University in La Plata, Argentina (UNLP), for which I am deeply grateful for the education and formation that made me an engineer, my greatest desire was to embark on a PhD. and continue down the path of research. As I write these acknowledgements, I am overwhelmed with emotions, knowing that thanks to immense effort and dedication, my goal has become a reality. Above all, this achievement is not the result of a single person's work, but a collaboration, sharing, and support among numerous individuals to whom I dedicate my sincerest gratitude in this section.

I would like to begin by thanking the French National Centre of Scientific Research (CNRS) for the funding of this PhD. through the 80 PRIME project. This founding gave me the opportunity to explore a subject that ignited a profound passion within me-Coastal Environments. Furthermore I had the privilege of doing this thesis in a wonderful city, within two laboratories, the Institute of Fluid Mechanics (IMFT) and the Space Geophysics and Oceanography Laboratory (LEGOS) both in Toulouse, who warmly welcomed and supported me throughout the entire process.

I extend my sincere gratitude to my supervisors, Laurent Lacaze and Rafael Almar, whose scientific guidance has been indispensable for this work. This research presented a unique challenge of combining two distinct scientific approaches to achieve a common goal, a task made even more complex by the disruptive influence of the COVID years during the early stages of the PhD. Together, Laurent and Rafael formed an outstanding team, driving this project forward within a consistently positive atmosphere. I deeply appreciated our scientific or non-scientific interactions, both as a team or with each one of them individually. Thank you, Laurent, for your daily availability and continued encouragement. Your great benevolence, constructive scientific feedback, and guidance on my work have been invaluable in improving its quality and direction. Additionally, thank you, Rafael, for your innovative ideas that constantly propelled this research forward, offering valuable scientific perspectives. Thank you both, you have been great mentors and I hope we will have the opportunity to continue working together.

I wish to express my deep appreciation to the entire IMFT research support team, whose direct involvement has been crucial for the success of this research. A special acknowledgement goes to Jean-Dominique Barron, who played a key role in this work by setting up the entire experimental device. Thanks to his exceptional expertise and dedication, even our "most craziest" ideas were able to became reality. I'd also like to extend my special thanks to Sébastien Cazin, the head of the Image Signals department, as well as Hervé Ayroles and Frederic Bergame, from the Image Signals department. Their technical expertise and availability during the experiments where essential for the correct execution of the laboratory experiments.

During my PhD., I was a member of the Fluid and Particles group (FEP) at IMFT. I would like to thank the entire FEP group and some of its members in particular. Sylvain

Viroulet and Matthieu Mercier, thank you both for your dedication and involvement in my PhD. Your friendly attitude made my work very enjoyable, especially when we explored new sports outside the laboratory. I'm also thankful to Thomas Bonometti for his guidance during my teaching experience and Sylvie Senny for her kindness and availability. I would like to acknowledge Marius Aparicio, whose contributions during his final master's internship were very useful for the perspectives of this work. Of course, I cannot forget to mention all my fellow doctoral and post-doctoral friends at IMFT, especially my desk mate, Abigael, who contributed to creating a super-friendly ambience in our shared office, always filled with good vibes. I want to thank Corentin, with whom I shared exceptional moments, especially during our 'mate sessions' with Abigael. I hope you both continue and pass on the mate tradition. Thanks to Guillaume, who has been a true friend since my very first day in the laboratory. And thank you to the IMFT football team for the great fun we had every Friday!. Your camaraderie has been a significant part of my this journey, and I'm truly thankful for the experiences I had at the IMFT.

I would like to thank Vincent Regard and Hervé Michallet for agreeing to form my thesis monitoring committee. Thank you both for our annual meetings that enriched this work. A sincere acknowledgement goes to my entire PhD. jury: Marissa Yates, Damien Sous, Bruno Castelle, and Frédéric Bouchette. Thank you all for your instructive questions and remarks in the reports and during the defence; they provided valuable insights and inspiration for future reflection.

One of the most challenging parts of this PhD was the defence, and for this, I extend my sincere thanks to everyone who patiently supported and assisted me during this demanding time. Again I would like to mention my colleagues Guillaume, Matthieu, Abigael, and Corentin for actively participating in my rehearsals. Additionally, I am immensely grateful to my partner, Francisco, who not only encouraged me and continuously assisted me during this final stage but has been by my side since the very beginning of the PhD, especially during the toughest times. I have no doubt that he has a very deep understanding of my research topic, as I bombarded him with it daily. Thank you Francisco for your love. Now, a warm thanks go to my lifelong Argentinean friends: Sofi, Noe, Nanu, Lula, Fofi, Chuchi, Agus, Lupe, and Aye. Despite not understanding a word of my final rehearsal in French, they attended, offering me their precious support. Their presence not only gave me great courage to successfully pass the defence but also, every year during my trips to Argentina, they helped me disconnect and recharge my energy.

Finally, I would like to express my profound appreciation to my dear family. My Mum and Dad deserve special mention for their unwavering love and encouragement, providing me with the opportunity to pursue my doctoral studies in France and always standing by me when I needed them. To my brothers, Leonel and Mauro, who made the effort to be by my side during the final stretch. A special acknowledgement goes to my brother Mauro for his consistent review of my work. And above all, to conclude, I want to dedicate this work and offer my deepest gratitude to my dear mother, who, with her profound love and consistent encouragement, passed her passion for research and instilled it in me. From the bottom of my heart, I will always love you, Mum!

Contents

List of Figures

List of Tables

Acronyms

UPCC	*Intergovernmental Panel on Climate Change*
NE-SW	*Northeast-southwest*
NT	*Nha Trang*
GP	*Grand Popo*
RGB	*Red, green and blue*
EBP	*Equilibrium beach profile*
RTR	*Relative tidal range*
MSL	*Mean sea level*
MLWS	*Mean low water spring level*
MHWS	*Mean high water spring level*
MLWN	*Mean low water neap level*
MHWN	*Mean high water neap level*
LBT	*Longshore Bar and Trough*
RBB	*Rhythmic Bar and Beach*
TBR	*Transverse Bar Rip*
LTT	*Low Tide Terrace*
SRB	*Surf regulated beach*
SwRB	*Swash regulated beach*
Wr	*Wave regime*
Tc	*Characteristic capture time*
D_{50}	*Mean sediment size*
H_s	*Mean peak wave height*
T_p	*Average peak period*
Ω_0	Offshore Dean number
Ω_{sf}	Surf Dean number

Ω_{sw}	Swash Dean number
γ	Breaker index
γ_{br}	Breaker index at wave breaking
ξ_0	Iribarren number
ξ_{br}	Iribarren number at wave breaking
Ro	*Rouse number*
s	*Wave steepness*
s_0	*Offshore wave steepness*
s_sw	*Swash wave steepness*
λ	Offshore wavelength
λ	Offshore wavelength
β	Beachface slope
β_{eq}	Equilibrium beachface slope
β_i	Initial beachface slope
β_f	Final beachface slope
α	Slope value of the shoreface (wave shoaling)
S_l	*Shoreline position*
H_0	*Off-shore wave height in the laboratory model*
H_b	*Breaker wave height in the laboratory model*
H_T	*Water depth on the terrace in the laboratory model*
T_0	*Off-shore wave period in the laboratory model*
W_s	*Sediment fall velocity*
L_t	*Terrace length*

Introduction

Context and purpose for research

From a geomorphological and geological perspective, a beach can be defined as an accumulation of sediment deposit along the coastlines, forming the land and ocean boundary. The location and shape of a beach depends on various factors such as the sources of sand, coastal processes, and the underlying geology (Bird, 2011). Depending on the type of substrate, there exists a wide variety of different beaches around the world, from fine sandy beaches to rocky shores, as represent in Figure 1. The variations in beach morphology are shaped by the interactions of different factors such as waves climates, sediment supply and geology.

Figure 1: Photograph examples of 3 different types beaches in Europe (France, Spain and Greece) with different substrate.

Sandy beaches, which account for over one-third of the global coastline, are of significant socioeconomic importance, supporting recreation, tourism, and diverse ecosystems. They also serve as a crucial interface between land and ocean, offering natural coastal protection from marine storms. However, this valuable coastal area is increasingly at risk due to the adverse effects of climate change and human actions, leading to substantial alterations in the coastline. During the past decades it has been observed an increase in frequency of storms occurrence leading to more severe episodic coastal erosion (Callaghan and Helman, 2008; Masselink et al., 2016; Mentaschi et al., 2018). Severe storms can have dramatic changes to the coastline and devastation to the coastal settlements, as shown in Figure 2. In addition, rising mean sea level is leading to coastal retreat (Bruun, 1962; Dean and Houston, 2016). According to the Intergovernmental Panel on Climate Change (IPCC), global sea level has risen by about 15 cm since the late 19th century, and the rate of sea level rise has been accelerating in recent decades (Pachauri et al., 2014). The impacts of sea level rise on coastlines are expected to be significant and widespread, with consequences such as increased coastal flooding and erosion, loss of coastal wetlands and other ecosystems, and displacement of coastal populations. Another effect of climate change is the growth of wave energy, which directly impacts coastlines and affects storm wave characteristics (Sterl et al., 2009; Hemer et al., 2013; Morim et al., 2020).

Figure 2: Photograph examples of devastating coastal erosion and storm damage from around the world. From beach erosion to property damage, the consequences of these natural hazards can be severe.

Meanwhile, as the global population continues to grow exponentially, coastal systems are facing increasing pressure, particularly as more than 40% of the world' population resides in this area, and which continue to attract more inhabitants (Merkens et al., 2016). This trend is exacerbating the vulnerability of coastlines and increasing the risk of flooding and other hazards.

As human activities continue to focus on the land-ocean boundary, natural resources are being consumed and altered at an unprecedented rate, directly impacting the integrity of coastal environments in different time and spacial scales. In fact, some scientists argue that the changes brought about by human activities have exceeded those resulting from "natural" or non-anthropogenic forces in the 20th century (Valiela, 2009). The substantial alterations of the coastal environment induced by these human activities are for instances the construction of harbors and other structures that disrupt sediment flux dynamics, resulting in significant changes in coastal erosion patterns. These structures impede the natural flow of sediments, leading to sediment buildup on one side and erosion on the other, a process known as sediment starvation. This phenomenon has been observed in numerous locations worldwide, as documented in Yang et al. (2017); Hsu et al. (2007).

Moreover, human activities also modify the possible source of sand required for the natural evolution of beaches, such as for instance dams in rivers. Dams indeed trap sediment and prevent it from reaching the coast, reducing the supply of sediment and therefore contribute to coastal erosion. This has been observed in many river systems all over the world. For example, a study conducted on the Western Gulf of Lions shoreface in France used an integrated method to study sediment coastal reservoirs (Brunel et al., 2014) and found that the variation of the

overall morphology of the beach leading to coastal erosion was a consequence of sedimentary deficit linked to sand extraction and constructions of dams. Figure 3 illustrates an example of the impact of dams construction in 1978 at Perpignan, where it is clear how the maximum river discharge has been strongly affected after the construction of the dam.

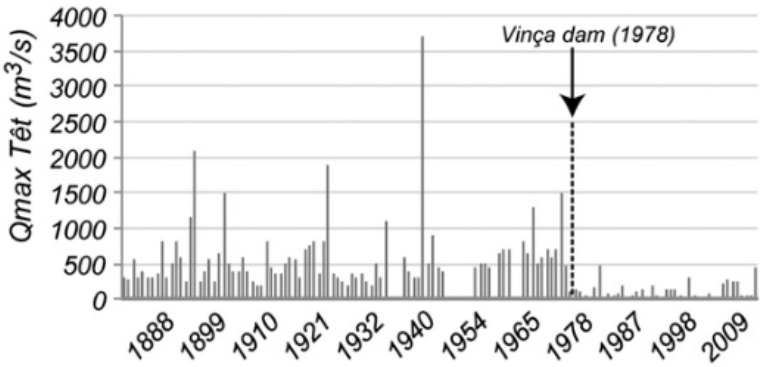

Figure 3: Annual Qmax (m3/s) for Têt river at Perpignan from 1876 to 2010, before and after construction of Vinça dam in 1978. Figure taken from (Brunel et al., 2014).

More recently, human-based solutions to beach erosion can also have an impact on the coastal environment as of instance beach nourishment, which involves adding sand to eroding beaches. While this can help to protect the coastline, it can also have unintended consequences, such as changes to the local ecosystem and the creation of a false sense of security for coastal communities. Overall, human activities have had a significant impact on the coastal environment, and it is important to understand these impacts to effectively manage and protect the coastal zone and resources.

This global issue calls for immediate attention, with many locations worldwide experiencing similar impacts. All these current pressure on the coastline, related to natural or human actions is leading coastal communities on having to intervene quickly on this zone to avoid coastal flooding, erosion or accretion problems or to conserve coastal ecosystems (Valiela, 2009; Lipiec et al., 2018). In response, many of these communities turn to a range of engineering techniques, from soft to hard, to mitigate the risks. While some of these techniques show promising results (Bayle et al., 2021), they are often applied based on examples from elsewhere (Allan et al., 2023), rather than a deep understanding of their underlying physical mechanisms. Moreover, the long-term consequences of these actions are not well understood, and the dynamic nature of coastal systems makes it essential to consider the impacts on adjacent zones. Given the global nature of this problem, localized solutions will not suffice, what could be needed is a comprehensive and accessible global management plan that takes into account the ecological, economic, and social dimensions of the issue. The scientific community, particularly coastal scientists, has a responsibility to take up this challenge and develop innovative solutions that can balance the needs of different stakeholders while ensuring long-term sustainability. Only through collaborative efforts can we hope to address the pressing challenges that are facing coastal communities and secure a more resilient future. To achieve this goal a solid understating of theses complex coastal systems is essential. In-

sufficient knowledge of coastal processes can lead to inappropriate or ineffective interventions that may worsen coastal problems. Therefore, it is crucial to increase our knowledge of the physical processes impacting the coast, specifically focusing on swash zone, that is defined as the part of the beach intermittently covered and uncovered by waves forming the land-ocean boundary.

One of the main challenges faced by communities when addressing coastal issues is the availability of predictive models to make informed decisions. Despite significant advancements in modeling techniques, there is still a lack of understanding, particularly in the highly dynamic swash zone. Unfortunately, useful and classical models such as the Brunn rule (Bruun, 1954, 1962), the Dean equilibrium profile (Dean, 1977, 1991) or more complex cross-shore equilibrium models (Yates et al., 2009; Castelle et al., 2014b; Lemos et al., 2018) are not necessarily designed on predicting rapid morphological changes such as those observed in the swash zone, i.e beachface recovery after a storm, as these models are either based on seasonal or annual time scales equilibrium approaches or focus mainly on the global evolution of the shoreline position.

Therefore to improve the predictions of swash evolution, numerical models have been developed to capture swash dynamics with different levels of complexity (Larson et al., 2004; Pritchard and Hogg, 2005; Steenhauer et al., 2012; Briganti et al., 2016, see for example). These models have been obtained and/or validated from extensive series of experimental and field measurements and are used to help in the understanding of swash morphodynamic systems. Despite these recent advances in swash modelling, the prediction of the correct net sediment transport rates and morphological changes in the swash zone are still lacking specific details and need to be improved (Chardón-Maldonado et al., 2016; Bakhtyar et al., 2009). In addition, high quality field measurements are needed to validate and develop all these numerical models. This is a concern because field measurements of sediment transport and fluid motions in the swash zone are very difficult to obtain and analyze due to the complexity of the highly nonlinear and unsteady processes occurring simultaneously in this zone (Guza and Thornton, 1982; Puleo et al., 2003; Miles and Russell, 2004; Masselink et al., 2005; Masselink and Puleo, 2006; Turner et al., 2008). Often, these models require a significant amount of data to validate them, which can be a challenge to all coastal communities, but specially in developing countries, due to the need for resources, time, and skilled personnel.

Within this general context, this thesis proposes to simplify these complex coastal systems by applying a physical-based approach through a combined study of laboratory experiments and field data analysis. More specifically, in light of the coastline experiencing multiple changes, this work centers around the concept of rapid equilibrium and transitional states of swash zone morphology associated with transitions between different hydrodynamic forcing states (such as storms or seasonal changes). By gaining a deeper understanding of swash zone dynamics via a physically-based simplified approach, it would be possible to develop more accurate and effective prediction models. This, in turn, will enable the formulation of sustainable and practical management strategies with broader applicability.

Main objectives

To address the urgent need for sustainable coastal management strategies and contribute to the scientific community's effort to better characterize the resilience of coastal zones, particularly in natural post-storm recovery processes, it is imperative to improve nearshore modeling on relative short times scales. This issue remains a challenging task due to the complexity of swash dynamics. To this end, this thesis propose to tackle this challenge by the definition of the following 3 objectives:

1. **Simplify the coastal hydro-sedimentary system**

   Coastal hydro-sedimentary systems are inherently complex and pose a significant challenge for accurate modeling as these systems undergo continuous adjustment caused by hydro-morphological coupled interactions that are highly scale-dependent, both temporally and spatially (Stive et al., 1991; Cowell and Thom, 1994; Larson and Kraus, 1995). Despite significant advances made by researchers in developing models that incorporate the coupling between hydrodynamics and seabed morphology at varying levels of complexity (Anthony, 1998; Davidson and Turner, 2009; Grasso et al., 2009; Yates et al., 2009), predicting sediment transport in the nearshore remains a challenge. This is especially true in the swash region, which is highly dynamic and subjected of significant portions of sediment transport (Chardón-Maldonado et al., 2016).

   Although numerical models have been develop to incorporate the coupling between hydrodynamics and sediment transport, they quickly become computationally expensive and impractical for long-term or large-scale engineering projects (Brocchini and Baldock, 2008; Kalligeris et al., 2020). As a result, a simplified approach is necessary to study these complex systems.

   The first objective of this thesis is therefore to develop a simplified yet physically-based approach characterizing nearshore coastal hydro-sedimentary systems, with a focus on accurately describing swash dynamics and its interactions with other nearshore regions. The scope and limitations of this simplified approach will also be carefully evaluated and discussed.

2. **Characterize the role of swash dynamics within the coastal system**

   The physical description of the entire coastal region can be complex, and it is often necessary to focus on sub-regions. Coastal hydro-sedimentary systems can be divided into different zones such as the breaker, surf, and swash zones based on the shoreward propagation of waves. The swash zone is the last zone in the nearshore, and its hydrodynamics have been observed to be influenced by the inner-surf zone, while interactions the other way around have often been disregarded. Nevertheless, studies have shown that the swash zone plays a key role in wave reflection and feedback on incoming waves, which are commonly referred to as swash-swash interactions (Almar et al., 2016, 2018; Brocchini and Baldock, 2008; Bakhtyar et al., 2009). The swash is a highly dynamic region, and its morphological response to wave forcing could be quasi-instantaneous, potentially influencing the hydrodynamics of the entire nearshore system.

The question remains as to whether the rapid morphological response of the swash zone controls the hydrodynamics of the nearshore system or if it is the other way around. Although some studies have analyzed feedback processes linking surf and swash dynamics, it is still unclear which physical parameters govern these behaviours. Both situations are observed in the field, making it important to understand which cases clearly show that swash dynamics is controlled by surf processes and vice versa (Elfrink and Baldock, 2002; Brocchini and Baldock, 2008; Masselink and Puleo, 2006; Svendsen and Putrevu, 1996)).

Therefore, a further objective of this research is to investigate the impact of swash dynamics on the coastal hydro-sedimentary system and establish a physically-grounded methodology for characterizing swash dynamics and its hydro-morphodynamic interactions with adjacent nearshore areas. Through this investigation, we aim to identify the physical parameters that govern these phenomena.

3. **Highlight the rapid evolution of the beachface slope**

The slope of the beachface plays a critical role in the stability of the shoreline and the dynamics of the coastal hydro-sedimentary system. Alterations in the beachface slope can affect wave energy dissipation and reflection, wave run-up excursion, and sediment exchange between land and ocean. While numerous studies have established a positive correlation between the beachface slope and the sediment size (Bagnold, 1940; Masselink et al., 2016; Bascom, 1951; Turner, 1995; Reis and Gama, 2010; Bujan et al., 2019), resulting in the development of empirical relationships that demonstrate a power-law dependence between the beachface slope and the mean sediment size (Sunamura, 1984; Soares, 2003; Reis and Gama, 2010). These relations have proven to predict the slope in a generalize form but, they lack of physical basis to provide a clear link to swash dynamics and they mask the physical processes occurring in this area. In particular, the strong influence of the grain diameter D_{50} on the beachface slope is probably due to the sediment fall velocity, which is known to influence the transport regime relative to wave dynamics.

Therefore, this study aims to approach the dynamics of the beachface slope from a different perspective by identifying the main parameters controlling swash dynamics and use them to develop a dimensionless analysis that could explain the physical processes occurring in the swash zone. A particular attention is focused on the relation between the beachface slope and the dimensionless fall velocity also known as the Dean Number (Dean, 1991). This number is commonly used in coastal morphodynamics as a parameter controlling the equilibrium beach states on seasonal to annual timescales (Wright et al., 1984). As it has been observed that the beachface slope reacts very quickly to wave action in order of hours to days (Hughes et al., 1997; Butt and Russell, 1999; Puleo et al., 2003; Masselink and Puleo, 2006), we aim to investigate the relevance of the Dean Number as a potential control parameter of the beachface slope dynamics.

This research also focuses on the dynamics of the beachface as it transitions from an out-of-equilibrium position to an equilibrium state under varying wave forcing conditions. This is crucial as it can be linked to the beachface's ability to recover after severe events such as storms and hurricanes.

To achieve these objectives, an interdisciplinary approach combining laboratory experiments with field data analysis is undertaken. This thesis was conducted at two institutions in Toulouse: the Institut de Mécanique des Fluides (IMFT) and the Laboratoire d'Etudes en Géophysique et Océanographie Spatiales (LEGOS). The research was supported by the French National Centre for Scientific Research (CNRS) through the 80 PRIME project, which is a multi-disciplinary research initiative.

The choice to conduct laboratory experiments in this study is well-justified for several reasons. Firstly, laboratory experiments allow a control of the physical parameters involved in complex hydro-sedimentary systems, enabling the extraction of models based on physical processes. Secondly, fine hydro-sedimentary measurements can be developed in the laboratory resulting in a better understanding of the physical processes. Finally, equilibrium states that are rarely observed in natural environments can be achieved in the laboratory, leading to a more accurate understanding of both equilibrium beach states and out-of-equilibrium evolutions.

The experimental setup consists of a wave flume with dimensions of 12.0 x 0.15 x 0.30 m (L x W x H) which is available at the IMFT. Although this is a small-scale laboratory device, it offers several advantages over larger-scale laboratory devices. For instance, small-scale laboratory experiments are generally simpler and less expensive, and different physical parameters can be easily varied in the laboratory to recreate a wide range of situations in a relatively short amount of time. The limitations of the small-scale physical model include the risk of an inaccurate idealization and the possibility of overlooking important parameters. These limitations will be discussed when presenting the results of this physical model.

However, it is important to note that laboratory experiments can create physical situations that are rarely observed in nature, and it can be challenging to recognize when these situations are not reflective of real-field conditions. Therefore, it is crucial to compare laboratory results with field data to ensure that the physical and geometrical scaling of the model is accurate. This is where a coupled laboratory-field study becomes necessary. In this work, we have access to a high-quality database of field experiments conducted at two different beaches, which will serve as a basis for the laboratory physical scaling.

By combining laboratory and field data analysis with a simplified approach to understand the intricate hydro-sedimentary systems, we can gain valuable insights that can effectively describe real field situations. This, in turn, can improve the accuracy of predictor models, contributing to the development of practical coastal solutions.

Thesis Organization

The thesis manuscript begins with an overview of the research, followed by a general introduction that provides context, outlines the major issues, and presents the objectives of the PhD. The first chapter includes a bibliographic analysis of the existing knowledge on littoral and sandy beaches, as well as a more specific study of the nearshore hydro-morphodynamics

of these hydro-sedimentary systems. The objective of this chapter is to simplify these complex systems, as explained in objective 1 of the thesis. After developing a simplified model of these hydro-sedimentary systems, the thesis is divided into two main axes: field data analysis (Chapter 2) and laboratory study (Chapter 3).

In order to achieve objective 2 of the thesis, the first step within the two main axes was to analyze the available field data using the simplified model to characterize the role of swash dynamics within the nearshore coastal hydro-sedimentary systems. Chapter 2 presents the results of this analysis and leads to a publication in Coast, an open-access journal on coastal engineering published by MDPI, titled "Surf and Swash Dynamics on Low Tide Terrace Beaches" (Mingo et al., 2021). This chapter provides a detailed description of the available field data, followed by a presentation of the results in the format of an article.

Based on the field observations done in Chapter 2, it was determined that further study was needed in the laboratory to achieve objective 3 - highlight the rapid evolution of the beachface slope. This laboratory work begin with the design and assembly of the nearshore physical model, including hydrodynamics test and numerical simulation to understand its hydrodynamics. Based on field data, the physical model was physically and geometrically scaled, and once we validated the model, it was used to study swash dynamics by highlighting the dynamics of the beachface slope. This physical model allowed as to describe the role of the swash zone in the nearshore region and focus on the response of the beachface slope to variation in wave forcing. As a result, we were able to develop two articles: (i) titled "A Semi-Empirical Formula of Beach Slope on Flat Lower Platforms" which was submitted to the journal Coastal Engineering in March 2023 and is in revision, while the second article, titled "Beach adaptation to rapid wave changes" is currently being prepared for submission.

The final section of the manuscript presents the perspectives and overall conclusions of the thesis. In the perspective, we revisit the field data results in light of the new insights gained from the laboratory experiments and introduce a new device in the physical laboratory model to extend the investigation of beachface dynamics to not only waves change but also to incorporate the influence of sediment inputs. Figure 4 illustrates the organizational structure of the thesis.

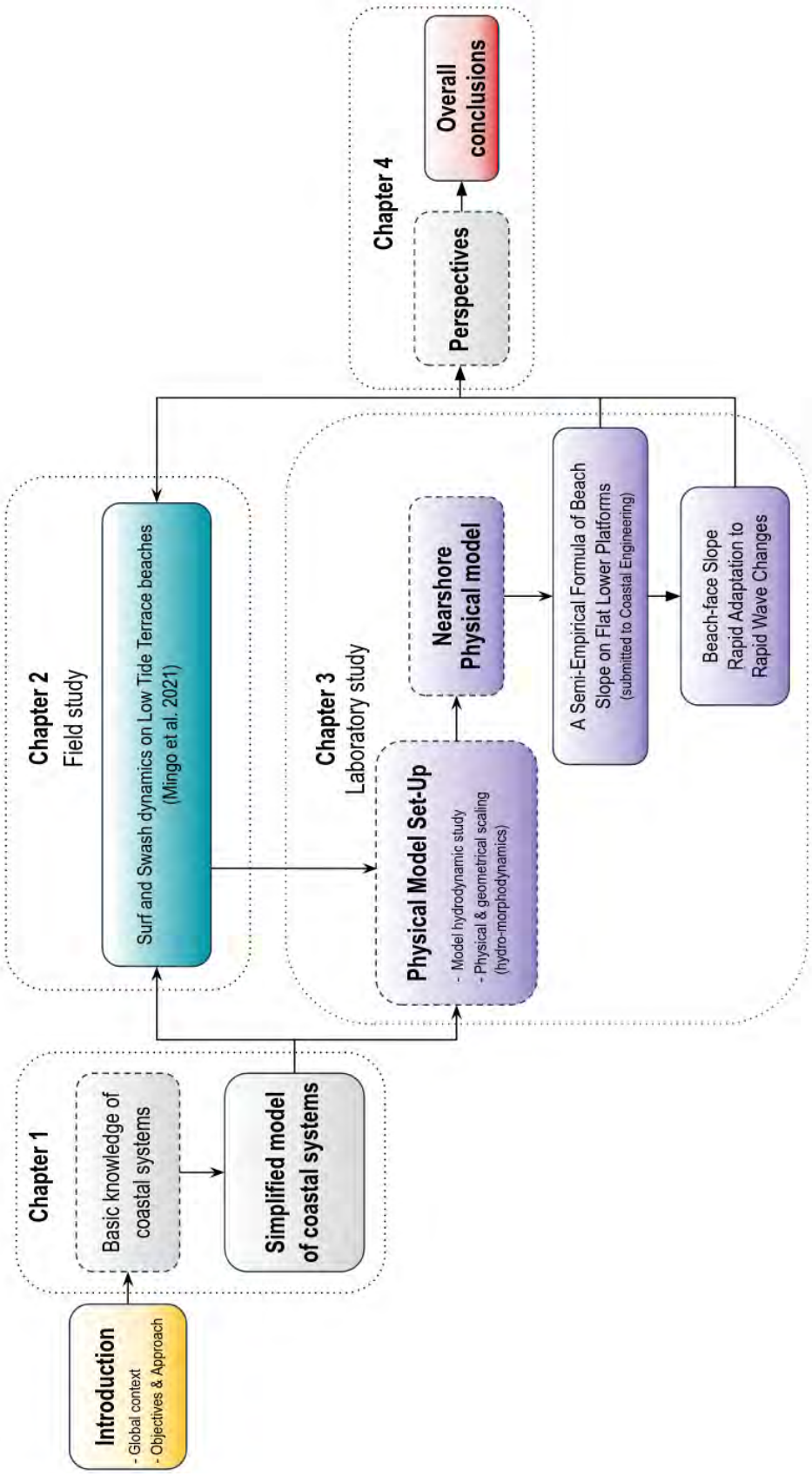

Figure 4: Schematic diagram explaining thesis organization.

Chapter 1

Beach morphology: from a complex hydro-morphodynamics to a simplified model

Contents

1.1 State of the art of coastal dynamics

1.1.1 Basic knowledge on littoral and sandy beaches

The littoral zone refers to the area that is adjacent to a coastline, specifically the area that is affected by the interaction of land and sea. The littoral is a dynamic environment that is subject to constant changes due to wave action, tides, currents and other natural forces or human interventions. Depending on all these factors a variety of different environments can be observed within the littoral zone, such as: sandy or gravel beaches, rocky shores, estuaries and salt marches.

From a geological perspective, a beach can be defined as an expanse of sediment deposit, such as sand, gravel or pebbles, that are accumulated on the coast by the action of waves and currents (Carter, 2013). The shape, position and proportion of beaches in the littoral zone depend on several factors for instance, sources of sand (i.e, coastal rock erosion, sediment runoff from rivers), coastal processes (i.e, the effect of tides, waves and currents) and underlying geology (i.e, the nature of the underlying rocks).

Sandy beaches are a common feature of many coastal areas around the world as they are one of the most visible part of the littoral zone. The proportion of sandy beaches in the coastal zone around the world is not easy to estimate due to all the factors just mentioned above, that act on continuously evolving system. However a recent study, based on satellite images to identify sandy shorelines (Luijendijk et al., 2018) show that 1/3 of the ice-free world shoreline is sandy. The global distribution of sandy shorelines is illustrated in Figure 1.1, where it is shown that the coast of Africa are mostly sandy beaches, while the rest of the continents have around 30% of sandy shorelines.

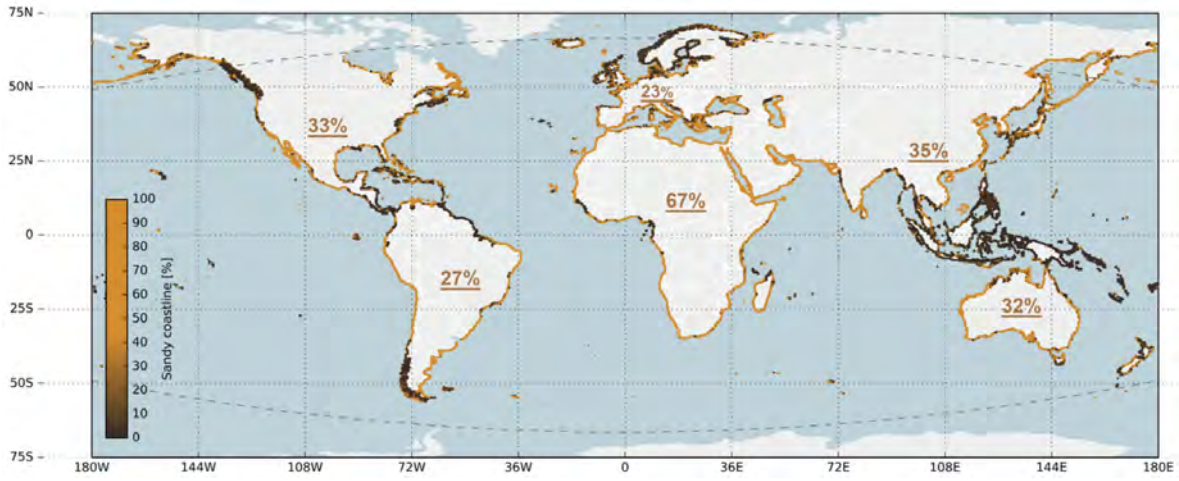

Figure 1.1: Global distribution of sandy shorelines; the coloured dots along the world's shoreline represent the local percentage of sandy shorelines (yellow is sand, dark brown is non-sand). This figure is extracted from Luijendijk et al. (2018).

A sandy beach can be defined as coastal hydro-sedimentary system. These systems are governed by complex hydro-morphological interactions resulting in sediment transport, deposition and erosion due to coastal water motions. The difficulty to approach this systems is due to the complex feedback interactions occurring between the fluid/sediment, as they are strongly non linear and unsteady physical processes. This means that a variation in the hydrodynamics forcing will induces sediment transport responsible for morphological changes and this changes will then modify the incoming wave forcing. In addition, there are external drivers that can also alter the global system, such as waves that change over time, tides, storms, etc., as well as morphological sources related to sediment input or deficit. These non-linear interactions between fluid/sediment are one of the main mechanisms responsible for the morphodynamic evolution of coastal systems (Stive et al., 1991; Cowell and Thom, 1994; Milliman and Farnsworth, 2013). An schema of this coastal hydro-sedimentary systems is represented in left side of Figure 1.3. Further more, coastal hydrodynamic processes occur at different spatio-temporal scales, ranging from seconds to millennial timescales (Phillips, 1992; Cowell and Thom, 1994; Larson and Kraus, 1995; Stive et al., 1991; Ruggiero et al., 2016; Luijendijk et al., 2018). In particular Figure 1.2 provides a summary of these processes associated with their time and spatial scale.

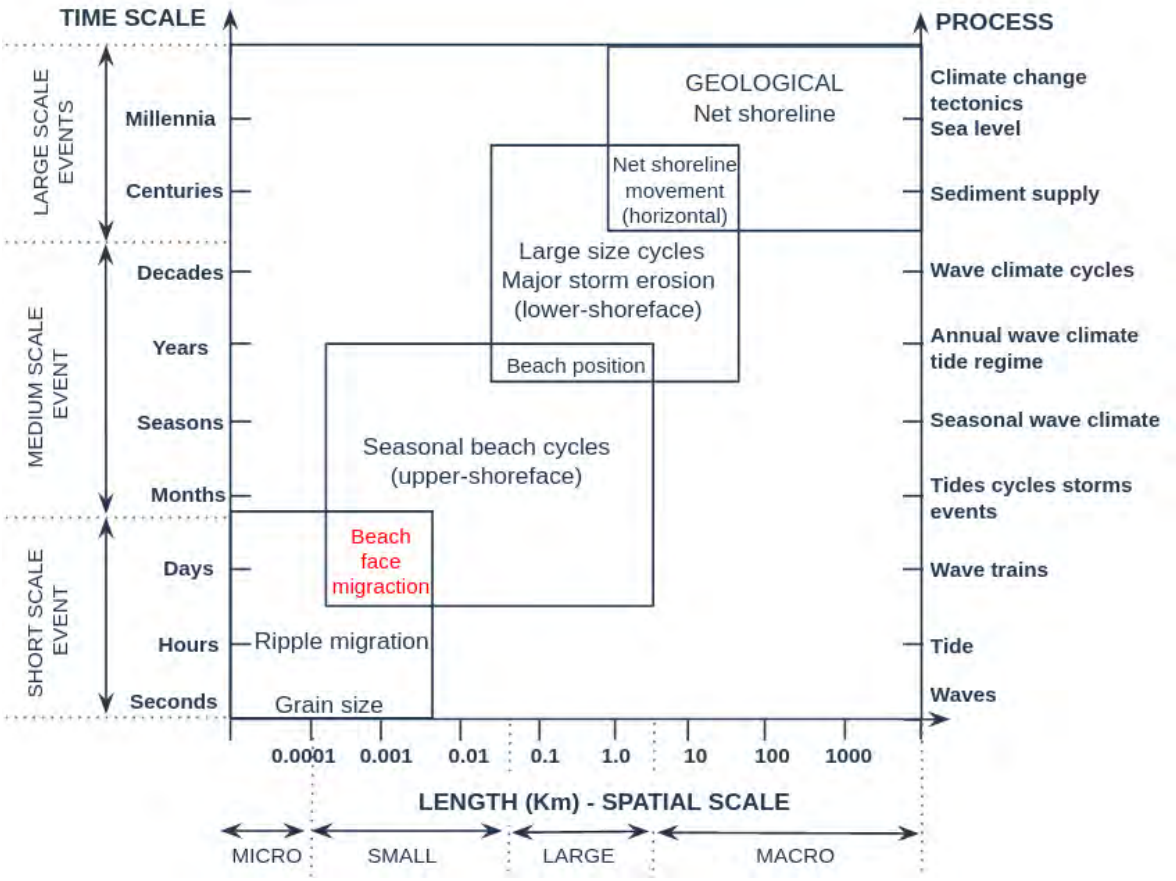

Figure 1.2: Spatio-temporal scales and associated dominant processes. Figure adapted from Cowell and Thom (1994).

The processes associated with grain size and movement can be resolved in seconds, while those associated with ripples occur over hours. The beach migration can occur over hours to days for the beachface, while seasonal to annual timescales are are observed for the upper-shoreface. Large-scale beach cycles associated with major storm can influence the lower shoreface and occur over decades, while net shoreline movement occurs over centuries, and littoral cell and hydrographic network evolution occur over millennial timescales.

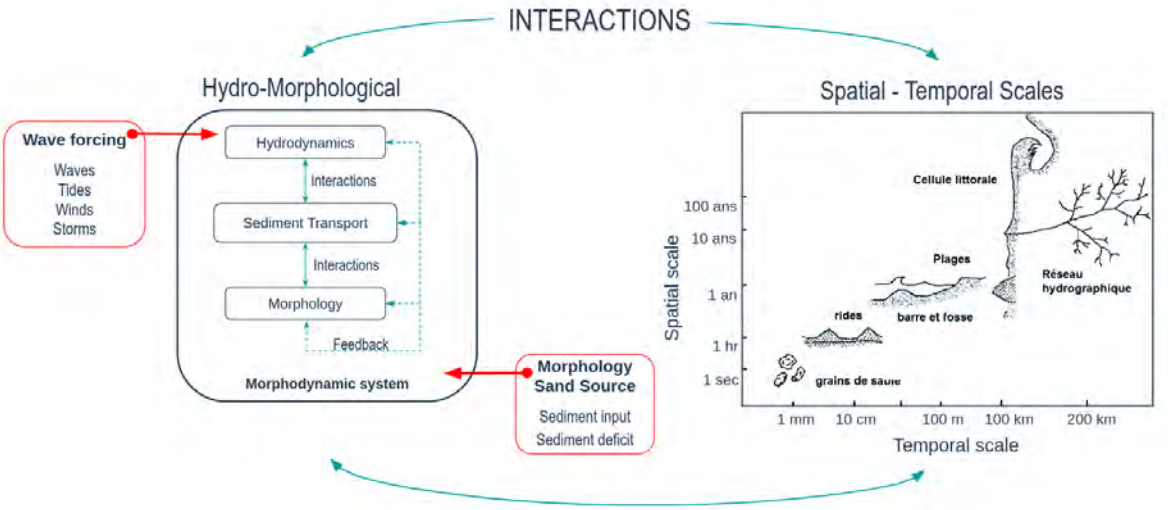

Figure 1.3: Interactions of an hydro-sedimentary system. Left figure shows the schematics of an hydro-morphodynamic system (Figure modified from Stépanian (2002)). Right figure illustrates the spatial and temporal scales of littoral processes (Figure adapted from Astier (2014); Sabatier (2001)).

Moreover, short-term morphological dynamics of beach profiles are linked to hydrodynamic conditions on the scale of tides (typically a few hours) or an short scale event (typically a few days to weeks). This short-scale dynamics can interact with the seasonal scale and affect the beach cycles, especially in environments with marked seasonality in the wave regime. The seasonal events acts on larger space and time scales, playing an important role in the dynamics of the coastline. Thus, the different time and space scales are interconnected, creating interactions and feedbacks between them. As a result, predicting the behaviour of hydro-sedimentary systems is a challenging task due to the complex spatio-temporal interactions between the coupled non-linear hydro-morphological mechanisms (Figure 1.3).

Based on such complex non-linear and multi-scale processes, it seems natural to first discuss the possible existence of equilibrium systems, at least when a given hydro-sedimentary beach system is subjected to a given forcing. This is discussed in the following sections.

1.1.2 Concept of beach equilibrium profile

The concept of beach equilibrium profile is a fundamental and ongoing question in coastal engineering. According to conventional concepts, a beach exposed to constant wave forcing (monochromatic or random) evolves towards a stationary state, known as an equilibrium beach profile (EBP). This concept is supported by laboratory experiments (Waters, 1939; Grasso et al., 2009), empirical models (Bruun, 1954), and semi-theoretical models (Dean, 1991).

Bruun (1954) was the first to develop an expression for EBP in 1954 based on an extensive empirical analysis. According to Bruun, the mechanisms leading to and EBP depends on a balance between destructive and constructive forces acting on the beach. This forces are responsible of sediment transport offshore and onshore directions. If either of these forces acting on the beach is modified there will be an unbalance and an adjustment of the beach profile to bring the forces back into balance. On this basis Bruun proposed the empirical Equation 1.1.

$$h(x) = Ax^m \tag{1.1}$$

Where h is the water depth at a distance x from the mean sea level shoreline, m is a shape factor associated to the type of the destructive forces and A is a scale parameter that depends on the stability characteristics of the bed material. Based on the values of m and A, the EBP proposed by Equation 1.1 varies from a concave upward profile when $m < 1$ to a convex upward profile when $m > 1$. When $m = 1$, a linear profile is described. Dean (1977) validated this equation proposing that m should be fixed in 2/3 and that the only free variable should be the scale parameter A.

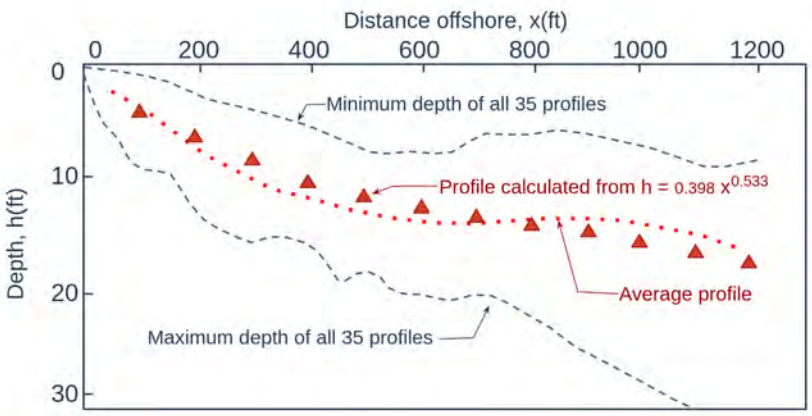

Figure 1.4: Equilibrium Beach Profile (EBP), water depth h as a function offshore distance based on 35 beach profiles. The red dotted line represents the average profile, blue dashed lines represent maximum and minimum depths, and the red triangles represent the best fit from Equation 1.1. This figure is extracted from Dean (1977).

Since the validation of this EBP equation numerous works have been done to approach the scale parameter A and its interactions with the shape parameter m in order to obtain the most suitable representation of an equilibrium beach profile (Boon and Green (1988)). It has been concluded that A is a dimensional parameter that depends mostly on sediment characteristics such as settling velocity and diameter (Moore (1982); Larson (1991); Kriebel et al. (1991); Bodge (1992)).

Equilibrium profiles are established from field observations of global beach profiles, which represent the entire nearshore region. Figure 1.4, extracted from Dean (1977), illustrates this concept with a data group of 35 beach profiles used to establish the EBP. The figure shows the average profile (represented by the red dotted line), the maximum and minimum depth performances (represented by the blue dashed line), and the best fit from Equation 1.1 (represented by the red triangles). However, global equilibrium states, even if they can be associated with seasonal or annual timescales, can easily vary due to external processes, such as changes in wave forcing or sediment flux along the coast. These variations are not captured by EBP, and as a result, these profiles are rarely observed in the field. The concept of dynamic equilibrium of the beach, introduced by Wright et al. (1984), complements the concept of beach equilibrium profile, as it highlights the permanent adjustment of the beach with hydrodynamic forcing.

The Wright and Short beach classification model is an empirical model based on field observations. This model is founded on the concept of equilibrium between hydrodynamic conditions (mainly waves) and beach morphology. The dimensionless sediment fall velocity, known as the Dean number (Ω), is used to classify beaches in micro-tidal environments. This dimensionless number relates off-shore wave height (H_0) and peak period (T_p) with sediment fall velocity (W_s), controlling suspended sediment transfers. The Dean number is defined as a dimensionless fall velocity $\Omega = H_0/W_sT_p$ or it can also be interpreted as a length scale ratio $\Omega = H_0/H_g$, where $H_g = W_sT_p$ represents the typical height over which sediment settles during a wave period. The Dean number is typically used at micro-tidal beaches, where the environment is wave-dominated, to classify beaches into different morphological states. Using this dimensionless number, global cross-shore beach profiles can be described and classified into dissipative ($\Omega > 5$), intermediate ($1 < \Omega < 5$), and reflective ($\Omega < 1$) states. Over time, sandy beaches can evolve from one state to another, depending on wave conditions.

Masselink and Short (1993) proposed a modification to Wright and Short classification model by linking two parameters that affect beach morphodynamics: the dimensionless fall velocity (Ω) and the ratio between tidal range and wave height (RTR). With this modification beaches are no longer classified only based on their morphology, but also according to dominant processes, always related to hydrodynamic conditions. This modified model (Masselink and Short, 1993) provides a more detailed classification of coastal system, as shown in Figure 1.5.

While the Masselink and Short beach classification model provides a useful tool for classifying beaches into different morphological states based on the concept of equilibrium between hydrodynamic conditions and beach morphology, it has its limitations. The model is primarily focused on capturing average global equilibrium profiles that can be associated with seasonal

or annual timescales. Hence, the question arises as to whether the global equilibrium concept is relevant for field applications or if we should focus on pseudo-equilibrium on timescales such as tides, storms, or waves.

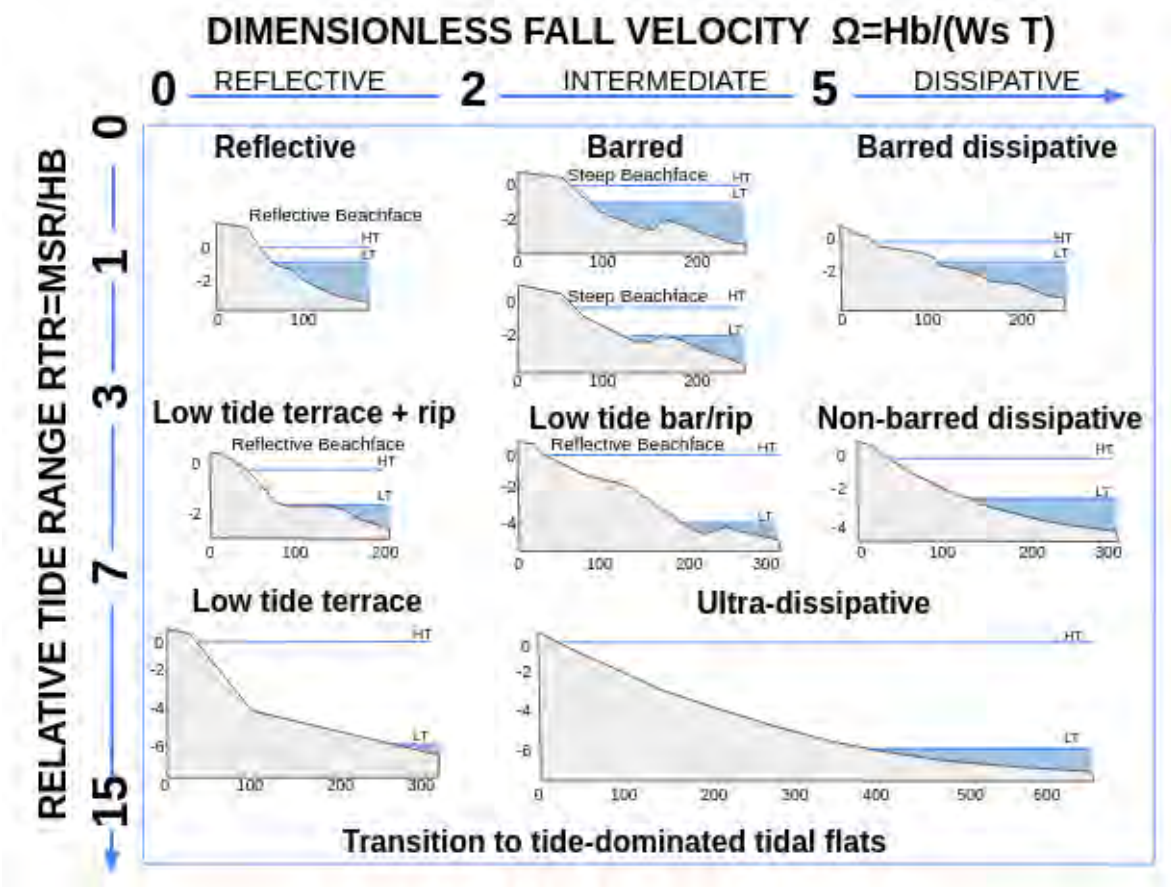

Figure 1.5: Beach classification model according to the Dean number (Ω) and the relative tidal range with respect to the wave height (RTR) at breaking (Figure reproduced from Masselink and Short (1993)).

It is important to note that the concept of beach equilibrium profile is relative to the timescale considered. It has been defined that there is an equilibrium profile for every incident wave conditions, but due to the stochastic nature of hydrodynamic forcings, this equilibrium states are unstable and will oscillates at a rate proportional to the disequilibrium: the distance from the present to the equilibrium states (Ludka et al., 2015). Different disciplines have different interpretations of the term equilibrium, highlighting the complexity of this concept (Thorn and Welford, 1994). Therefore, from a dynamic perspective, when studying beach systems, it is crucial to consider not only the equilibrium state but also the dynamics processes that can cause changes over time. Accordingly, the full hydro-morphodynamics need to be understand to access such processes.

1.1.3 Coastal hydro-morphodynamics

Beach morphodynamics is the spatio-temporal evolution of the beach morphology under the influence of hydrodynamic forcing. The coastal hydro-morphodynamic system is influenced by both local fluid-sediment interactions as well as external factors such as storms, winds, currents, tides, sediment deficits or in-punts, as shown in Figure 1.3. Through sediment transport the beach evolves under the action of hydrodynamics forcing, leading to changes in the sea-bed and sediment transport patterns.

1.1.3.1 Hydrodynamics forcing

The surface of the ocean is influenced by various forces, such as wind and atmospheric pressure, which result in the formation of waves and currents. Additionally, the gravitational pull of the Moon and the Earth's rotation generate slow-moving tides on the ocean's surface. These forces operate on different time and spatial scales, ranging from seconds to centuries and millimeters to kilometers, as shown in Figure 1.6.

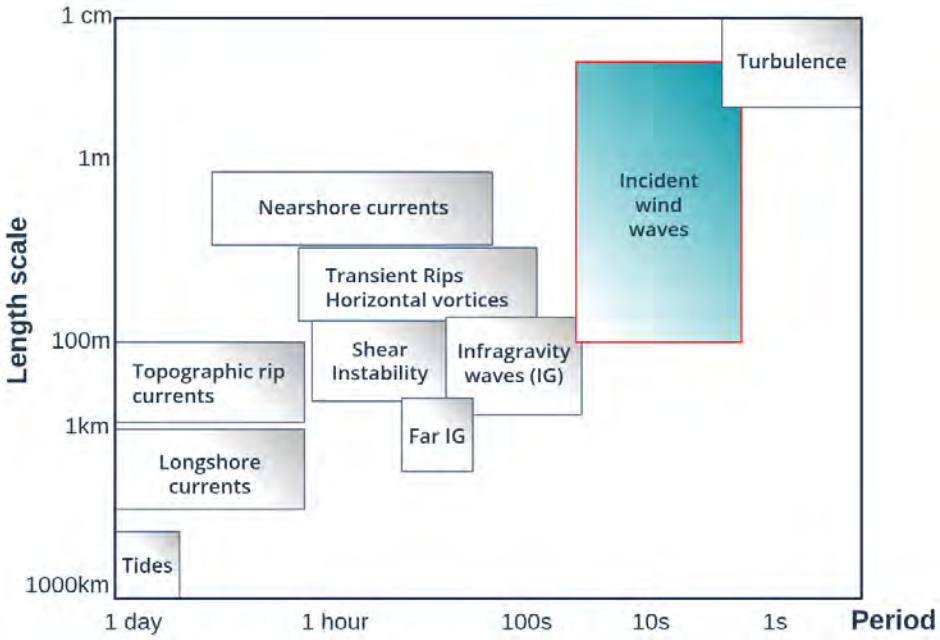

Figure 1.6: Space-time scales of coastal hydrodynamic processes (Figure reproduced from Souza et al. (1997)).

Generally speaking, for a wave to exist there must be an initial equilibrium state, which is perturbed by an initial disturbance and compensated by a restoring force. For gravity wave at a free-surface of a liquid initially at rest, the free-surface then oscillates around it equilibrium state. The different origin and nature of surface oscillations affect the waveform in terms of height and period (and associated wavelength), generating a large variety of waves. Ocean

waves can be categorized in various ways, with one of the most common classifications being based on either their period or wavelength. A graphical representation of this classification, showing the type of wave, the generating and reacting forces, has been provided by Holthuijsen (2010) and is presented in Figure 1.7.

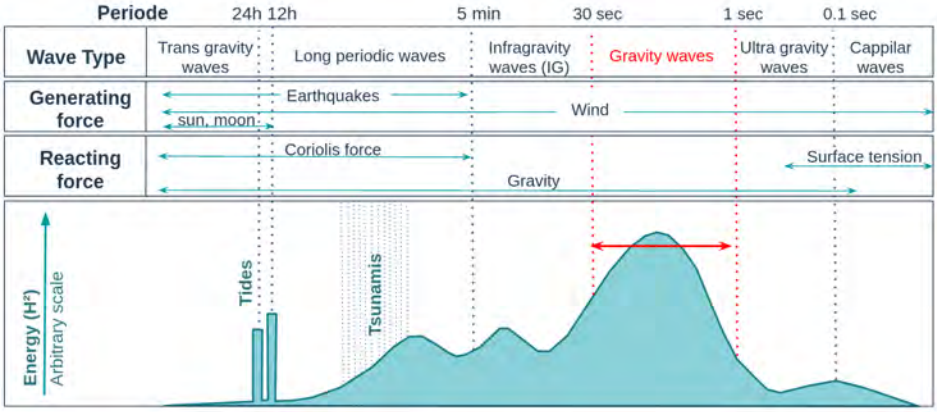

Figure 1.7: Wave classification based on the wave period (Figure reproduced from Holthuijsen (2010).

In the upcoming section, our primary focus will be on the transformation of incident gravity waves up to the swash zone. We will also provide a conceptual description of infragravity waves that can be observed in the coastal zone. Understanding the physics of the incoming incident waves is crucial to our study of how nearshore morphodynamics respond to changing wave conditions.

Incident gravity wave transformation up to the swash zone

The movement of ocean surfaces is mainly driven by atmospheric conditions, such as wind, which generates undulations upon contact with the water surface. These perturbations, known as gravity waves, propagate due to pressure gradients induced by the variation of water height. The characteristics of these waves will depend on the intensity and duration of the winds, as well as the distance of wind action, known as fetch (see Figure 1.8).

The basic wave dynamics is detailed in Holthuijsen (2010); Toffoli and Bitner-Gregersen (2017), where it is establish that when waves propagate over a depth much larger than the wavelength (Deep water can be considered as of infinite depth), longer waves travel faster than shorter ones, dispersing from one another. As a consequence, long waves rapidly move outside the generating area propagating in the ocean and become swells (mechanical waves that propagate under the predominating influence of gravity). Swells have a typical wavelength that is greater than 260 m up to a maximum of approximately 900 m . Gravity waves assume periods ranging from a minimum of about 1 s up to maximum of approximately 30 s (see Figure 1.8).

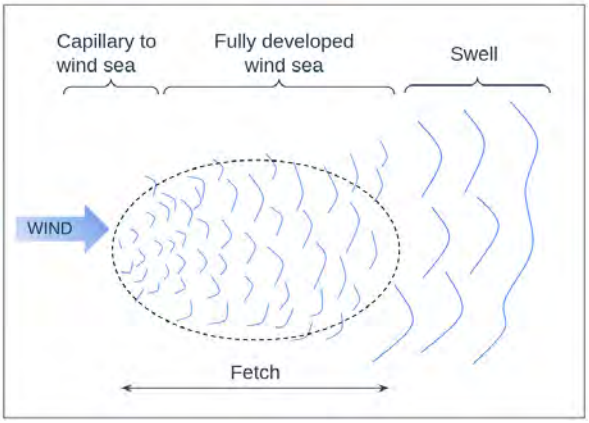

Figure 1.8: Schematic representation of wave generation (Figure reproduced from Toffoli and Bitner-Gregersen (2017)).

When waves travel across the water surface, the movement of water particles is predominantly characterized by vertical oscillation, with minimal horizontal displacement in the direction of wave propagation. This creates circular paths with a diameter matching the wave amplitude for individual points on the water surface. This motion extends to the underlying water, disturbing it to a depth of approximately half the wavelength, as depicted in the deep water section of Figure 1.9. However, as waves approach the shallow waters near the shore, their interaction with the seabed causes a transformation in their motion. The wave orbits become flattened and transform into elliptical paths, as illustrated in the shallow depth section of Figure 1.9.

As waves approach the coastline, they undergo a series of changes due to their interaction with the seabed (Figure 1.9). The decreasing water depth near the shore causes an amplification in wave height (from crest to trough) due to a decrease in wave celerity caused by bottom interaction. This process, known as shoaling, results in waves that develop an asymmetric shape with large crests and wide troughs. Once the asymmetry reaches a critical point, the waves break and surge, creating a breaking zone. All gravity waves, or swells, experience an increase in amplitude and a decrease in wavelength over rapidly shoaling regions before breaking near the shore and expend their energy on the shoreline.

After the wave transformation asymmetric waves (wave fronts or bores) can reach the shoreline. This asymmetry generates an additional fluid supply towards the coast, causing a rise in the mean sea level (wave set-up). However this increase cannot be sustained indefinitely, and to maintain an equilibrium the water must return offshore directions, creating a bed return current. This current is know to contribute to the formation of sandy bars and erosion of the coastlines. Beyond these gravity waves, their non-linear interaction leads to the generation of low-frequency wave know as infra-gravity (IG) waves which can strongly affect the dynamics close to the shoreline.

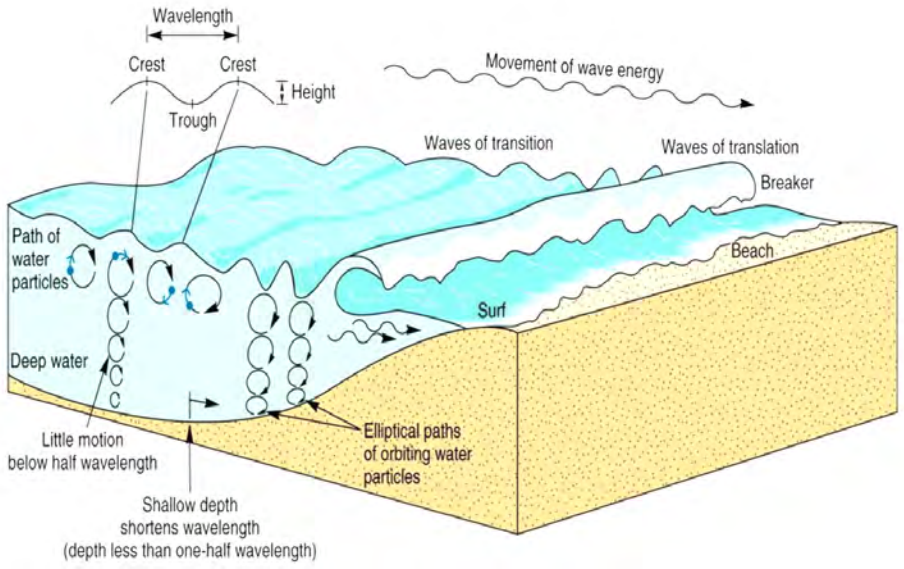

Figure 1.9: Modification of wave shape near the coast. (Figure extracted from Biausque (2018)).

Infragravity waves

Infragravity waves, also known as low-frequency waves or long waves, are an important type of ocean waves that are generated through nonlinear interactions between wind-generated gravity waves. These interactions convert a portion of the energy of the gravity waves into subharmonics with periods ranging from about 20 to 30 seconds up to a maximum of approximately 5 minutes (Guza and Thornton, 1985; Herbers et al., 1995). The existence of infragravity waves was first observed by Wunk (1949) and Tucker (1950), and subsequent studies have provided further details and characteristics of these waves (Longuet-Higgins and Stewart, 1962; Holman and Bowen, 1984; Ruessink, 1998; Toffoli and Bitner-Gregersen, 2017; Thomson et al., 2006; Bertin et al., 2018).

Gravity waves, discussed in the previous section, propagate in trains which are groups of waves that travel together with a similar wavelength and frequency. These waves interact with each other, creating wave packets or trains, and can travel great distances across oceans and seas. Infragravity waves are closely related to incident wave groups or packets, as the energy associated with these long oscillations is bound to the generating wave trains. Due to wave shoaling and breaking processes infragravity waves are released as free waves in the nearshore, i.e. evolving independently of their initial gravity wave origins. They can also be reflected back offshore directly or trapped by refraction (Ruessink, 1998).

Beyond infragravity waves, it has been observed that various long waves actually coexist near the shoreline (Holland and Holman, 1999). Waves trapped at the nearshore during the realise of IG waves are know as edge waves. This waves can reach the beachface and be reflected directly offshore, ,creating either offshore direction leaky waves or trapped standing waves in the surf zone. A schematic representation of the generation and propagation of IG

waves is shown in Figure 1.10. For more details of these long waves in the nearshore zone, the reader should refer to Ruessink (1998); Bertin et al. (2018).

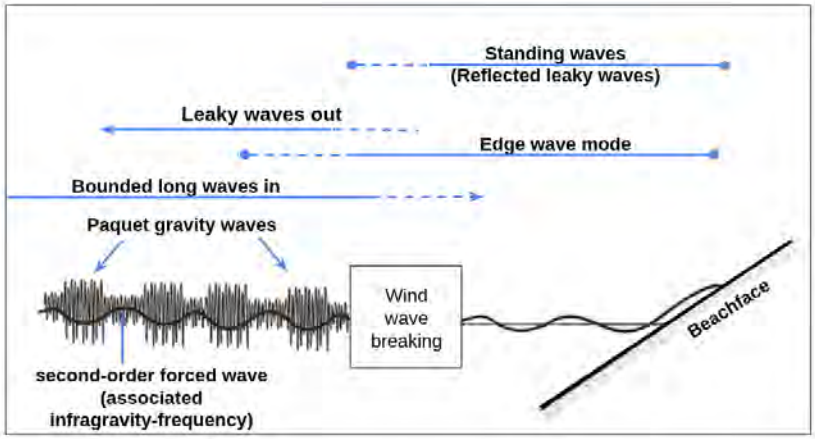

Figure 1.10: Schematic representation of infragravity wave generation (according to Oltman-Shay and Hathaway (1989); Ruessink (1998)).

Infragravity waves play a significant role in the nearshore region, as these free waves exhibit small amplitudes that may not break, allowing them to transfer their energy shoreward. This aspect becomes particularly relevant in dissipative beach states, where the extended dissipative zone has the potential to dissipate shorter wind or gravity waves, making long waves the predominant waves reaching the shore.

1.1.3.2 Sandy beach morphodynamics

A morphodynamic system consists on geomorphological adjustments in response to changes in the environment around it. In coastal hydro-sedimentary systems, the topography of the seabed is constantly adjusting to hydrodynamic forcing. These morphological changes are driven by sediment transport gradients (see Figure 1.3).

The evolution of sandy beach topography over time and space is largely influenced by the water level on the seabed, which is a key parameter that controls the hydrodynamic forcing. Offshore topography, being subject to low-frequency phenomena, tends to operate on larger temporal scales. On the other hand, the intertidal zone, being a highly dynamic area, is characterized by rapid morphological changes occurring over shorter time scales.

The morphology of sandy beaches is a crucial element in understanding coastal morphodynamics. The beach profile, which provides a vertical cross-sectional view of the coast, is commonly used to characterize beach morphology. In 1982, Wright and Short introduced a representative beach profile, which is still widely used today and typically displays a concave shape from the dune towards the sea (as already mentioned in Section 1.1.2). An updated version of this profile is presented in Figure 1.11.

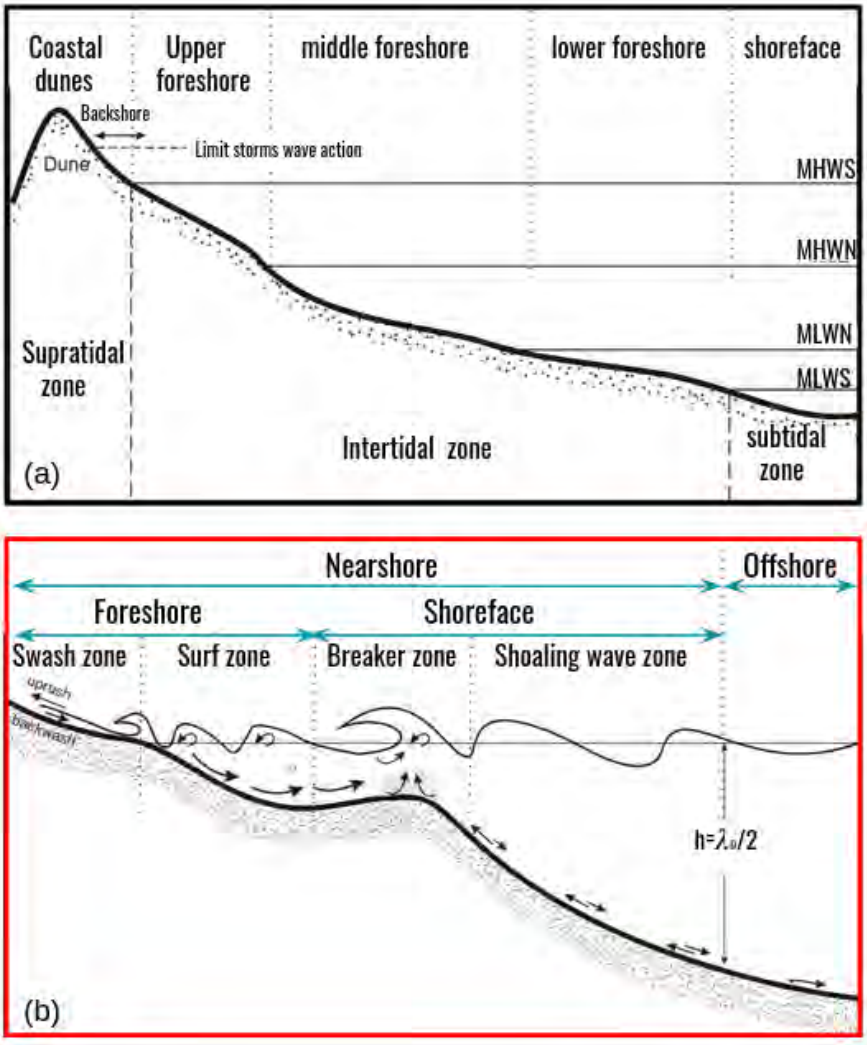

Figure 1.11: (a) Beach morphology in a macro-tidal environment. (b) Beach profile morphology based on incidents waves propagation towards shore. Figure modified from Wright et al. (1982a); Stépanian (2002).

The beach profile can be divided into three distinct tidal zones based on water level, as shown in Figure 1.11a. The subtidal zone is defined as the area below the mean low water spring level (MLWS), which is perpetually submerged and subject to constant wave action, tidal currents, and general currents. The intertidal zone is defined as the area between MLWS and the highest spring level (MHWS), which is a highly dynamic zone also referred to as the foreshore of the beach profile. In macro-tidal environments, the foreshore can be further divided into sub-zones based on neap (MLWN and MHWN) and spring (MLWS and MHWS) tidal fluctuations.

It is important to consider the role of wave propagation and transformation towards the shore in shaping coastal morphology, as discussed in the previous section, which is very commonly used to subdivide coastal zones (i.e Pilkey et al. (1993); Ruggiero et al. (2005),

in addition to tidal effects. In particular, the nearshore region extends from the wave base to the limit of run-up and comprises several zones, including the shoaling, breaker, surf, and swash zones (Figure 1.11b). It is further divided into two main regions: the shoreface and foreshore. The foreshore is a critical zone as it acts as a sediment transport corridor, a source of sediment, and facilitates the exchange between the beach and the outer beach zone (shoreface). It exerts a significant influence on the dynamics of beach behaviour (Short and Jackson (2013)). Each zone of the nearshore is characterized by different hydrodynamic processes and interactions between zones, which have been extensively studied. However, the highly complex nature of these interactions means that the nearshore remains a current topic of research, with much still to be learned. The complexity arises due to the interplay between various factors such as wave energy, sediment dynamics, and beach morphology, which can vary significantly over short distances and timescales. Our work focuses on understanding the link between morphodynamics and wave transformation.

Basic concepts of nearshore sediment transport

As mention earlier beach evolution will be conducted by sediment transport. The spatial-temporal evolution will depend on the location of the area on the beach profile. The offshore beach morphology will be associated to longer temporal scales while the nearshore or inter-tidal zone will be associated to shorter temporal scales. These two scale and frequencies of the morphological response based on the coastal zone area is schematically represented in Figure 1.12.

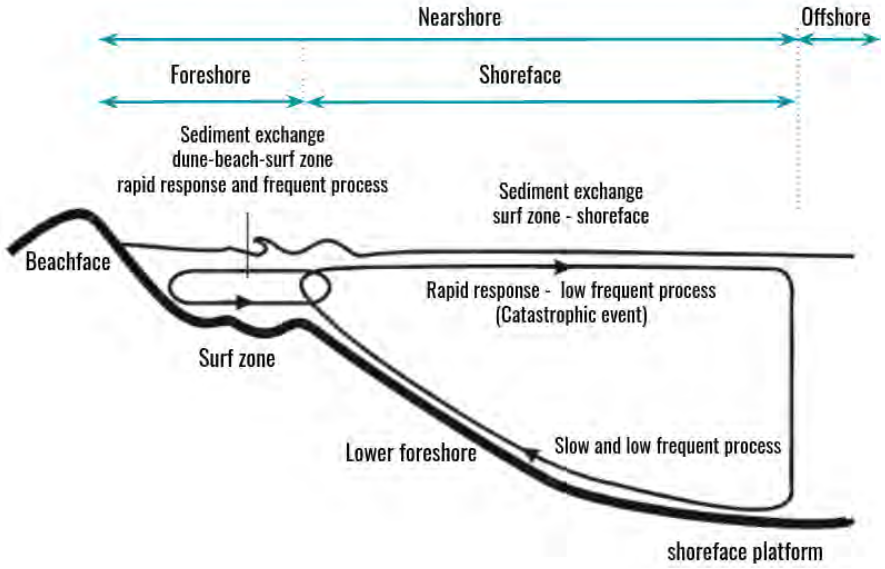

Figure 1.12: Scales and frequencies of morphological responses of the different zone of the coastal domain (According to Wright et al. (1985) and extracted from Stépanian (2002).

Both waves and currents are essential for sediment transport in coastal environments, as highlighted by several studies (Soulsby and Humphery, 1990; Wang et al., 2007). However, their interaction can be intricate and highly dependent on local conditions. The net sed-

iment flux resulting from the balance between waves and currents is influenced by various factors, including the characteristics of waves and currents, sediment properties, bottom topography, and their location within the coastal area. To understand this complex system it is common to analyze sediment transport in two main directions: longshore and cross-shore directions. Longshore transport occurs parallel to the coastline, while cross-shore transport is perpendicular to the coast.

Longshore currents are a well-studied concept in coastal science, as several currents can be generated in the nearshore. These currents travel parallel to the coast and are due to the incidence angle of incident waves during their breaking (Komar and Inman, 1970; Longuet-Higgins, 1970). The intensity of these currents is proportional to the wave height at the breaking point, as well as its incidence angle. This longitudinal current can develop at different locations along the beach profile and based on the sea-bead topography they can be confined in the surf zone, as shown in Figure 1.13a. These longshore currents have the ability to transport sand from one adjacent area to another over a considerable distance, while waves shape the beach in the cross-shore direction, due to currents generated from wave propagation towards shore, as explained in the previous section, shown in Figure 1.13b. The direction of cross-shore currents will depend on the water depth profile and the intensity of this current is generally lower than that of long-shore currents.

Rip currents, which are a type of surface current, can occur at various beach types and in different wave climates, as observed in studies such as Wright et al. (1984); Gallop et al. (2011); Castelle et al. (2017). These currents are typically fast, narrow, and flow offshore. They occur after the breaking point due to an excess of energy that flows along the coastline, causing the water to converge into a narrow channel that rapidly flows offshore, as illustrated in Figure 1.13c. Rip currents are known to induce a strong sediment transport offshore, especially during storm periods. They are extremely dangerous for swimmers and are a leading cause of drowning worldwide (Barlas and Beji, 2016).

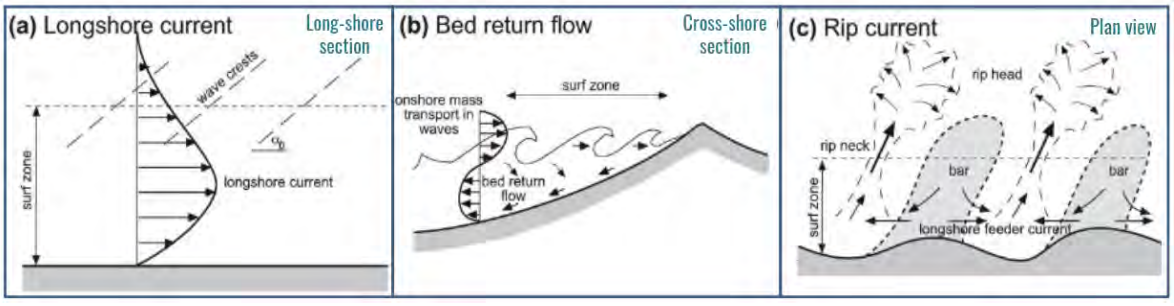

Figure 1.13: Currents in the nearshore: longshore drift (a), cross-shore bed return flow (b) and rip currents (c). This Figure is proposed by Masellink and extracted from Biausque (2018).

The transport of sediment induced by the propagation of incident waves depends on various factors, including the symmetry of the wave and the bottom topography (Grasso et al., 2011; Hsu and Hanes, 2004). When a wave is perfectly symmetrical, its net transport

is zero because the path of water particles follows circular motion (see Figure 1.9). However, if there is sediment available in suspension, a net transport can occur when the wave interacts with the bottom topography and creates an asymmetry in the wave velocities (known as wave skewness). This phenomenon has been detailed by various researches such as Dohmen-Janssen and Hanes (2005, 2002); Hsu and Hanes (2004);

In conclusion, net sediment transport that shapes beach profiles is controlled by complex wave-current interactions occurring at different spatial and temporal scales and in different longshore and cross-shore directions. These processes are typically studied separately, and models that consider coupled long-shore and cross-shore or current-wave interactions remain a challenge. Additionally, the type of sediment and bottom seabed are crucial in determining the mode of sediment transport, with sediment fall velocity playing a crucial role in determining the vertical distribution of sediment in the water column. Coastal sediment transport modes can be classified into several types based on the dominant transport mechanism, including bedload transport, suspended load transport, and wash load transport (i.e Foster et al. (2006)).

1.1.3.3 Focus on hydro-moprhodynamics of nearshore sub-regions

Shoaling and breaking zone

Shoaling happens when waves experience force from the seabed due to the decrease of water depth when approaching shore. This processes induces wave to change in shape and behaviour as they propagate to shallower water. Wave breaking occurs when the water depth becomes to shallow compared to the wave height. To describe this processes in literature a breaking criteria has been established, known as the breaker index (γ), which is the ratio of the water depth (H) to the wave height (H_b) $\gamma = H_b/H$. At the shallow water boundary, the breaker index indicates that the breaking process begins when the wave height becomes greater than a fraction of the water depth. Accordingly, the estimation of γ at breaking can be found around $\gamma_{br} = 0.8 - -1$ in the literature (Miche, 1944; McCowan, 1891).

The shoaling and breaking zone has been extensively investigated and is detailed in the following research works Thornton and Guza (1982); Drazen et al. (2008); Banner and Peregrine (1993); Power and Hughes (2008); Robertson et al. (2013); Chella et al. (2015). An important parameter in this zone is the Iribarren Number which is an hydro-morphodynamics control number that classifies the type of wave breaking. The Iribarren Number, also known as the surf similarity parameter is named after Iribarren who introduce the concept that describes wave breaking on sloping beaches. Then Battjes (1974), extended this concept and proposed a classification for periodic waves propagating on sloping beaches as a function of either offshore wave height (H_0) or wave height at the breaking point (H_b). This number is defined in Equation 1.2 and the different types of wave breaking is shown in Figure 1.14.

$$\xi_0 = \frac{tan\alpha}{\sqrt{H_0/\lambda_0}} \quad \text{or} \quad \xi_b = \frac{tan\alpha}{\sqrt{H_b/\lambda_0}} \tag{1.2}$$

where ξ is the Iribarren number, α is the angle of the seaward slope, λ_0 is the deep-water wavelength, H_b and H_0 is wave height associated at breaking or offshore respectively.

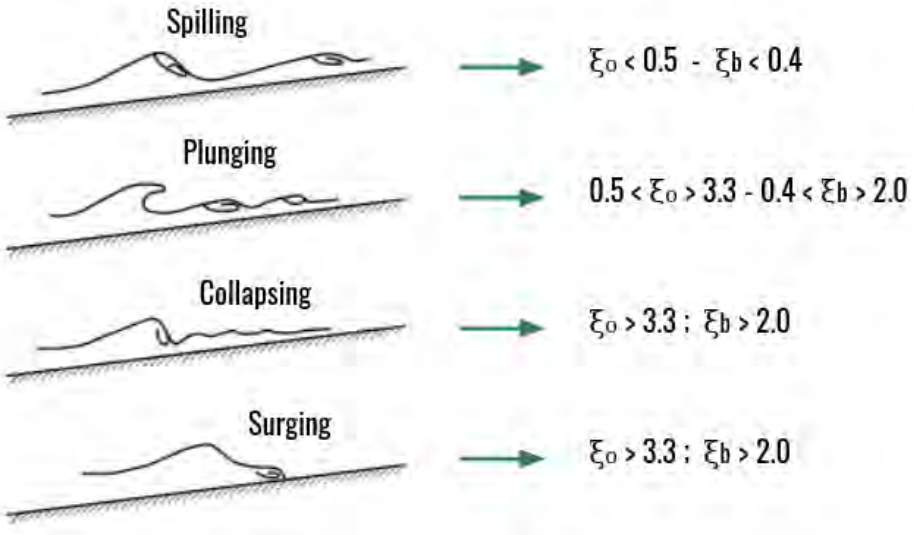

Figure 1.14: Breaker type following Battjes (1974) classification based on the Iribarren number.

The type of wave breaking will affect flow patterns, turbulence, and wave shape (skewness) and therefore will directly affect the sediment transport in the foreshore (Hsu and Hanes, 2004; Grasso et al., 2011). For instance Hsu (1998) performed a combined theoretical and experimental study showing that sediment transport in the foreshore (see Figure1.11b) is strongly linked to the Iribarren Number. In particular, they show that the geometric characteristics of a storm-beach profile is governed by a modified Iribarren number which includes the effects among the factors of beach slope, breaking wave angle and wave steepness.

Sediment transport on the foreshore is influenced by numerous factors, including tides, sediment characteristics, wave reflection, infiltration, groundwater, and more (Mason and Coates, 2001). Nevertheless, a primary driver of sediment transport is the dissipation of wave energy resulting first from the breaking process. As a result, the Iribarren Number and the breaker index parameters (ξ and γ) remain crucial in understanding and predicting sediment transport in the foreshore.

Surf zone

The surf zone, located between the breaking zone and the swash zone, is a well-known dissipative area for incoming waves (Wright et al., 1982b; Battjes, 1988). Due to its complexity, it exhibits a wide range of hydro-morphodynamic systems. The equilibrium beach classification model proposed by Wright et al. (1985) and modified by Dean Dean (1991) classifies beach morphology based on the Dean number ($\Omega = H_b/(T_p W_s)$) and the relative tide range (see Section 1.1.2). This results in different hydrodynamic systems for each type of beach,

with a primary difference being the morphology of the surf zone, as shown in Figure 1.5. For example, a reflective beach profile is characterized by a steep foreshore with a relatively narrow surf zone and a near-vertical beach face, while a dissipative beach profile has a gentle foreshore with a wide surf zone and a relatively flat beach face, according to the Wright and Short classification model.

Intermediate beaches exhibit a more complex bottom topography, resulting in more complex hydrodynamic systems, particularly in the surf zone. Wright et al. (1984) have well-described the diversity and the hydro-morphodynamics of these intermediate beaches, leading to the subdivision of four beach states: Longshore Bar and Trough (LBT), Rhythmic Bar and Beach (RBB), Transverse Bar Rip (TBR), and Low Tide Terrace (LTT). A summarised version of Wright et al. (1984) classification is shown in Figure 4.1. The intermediate beaches are characterized by different types of bar formation in the surf zone, such as double bar beaches, bars closer to the breaking point or closer to the swash zone, merging within it. These complex topographies, when viewed from the air, generate different return channels. The morpho-dynamics of the bar and its influence on the hydrodynamic forcing have been extensively studied, with a good understanding of it, including research by Oltman-Shay and Hathaway (1989); Lippmann and Holman (1989); Short (1996); Masselink and Short (1993); Castelle et al. (2016); Leckler and Dubardier (2010); Benoit et al.; Madsen et al. (1997) .

While this zone has been extensively studied by coastal scientists, understanding how the surf zone interacts with other coastal zones is still an active area of research.

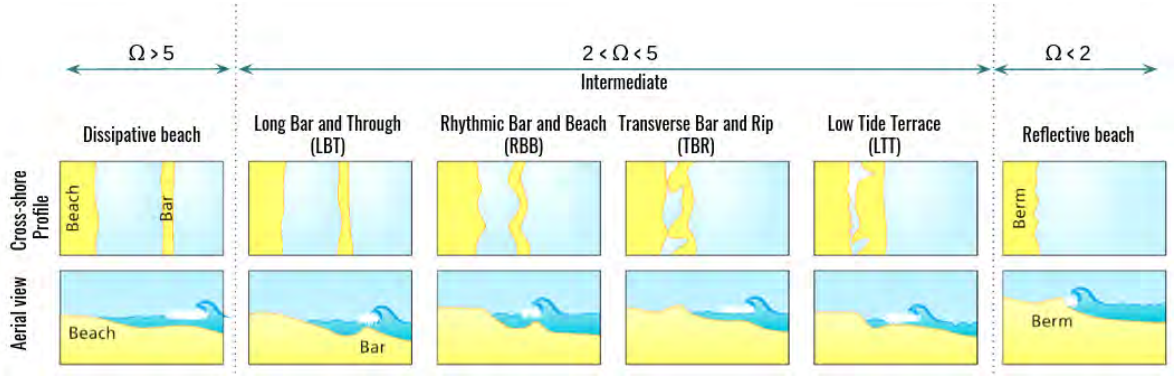

Figure 1.15: Beach state classification based on the Dean number (Wright et al. (1984); Short (1996)). Figure extracted and adapted from Ondoa (2020); Oerlemans et al. (2022)

Swash zone

The swash zone is the last zone of the beach where breaking waves dissipate or reflect their remaining energy at the bottom of the emerged beach profile (Brocchini and Baldock, 2008), as shown in Figure 1.11b. The cycle of wave motion implies that the top of the beach is intermittently covered and uncovered by waves defining the beachface, which is the land-ocean boundary. The swash zone is characterized by strong unsteady flows, high turbulence, large sediment transport rates and rapid morphological changes (Masselink and Puleo, 2006). Additionally, in the swash zone, the set-up induced in the breaker zone is

compensated, generating an additional offshore bottom current that has a significant influence on sediment transport, as already explained in Section 1.1.3.1 (Longuet-Higgins and Stewart, 1962; Svendsen, 1984). Therefore the swash zone is continually under these two mechanism: set-up and wave driven oscillation above this set-up level which are know as swash up-rush and down-rush (Guza and Thornton, 1982). Based on these two mechanisms, the swash zone is one of the most energetic and dynamic region of the nearshore.

The water motions oscillations in the swash occur over a wide range of frequencies that can be grouped into three categories according to the most energetic wave frequency in the foreshore (Hughes (1992)). The first category are the IG waves, that have frequencies ranging from between 30 sec and 5 min (see Figure 1.7). The second category is referred to the sub-harmonic edge waves, which period have twice the incident wave period typically 15 to 25 sec. And the third category is directly associated with up-rush and down-rush of gravity waves and have periods between 5 to 15 sec. All these waves have been discussed in Section 1.1.3.1.

The spatial boundaries and time period of swash events are difficult to define due to the intermittence of incident waves and water levels. Typically, the third category of swash oscillations related to up-rush and down rush is used to determine a swash cycle (Puleo et al., 2000). Despite the complexity of the swash morphology and wave signal, a single swash event can then be defined by the covering and uncovering of the beachface by a single wave, shown in Figure 1.16. These swash events are associated with highly non-linear waves that can be described as a "bore," which is a steep wave front generated due to nonlinear interactions between waves in shallow water.

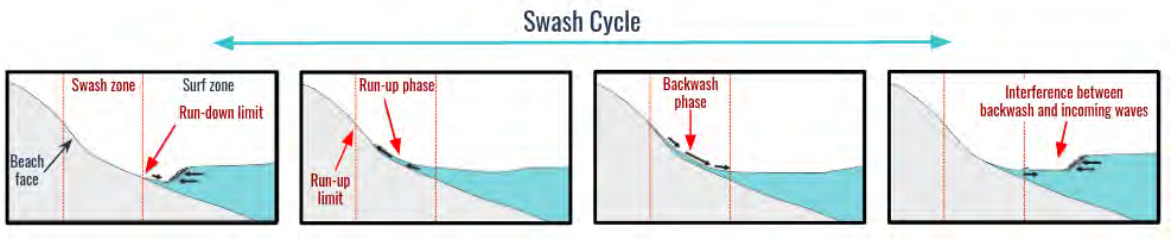

Figure 1.16: Representation of a swash cycles where black arrows represent flow direction with size indicative of relative magnitude. Red doted line illustrated swash zone limites generated by the up-swash and backwash. Figure proposed by Masselink and Puleo (2006) and adapted from Pitman (2014).

During the uprush phase, flows are generated by the collapse of the propagating bore on the beachface. An interaction between these flows and the preceding backwash can be then observed trough collision (Hibberd and Peregrine, 1979; Jensen et al., 2003). The motion during the backwash is mainly dominated by bottom shear, while that during the uprush is dominated by turbulent flows generated within the bore propagation.

The thickening of the boundary layer during backwash is more significant than during uprush, leading to a longer duration of the downward motion than that of the upward motion (Masselink et al., 2005). It has been observed that the duration of backwash is generally

much longer than that of uprush, while the peak velocities reached during backwash can be comparable to or slightly lower than those reached during uprush (Puleo et al., 2000; Hughes and Baldock, 2004). Thus, the velocity asymmetry in the swash zone is often observed as negative, which would mostly lead to offshore sediment transport (Masselink and Puleo, 2006). Even though, the relative role of uprush and backswash on sediment transport, leading to either onshore or offshore transport remain unclear.

Hydro-moprhodynamics equilibrium of the swash zone

Defining the swash zone can be challenging due to its energetic nature, which can be affected by tide fluctuations. At low tide, the swash morphology is dominated by incident wave action, including wave excursion and up-down rush interactions (Wright et al. (1982b)). However, at high tide, tidal effects leading to over-swash or surf dissipation processes can also affect the swash morphology at different positions, making it difficult to define an equilibrium slope of the beachface (see Figure 1.17).

In microtidal beaches where tidal effects are negligible, the swash equilibrium can be more easily related with the hydrodynamic motion of the swash zone. When the volume of water displaced during uprush (toward the shore) is equal to that transported during backwash (toward the offshore), a balance is achieved. This resulting slope represents the equilibrium between the asymmetry of swash toward the shore and the gravitational component toward the offshore, as described by Wright et al. (1982b). In this case, tidal effects are ignored, and a single beachface slope can be associated with the swash zone.

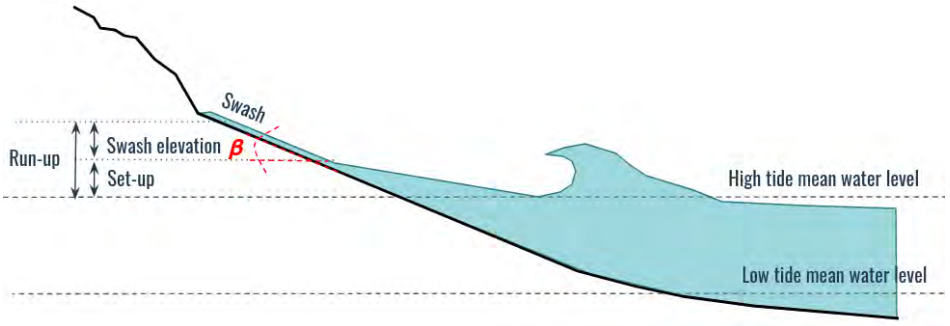

Figure 1.17: Sketch of run-up in the swash zone and definition of the beachface slope (β). Figure proposed by Komar (1977) and modified from Astier (2014).

Masselink and Puleo (2006) proposed an equilibrium slope that depends on the balance between uprush and backswash of the incoming waves, resulting in two possible scenarios: either the beach profile is steeper than the equilibrium slope, or it is flatter. Therefore the beachface morphology will adapt to these individual waves forcings implying a net sediment transport toward offshore or onshore directions. When the beachface slope (β) is steeper than the equilibrium slope, the wave forcing generates a net sediment transport towards the offshore because the transport by uprush is less efficient than by backwash. As a result, sand moves from the top to the bottom of the beach profile, as shown in Figure 1.18(a).

On the other hand, when the beachface slope (β) is flatter than the equilibrium slope, we observe a sediment transport towards the shore, resulting in a steepening of the beachface slope, as shown in Figure 1.18(b). In both scenarios, the beachface will continue to undergo morphological changes until a new equilibrium slope is reached. As the morphology of the swash is partly characterized by the local bechface slope (β) and is significant retroaction on hydrodynamics, this slope remains a key parameter on the swash and nearshore dynamics.

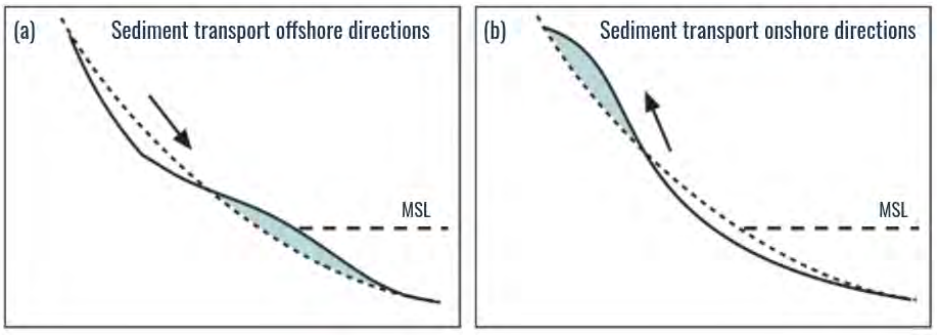

Figure 1.18: Shows erosion (a) and accretion (b) occurint in the swash zone as a result of individual wave action.Figure proposed by Masselink and Puleo (2006) and modified from Astier (2014).

Depending on the type of substrate, there exists a wide variety of different beaches slope around the world, from fine sandy beaches to rocky shores. Field observations and laboratory models have shown that beaches with finer sediment size are associated with lower beachface slopes. Since early research it has been admitted that the beachface slope increases with the increase of the average sediment size D_{50} Bagnold (1940); Bascom (1951); Turner (1995); Bujan et al. (2019). This statement has been partly explained by the effect of swash infiltration and exfiltration of water through the beach profile in the swash zone (Kemp, 1975; Turner, 1995; Masselink and Hughes, 1998; Masselink and Puleo, 2006; Sous et al., 2013). The infiltration process, which occurs as water percolates from the uprush into the unsaturated beach profile specially influences the equilibrium beachface slope for beaches with coarse sediment ($D_{50} > 1mm$). This infiltration weakens the backwash, resulting in an asymmetry of the swash and enhancing sediment transport towards the shore. This causes the beach profile to stiffen until it reaches a slope where the gravity component directed offshore balances the onshore force due to the asymmetry of the swash (Butt and Russell, 2000). A great deal of effort has thus been invested on this relationship between the beachface slope with sediment size (β-D_{50}), providing a significant amount of empirical equations to predict the slope. Most of these expression show a power law dependency of the slope with the mean sediment size (Sunamura, 1984; Soares, 2003).

In a recent work by Bujan et al. (2019), 2000 measurements of beachface slope for different grain size were extracted from the literature. Different models relating slope and grain size were tested on this data base (see Figure 1.19a). They showed that even the most representative of the empirical equations cannot describe the full distribution of the data sets. Nonetheless, they derived a universal equation that best fit the large data set, based on sed-

iment size (D_{50}), shown in Figure 1.19b. However the data shows a large variability of the beachface slope, especially for the smallest sediment size. Probably due to the wide range of data sources and therefore beach specificity's, as for instance their instantaneous state compared with equilibrium profile to wave forcing.

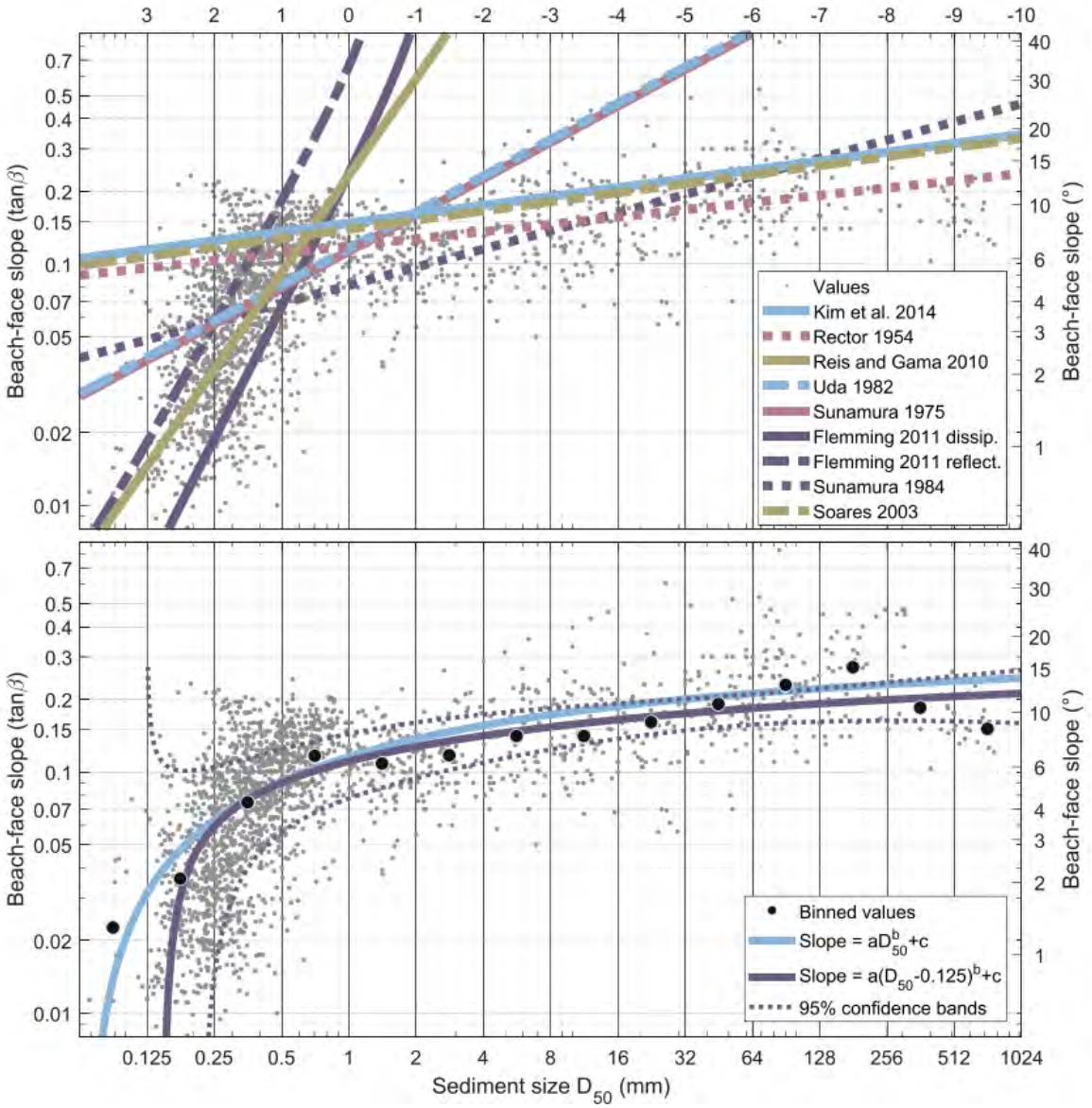

Figure 1.19: Top: plots of different empirical beachface slope equations over the big data sets. Bottom: best fit equations of the data set provided; where for the firs equation (light blue line) $a = 0.178$; $b = 0.187$; $c = 0.294$ and for the second equation (violet line) $a = 0.154$; $b = 0.145$; $c = 0.268$. This Figure is extracted from Bujan et al. (2019).

Therefore these empirical relations between the beachface slope and the sediment size can be used to predict the beachface slope in a highly generalized form, but they still lack of physical basis to provide a clear link with swash dynamics and the associated dimensionless

numbers characterising the relevant processes. In particular, the strong influence of the grain diameter D_{50} on the beach slope could also be influenced by the sediment fall velocity, which is known to influence the transport regime relative to wave dynamics. Therefore to reach a proper understating of these beachface slope variability's, the problem should be tackled from a physical approach taking into account not only the sediment but the interaction between sediment and hydrodynamic forcing acting on it.

Beyond this influence of the average grain size (D_{50}), the swash zone involves a wide range of hydrodynamics feedback mechanisms driving the evolution of the system and therefore probably the associated beachface slope. In particular, several researches such as Baldock et al. (2010); Holland and Puleo (2001); Masselink et al. (2005) highlighted the importance of these feedback mechanisms in swash modelling. For instance Masselink et al. (2005) hypothesized that the morphological response of the swash zone "represents an attempt to minimize the difference between the duration of the swash event D and the period of the incident wave T". Three cases where then distinguished: (i) when $D/T < 1$ the beachface slope tends to flatten due to the interrupted swash events since uprush and backwash do not interact, resulting in sediment transport towards the offshore direction (predominantly negative velocity asymmetry in the swash zone). (ii) When $D/T = 1$, the beach slope has reached its equilibrium condition. (iii) In the case where $D/T > 1$, there is a tendency towards steepening of the slope induced by the numerous uprush-backwash interactions that result in sediment transport towards the shore (Holland and Puleo, 2001). Indeed, the swash-swash interaction contributes to the increase of turbulence and sediment suspension, which plays an important role in the net sediment transport and makes the equilibrium beachface slope difficult to predict.

Despite recent advances in swash modelling, due to the high complexity of these systems and the difficulty to obtain high quality field measurements (Guza and Thornton, 1982; Puleo et al., 2003; Miles and Russell, 2004; Masselink et al., 2005; Masselink and Puleo, 2006; Turner et al., 2008), the prediction of the correct net sediment transport rates leading to rapid morphological changes in the swash are still lacking of a correct physical understanding and need to be improved (Chardón-Maldonado et al., 2016; Bakhtyar et al., 2009). Consequently, the local shape of the beach face remains not fully predictable.

1.1.4 Modelling coastal systems: a scale issue

Over the past few decades, coastal modeling have increasingly improved and different methods have been developed to approach the complex hydro-sedimentary systems, strongly temporal and spatial scale dependent (as discussed in the previous sections). Coastal morphodynamic evolution models are available in a wide range of complexities, computational demands, stability, and prediction horizons, with each method has its own advantages, disadvantages, simplifications, and assumptions. Hunt et al. (2023) proposed a diagram to summarise the range of validity of models resulting an a useful connection between the spatial and temporal scales of hydro-morphodynamic processes and various types of model approaches, such as empirical, reduced complexity and physics-based models, shown in Figure 1.20.

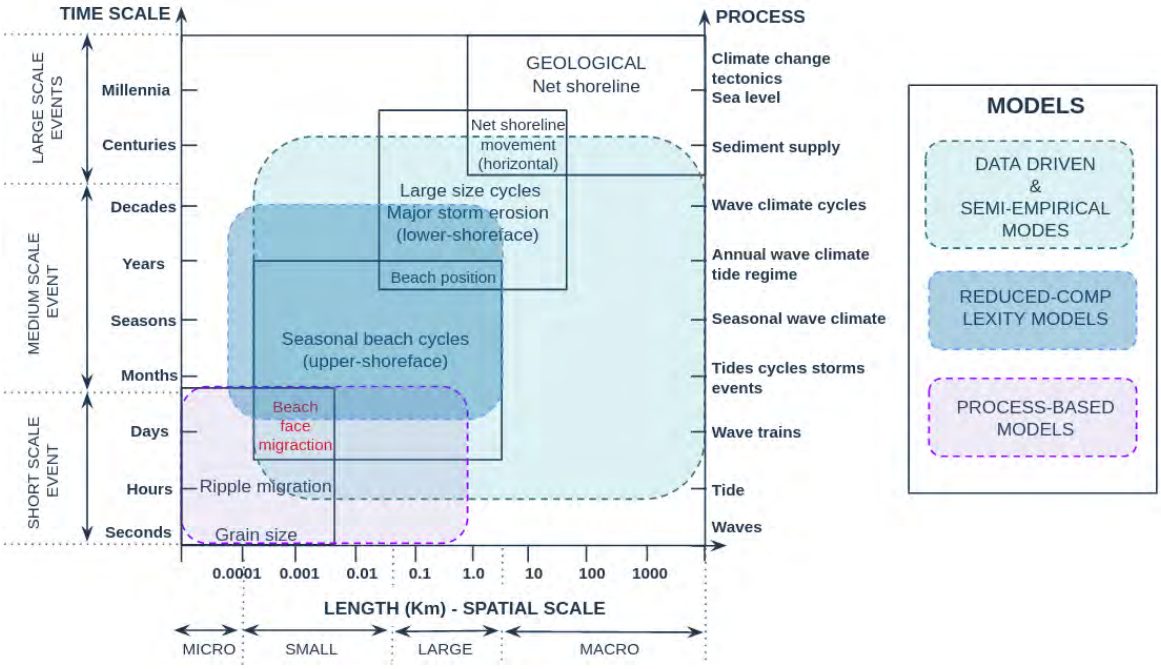

Figure 1.20: Schematic diagram presenting spatial and temporal modelling scales and approaches appropriate to hydro-morphodynamic processes. The range of validity of the different models is extracted from Hunt et al. (2023).

Coastal evolution has been studied for many decades using simple conceptual models (e.g. Bruun (1988); Dean (1977)). In the 1990s, the development of modern computers, better field measurements, and coastal monitoring technology allowed for the development of physics-based models. These models use mathematical aggregations of small-scale processes to predict coastal changes. However, computational limitations quickly hindered their medium-to-long term (years/decades) and regional spatial scales application. To overcome these limitations, a new data-driven approach emerged that challenged the dominance of physics-based models. This approach was based on large and high-quality datasets that omitted much of the process knowledge and were far more empirical, as seen in models like Hsu et al. (1994); Southgate et al. (2003). Today, the quality and duration of these datasets continue to improve, with better long-term monitoring and improved technology, including coastal video monitoring systems (e.g., Holman et al. (1993); Smit et al. (2007); Kroon et al. (2007); Siegle et al. (2007); Almeida et al. (2020)) and satellite data (e.g., Castelle et al. (2021); Vos et al. (2019); Luijendijk et al. (2018)).

Today, coastal science has witnessed a shift towards reduced-complexity models that combine the most impactful processes with the stability and computational efficiency of data-driven models. This trend has emerged as an intermediate state between traditional physics-based models and purely data-driven approaches. This new approach has been made possible by advances in technology and long-term monitoring, which continue to enhance the quality and duration of datasets.

The coastal morphodynamic models can be considered as a continuum from complex process-based models to simpler data-driven models. Figure 1.21 illustrate the complexity spectrum coastal models. In the left side of this Figure we can appreciate that appropriate choice trajectory is dependent on both data availability and process knowledge. Higher process understanding facilitates the use of process-based models, whereas data-driven models may be more appropriate in the absence of process understanding but with an abundance of relevant data.

The right side of Figure 1.21 presents the complexity model spectrum with a corresponding simplified model example. The advantages related to increasing simplicity stability, computational efficiency, data dependency and application rates are illustrated in green and the disadvantages related to the same features are illustrated in red.

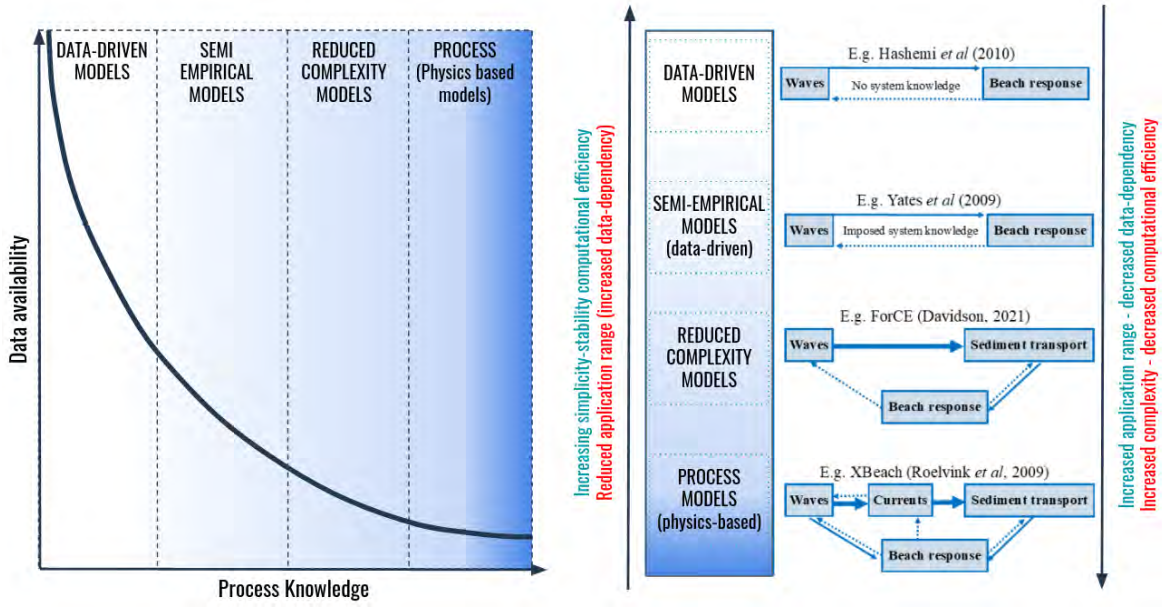

Figure 1.21: Coupling of small, intermediate and large scale coastal processes. Figure extracted from Thornton et al. (2000).

Inevitably, the future of daily-to-decadal coastal modelling will be dynamic within the complexity spectrum shown in Figure 1.21. As computational capabilities improve and process knowledge advances, progress towards the process-based end of the spectrum will continue. However, the rapidly increasing availability of coastal data and data assimilation techniques also promises opportunities to migrate towards the data-driven end of the spectrum. Reduced-complexity models, occupying the middle ground, are well-positioned to benefit from these advances and provide immediate practical, community-accessible capability to predict, for instance, shoreline change across various timescales. Therefore, it is important to continue improving simple physical-based approaches to study coastal systems, as all modeling categories can directly benefit.

1.2 Simplified approach of nearshore coastal systems

In this section, we propose a simpler way to study nearshore coastal systems, which will be the basis of the physical model used in this study. This is important for advancing our understanding of these complex hydro-morphological systems and developing practical solutions with broader applicability. As already mentioned, one of the key indicators of coastal changes is the coastlines evolution (Davidson and Turner, 2009), i.e the swash zone. Again, due to wide range of spatial and temporal scales this area presents significant challenges for research. To overcome these locks we suggest to focus on swash dynamics and its interactions with other nearshore regions by reducing the complexity of these coastal systems. To this end, we propose to focus on cross-shore sections, as they provide a clear hydrodynamic subdivision of the system based on the incoming wave transformation when approaching the coast, and modelling the shape of the beach. Instead of considering all hydro-morphological interactions, we will focus on key parameters that best characterize each sub-region and study their interactions between them.

While many models rely on empirical equations derived from field and experimental observations, these equations may not fully capture the underlying physics of the system, i.e the relationship between β and D_{50}. To address this issue, we conduct a dimensionless study using physical parameters that can describe the processes occurring in each sub-region. For example, we can use the Irribarren Number to characterize the wave breaker zone. Therefore by identifying the key parameters that best represent the coastal system, we can construct or use existing dimensionless parameters as control parameters to describe the hydro-morphological dynamics of the nearshore. Based on existing knowledge of coastal systems (as summarized in the previous sections) we propose to define each cross-shore sub-region using simplified physical models and associated relevant parameters, as sketched in Figure 1.22:

- Off-shore: This zone is characterized by the propagation of waves in deep water, where the interaction with the bottom is assumed negligible. A first attempt to provide the influence of individual gravity waves onto the shoreline is first to simplify the complex wave signal. In particular, we will focus here on monochromatic gravity waves and thus characterize the wave forcing by its offshore wave period and wave height (T_0 and H_0, respectively).
- Shoreface (shoaling and breaker zone): The hydrodynamics of this zone is mostly controlled by the interactions between the incoming waves and the bottom topography, resulting from the water depth decrease as waves approach the coast (see Section 1.1.3.3). Thus, the main parameters highlighted here are the wave characteristics at breaking and the value of the sloping bottom tomography (referred as α).
- Surf-zone: This zone is the region between the breaking and swash zones, which is highly complex due to the multitude of sub-systems that can arise (see Section 1.1.3.3). It is characterized by highly asymmetrical waves, such as bore action, that propagate shoreward and eventually dissipate along a surf length (l_s). The surf zone can be considered a transitional zone between breaking and swash zones, and can be identified

by a wave energy dissipation function based on shallow water theory. This function will depend on the surf dissipation length, water depth of the surf zone, and surf beach state $L(l_s, h_s, \Omega_0)$.

- Swash zone: the last zone of the beach under wave action is the swash zone. As discussed in Section 1.1.3.3, a key parameter for this zone is its slope (β), which is a dimensionless parameter associated with several coastal processes such as local sediment transport rates, wave excursion, dissipation and reflection, controlling directly the shoreline position ($s_l(x,t)$).

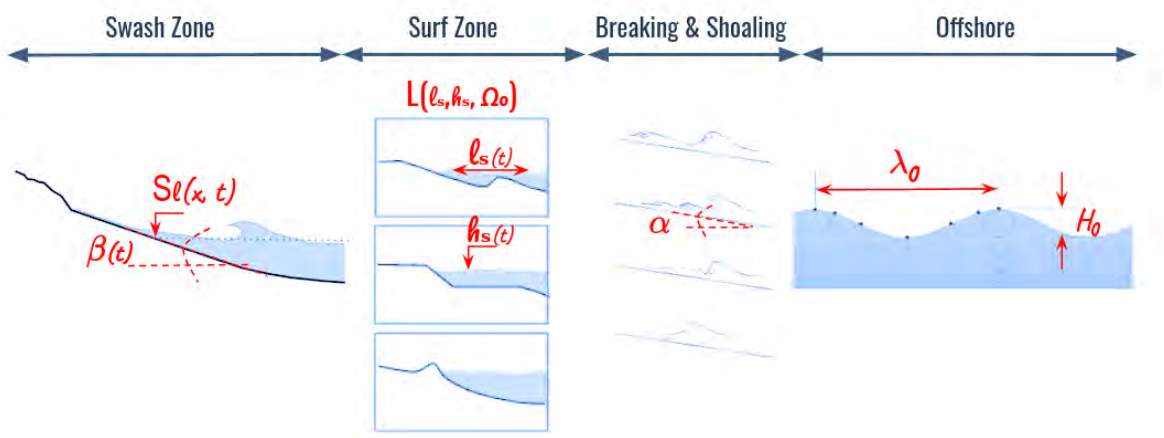

Figure 1.22: Main hydro-morphodynamic parameters that characterize each sub-section of a cross-shore profile. Where H_0 and λ_0 are the offshore wavelength and wave height, α is the slope value of the shoreface, $l_s(t)$ is the surf dissipation length, h_s is the surf water depth, $L(_0)$ is the wave energy dissipation function on the surf zone, β is the beachface slope and S_l is the shoreline position.

.

The simplified approach outlined is designed to analyse the cross-shore coastal region and identify its key parameters (illustrated in Figure 1.22). To fully simplify the system it is necessary first to determine the beach state of the surf zone resulting in an specific bottom topography. In this study we focus on low tide terrace (LTT) environment, which is a unique case within the intermediate beach state (Wright et al., 1984), characterized by a steep beachface slope (swash zone) followed by flat platform (surf zone). LTT environments are prevalent in both micro- and macro-tidal environments, including sandy beaches, coral and rocky reefs. Despite their prevalence, LTT environments are not well-documented, which makes them an important area for further research. Additionally, soft-engineering coastal protection methods, such as cobble berm revetments can change the dynamics of a dissipative erosive system into an artificial composite beach with a steep beachface and relatively flat dissipative surf zone, resembling to LTT environments. Given the promising results of such protection systems for shoreline stability in areas threatened by erosion (Bayle et al., 2020, 2021), further investigation of LTT dynamics could enhance also our understanding of these artificial coastal protection solutions.

Moreover, LTT environments are an ideal choice for this simplified approach due to their unique characteristics. These environments are characterized by a regular bottom topography and display a combination of dissipative and reflective beach states, as noted by Miles and Russell (2004). This makes them a suitable candidate for highlighting and studying the dynamics of both types of beaches. The resulting simplified model proposed to study nearshore hydro-moprhodynamics on LTT environments is schematized in Figure 1.23.

It has been shown that the beachface slope (β), a key parameter in this study, varies with at least three minimum parameters: mean sediment size (D_{50}), wave period (T_0), and wave steepness ($s = H_0/\lambda_0$) (King, 1972; Bascom, 1951; Rector, 1954). Therefore, a controlling hydro-morphological dimensionless number associated to these parameters could be the Dean Number ($\Omega_0 = \frac{H_0}{T_0 W_s(D_{50})}$, (Dean, 1977). As discussed in Section 1.1.2, this dimensionless number is used to classify equilibrium beach states (Wright et al., 1984) on seasonal or annual time scales. However for short times scales associate to instantaneous wave variations their is a poor correlation with the morphological response. This is observed spatially for storm-dominated environments characterized by intermittent and seasonal recovery periods (Morton et al., 1995; Anthony, 1998; Lee et al., 1998).

Nevertheless, recent research has shown that equilibrium beach response concepts associated with the Dean Number are useful for modeling short-term processes that focus on local morphological parameters, rather than on the global morphological equilibrium state, i.e cross-shore shoreline evolution Miller and Dean (2004); Yates et al. (2009); Davidson et al. (2013); Castelle et al. (2014b); Splinter et al. (2014). These models have proven good skills to predict the evolution of the shoreline in shorter times scales for different morphology states (dissipative, reflective and bared beaches). Another local morphological important parameter that has been observed to respond quickly to wave action over short time scales is the beachface slope (Hughes et al., 1997; Butt and Russell, 1999; Puleo et al., 2003; Masselink and Puleo, 2006). In line with these recent results, we only consider the beachface as an erodible material. The surf zone and breaking zone topography are assumed to be evolving on a slightly larger time scale, allowing to first focus on the only beachface response to waves. Then, this work aims at investigating the relation between the beachface slope and changes in wave conditions characterized by the offshore Dean Number, focusing on low tide terrace environments. We will apply the simplified approach in LTT conditions and use the Dean number as a control parameter. The resulting model is shown in Figure 1.23, and it will enable us to highlight the response of the beachface slope to changing waves conditions on short time-scales periods.

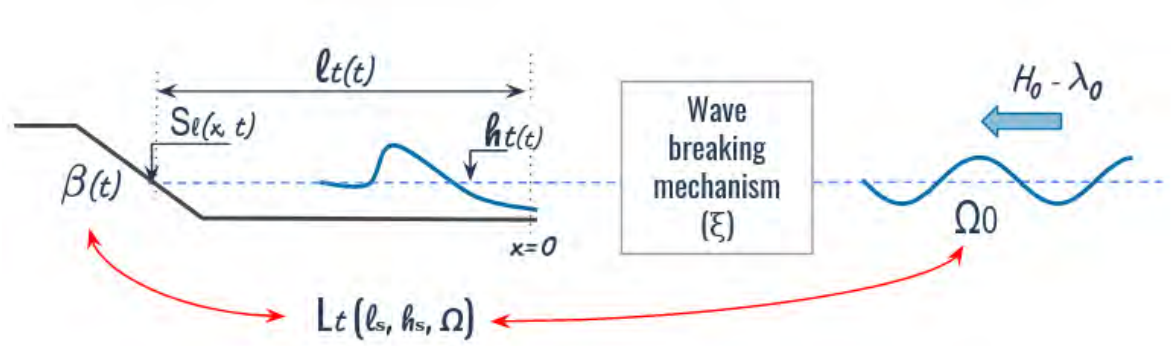

Figure 1.23: Simplified approach of coastal systems applied for LTT environments. Where H_0 and λ_0 are the offshore wavelength and wave height, α is the slope of the shoreface, $l_t(t)$ is the terrace dissipation length, h_t is the water depth on the terrace, $L_t(l_t, h_t, \Omega)$ is the wave energy dissipation function on the surf zone for LTT topography, β is the beachface slope and S_l is the shoreline position.

.

Chapter 2

Field study

Contents

2.1 Summary

This chapter presents the study of nearshore dynamics on LTT environments based on a robust data set that was collected during several field experiments at two different field site, one at Nha Trang beach on the East coast of Vietnam and the other at Grand Popo, Benin (located in the Gulf of Guinea, West Africa). The data collection spanned from 2013 and 2016.

It is important to have a correct understanding of the local environments as it can influence many of the coastal processes taking place at the beach. Therefore the first section of this chapter is dedicated to detail the data sets and the previous work that resulted from the analysis of these field experiments. This will involve a description of local wave climate, beach morphology, methods used for field measurements and the previous results published.

The main section of this chapter is dedicated to introduce the new results reached on dynamics of sandy beaches with a low tide terrace, based on the simplified concept of coastal systems on LTT environments explained in Section 1.2. These results where published in MDPI open access journal in 2021 titled "Surf and Swash dynamics on Low Tide Terrace Beaches" Mingo et al. (2021). The interesting correlation found between local parameters of the nearshore LTT beaches with off-shore wave forcing encouraged this work to continue the research in the laboratory. The main insights of the article and the remaining open questions are presented in the last section of this chapter.

2.2 Data and methods

Several intensive field experiments were conducted at two sandy beaches between 2013 and 2016, with two main objectives: (i) to investigate short and long term inner-shore interactions under variable wave conditions (Almeida et al., 2020; Almar et al., 2014, 2016) and (ii)to validate extraction methods obtained from video camera estimates, in particular asses error on beach profiles obtained from a combination of depth inversion from wave kinematics and intertidal beach mapping using the shoreline (Almar et al., 2016; Thuan et al., 2019; Ondoa et al., 2016).

These field experiments were conducted by LEGOS/IRD in France with local collaborations, Thuy Loi University at Nha Trang, Vietnam and ICMPA-UNESCO Chair University of Abomey-Calavi at Benin. They have collected over 3 years time series of daily measurements of beach morphology and wave conditions based on bathymetry inversion methods.

Both beaches, Nha Trang and Grand Popo have a very different wave climate but the common point is that both have a uniform low tide terrace and a similar sediment mean size. For this reason these data set is perfectly adequate to study surf and swash dynamics on LTT environments focusing on the morphological response of the beach to the variation of wave regimes. From now, in this manuscript Nha Trang is referred as NT and Grand Popo as GP.

2.2.1 Nha Trang LTT environment

Nha Trang is a sandy beach located in a semi-closed bay in the Southeast of Vietnam. The bay has an NE-SW coastal orientation and approximately 6km long extension, its location is represented in figure 2.1. This bay is partially protected from waves by a groupe of island located close to NT. The full description of NT beach is detailed in the following papers: Almeida et al. (2016, 2020); Thuan et al. (2019); Almar et al. (2017b).

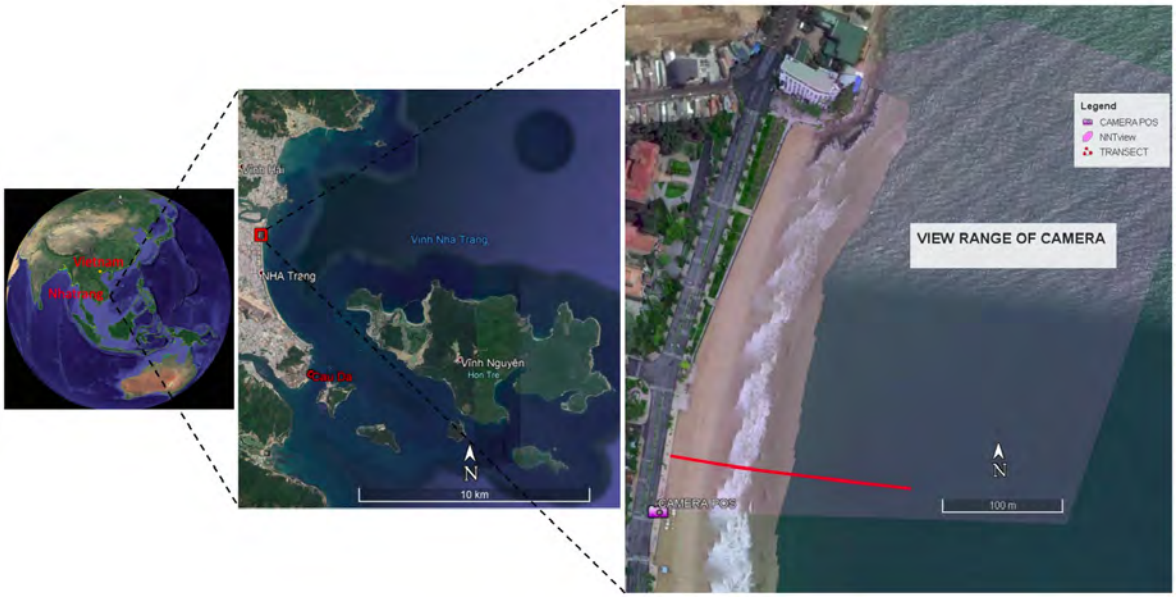

Figure 2.1: Left figure shows the location of Vietnam and Nha Trang. The middle Figure illustrates the location of the study area at the central part of the bay and some important local features such as the groupe of islands that protect the bay. The right figure presents the camera range view represented by transparent pink color and the red line presents the location where the cross-shore time stack images are generated for depth inversion. This Figure is extracted from Thuan et al. (2019).

The wave climate in the area is subdivided into two seasons: spring-summer and fall-winter monsoon. The spring and summer monsoon (May to September) is characterized by weak wind waves with short periods. The fall and winter monsoon (October to April) generates more energetic waves that can reach values up to 4m. During winter NT can be exposed to extreme events such as typhoons (typically from North directions). Nevertheless NT is most of the time under local generated wind waves, that hit the bay-beach with near shore-normal incidence (Almar et al., 2017b; Thuan et al., 2019). Nha Trang bay has a diurnal and semi-diurnal tides with a micro-tidal range from 0.4m to 1.7m.

The field data extracted at Nha Trang and used in this work to study surf and swash dynamics on LTT environments is detailed in Figure 2.2. These figure shows the off-shore wave forcing and beach response over 3.5 years observations. The field data acquisition methods is based on bathymetry inversion (explained in the following paper Thuan et al. (2019)) from

a shore-based camera system . The location where the cross-shore time stack images are generated is presented in Figure 2.1. The offshore wave characteristics where extracted from ERA-Interim global atmospheric reanalysis produced by the European Center for Medium-Range Weather Forecasts (Dee et al., 2011). These offshore wave data was validated over a two month field local experiment using wave gauge (Almar et al., 2017b).

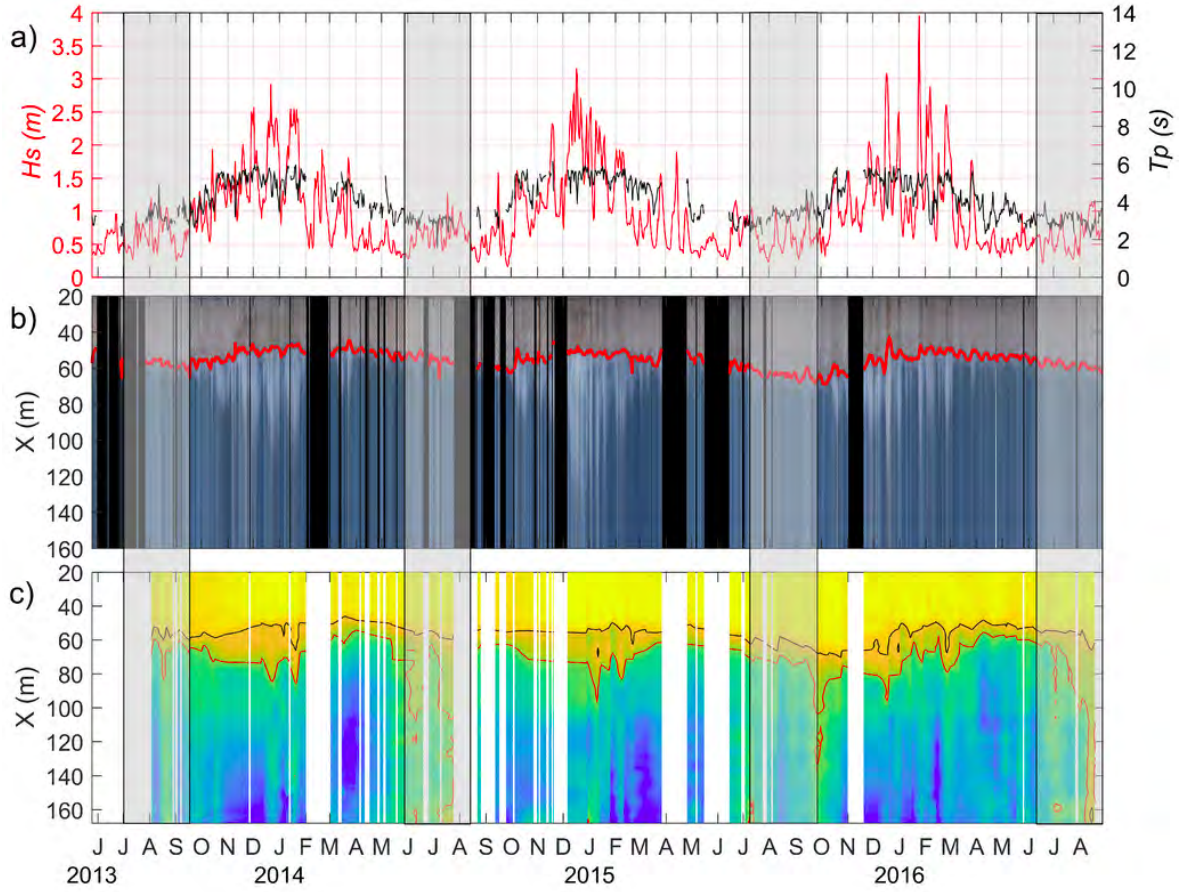

Figure 2.2: Long-term evolution of wave forcing and beach morphological response for 3.5 years observation. a) Off-shore wave forcing, where the black solid line represents the wave period (T_p) and the red solid line the significant wave height (H_s). b) Shoreline long-term evolution marked by the red line over daily mean cross-shore time stack video images in RGB band color. c) Daily bathymetry long-term evolution extracted from video inversion methods (in colors), the low tide terrace area is indicated between the black and red contours at an elevation -0.5m and -1.3m respectively. Note that the shaded bands in the summer season corresponds to wind waves period less than 3-4 seconds and cannot be used for depth inversion methods. This Figure is extracted from Thuan et al. (2019).

It can be appreciated from Figure 2.2 a correlation at the seasonal scale between the evolution of off-shore wave forcing and beach inner-shore response. Two main information can be extracted from this Figure 2.2 to characterize the beach dynamic of Nha Trang:

- Nha Trang shows a strong seasonal forcing from weak wind waves during summer with minimum values of $H_s = 0.5m$ and $T_p = 2s$ and moderate energetic waves during winter with maximum values of $H_s = 4m$ and $T_p = 6s$.

- The shoreline presents a correlation with the seasonal wave forcing: when the wave energy increases an erosive phase is produced from summer to winter, the LTT is created and expands leading to a LTT beach profile during winter. Then there is a recovery or accretion phase taking place during winter to summer when the wave energy decreases, the terrace width decreases and the terraces merges with the beach-face resulting in a reflective profile during summer. The shoreline doesn't appear to have absolute shifts from year to year during this 3.5 years field observations.

The mean summer and winter beach profile is represented in Figure 2.3. This Figure shows two different years of winter and summer mean profiles to illustrate the erosion and accretion phases observed during seasonal transitions. It can be appreciated in this Figure how there is an accretion phase when going from Winter to Summer and an erosion phase from Summer to Winter, this is also observed in the shoreline evolution in Figure 2.2b.

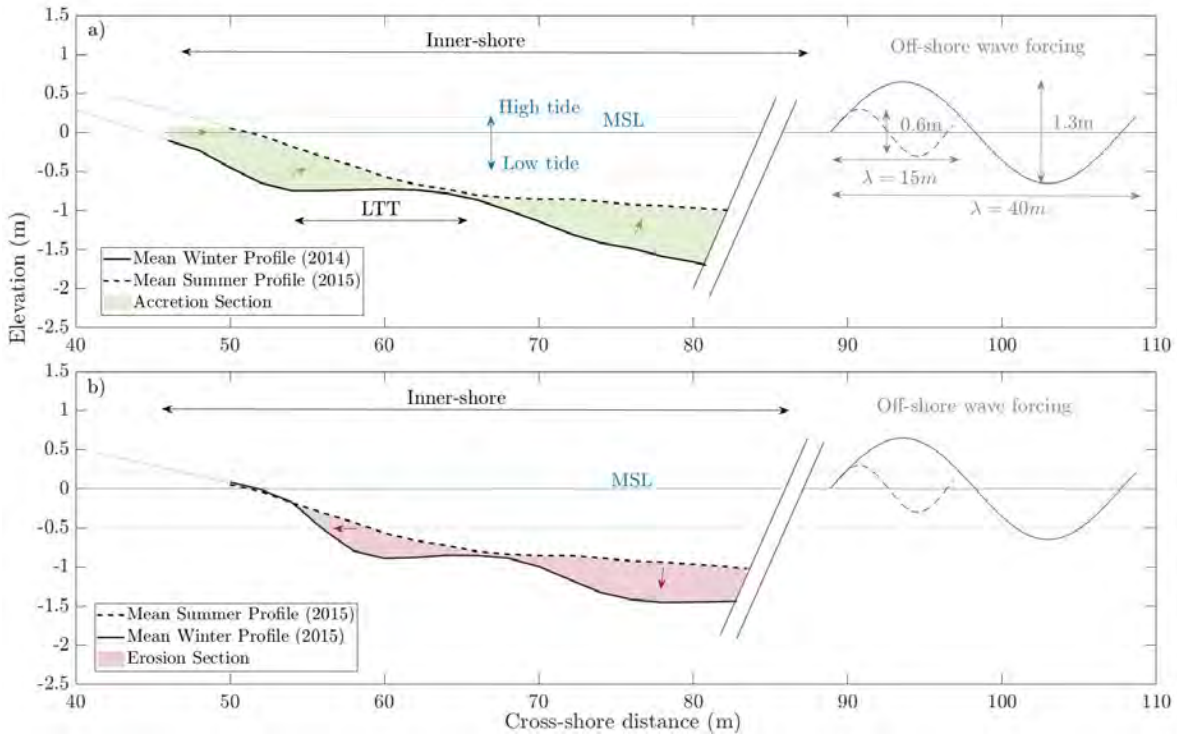

Figure 2.3: Winter and summer mean beach profile for 2014 (Figure a) and 2015 (Figure b). During the transition from winter to summer there is an accretion of the mean beach profile (green shadow in Figure a) and an erosion from summer to winter (red shadow Figure b). Both figures (a and b) have represented in their right side the winter and summer off-shore wave forcing, solid blue line and dashed blue line respectively. The wave vertical scale is respected 1:1 and the horizontal scale is 1:2.

The mean sediment size (D_{50}) can vary within the bay from $D_{50} = 0.9mm$ in the north of the bay to $D_{50} = 0.4mm$ in the south. Following the classic Wentworth grain size classification (Wentworth, 1922), this sand is classified as medium to coarse. The mean LTT winter beach profile associated to energetic wave conditions is characterized by a steep upper beachface where its slope is approximately 1:10 followed by a uniform and flat terrace, approximately 20m wide. The mean summer beach profile associated with low energetic waves conditions has a uniform foreshore, where the slope is approximately 1:10. The mean summer profile is characterised by reflective upper beach-face shape. These summer and winter mean beach profiles are shown in Figure 2.3.

The long term field experiments conducted at Nha Trang (Thuan et al., 2019)) show the overall stability of the shoreline and classified the beach into an intermediate to reflective states with a seasonal fluctuation. The short term field experiments (Thuan et al., 2019; Almeida et al., 2020)) proved as well a high resiliency of the LTT beach. During typhoon, monsoon events or seasonal cycles, it was observed rapid exchanges of sediment between the upper beach-face (swash zone) and the flat platform (surf zone). The upper beach recovery to these events where observed to be within a few days.

During the experiments launched for nine days (Almeida et al., 2020) at Nha Trang it was concluded that the inner-beach was continuously and rapidly adjusting to different tidal and wave conditions, distinguishing two clear phases of evolution: erosion and accretion. These morphological adjustments were associated to changes in water levels and off-shore wave height. It was evidenced that during low tide conditions, the LTT acts as a low-pas-filter dissipating a large part of wave energy in the short wave band (frequency between 0.05 and 0.3Hz) and potentially enhances energy transfer to the infragravity band (Almeida et al., 2020). This suggests a control off swash processes by infragravity waves (frequency<0.05Hz) that do not fully dissipate in the surf zone. On the contrary during high tide, due to the increases of water level on the terrace, the terrace becomes less effective at dissipating incident waves and the swash control parameters become less clear. Nevertheless, It has been demonstrated that the significant wave height, measured just seawards of the swash zone with the foreshore active slope improves predictions on the vertical run-up. The improvements of the vertical run-up was due mainly to the introduction of the beach-face slope information. Therefore predicting the beach-face slope dynamics is crucial for understanding swash dynamics.

2.2.2 Grand Popo LTT environment

Grand Popo is an open microtidal coast forming a 500km long mild embayment located at the Bight of Benin coast in the Gulf of Guinea. The location of this beach is shown in Figure 2.4. Short and long terms field experiments have been conducted in this beach, where the main results are presented in the following papers: Almar et al. (2014); Castelle et al. (2014a); Ondoa et al. (2016); Almar et al. (2016, 2019a)

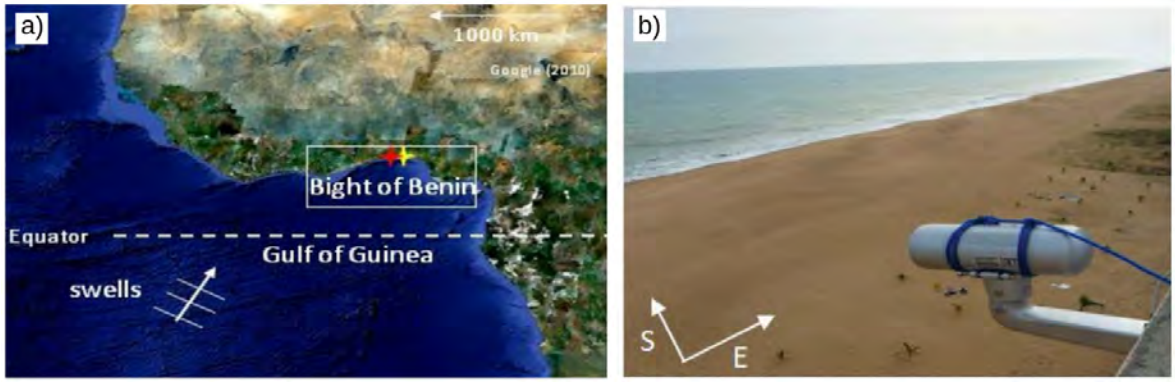

Figure 2.4: a)The Bight of Benin coast represented in a regional map, where the red and yellow crosses represent respectively the study site at Grand Popo and the city of Cotonou (local feature).b) Grand Popo beach in Benin, showing the video camera system for field experiments. Image extracted and modified from Almar et al. (2014)

Grand Popo is a representative of Bight beaches at Benin. This coast is an open wave-dominated environment exposed to a constant, moderate to high energy wave for the year. This open environment is exposed to long swell waves generated in the South Atlantic that travel from mid-latitude (45 – 60°) with a S-SW incidence (Almar et al., 2014, 2015). Grand Popo has a neap and spring tides with a microtidal range from 0.3 to 1.8 respectively. Note that this beach is not affected by human interventions and presence.

This work uses the morphological data extracted at Grand Popo during long and short term field experiment undertaken from March 2013 to June 2016. The long term field experiment consisted on deploying a video system at 80 m approximately from the shore that collected data continuously at 2Hz frequency creating a time stake images across-shore direction (Ondoa et al., 2016; Almar et al., 2014). The data extracted from the video system was validated by short terms field experiments that included both sea and beach morphological surveys with differential GPS and bathymetric sonar (Almar et al., 2016)). The off-shore wave forcing, waves and tides, were obtained by ERAInterim re-analyse (Dee et al., 2011) and validated by using a Acoustic Doppler Current Profiler (ADCP) moored at 10 m depth (Ondoa et al., 2016). These field data is summarised in Figure 2.5. From this Figure it can be observed that Grand Popo is exposed to a rather constant wave forcing during the year, where the wave annual averages are $H_s = 1.36m$ and $T_p = 9.4s$.

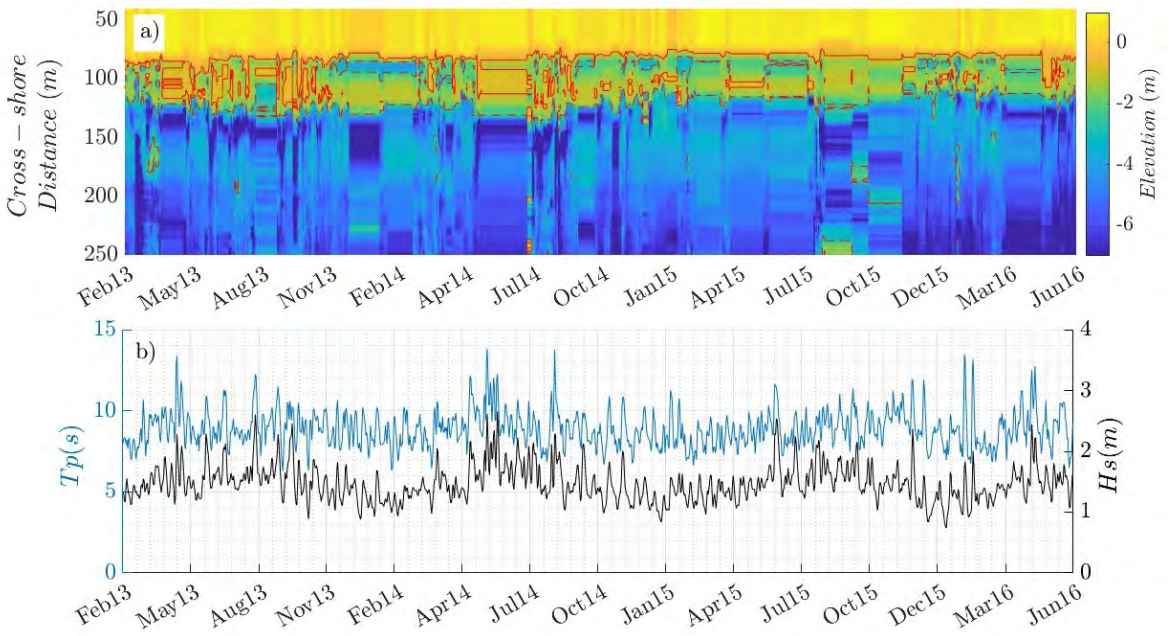

Figure 2.5: (a) Daily bathymetry long-term evolution obtained by video inversion methods (in colors), the low tide terrace are is indicated between the red lines at an elevation of -0.85 and -2.5 respectively. (b) Off-shore wave forcing long-term evolution, where wave period is represented by the cyan line and significant wave height by the black line.

An alongshore stable low tide terrace is observed during the whole time period. At Grand Popo the wave climate seasonal fluctuations are rather weak and an annual cross-shore mean profile can be extracted (see Figure 2.6).

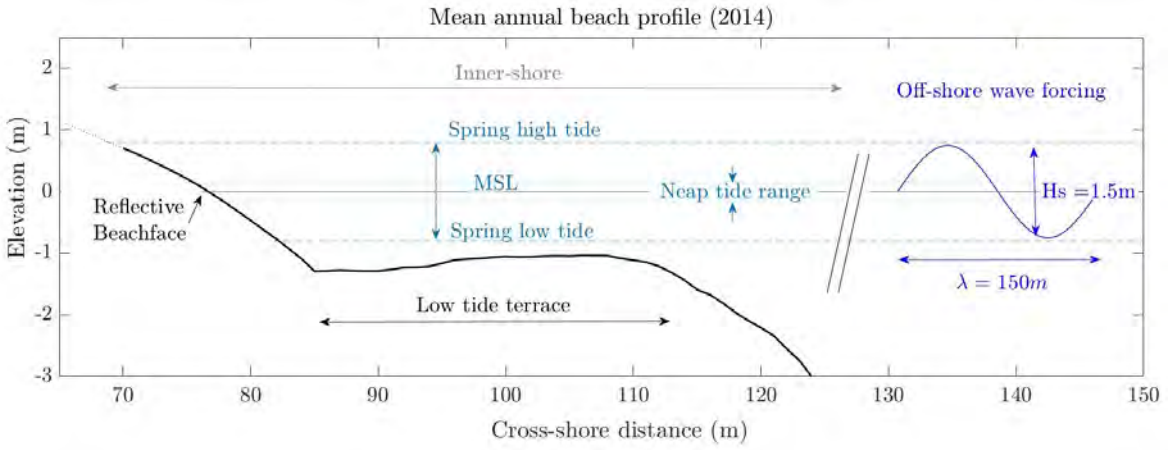

Figure 2.6: The black line represents the annual mean profile for 2014. The solid light blue line represents the mean sea level (MSL), the dashed light blue line represents the spring tide range and the doted light blue line the neap tide range. Off-shore wave forcing is represented in dark blue, where the vertical scale of the wave is 1:1 and the horizontal scale 1:7.5.

The bight of Benin coast is know to have a strong wave-induce long-shore sediment transport, which has been reported to be one of the largest in the world (Almar et al., 2015). These long-shore transport rates are dominantly due to both incident and swell waves from S-SW directions, resulting in an oblique wave forcing impacting the coastlines. Therefore any human interventions that could interrupt the input or output of sediment, e.g harbours constructions can affect this sediment exchange dynamics. Grand Popo is a coast far from any harbour, and as mentioned above it does not have much human interventions. It can be seen from Figure 2.5 that the coastline and the inner-shore shape remains more or less invariant and unperturbed on an annual time scale observation. Grand Popo annual beach profile presents an alongshore uniform low tide terrace with a rather steep beachface, where its mean slope is approximately 1:5. The beach average sediment size is medium to coarse with $D_{50} = 0.6mm$.

An interesting study has been carried at GPP by Almar et al. (2016) in which they analysed surf and swash interaction at GP low tide terrace site. The results of this study are based on an intensive field short time scale experiment conducted in March 2014. During this field experiment they capture the evolution of incoming and reflected waves and tides in 10m depth, characterising off-shore wave forcing. The surf zone was instrumented with Acoustic Doppler Velocimeters for measuring frequency wave transformation across the terrace all the way to the swash zone (see Figure 1 in Almar et al. (2016)). Time-series of wave run-up was extracted and spatio-temporal images were collected during daylight and treated in order to obtain instant wave run-up motion. Using this field data the relative contribution of surf and swash zone in dissipating wave energy was calculated using an approximated formulation proposed by Guedes et al. (2013). This energy formulation has been compared with a Boussinesq model SERR1D (Cienfuegos et al., 2010). This numerical model allows to calculate wave-breaking energy dissipation and energy transfer from short waves bands to IG bands (Rocha et al., 2017). The Boussinesq model was validated with the field data and allowed to study the influence of inner-shore parameters such as: terrace width, upper slope, and tide on the reflected wave and its interaction with the incoming wave. The most important parameter influencing surf dynamics is highlighted to be the beachface slope by controlling outgoing waves and also incoming waves through feedback mechanisms.

It can thus be concluded at GP that the beachface slope has an important role in controlling surf hydrodynamics, meaning that the beachface is adjusting to offshore wave forcing quicker than the surf zone. What would now be worth studying is how the beachface slope is responding to directly to changes in offshore wave forcing, disregarding surf zone processes.

2.2.3 Surf and Swash Dynamics on Low Tide Terrace Beaches

These two field data sets NT and GPP are particularly suitable for studying low tide terrace dynamics. As both beaches are classified as LTT sites that have similar sediment size and tidal range but very different wave climates and annual beach morphology dynamics. These differences and similarities provides then a fairly complete data set on LTT beaches.

Despite recent advances in inner-shore modelling, inner-shore morphological changes from simple formulation remains a current challenge to coastal researchers (Chardón-Maldonado et al., 2016)). The objective of this section is to study LTT dynamics by using the simplified analysis, explained on Section 1.2, of LTT environments. In particular, the present study of LTT beaches is limited to the nearshore morphological response to off-shore wave forcing. The wave breaking process which has already been deeply investigated in literature is thus disregarded in this study. This approach allows to simplify the very complex hydro-sedimentary system to a few key parameters that could describe the dynamics of LTT beaches. This is therefore a first step for validating the proposed physical model along the present study. The simplified approach of LTT environments is represented on Figure 2.7, where the main parameters are the off-shore wave characteristics (period and wave height), the terrace length and water level on the terrace representing the surf zone, and the beach-face slope to characterize the swash zone.

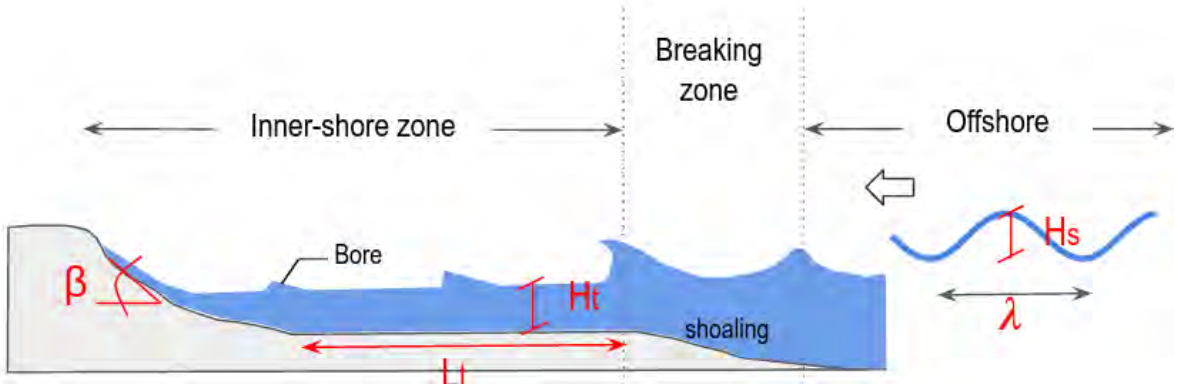

Figure 2.7: LTT simplified system. The beach-face slope is represented by β, Lt and Ht represents the terrace length and water level on the terrace and Hs and λ the off-shore wave length.

The results of this study are summarised in the following published paper in MDPI open acces journal in 2021 titled "Surf and Swash Dynamics on Low Tide Terrace Beaches" (Mingo et al., 2021).

2.2.4 abstract

Low tide terrace (LTT) beaches are characterised by a moderately steep beach face and a flat shallow terrace influencing the local hydro-morphodynamics during low tide. The upper beachface slope (β) and the terrace width (L_t) are the main morphological parameters that define the shape of LTT cross-shore beach profiles. This work aims at better understanding the behaviour of β and L_t and their link with the incoming wave forcing. For this purpose, our results are based on 3.5 years times series of daily beach profiles and wave conditions surveys at two different microtidal LTT beaches with similar sediments size but different wave climate, one at Nha Trang (Vietnam) and the other one at Grand Popo (Benin). While they look similar, two contrasting behaviour were linked to two sub-types of LTT regimes: the first one is surf regulated beaches (SRB) where the swash zone is highly regulated by the surf zone wave energy dissipation on the terrace, and the second is swash regulated beaches (SwRB) acting in more reflective regime where the terrace is not active and the energy dissipation is mainly produced in the swash zone, the terrace becomes a consequences of the high dynamics in the swash zone. Finally, extending the common view of an equilibrium beach profile as a power law of the cross-shore distance, the ability of a simple parameterised cubic function model with the Dean number as unique control parameters is proposed and discussed. This simple model can be used for the understanding of LTT environments but it can not be extended to the whole beach spectrum.

keyword: low tide terrace (LTT); surf zone; swash zone; hydro-mophodynamics systems; cross-shore beach profiles; Dean number; terrace width; upper swash slope.

2.2.5 Introduction

Sandy beaches are loose deposits of sand accumulated at the shoreline that have been carried alongshore and cross-shore by currents and waves. The location of theses beaches is a function of sand sources, coastal processes and geology Gallop et al. (2020). The modal beach morphology of sandy beaches changes in response to environmental conditions (waves and tide forcing, sediments, geology, etc.). This has been studied for a long time and has led to the development of several beach classification models. All of them include the occurrence of distinct beach morphologies linked to the key environmental conditions like wave climate, tidal regime and beach sediment characteristic Wright et al. (1984); Power et al. (2013); Masselink and Short (1993). Wright et al. (1984) formulated one of the first of such beach classification model based on the dimensionless fall velocity also know by the Dean number (Ω). The dimensionless fall velocity is an important parameter influencing both surf zone hydraulics and the form of the resulting equilibrium profile, this was first proven by Gourlay (1981).

The Dean number ($\Omega = H_s/W_sT_p$) is a dimensionless parameter that relates breaker wave height (H_s), wave period (T_p) and sediment fall velocity (W_s), in other terms it refers to the ratio of a particle settling time (H_s/W_s) to the wave period. On microtidal beaches, where the environment is wave-dominated, beach systems can be classified in three distinctive

beach types: dissipative ($\Omega > 5$) and reflective ($\Omega < 1$) states linked by an intermediate state ($1 < \Omega < 5$). Dissipative beaches are normally characterized by a smooth slope and spilling breakers while reflective beaches are the opposite having a steep slope and surging breakers Wright et al. (1984); Short (1996).

This research work is focused on Low tide terrace (LTT) environments. LTT beaches are a specific but common type of sandy beaches widely studied in the coastal community (Wright et al., 1984; Short, 1996; Miles and Russell, 2004; Stringari and Power, 2019; Lemos et al., 2018; Anfuso and Ruiz, 2004; Power et al., 2013)). Nevertheless our understanding on LTT beach dynamics is still not sufficient and needs to be improved.

Following Wright and Short classification model at microtidal beaches, the LTT state is a particular case inside the intermediate state. Theoretically, as the rip channels of transverse bar and rip state (TBR) are infilled the LTT state is reached. The terrace formation is due to a coupling between the effects of tides and waves and are commonly formed out of coarse sand. A terrace beach can be seen also at macro- and meso tidal regimes Short (1996); Short and Jackson (2013).

LTT beaches have been observed to exhibits characteristics of both dissipative and reflective sites Miles and Russell (2004). During low tide, lower levels favour wave breaking on the gently sloping LTT, creating a very dissipative conditions of the surf zone but at high tide, they may pass across the terrace unbroken to surge up the steep beach face producing reflection. Recent work suggests that the terrace acts as a low-pass filter to the swash-zone dissipating a large part of the wave energy in the short wave band (frequency between 0.05 and 0.3 Hz) resulting in a dominance of infra-gravity waves (f < 0.05 Hz) that do not fully dissipate in the surf-zone Almeida et al. (2020). The morphological response of the swash zone to varying offshore waves is highly modulated by the surf zone conditions, being the terrace width a key parameter of the wave energy dissipation rate. Continuing these resents results Miles and Russell (2004); Almeida et al. (2020); Almar et al. (2014, 2016); Almeida et al. (2016), the present work intends to describe the swash and surf dynamics of LTT beaches by doing a simple characterisation of these zones using two main morphological parameters of LTT cross-shore beach profiles: the upper swash slope (β) and the terrace width (L_t) of the surf zone. These are key parameters that defines the shape of cross-shore LTT profiles and their relationship with the hydrodynamics wave forcing will provide information of their behaviour. In the following sections we aim to explain how these parameters work, search their relationship between them and their interactions with the offshore wave forcing. This paper aims at improving our knowledge on LTT beach morphodynamics by analysing two field data set at LTT environments with two different wave climate. Understating the morphodynamic response of LTT beaches to different wave climates is an important issue for coastal erosion, especially as rising sea levels can invade upon coastal infrastructure and climate change may modify the variation of extreme events frequency and intensity (IPCC Working Group 1 et al., 2013).

2.2.6 Methodology

Field Data

Several field experiments were conducted at two sandy beaches between 2013 and 2016, one at Nha Trang, Vietnam and the other at Grand Popo, Benin. The objective of these field campaigns were to investigate short-term swash-zone hydrodynamics, and morphodynamics under variable wave conditions based on bathymetry inversion methods. These datasets revealed the characteristics of Nha Trang and Grand Popo beaches as low tide terrace beaches Almeida et al. (2020); Almar et al. (2016); Ondoa et al. (2016). A secondary objective of these experiments was to validate video camera estimates, and in particular asses error on beach profiles Thuan et al. (2019); Ondoa et al. (2016) obtained from a combination of depth inversion from wave kinematics Almar et al. (2016); Bergsma and Almar (2018) and intertidal beach mapping using the shoreline Almar et al. (2012).

Figure 2.8 presents the beach profiling location (cross-shore transect) of Nha Trang and Grand Popo where cross-shore time-stack images are created for depth inversion. Inversion method relies on the linear wave theory that provides a dispersion relation between wave propagation and bathymetry for shallow and intermediate depths.

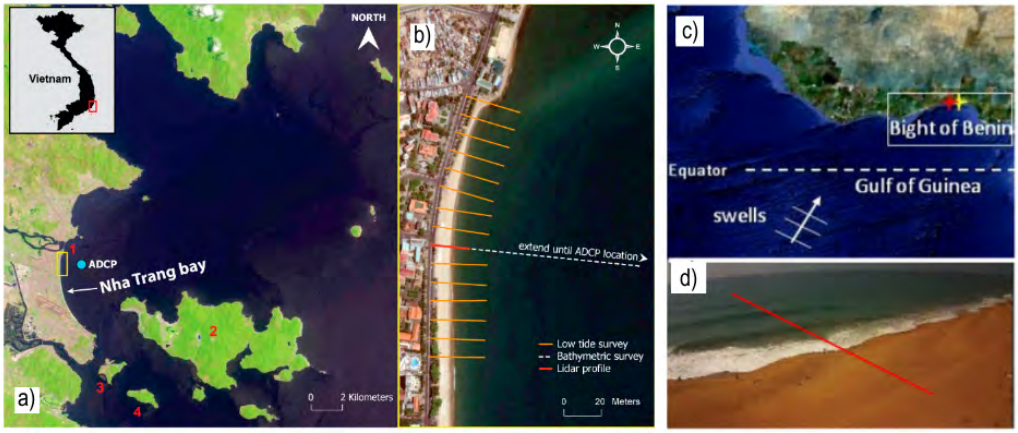

Figure 2.8: (**a**) Location of Nha Trang bay and some important local features including:1—Cai estuary; 2—Hon Tre island; 3—Hon Mieu island; 4—Hon Tam island. The yellow box indicates the section of the beach studied (zoomed in figure **b**). (**b**) Aerial photograph of the study site where the red solid line presents the profiling location where cross-shore time stack images are created for depth inversion. (**c**) Focus in the Bight of Benin where Grand Popo beach is located. (**d**) Grand Popo beach. The red solid line presents the profiling location where the cross-shore time stack images are created for depth inversion.

For Nha Trang a shore-based video system Lippmann and Holman (1989); Holman et al. (1993) was installed in May 2013 in the central part of Nha Trang bay by researchers of Thuy Loi University in collaboration with LEGOS/IRD-France. The video station contains two color cameras (VIVOTEK IP7361, max-resolution 1600 × 1200 pixels) fixed on an existing light pole nearby, located 70 m from shore and at 14.3 m above mean sea level (MSL). Time-

stack images are interpolated on a regular grid using MSL reference and parameters obtained in the rectification step, with the native time resolution (2 Hz) and a regular space resolution of 0.5 m Thuan et al. (2019).

For Grand Popo a low-cost video system was installed on the top of a tower of the Navy forces of Benin, about 70 m from the shoreline. As detailed in Ondoa et al. (2017), the system was composed of a VIVOTEK IP 7361 camera (1600 × 728 pixels), which collected data continuously at 2 Hz.

Video-based bathymetry inversion has been developed for more than 20 years Bergsma and Almar (2018); Thuan et al. (2019) with a range of errors between 0.1–2.0 m (RMSE). At Nha Trang it was proved that the error obtained on the bathymetry data increased with the distance to shore but the main aspect of the beach profile, i.e., the terrace, was well captured by the inversion method Thuan et al. (2019); Ondoa et al. (2016). The Root Mean Square Errors (RMSE) on the elevation for Nha Trang and Grand Popo is 0.26 m and 0.14 m respectively. these values were obtained from comparison between observed beach profiles during field surveys and those calculated with inversionmethods (Ondoa et al., 2017; Thuan et al., 2019). Note that wind waves period less than 3–4 s cannot be used for depth inversion as it produces significant errors on the extraction of the bathymetry (shaded bands converging the summer season at Nha Trang, Figure 2.9).

Figure 2.9 illustrates the data sets from these fields experiments where it is possible to appreciate 3.5 years bathymetry evolution, offshore wave forcing parameters such as wave period (T_p) and height (H_s) and the Dean number evolution (Ω) defined in the previous section. For both cases (Nha Trang and Grand Popo), wave height and period (zero-crossing) are derived from the video images and thus better accounts for local waves than model hindcasts. These estimations were already calibrated/validated using insitu measurements during field experiments (see more details in Thuan et al. (2019); Ondoa et al. (2016)).

Figure 2.9a,d show the daily cross-shore video-derived beach profile, where the low tide terrace area is indicated. For the location of the terrace zone, the elevation values were fixed at −0.4 m to 1 m for Nha Trang and −0.85 m to −2.5 m for Grand Popo as those values have proven to best capture the terrace evolution on the daily bathymetry figure obtained from video inversion.

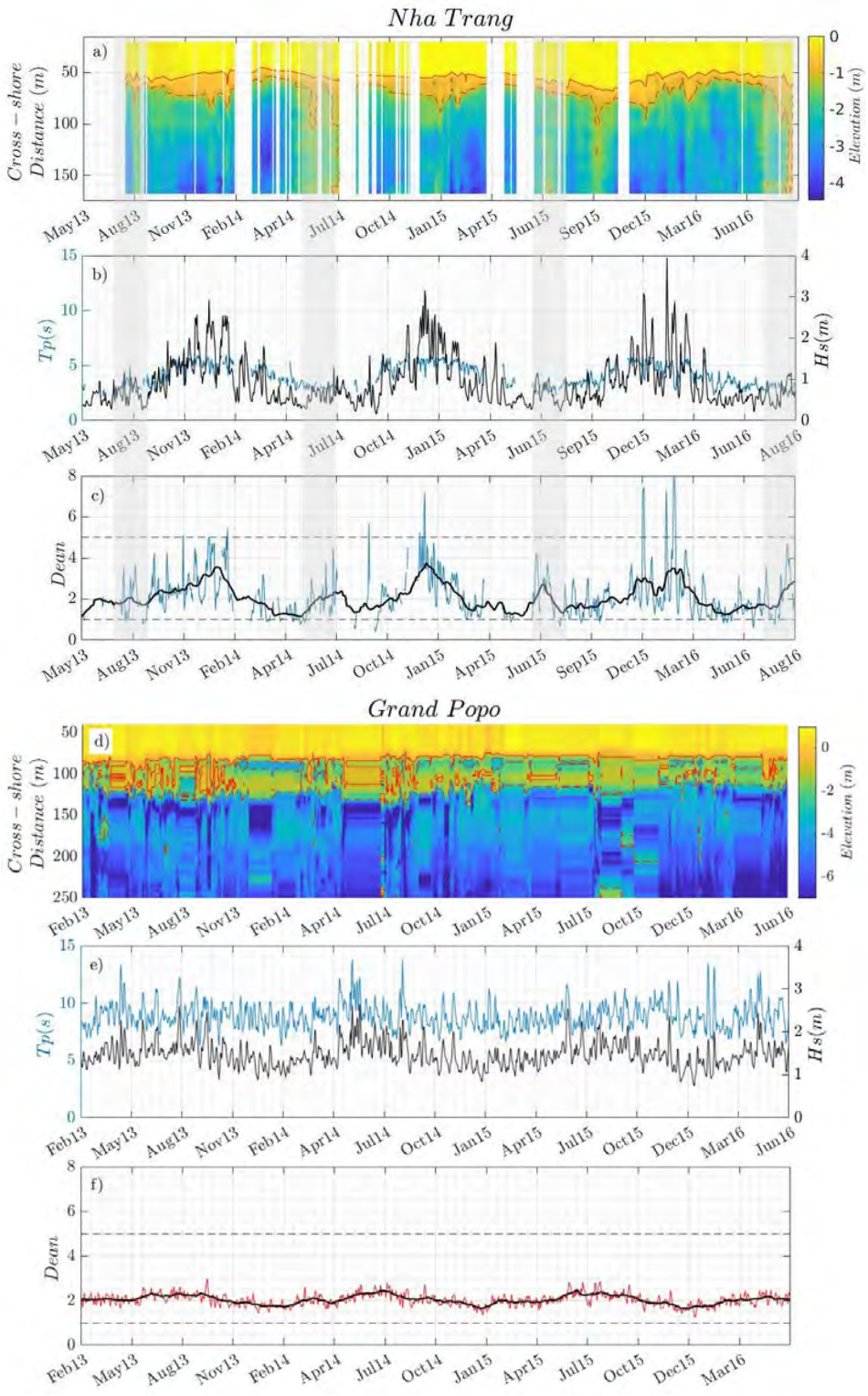

Figure 2.9: (**a**,**d**) show the long−term evolution of the daily bathymetry at Nha Trang and Grand Popo. The LTT is indicated between a red contour between −0.4 m and −1 m for Nha Trang and −0.85 m and −2.5 m for Grand Popo. Note the shaded bands covering the summer season. They roughly indicate that wind waves with period less than 3–4 s cannot be used for depth inversion (more on error estimation in Thuan et al. (2019)). (**b**,**e**) illustrates the offshore wave forcing evolution at Nha Trang and Grand Popo, wave period in cyan and wave height in black. Figure (**c**,**f**) show the Dean number evolution calculated for Nha Trang and Grand Popo, daily evolution in cyan and monthly moving average evolution in black.

The tidal level at Nha Trang and Grand Popo were extracted from previous work Thuan et al. (2019); Almar et al. (2014) for a first location of the swash zone. To define the upper swash slope (β) the berm crest point and the upper limit of the terrace was used as reference for each beach profile, then β is defined as the linear part of this zone representing the beachface slope (Figure 2.10). Thus to extract the upper swash slope (β), the linear limits were not fixed and were calculated for each profile from its berm crest.

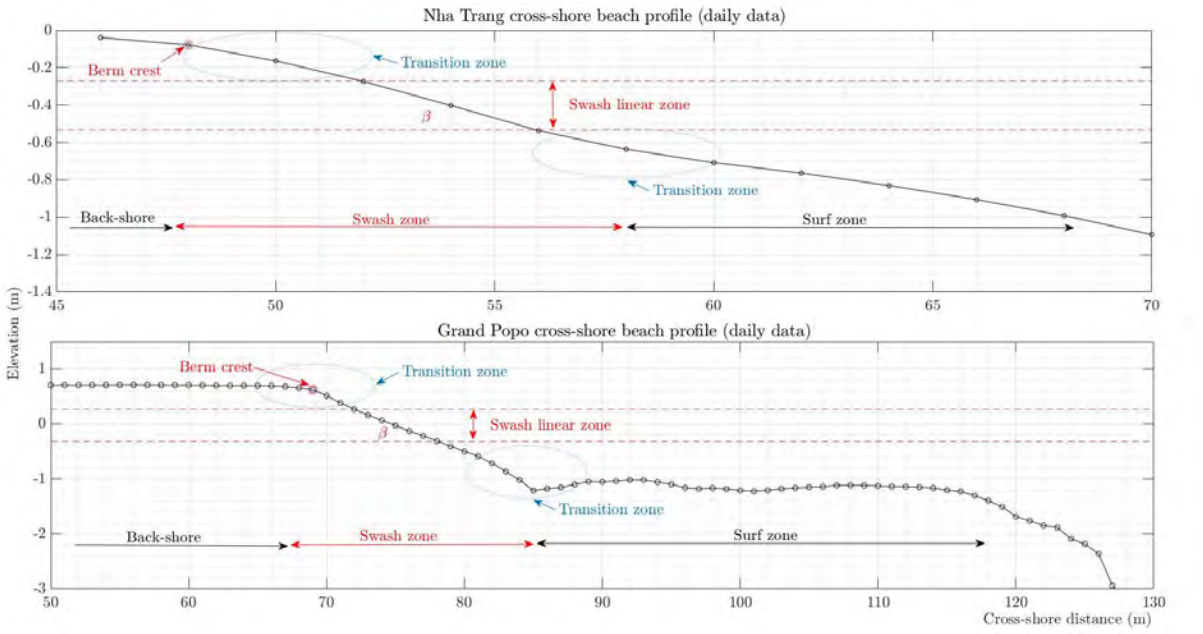

Figure 2.10: Typical WNT and GP cross-shore profiles. Definition of the swash zone and upper swash slope (β) for Nha Trang (top Figure) and Grand Popo (bottom Figure).

To summarise, Nha Trang is a along−shore uniform LTT beach located on a semi-closed bay with a microtidal range from 0.4 m to a maximum of 1.7 m and a low to moderate energy wave climate where waves show seasonal variability. The annual mean significant wave height ($\widehat{H_s}$) is 0.95 m, with an associated averaged peak period ($\widehat{T_p}$) of 6.2 s. On the other hand Grand Popo is an open microtidal coast forming a 500 km long mild embayment in the Gulf of Guinea. This coast is exposed through the year to constants, moderate to high energy waves (mean significant wave height $\widehat{H_s}$ = 1.36 m; mean peak period $\widehat{T_p}$ = 9.4 s). Grand Popo coastal area is a swell-dominated environment where oblique waves (South/Southwest) and tides are the main drivers of nearshore dynamics. The sediment size is medium−to−coarse with a mean grain size of D_{50} = 0.6 mm for both, Nha Trang and Grand Popo. Therefore this are two LTT microtidal beaches with similar sediment size but different wave climate and coastal environments. The coastal characteristics of Nha Trang and Grand Popo are summarised in Table 2.1.

Table 2.1: Nha Trang and Grand Popo coastal characteristics. $\widehat{H_s}$, $\widehat{T_p}$, $\widehat{\lambda}$ are the offshore seasonal mean wave height, period and wavelength and $\widehat{\Omega}$ the seasonal mean Dean number.

	D_{50} (mm)	Micro-Tidal Range (m)	$\widehat{H_s}$ (m)	$\widehat{T_p}$ (s)	$\widehat{\lambda}$ (m)	$\widehat{\Omega}$	Beach State
			0.92 (annual)	4.09	27.76	2.85	-
NT	0.60	0.4 to 1.7	0.63 (summer)	3.14	15.77	2.50	Intermediate to Reflective
			1.30 (winter)	4.91	38.45	3.50	LTT
			1.47 (annual)	8.89	125.51	2.05	LTT
GP	0.60	0.8 to 1.8	1.64 (summer)	9.04	129.00	2.27	LTT
			1.25 (winter)	8.07	112.23	1.85	LTT

Dimensional Analysis and LTT Classification

The hydro-morphodynamic processes can differ dramatically as function of the beach states. To classify these states we used the Dean dimensionless number. The evolution of the dimensionless fall velocity, also known as the Dean number, shown in Figure 2.9 is analysed in order to understand the temporal variability of cross-shore beach profiles. As mentioned previously, this dimensionless parameter can be written as :

$$\Omega = H_s/(T_p W_s), \tag{2.1}$$

with W_s the sediment settlement velocity, or equivalently

$$\Omega = H_s/H_g, \tag{2.2}$$

with H_g the typical height over which sediment settled during a wave period. Then, if $\Omega = H_s/H_g >> 1$, sediments in suspension fall on a short height compared to the spatial dimension of the wave. This means that sediments might remain in suspension and therefore be more subjected to transport between the different zones of the inner-beach.

At Nha Trang the seasonal variability of the hydrodynamics offshore wave forcing is more pronounced than at Grand Popo, as shown in Figure 2.9. This implies a variation of the Dean number at Nha Trang which can go from 1 up to 5 approximately, while the Dean number remains almost constant at Grand Popo, around 2. This phenomenon reflects the beach states morphodynamics classified by the Dean number. In particular, two clear beach states are identified at Nha Trang, one during summer and the other during winter, while only one beach state is observed at Grand Popo with a roughly unchanged LTT shape. At Nha Trang an erosive phase is observed from September until the end of February due to winter monsoon conditions. This leads to a LTT beach state during winter (Ω increases). Then an accretion phase imposes the terrace to merge with the beachface resulting in a more reflecting state during summer (Ω decreases). This seasonal variability of beach states show how beach morphology adapts to changing wave conditions, implying a fast exchange of sediment between the upper beach part and the terrace (Thuan et al. (2019)). In contrast at Grand Popo a uniform shaped LTT is observed throughout the whole time series. Actually,

Grand Popo is usually classified as a LTT beach state with a highly dynamic swash zone (Almar et al. (2016); Ondoa et al. (2017); Thuan et al. (2019)).

Nha Trang and Grand Popo beach states are illustrated in Figure 2.11. There are clearly three different cross-shore mean profiles. In particular and as discussed previously, Nha Trang clearly highlights a difference between the summer and winter profile, referred for now to as SNT and WNT respectively, while a similar beach profile is observed at Grand Popo during the whole year, referred to as GP. The morpho-hydrodynamics annual mean parameters of both sites are summarised in Table 2.2 accordingly.

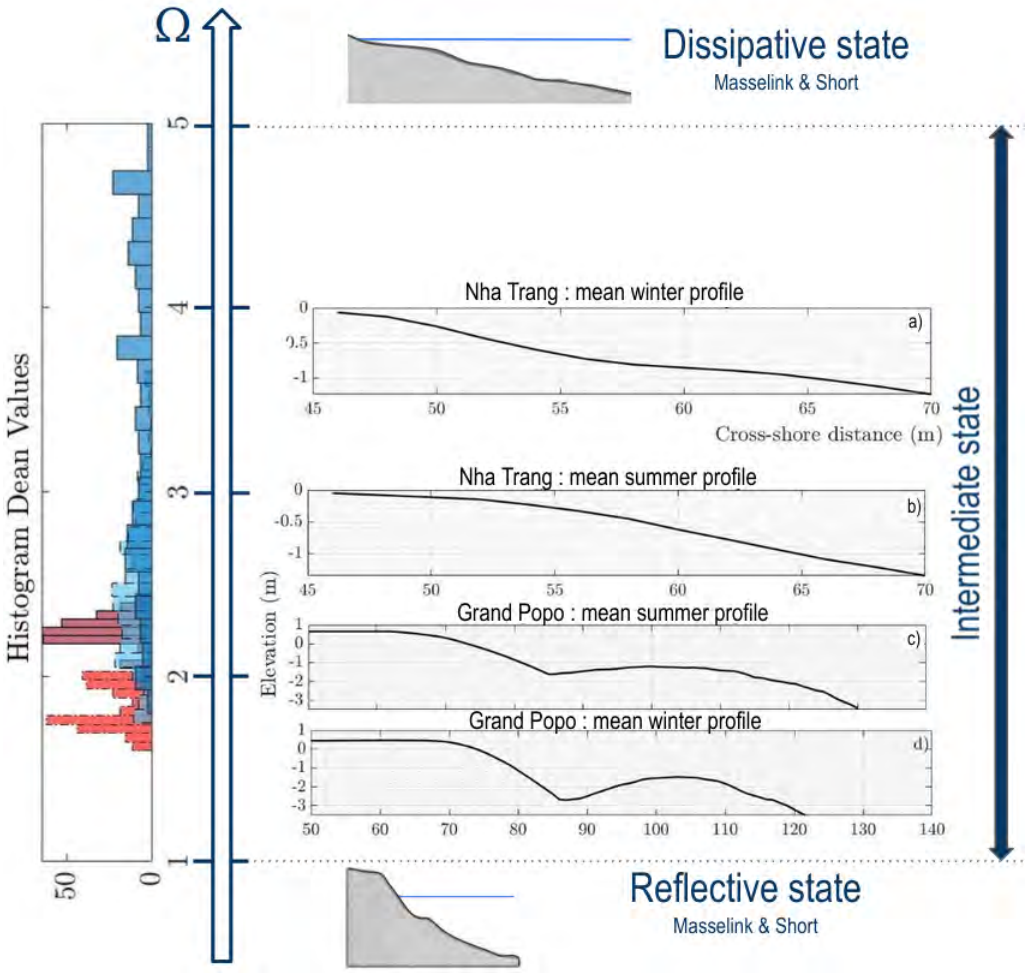

Figure 2.11: Nha Trang and Grand Popo Summer and winter mean cross-shore beach classified according to the Dean number (Ω). The figure on the left shows an histogram of the monthly Dean values of the Nha Trang (in blue) and Grand Popo (in red) cross−shore profiles.

WNT is characterised by a fairly steep upper beachface slope ($\beta \sim 0.1$) and a 14 m wide terrace and GP profile has a steeper beachface slope ($\beta \sim 0.19$) and a 42 m wide terrace. The only geometric relationship that is maintained between these two LTT states (WNT and GP) is the ratio between the terrace width and the wavelength ($L_t/\lambda = 0.3$). The Dean

number at Grand Popo is smaller than Nha Trang Dean numbers meaning that there is more sediment transport between the surf and swash zone at Nha Trang, this is also reflected on the dimensionless parameter $\widehat{H_t}/\widehat{H_g}$. Note that the Dean number of SNT is actually closer to the value of GP one, but no terrace is observed in this case, while the upper beachface slope remains relatively smaller for SNT than GP. These observations are therefore not fully captured by using only the Dean number. However, we propose to analyse LTT in term of the Dean number to highlight the influence of this parameter on the evolution of the profiles specifying its advantages and limitations.

Table 2.2: Nha Trang and Grand Popo moprho-hydrodynamics parameters. $\widehat{L_t}$, $\widehat{\beta}$ and $\widehat{H_t}$ are the annual mean terrace width, upper swash slope and water depth on the terrace.

	Morpho Parameters			**Hydro Parameters**			**Morho-Hydrodynamics Parameters**				
Beach State	$\widehat{L_t}$	$\widehat{\beta}$	$\widehat{H_t}$ (m)	$\widehat{H_s}$ (m)	$\widehat{T_p}$ (s)	$\widehat{\lambda}$(m)	$\widehat{H_g}$	$\widehat{H_t}/\widehat{H_g}$	$\widehat{h_s}/\widehat{\lambda}$	$\widehat{L_t}/\widehat{\lambda}$	$\widehat{\Omega}$
Reflective (SNT)	–	0.10	0.6 m	0.63 m	3.14 s	15.77 m	0.25 m	2.4	0.04	–	2.47
LTT (WNT)	14 m	0.10	0.9 m	1.30 m	4.91 s	38.45 m	0.40 m	2.25	0.03	0.3	3.50
LTT (GP)	42 m	0.19	1.30 m	1.47 m	8.89 s	125.51 m	0.72 m	1.80	0.01	0.3	2.05

Key Low-Tide Terrace Morphological Parameters Extraction

The morphological key parameters of LTT beaches inner-zone are the upper beachface slope (β) and the terrace width (L_t). These parameters can define the shape of LTT cross-shore beach profiles. To analyse the behaviour of these key parameters, the first step is to process the data sets by calculating correlations between the morpho parameters (β, L_t) with the Dean number (Ω) for different times scales moving average to smooth out short terms fluctuations (out-of-equilibrium states). Interestingly for these correlations it was observed that for both cases, Nha Trang and Grand Popo, the correlations improved with the increase of the days mean moving average, converging around the monthly mean average, these correlations values are indicated in Figure 2.12.

The correlations between the terrace width (L_t) and the Dean number (Ω) is considerably better for Nha Trang than for Grand Popo when analysing monthly data. This is a fact as theses values depend on the wave climate; the wave climate is monsoonal at Nha Trang, therefore the beach profile and the Dean number are more variable than at Grand Popo were the wave climate is more or less constant being the beach profile response also more or less constant. This fact highlights that there is a time delay between the wave action and the changes in the beach profile parameters. Note that the upper swash slope for Nha Trang cross-shore beach profile (β) is never correlated with offshore parameters meaning that this parameter may be dominated by surf zone processes and not directly driven by incoming waves.

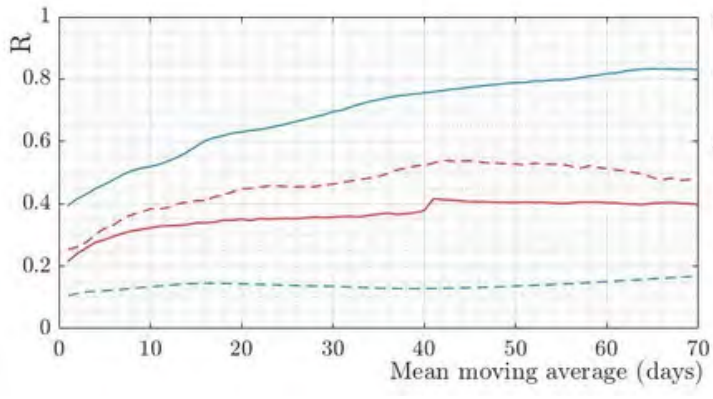

	Variables	Daily (R)	Monthly (R)
Nha Trang	Lt - Ω	0.39	0.70
	β - Ω	0.10	0.14
Grand Popo	Lt - Ω	0.21	0.35
	β - Ω	0.25	0.46

Figure 2.12: Left figure illustrate the correlation coefficient between the morpho parameters (β, L_t) with the Dean number (Ω) for different times scales moving average

On the following sections all morpho and hydro parameters analysed are referred to the monthly mean moving average data (β, L_t, Ω).

Morphology Scaling

As it was seen from field data observations the morphodynamic behaviour of WNT and GP are very different. To characterise this two kinds of LTT beaches and understand the processes intervening we study the interactions of LTT morpho parameters (L_t, β) with their corresponding Dean number (Ω).

Dimensionless parameters are calculated from the two morpho parameters in order to relate them with the Dean number and compare both LTT beaches. These morphological dimensionless parameters are: the ratio between terrace width and seasonal mean terrace depth ($L_t/\widehat{H_t}$), the ratio between terrace width and offshore wavelength (L_t/λ) and the upper swash slope (β). The results between these dimensionless parameters with the the Dean number (Ω) are illustrate in Figure 2.13 highlighting the hydro-morphological relations at Nha Trang and Grand Popo.

On Figure 2.13, Nha Trang data is represented in blue and Grand Popo in red. Note that when $\Omega < 2.5$, no terrace is observed for (SNT). These results allows us to identify 2 different behaviours of the dimensionless morphodynamics parameters ($L_t/\widehat{H_t}$, L_t/λ and β) in relation with their Dean number (Ω). The first case is for $\Omega > 2.5$, for which the morpho parameters remain rather constant. In the other case, when $\Omega < 2.5$, the upper swash slope (β) and $L_t/\widehat{H_t}$ decrease with the Dean number (Ω). More surprisingly, the parameter L_t/λ seems invariant with Ω, suggesting geometric similarities for LTT beaches (WNT & GP).

To finish, note that a dispersion of the data is observed in Figure 2.13, suggesting a strong variability of the LTT morphology on a short time scale, as highlighted in Figure 2.9.

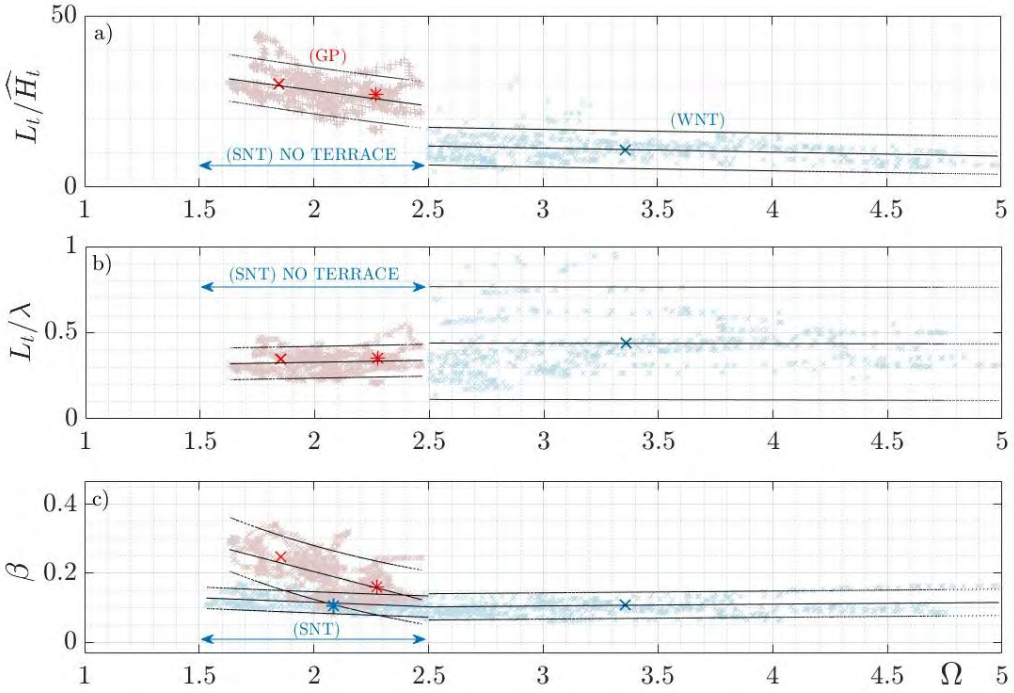

Figure 2.13: In these figures the blue and red color represents Nha Trang and Grans Popo dimensionless values. The little crosses (x) represents the monthly average values, the big ones (X) the summer average values and the big asterisks the winter average values. The two external black lines are the 90% confidence intervals (CI) and the middle one is the data regression. (**a**): Ratio between monthly moving average terrace width (L_t) and annual mean terrace water depth ($\widehat{H_t}$) vs. the Dean number (Ω). (**b**): Ratio between monthly moving average terrace width (L_t) and annual mean terrace water depth ($\widehat{H_t}$) vs. the Dean number (Ω). (**c**): upper beach face slope (β) vs. Dean number (Ω).

Discussion on the Swash Versus Surf Morphodynamical Process

We have therefore shown that even if Nha Trang and Grand Popo are classified as LTT microtidal environments, their nearshore behaviour is very different. A fundamental difference between them is their wave climate. However, a clear analogy in term of Dean classification can be done between Nha Trang during summer (SNT) and Grand Popo (GP). In contrast, Nha Trang during winter (WNT) has somehow a different evolution and structure with Ω. The difference between these different observations is discussed in the following.

Field observations suggest that the dynamic of the nearshore zone exhibits characteristic of a dissipative and a reflective beach for WNT and SNT, respectively. According to such classification with Ω (a beach profile being more reflective for decreasing Ω), this suggestion is here based on the profile structure shown in Figure 2.11. In particular, one observes that the terrace for WNT actually disappears for SNT, suggesting a lower dissipation on a shorter inner surf zone for the latter. Such observation would suggest a reflective beach for GP profiles, as Ω is closer to SNT than WNT. Yet, GP highlights a stable terrace profile. We suggest here that such terrace is therefore inactive, and probably to be attributed to a swash

evolution, rather than a surf-dominated dynamics, as explained in the following.

Based on Figure 2.13 and according to the previous discussion, two different behaviour are thus dissociated only depending whether the Dean number is actually lower or higher than 2.5, independently of the considered site. Then, for Ω is > 2.5, the three morphological dimensionless parameters ($L_t/\widehat{H_t}$, L_t/λ and β) remain roughly constant with Ω. The terrace and swash shapes become independent of the Dean number (Ω). This behaviour suggests that the inner-surf dynamics is strongly affected by the terrace which dissipates wave energy, as mentioned previously. The swash zone is thus only regulated by the surf zone. On the other hand for $\Omega < 2.5$ (SNT & GP) we can see that the upper swash slope (β) has a decreasing trend with Ω (Figure 2.13c), suggesting a more intense action of the local slope in the swash zone on the inner surf dynamics (even if Nha Trang and Grand Popo highlight a slightly different evolution of $\beta(\Omega)$ in this regime as shown in Figure 2.13c for $\Omega < 2.5$). These two different morphodynamic behaviours, depending only on Dean number, allows us to classify LLT beaches in two different families. The first one is when the terrace becomes active at dissipating wave energy, hence the dynamics of the swash zone will be regulated by the surf zone ($\Omega > 2.5$). This case is referred to as Surf Regulated Beach (SRB). The second situation ($\Omega < 2.5$), referred to as Swash Regulated Beach (SwRB), is when the dissipation of the wave energy occurs mainly close to the beachface producing a highly dynamic swash zone. SNT and GP can be classified as SwRB.

To finish, The difference in $\beta(\Omega)$ observed between the two sites at $\Omega < 2.5$, i.e., for SwRB state, could be attributed to different processes, which are not accounted in the present classification. The first one is that Grand Popo is probably close to equilibrium, while Nha Trang is clearly evolving between two states, i.e., is out-of-equilibrium. The second one is that the beach slope depends on other parameters, such as the longshore sediment transport for instance (probably more intense in Grand Popo due to oblique wave impact) or the beach profile history.

2.2.7 Extending the Dean Profiles to 3rd Order Profiles

3rd Order Regression of the Bathymetry for the Study of a Parametric Model

Having found interesting correlations between Lt and β with the Dean number for LTT cross-shore profiles, the objective in this section is to build up a simple parametric model from this correlations and see if it is possible to recreate the beach profiles bathymetry evolution using as input the Dean number (Ω).

Cross-shore beach profiles can be approached using the theoretical equilibrium beach profiles proposed by (Bruun, 1954) and Dean (1991). These equilibrium profiles derived from field observations have the following form :

$$h = Ay^n \tag{2.3}$$

in which A, representing a sediment scale parameter, depends on the sediment size D and an exponent n equal to 2/3. This well known expression proposed by Dean it's normally used to generalise the entire beach profile, but as it has a simple form it's not adequate to capture local variation of the inner surf zone, which is the zone of interests in this research work. Therefore a 3rd order polynomial is chosen to model this specific zone. Even if no theoretical background supports such power law coefficient, the third order polynomial is the minimum order allowing to capture the shape profile including both swash and terrace as it includes the required curvatures of opposite sign. The model is not efficient to capture the beach profile shape in other locations (Figure 2.14).

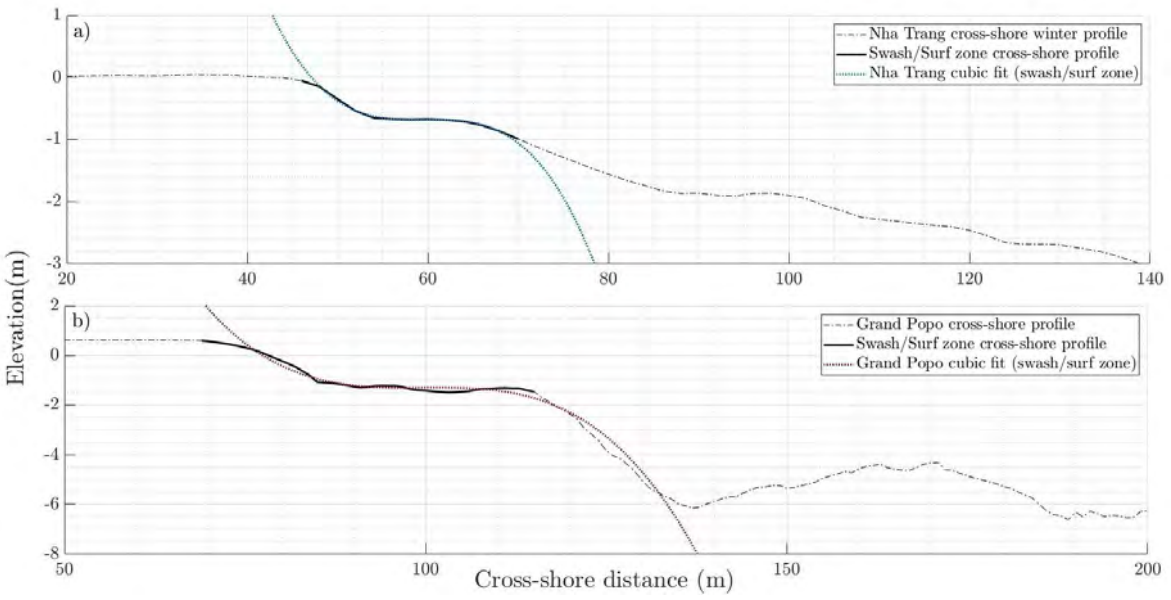

Figure 2.14: Typical WNT and GP cross−shore profiles. (**a**): The black dashed line represents Nha Trang mean winter cross−shore beach profile. The bold black line shows the zone of interest (surf and swash zone). The blue doted line is the cubic function that fits the zone of interest. (**b**): The black dashed line represents Grand Popo annual mean cross-shore beach profile. The bold black line shows the zone of interest (surf and swash zone). The red doted line is the cubic function that fits the zone of interest.

The parametric model consists of a two-parameter polynomial equation formed by only keeping the cubic and the linear terms, such as

$$y(x) = A(x - \hat{x})^3 + B(x - \hat{x}) + \hat{y}, \tag{2.4}$$

where x is the cross-shore distance and $y(x)$ the elevation of the beach profile. $\hat{x}$ and $\hat{y}$ refers to profiles offset allowing to center each profile around the zone of interest. The coefficients A and B define the shape of the beach profile. The variation of these coefficients can represent three key types of cross-shore profiles which are useful to represent the reflective profiles, LTT states and their transitions. In other words three profiles can be distinguished

from the variation of the cubic and linear terms, as represented in Figure 2.15. In particular, Figure 2.15a shows an example of a LTT inner-shore environments observed for WNT profiles compared with a purely cubic profile, i.e., $B \to 0$. On the other hand, a SNT profile (reflective state) is well fitted by a linear shape, i.e., $A \to 0$ (see Figure 2.15c). Finally, ass shown in Figure 2.15b, transient profile between these two cases can be captured by the full model (2.4) when both $A \neq 0$ and $B \neq 0$. The evolution of the beach states from a LTT to a reflective state can therefore be captured by model (2.4) with A and B to be determined.

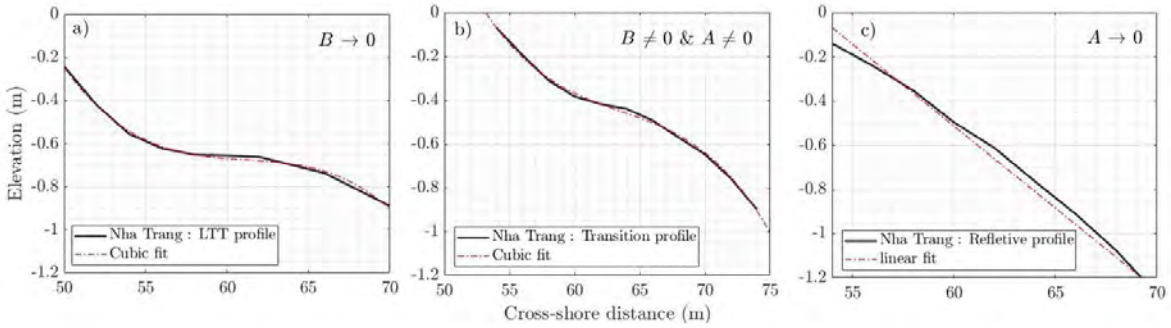

Figure 2.15: LLT cross−shore to reflective beach profiles obtained with the variation of the shape coefficients (see Equation (2.4)). (**a**): example of a LTT profile environment at WNT fitted with a purely cubic profile ($B \to 0$). (**b**): example of a LTT profile environment at WNT fitted with a cubic profile ($A \neq 0$ and $B \neq 0$). (**c**): example of a SNT profile (reflective state) fitted by a linear shape ($A \to 0$).

In order to show the relevance of model (2.4) over the entire set of measurements, the evolution of both L_t and β can be compared between measured profiles and fitted profiles. This is shown in Figure 2.16 for Nha Trang and Figure 2.17 for Grand Popo. Here, the 3rd degree regression model (2.4) was applied on the monthly moving average measurements data (as explained in Section 2.2.6).

The obtained terrace shape parameters, $Ltfit$ and βfit, are in good agreement with those obtained from field data measurements (Lt and β). Note that, even if the evolution of both parameters L_t and β is nicely captured by the cubic fit, L_t highlights a slightly better accuracy that β in both cases (Nha Trang and Grand Popo). Nevertheless, as already mentioned, Figure 2.16c clearly shows a seasonal fluctuation of the terrace shape which is actually captured by the proposed polynomial model. On the other hand, β does not seem to follow a clear seasonal trend, and is more likely affected by short term fluctuations. On the contrary, Figure 2.17c shows that the terrace length L_t at Grand Popo remains roughly invariant while the upper swash slope β highlight a slight correlation with seasons, beyond a rapid short term fluctuations.

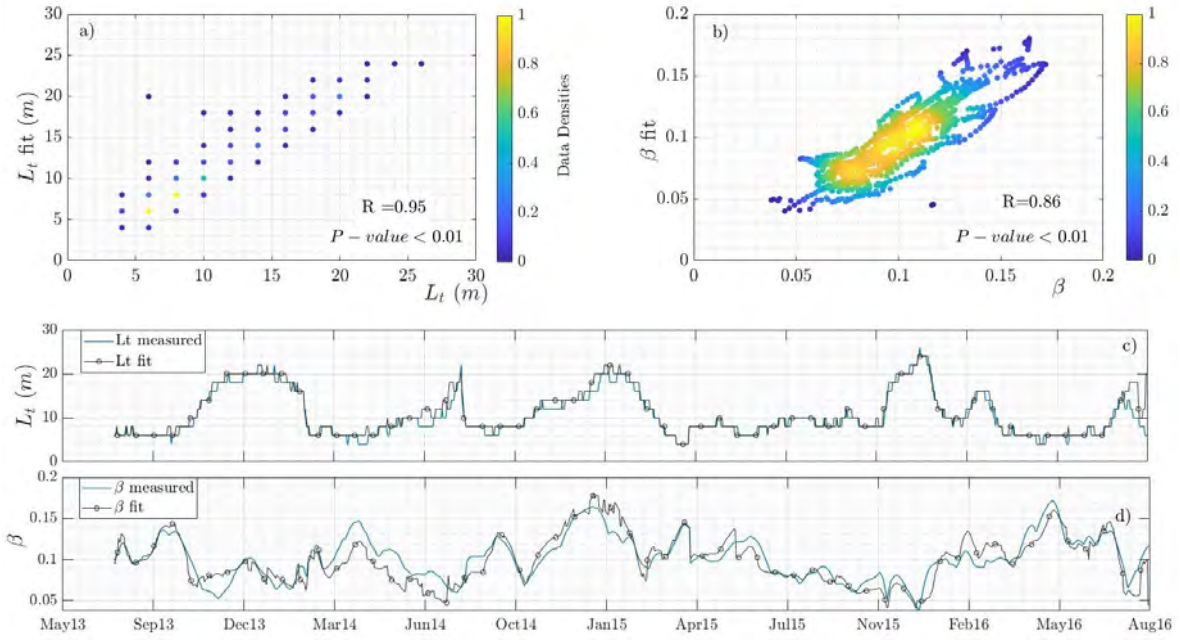

Figure 2.16: Nha Trang fit results. (**a**): Lt monthly average field data (L_t) vs Lt fit. (**b**): betas monthly average field data (β) vs betas fit. (**c**): terrace width (L_t) evolution observed from field data and L_t evolution calculated from fit profiles (L_t fit). (**d**): upper swash slope (β) evolution observed from field data and β evolution calculated from fit profiles (β fit).

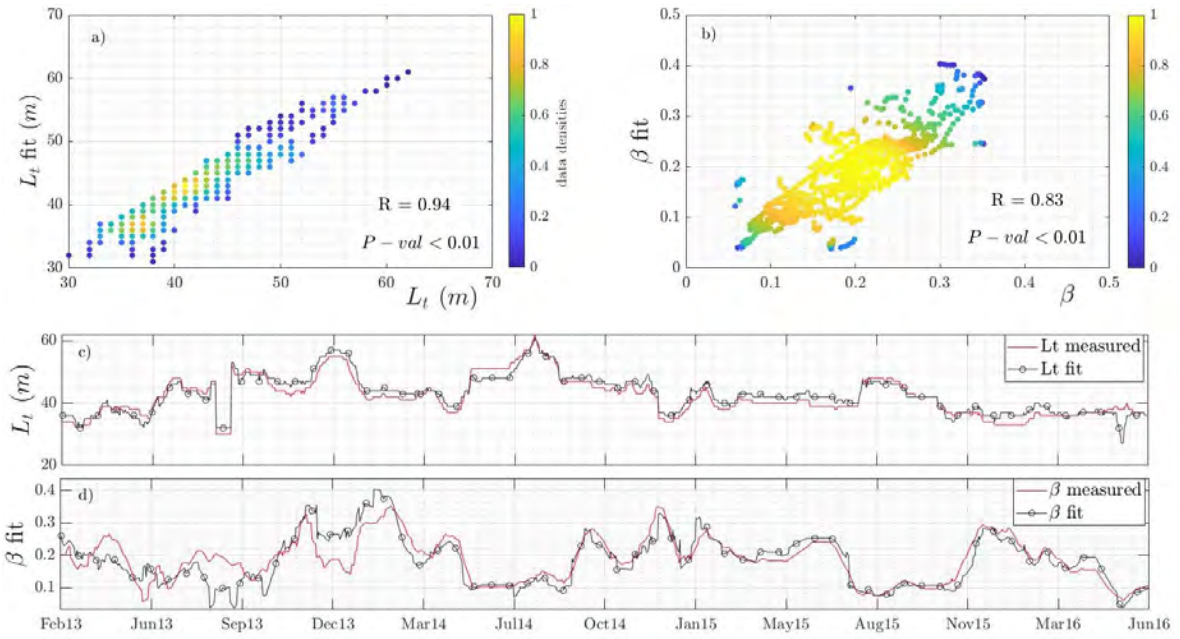

Figure 2.17: Grand Popo fit results. (**a**): Lt monthly average field data (L_t) vs Lt fit. (**b**): betas monthly average field data (β) vs betas fit. (**c**): terrace width (L_t) evolution observed from field data and L_t evolution calculated from fit profiles (L_t fit). (**d**): upper swash slope (β) evolution observed from field data and β evolution calculated from fit profiles (β fit).

2.2.8 A Simple Parametric Model to Understand the Behaviour of LTT Beach Profile

In the previous section, we have shown the ability of a simple polynomial shape (2.4) to capture the basic trend of LTT beaches. Moreover, it was also shown in Section 2.2.6 how the Dean number Ω controls the main geometrical characteristics of the shape profiles L_t and β. Now, in order to link these two results, a unique parametric equation that only depends on the dean number (Ω) is tested. For this purpose, the link between A, B and Ω has to be evaluated.

Model (2.4) can therefore be simply written as:

$$y(x) = F(\Omega)\ (x - \hat{x})^3 + G(\Omega)\ (x - \hat{x}) + \hat{y} \tag{2.5}$$

The models were trained separately for Nha Trang and Grand Popo as we found that both beaches had very different responses of their inner-surf zone to offshore wave forcing. The training of the parametric model consists on obtaining the shape coefficients (A and B, Section 2.2.7) and relate them to the Dean number (Ω). Therefore the model coefficients F(Ω) and G(Ω) modelling A and B, respectively, as a function of Ω, are obtained from a linear regression between the shape coefficients A and B with respect to Ω illustrated in Figure 2.18.

It is interesting to note that the strongest correlations between the shape coefficients with Ω is not the same for both beaches. For Nha Trang the dominant coefficients is coef. B (Figure 2.18b left) and for Grand Popo is coef. A (Figure 2.18c left). For Nha Trang it is possible to appreciate a seasonal fluctuations of the shapes coefficients; coefficient B tends to zero when there is a terrace profile meaning that the linear terms goes to zero in these cases. It is found that the dominant coefficient for Nha Trang (coef. B) and Grand Popo (coef. A), are well captured by this linear models $G_{NT}(\Omega)$ and $F_{GP}(\Omega)$ respectively (Figure 2.18b,c). Even if less accurate, the trend evolution of coef. A for WTN is also captured by the linear model $F_{NT}(\Omega_{WNT})$ (Figure 2.18a left). Moreover, at Grand Popo it was proved that coef. B does not influence the obtained results. This conclusion was reached by performing two tests, one with a linear regression between Ω and coef. B and the other one with $G_{GP}(\Omega) = 0$ (right Figure 2.18d), the results were basically the same for both cases. Thus to simplify GP model G(Ω) is zero.

The results of each model are illustrated in Figures 2.19 and 2.20 for these two sites respectively. The evaluation of the model is estimated by the differences between the monthly average evolution of the terrace width (L_t) and the upper swash slope (β) obtained from field data with the values calculated from the model (L_t model and β model). The root-mean-square error (RMSE) and root-mean-square-relative error (RMSRE, %) are shown in Table 2.3.

Note that the values correspond well with the discussion in Section 2.2.6, that there are two families of LTT beaches : one controlled by the swash zone (SwRB) and the other by the surf zone (SRB). The highest RSMRE corresponds to the swash slope evolution (RSMRE =

46%) at Nha Trang which is the case of SRB, thus it make sense that the variations of the swash slope (β) can not be capture with the variation of off-shore parameters such as the Dean number (Ω) as it is controlled by surf zone process.

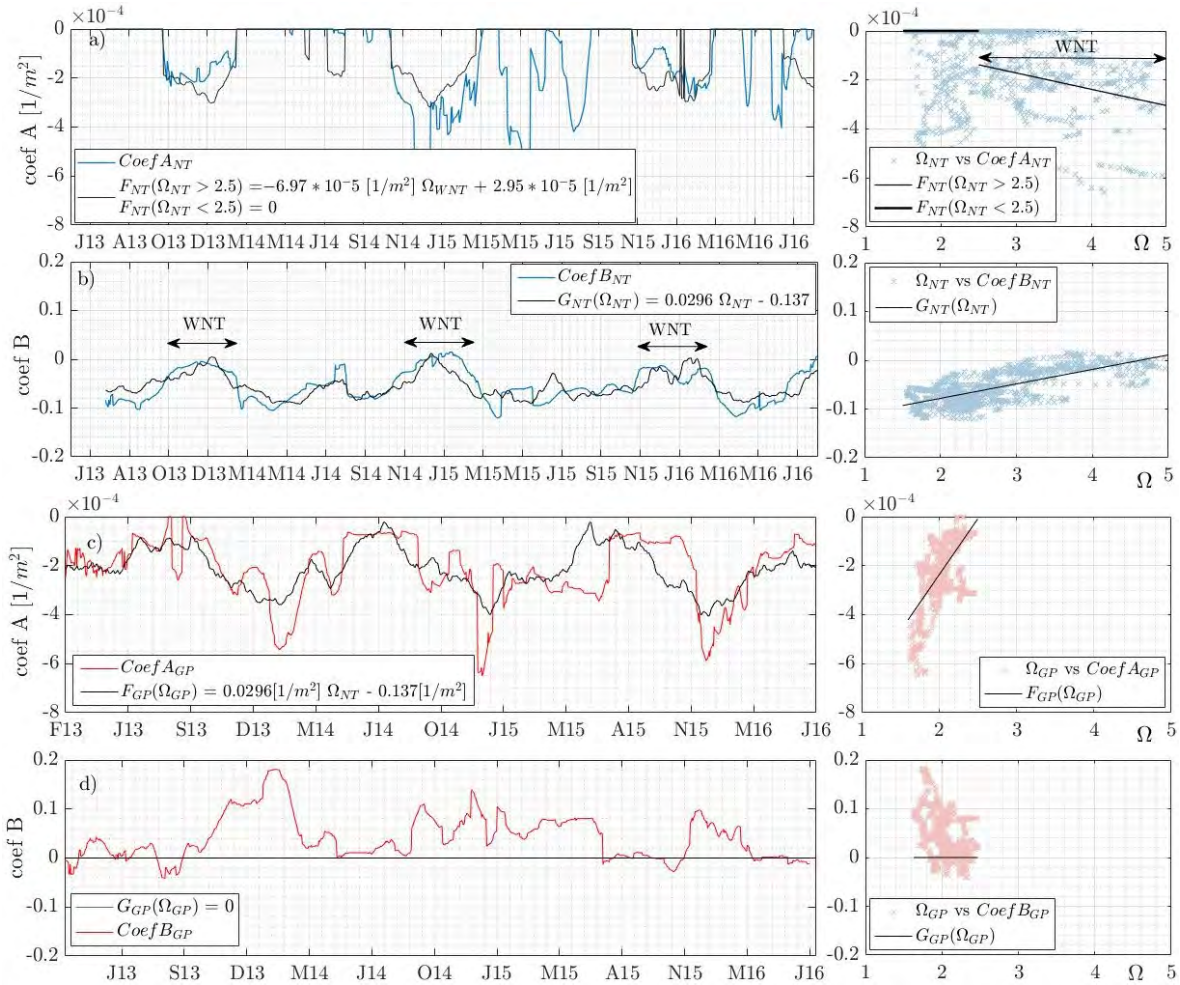

Figure 2.18: Left Figures: represents the shape coefficients evolution for Nha Trang (Figure **a** and **b**) and Grand Popo (Figure **c** and **d**). Right Figures: shape coefficients vs their respective Ω. Represented in black are the linear regressions obtained between the shape coefficients A and B respect to Ω.

It is important to analyse not only the errors obtained by the models predictions, but also the trends of the morpho-parameters (L_t and β), Figures 2.19 and 2.20. From these comparisons, one can observe that the general trend of the beach profiles over time is recovered by the model (see Figures 2.19a,b and 2.20a,b for comparisons). A more quantitative comparison is also proposed by plotting the evolution of L_t and β (from data and model) as a function of time in Figures 2.19c,d and 2.20c,d. Seasonal variation seems to be well captured by the model. This is more clearly highlighted by L_t at Nha Trang (Figure 2.19c) and β at Grand Popo (Figure 2.20d). On the other hand, rapid fluctuations are slightly more poorly prescribed by the model, indicating that transient evolution probably includes physical

ingredients not accounted for in the Dean number Ω.

Table 2.3: Root mean square error(RMSE, m) and relative error (RMSRE, %) obtained from the model prediction.

	RMSE		**RMSRE**	
2-5	**Lt-Lt Model**	**β-β Model**	**Lt-Lt Model**	**β-β Model**
Nha Trang	2.9 m	0.04	21%	46%
Grand Popo	5.9 m	0.05	14%	28%

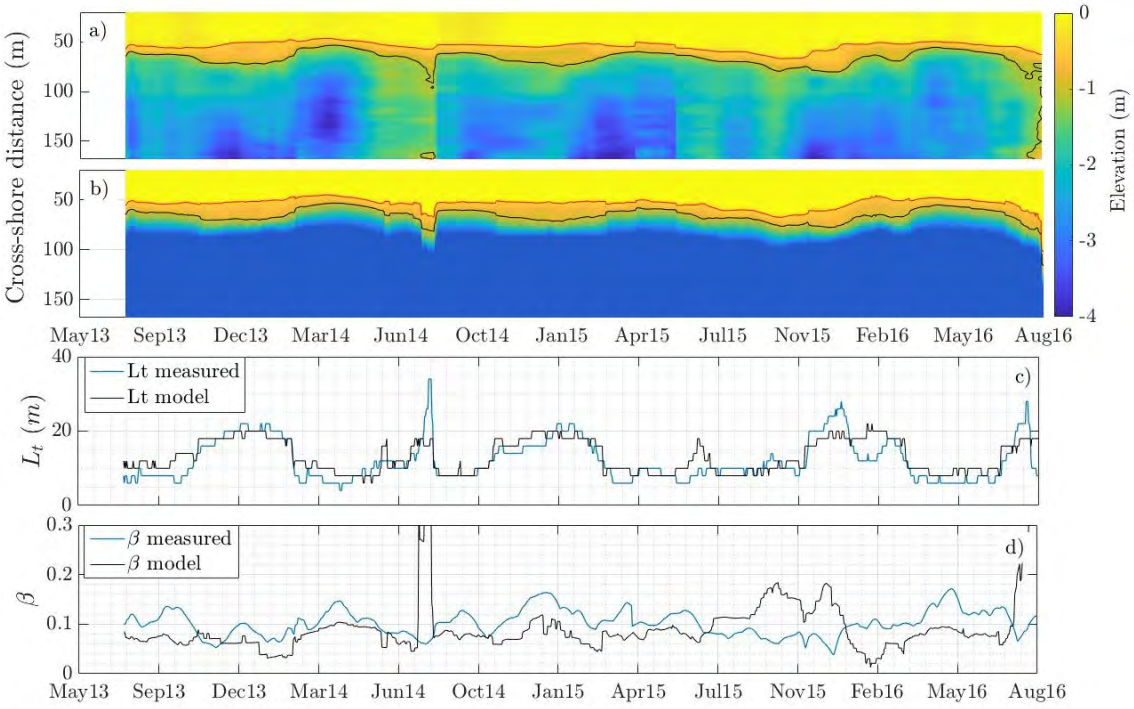

Figure 2.19: Nha Trang model results. (**a**): Monthly average bathymetry evolution. (**b**): Bathymetry evolution calculated with the parametric model. (**c**): terrace width evolution obtained from field data and those calculated from the parametric model (L_t & L_t model). (**d**): upper swash slope evolution obtained from field data and those calculated from the parametric model (β & β model).

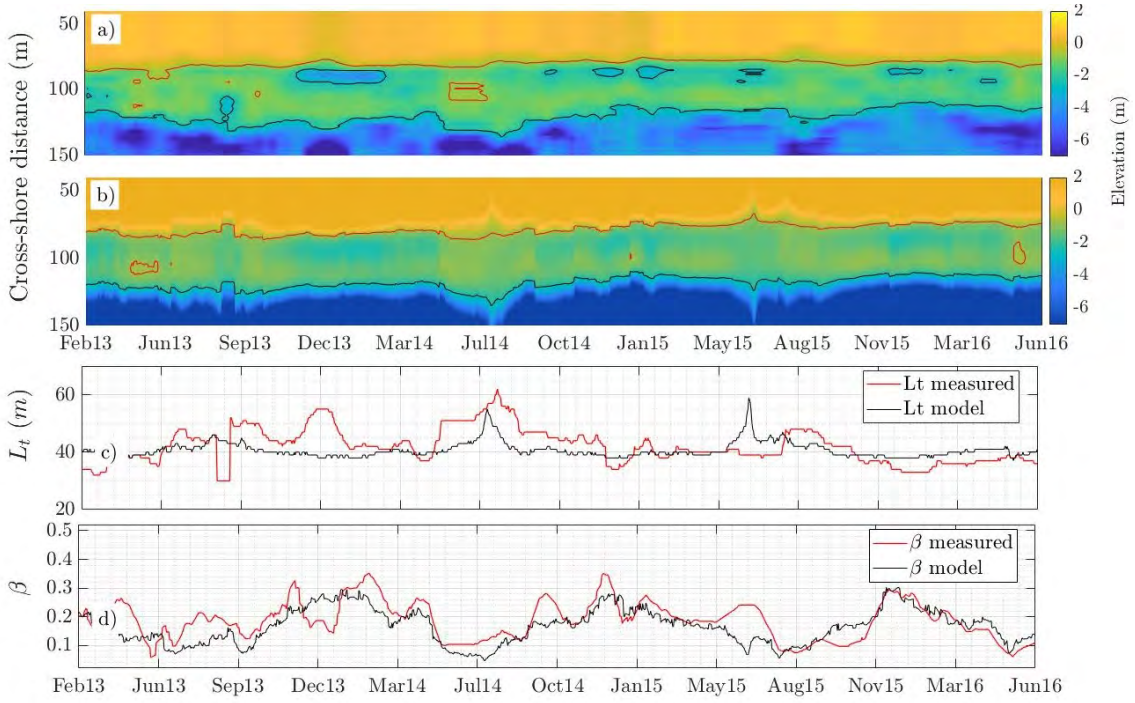

Figure 2.20: Grand Popo model results. (**a**): Monthly average bathymetry evolution. (**b**): Bathymetry evolution calculated with the parametric model. (**c**): terrace width evolution obtained from field data and those calculated from the parametric model (L_t & L_t model). (**d**): upper swash slope evolution obtained from field data and those calculated from the parametric model (β & β model).

2.2.9 Conclusions

From the morphological scaling at Nha Trang and Grand Popo, two different morphological responses of the inner-surf zone were identified depending on wave climate. When swash processes dominate with large reflection such as in Grand Popo, the terrace can be seen as a result of the sediment deposition from the swash zone (and reflected waves) and not directly driven by incoming waves, we refer this case as Swash Regulated Beach (SwRB). The other situation refers to a Surf Regulated Beach (SRB) being the case of Nha Trang where the terrace is active at dissipating wave energy hence the dynamics of the swash zone is regulated by the surf zone and not by offshore wave forcing. This two families (SwRB and SRB) were also observed from the results of the simple parametric model proposed in Section 2.2.7. based on the Dean number (Ω) as a control parameter. Note that this simplified model should be use to help understand LTT environments and not as a predictor as a single parameter is surely not enough to describe the whole spectrum of beaches. Such single parameter analysis can not explain and capture the entire hydro-morphodynamics of the system: as for instance site-to-site unification remains difficult, but also rapid variation of the upper swash slope (β) are not captured. This remains an open question that would require more field data and probably a more refined out-of-equilibrium state model.

2.3 Global conclusions and discussions

The main highlight of this paper (Mingo et al., 2021) is to use the off-shore Dean Number as a control parameter of inner-shore morphodynamics for LTT environments, on monthly time scales. The Dean Number is known to describe well global equilibrium beach states observed in seasonal or annual time scales (Wright et al., 1984; Short, 1996; Dean, 1991). Nevertheless for these two LTT environments (NT and GPP), it was established a strong correlation between either the monthly mean Dean Number evolution with the beach-face slope dynamics (swash zone) at GP or the the monthly mean Dean Number evolution with the terrace length dynamics (surf zone) at NT.

Through this correlations found at NT and GPP of the nearshore response with the Dean number, a third order parametric model was defined separately for each beach, to recreate the inner-shore morphology (surf and swash zone) as a function of this single parameter (Ω). It was not possible to extracted a universal model for both beaches as it is concluded that NT and GPP had different inner-shore hydro-morphological responses to wave forcing. These different behaviours were referred to as Swash Regulated Beach (SwRB) for Dean Number lower than 2.5 or Surf Regulated Beach (SRB) for Dean Number higher than 2.5. Therefore the intermediate LTT beach state defined by Wright et al. (1984) can be sub-classified into: SwRB for $1 < \Omega < 2.5$ and SRB for $\Omega > 2.5$. Where for SwRB the beach-face slope could be directly responding to off-shore individual wave action (GP) and SRB the swash zone will be highly regulated by the terrace length.

A last result interesting to come back and highlight in this discussion is the result obtained from Figure 2.13. This Figure shows the ratio between the monthly terrace length and its associated wavelength plotted against its monthly mean Dean Number (L_t/λ vs Ω) for NT and GP. For Nha Trang only the winter cases with a LTT were plotted in that Figure. From this result a constant overall relation is defined as $Lt/\lambda \sim 0.4$. But a surf length could be associated for all beach states at NT, having a gentle or flat slope. This surf length is illustrated in Figure 2.2c between the black and red contours that correspond to an elevation of -0.5 and -1.3 respectively. Now if we re-plot the same Figure for the monthly ratio between the terrace and wave length as a function of the Dean Number (L_t/λ vs Ω) for all NT and GP beach states, we concluded that the overall constant relation ($L_t/\lambda \sim 0.4$) continues to work. Nevertheless this relation can be refined as it is observe a slight increase of the ratio between the terrace and wave length as the dean number increases. This result is presented in Figure 2.21, where the grey crosses represent NT and GP monthly relations between L_t/λ with Ω and the yellow dashed line is showing the trend of this relation.

The results of this field study encouraged to continue this analyse in the laboratory. This laboratory work is described in Chapter 3, where the morphological response of the swash zone to changing waves is studied with an experimental physical device specifically designed to highlight swash dynamics.

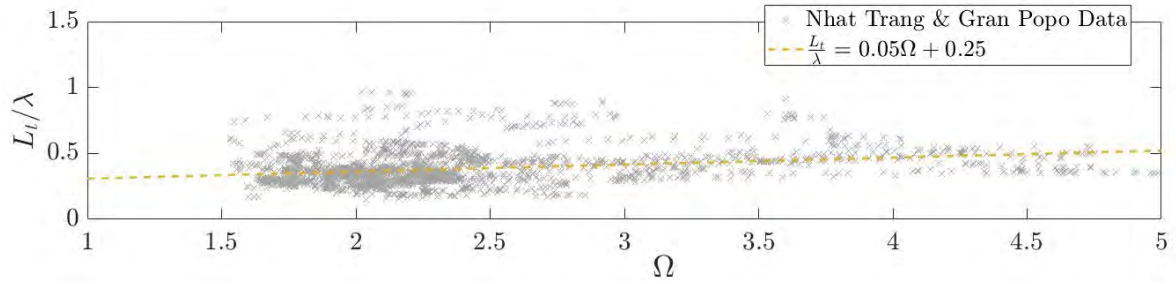

Figure 2.21: Grey crosses represents NT and GPP ratio between the monthly moving mean terrace and wave length (L_t/λ) vs the monthly moving mean Dean number (Ω). The yellow dashed line is a linear fit of this ratio (L_t/λ) evolution as a function of the Dean number.

Chapter 3

Laboratory Physical Model of the Nearshore

Contents

3.1 Set-Up of the Nearshore Laboratory Physical Model

A laboratory physical model is used to expand upon and clarify field observations results presented in Chapter 2. The model is designed to investigate the swash zone rapid adaptation to changing wave conditions on beaches with flat platforms, recreating LTT environments. Special attention is placed on exploring the relation between the beachface slope and the Dean number, as observed in field results.

This section is dedicated to describing the physical model of LTT beaches in microtidal environments, including the setup and measurement equipment, data extraction, its scopes, and limitations. The model is based on the simplified approach outlined in Section 1.2. The final part of the section presents preliminary results that provide important insights into the time scales of the hydro-sedimentary processes occurring in the model.

3.1.1 Physical model of microtidal environments with flat platforms

The modeling of microtidal environments with flat platforms involves replicating the typical geometrical form found in natural beaches within these environments. This allows us to delineate the different hydro-morphodynamic regions observed as waves approach the shore. For a more detailed explanation of this concept, the reader can refer to Chapter 1, Section 1.1.3, where it highlights the varying morphological time scale response of each region of the beach profile responding to wave action (Stépanian, 2002). The typical microtidal profile with its associated morphological time scale response to wave forcing is shown in Figure 3.1a.

Our model of LTT beaches in microtidal environments focuses on reproducing the hydro-morphodynamics regions of the cross-shore beach profile. A rigid gentle slope is introduced to generate a controlled wave-breaking mechanisms that keeps the interaction between wave shoaling and the seabed constant. Subsequently, a rigid flat platforms is imposed, and its length can be adjusted based on the starting point of the sandy beach, positioned at the end of the flat platform. This design simulates the shoaling and breaker region, the terrace and the upper beachface zone. A sketch of this physical model is shown in Figure 3.1b. The innovative aspect of this physical model is to only focus on the upper beachface and its beachface slope, very specific zone, disregarding the morphodynamics on the terrace representing the surf zone.

To this end, the model is divided into two distinct hydro-morphodynamics sections. The first one is an non-erodible section characterized by the rigid sloping bottom followed by the rigid flat platform that is under shalow water conditions. These sections recreates the wave shoaling and wave dissipation due to the interaction of the wave with the rigid bottom. And the second section is an erodible region recreating the upper beachface. The division of the model into a non-erodible and erodible region simplifies the hydro-sedimentary systems and it can be justified as research has shown that the upper beachface can respond to wave action in matter of minutes, hours or days. In contrast, other nearshore sub-regions require much longer response times ranging from seasonal to annual responses for the surf zone and decades to centuries for the shoreface (Short and Jackson, 2013). Thus, if we only focus on

the rapid morphological response of the upper beachface, the rest of the beach profile can be considered invariably during this time scale. The limitations of this assumption is discussed in the following sections.

Therefore, this simplified LTT model in microtidal environments can be reduce to a few key parameters that characterize different zones along the cross-shore beach profile. These hydro-morphological parameters include water depth, wave characteristics (period and height), length of the terrace, and the beachface slope. We will discuss these parameters in detail in the following sections. To draw an analogy with the field cross-shore typical profile, we refer to the different regions delimited in the model as "offshore", where the wave can be considered symmetrical and propagate with minimal interaction with the bottom; "shoaling and breaker zone," where waves become more asymmetrical due to the decrease of water depth on the rigid sloping bottom, ultimately causing wave breaking; "surf zone" where an asymmetrical wave front (bore) propagates and dissipates under shallow water conditions (flat platform) and finally the "swash zone," defined as the only erodible part of the model representing the upper beach. These zones and their analogy with the field are shown in Figure 3.1.

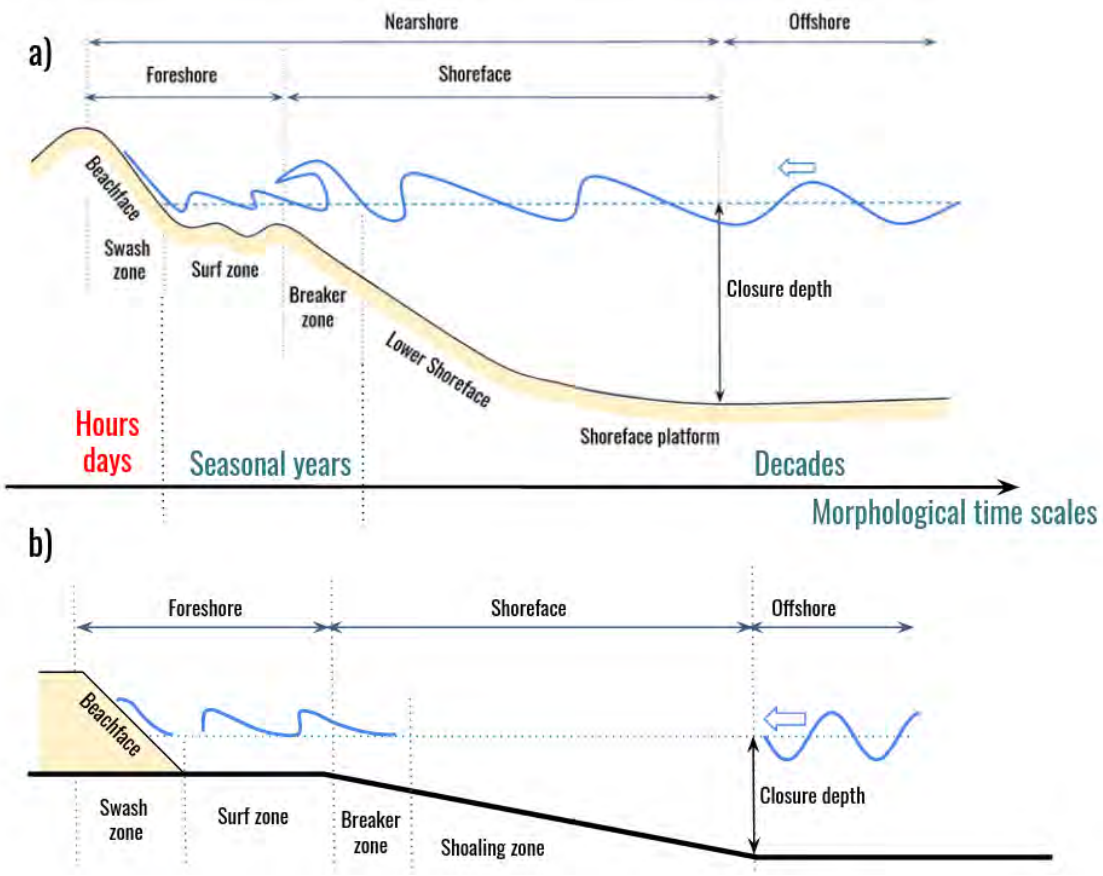

Figure 3.1: (a) Schematic representation of a typical beach profile in a microtidal environment. Adapted from (Wright et al., 1982b) and (Stépanian, 2002).(b) Sketch of the model proposed to interpret microtidal beaches in LTT environments.

3.1.2 Experimental set-up and data extraction

The setup of the model, along with the placement of the metrology devices, is illustrated in Figure 3.2. The LTT microtidal beach model is constructed within a small-scale water flume, specifically designed for this research. The flume measures 12.65 meters in length and has a cross-section with dimensions of 0.15 meters in width and 0.30 meters in height. The laboratory model is equipped with a flap paddle wave generator at one of its end as well as a rigid gentle sloping bottom to keep the breaker position fixed around $x = 0$ (with he axis x being aligned with the wave propagation along the flume). The erodible sandy zone, representing the upper beach, is located at the opposite end of the wave generator after the rigid sloping bottom. Between the wave generator and the rigid slope, two water gauges (S1) and (S2) are positioned to characterize the offshore wave forcing. Additionally, an optical metrology device is installed to monitor the hydro-morphodynamics of the shoaling, breaker, surf, and swash zones. This optical metrology device allows for the tracking of water/air/sandy bottom interfaces through digital shadowgraphy. The setup of the model, along with the placement of the metrology devices, is illustrated in

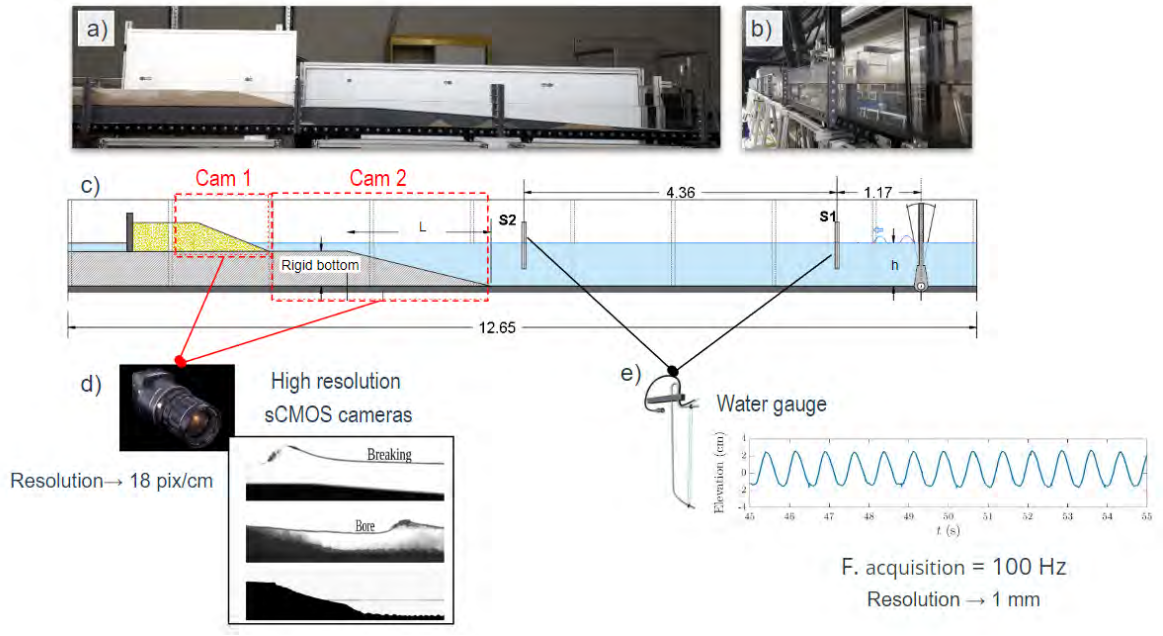

Figure 3.2: (a) Photograph of the laboratory model, featuring the rigid slope, the rigid flat platform, the sandy beach, and a water gauge (S2). (b) Close-up image of the flat paddle wave generator. (c) Schematic illustration of the laboratory model configuration, showing the locations of the metrology devices, with dimensions in meters. (d) High-resolution sCMOS-Lavision camera images. (e) Wave elevation data extracted from the water gauge.

As mentioned above, in this study, we use water gauge to measure both wave height (H_0) and period (T_0) before the slopping bottom to characterize the off-shore incoming wave. To ensure accurate measurements, we studied the associated errors in the measurements.

Figure 3.3 illustrates an example of data extracted from the water gauge, with the left side showing the calibration law and the right side depicting the free surface evolution.

During the calibration of the water gauge, we establish the relationship between the different water depth (h) with the voltage measured at the water gauge (V), extracting a linear relation $V = k * h$, where k is the calibration constant. The gauge precision is 0.01 V. Assuming a constant and normally distributed error along the gauge measurements, the Root Mean Square Error (RMSE) in adjusting the calibration constant (k) is determined to be 0.043 V, surpassing the gauge precision. The resulting calibrated value for k is established as 0.15 V/cm, implying an approximate 0.28 cm error in a single measurement of wave height (H_0). In a worst-case scenario, with a 2 cm wave amplitude, there is an estimated 14% error in the measurement. However the averaging of these measurements with 20 samples significantly reduces the error, resulting in an average wave height error of approximately 0.06 cm, or about 3%.

Turning our attention to the wave period (T_0) measurements, we identify the peak detection process as the primary contributor to error. The maximum error in detecting one peak is determined to be 0.025 seconds. As the period is determined as the mean value of 20 peaks, the error is divided by 20, resulting in an approximate 0.16%.

In conclusion, the errors associated with wave height and period extraction and calculations are negligible for the orders of magnitude under consideration in our analysis. Consequently, these errors are disregarded in the subsequent phases of our study, allowing us to focus on the fundamental aspects of beachface response to varying wave conditions.

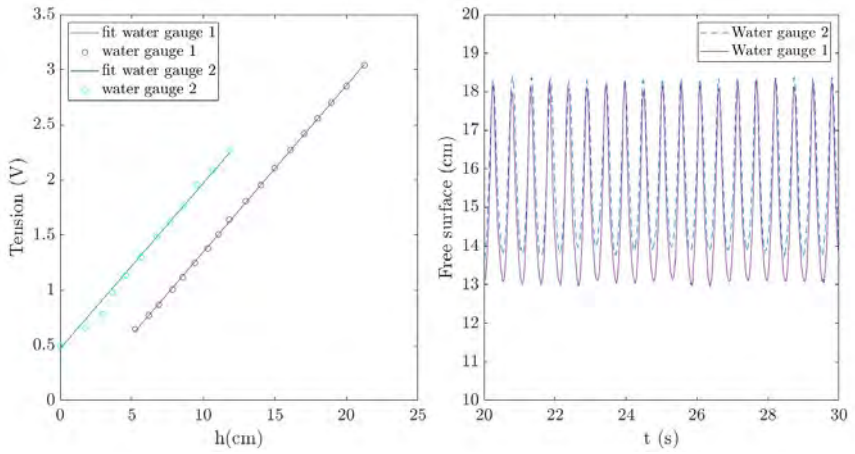

Figure 3.3: Example of water gauge data. The left figure displays the calibration law for four different water gauges, and the right figure illustrates the free surface evolution using the calibration law.

On the other hand, as we approach the inner-surf zone, represented by the sloping bottom, flat terrace, and the sandy region of the beachface, we employ two high-resolution cameras to monitor the free surface (Cam1) and beachface morphological evolution (Cam2). These

cameras capture images at a very high frequency. In our experiments, we adopt resolutions of 10.5 pixels/cm for Cam1 and 21.5 pixels/cm for Cam2 (position of the camera shown in Figure 3.2). For the lower resolution, errors in a single measurement are calculated as 0.047 cm. This error is ten times smaller than the error resulting from gauge calibration, making it a negligible contribution to our study and therefore not considered. However, potential errors may arise in the study due to the detection and extraction of free contours between water/air/sandy interfaces through the use of digital shadowgraphy. To achieve this, two-back-lights are placed in our area of interest (see Figure 3.2). This method involves illuminating the viewing window to enhance the contrast of surfaces for better detection. A post-processing code is developed to automatically analyze the collected images. For the hydrodynamics analysis of the free surface evolution, the acquisition frequency is 40 Hz, and for the morphological analysis of the beachface evolution, the image acquisition frequency is 2 Hz.

Figures 3.4 shows an example of the the free surface evolution on the sloping bottom calculated using the post-processor program for a given time capture.

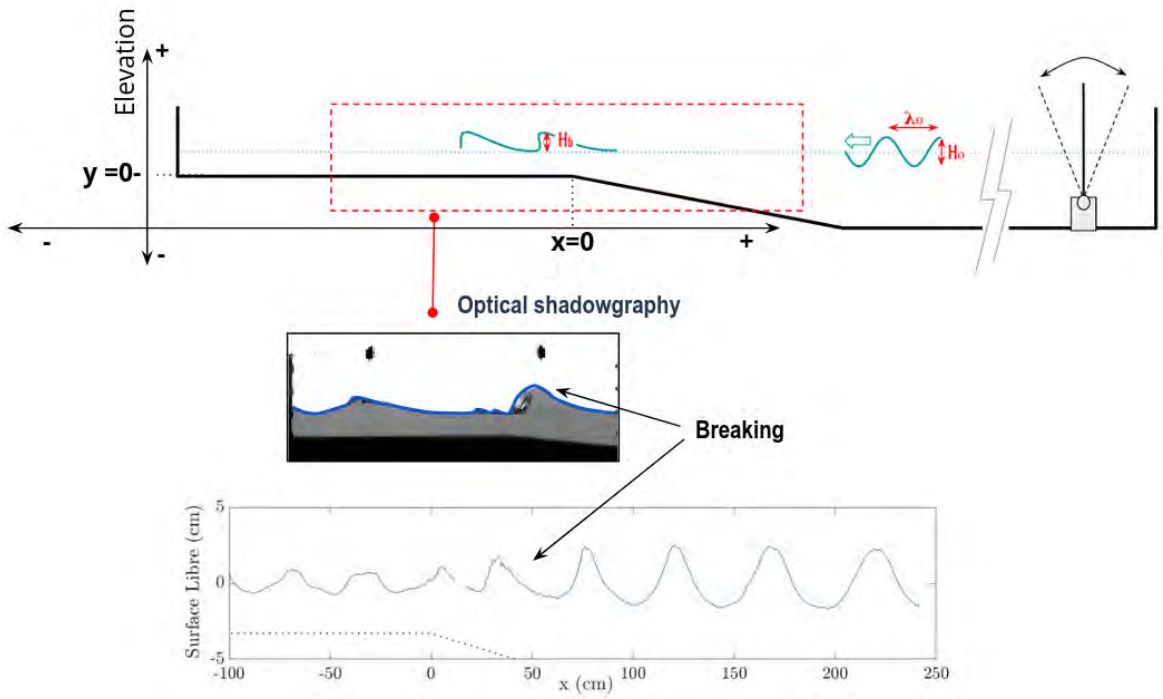

Figure 3.4: The top figure shows the sketch where the optical shadowgraphy is performed, the middle figure displays an example image captured by the high-resolution cameras with the detection of the free surface, and the bottom figure shows a plot of the free surface at a given time extracted after the post-processing code.

For the hydrodynamic study of the wave evolution on the sloping bottom and the flat platform, water dye is added to enhance the contrast, allowing the free surface to be clearly detected in each image. Therefore, with the high-frequency acquisition of the free surface,

it is possible to plot a spatio-temporal diagram of the free surface (see Figure 3.5), where the structure of the wave forcing and its evolution, perturbations, wave fronts, breaking, and deceleration can be visualised.

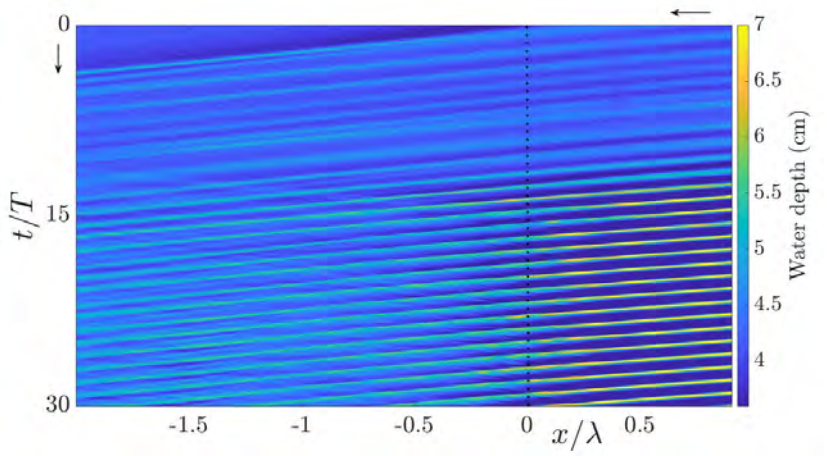

Figure 3.5: Spatio-temporal diagram of the free surface. Time evolves in the vertical axis from the top to the bottom, and x=0 corresponds to the beginning of the flat platform.

An example of the beach contour for a given time is shown in Figure 3.6. The detection of the beach contour from each photo allows the reconstruction of the beachface and the monitoring of its evolution.

While the beach profile evolves over time within a single experimental run, the limits may encompass an area that could introduce a slight error in the beachface. This area is associated with irregularities or breaks in the beach profile (see Figure 3.7).

The maximum error induced in one measurement due to these irregularities is calculated to be 20% in the worst-case scenario. However, given that one experimental test involves measuring more than 2400 beach profiles, the average evolution of the beachface slope is well captured, and the dispersion induced by the fixed limits can be considered negligible. This error does not significantly impact the analysis of the beachface slope evolution trend, as shown in Figure 3.8, which illustrates an example of the beachface slope evolution, where each measurements is plotted (blue circles) as well as it mean moving average between 50 measurements (black line). Furthermore, in the application of the model to study the beachface response to changing waves, we specifically focus on the equilibrium beach slope determined over a mean of 500 measurements, reducing the maximum error calculated for one measurement to 0.9%.

In conclusion, the errors introduced by the measurement equipment and extraction techniques for our main parameters are considered negligible in comparison to the magnitudes we are analyzing. Therefore, they will not be taken into account for the exploitation of this model. Although consideration of these errors could potentially lead to more quantitative estimations in future work, at present, their impact is minimal within the scope of our current analyses, and they do not significantly influence the conclusions drawn from our study.

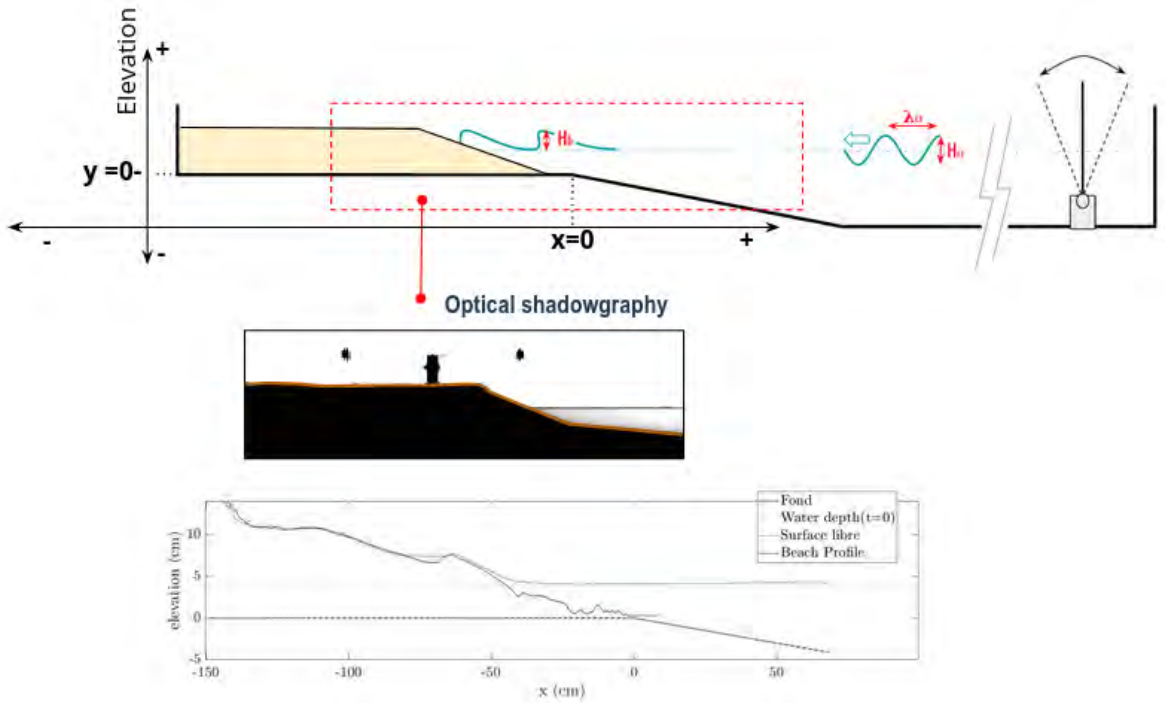

Figure 3.6: The top figure shows the sketch where the optical shadowgraphy is performed, the middle figure displays an example image captured by the high-resolution cameras with the detection of beachface contour, and the bottom figure shows a plot of the beachface profile at a given time extracted after the post-processing code.

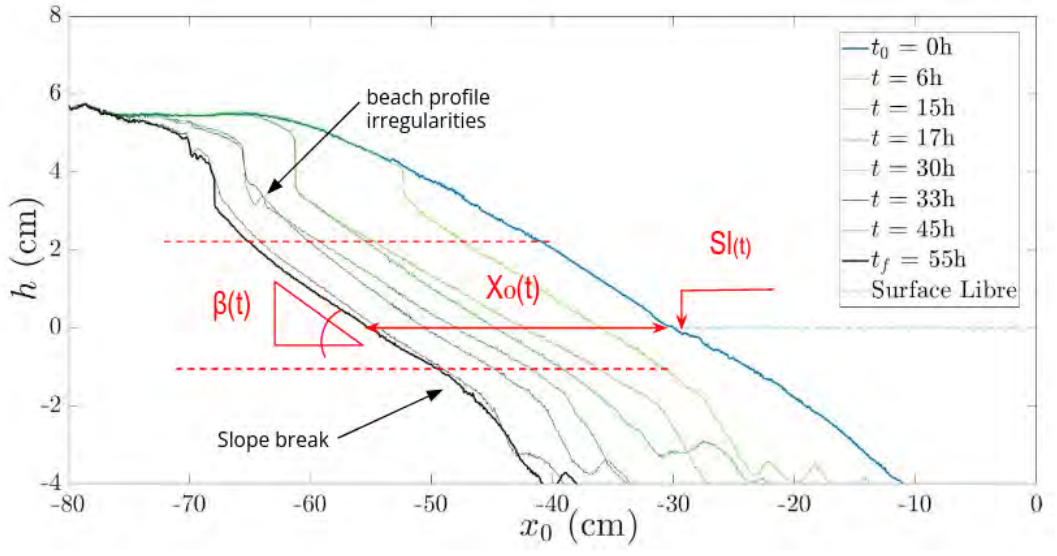

Figure 3.7: Beach profile extracted at 8 different moments of the experiments. The blue beach profile represents at start (no wave forcing) and the black profile (after 55 hours of receiving a constant wave forcing). The red dash line represents the limits for the extraction of the beachface slope ($\beta(t)$), the shoreline is represented by the parameter Sl(t) ad $X_0(t)$ represents the the distance of the shoreline to its initial position ($Sl(t = 0)$).

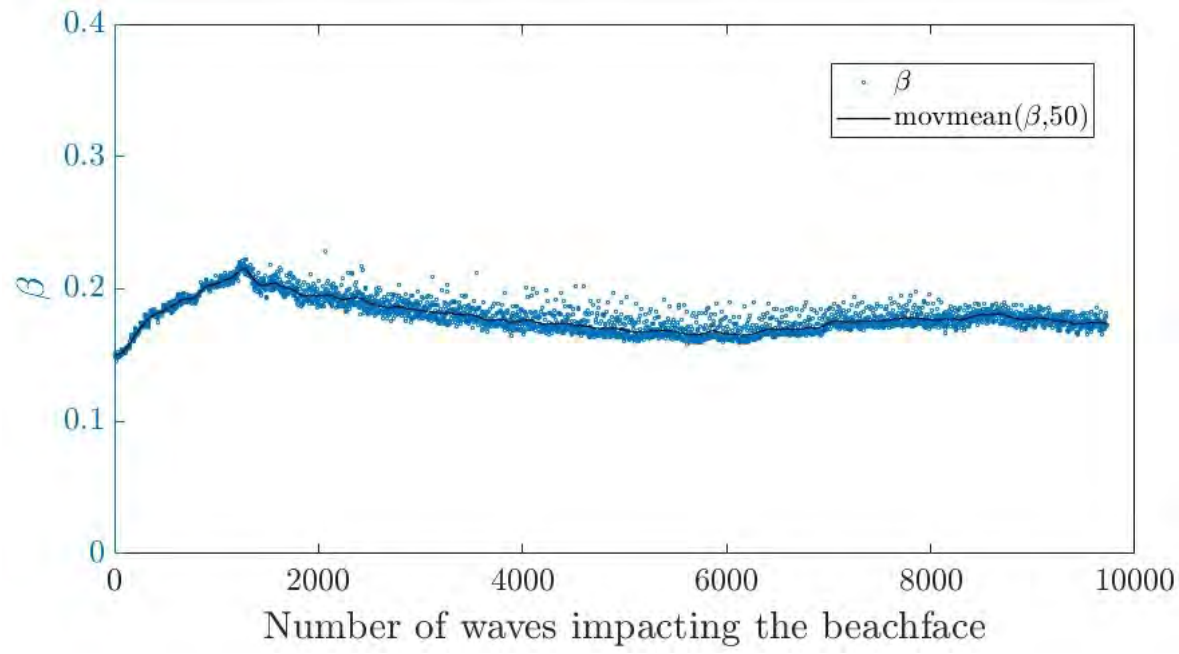

Figure 3.8: Example of beachface slope evolution extracted for a one test with an specific monochromatic wave action. Each circle represents a measurement of the slope taken in the experiment, and the black line is a moving mean of these measurements over 50 samples.

3.1.3 Characterization of wave regime in the LTT model

Off-shore wave forcing

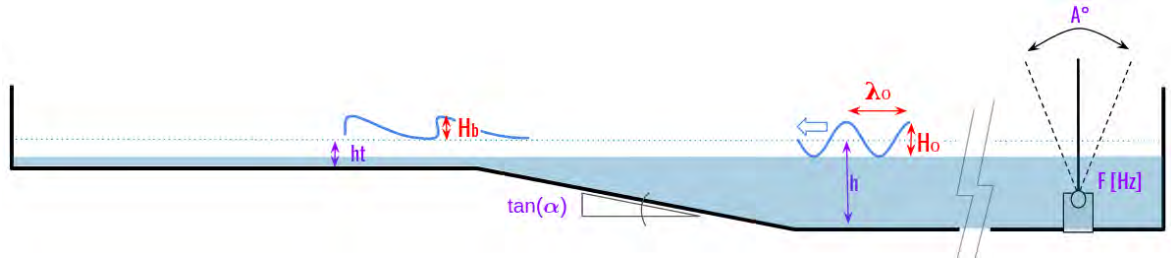

Figure 3.9: Hydrodynamic parameters of the LTT model.

A hydrodynamic study of the LTT model is conducted to examine the main controlling parameters and identify the hydrodynamics limitations of the model. Regarding specifically, the wave structure evolution in this unique bottom configuration (see Figure 3.9). The incoming waves characterised by the offshore wavelength and height (λ_0 and H_0 respectively) and the maximum bore height after breaking (Hb), is the responsible force for the upper beachface movement. These parameters are the governing parameters of the LTT model, and they can be manipulated either by adjusting the wave generator's amplitude and frequency (A an F), water depth (h referring to offshore and ht referring to the water depth on the

flat platform), as well as the rigid bottom slope (α) and length. Figure 3.9 provides a visual representation of these hydrodynamic parameters.

Therefore, it is essential to map the various types of waves that can be generated by manipulating the water level, wave generator, and the rigid bottom slope α. To avoid reproducing the same wave, and since our focus is on the rapid response of the upper beachface—rapidly adapting to changing waves compared to the rest of the beach profile—the rigid bottom slope and length are kept constant. The mapping of different wave types is achieved by adjusting the wave generator parameters and water depth. This approach allows the model to replicate natural conditions. Thus, the slope and length of the rigid bottom are set to $tan(\alpha) = 0.06$ and 2 meters, respectively, positioned 5.5 meters from the wave generator. These values were determined through a study of how the rigid sloping bottom dissipates wave energy. Additionally, this study provided a preliminary understanding and mapping of the waves that could be generated in this water flume, summarised in Figure 3.10.

Wave generator internal software inputs						Water Gauges				Observations
Test	Amplitude A (°)	Frequency F (Hz)	Periode T (s)	Speed Vmax (u/s)	Acceleration Acc (u/s2)	Wave height S1 (cm)	Wave height S2 (cm)	T_0 (s)	Wavelength λ(m)	Wave breaking
1	15	2,2	0,45	1037	12553	3,98	3,05	0,48	0,35	-
5	25	2,2	0,45	1728	20922	3,73	2,91	0,48	0,35	-
9	30	2	0,50	1885	20749	4	3,39	0,53	0,43	glissant
2	15	1,8	0,56	848	8403	4,09	3,58	0,57	0,49	glissant
6	25	1,8	0,56	1414	14006	5,54	4,67	0,58	0,5	glissant
10	30	1,8	0,56	1696	16807	4,46	4,06	0,58	0,5	glissant
13	10	1,6	0,63	503	4426	2,16	1,8	0,65	0,61	-
14	25	1,6	0,63	1257	11066	5,39	4,78	0,65	0,61	glissant
15	35	1,6	0,63	1759	15493	5,69	4,82	0,65	0,61	glissant
16	40	1,6	0,63	2011	17706	4,87	4,33	0,65	0,61	glissant
3	15	1,1	0,91	518	3138	2,12	1,61	0,93	1,04	-
7	25	1,1	0,91	864	5231	3,43	2,96	0,93	1,04	glissant
11	35	1,1	0,91	1210	7323	5,29	4,57	0,94	1,05	plongeant
17	50	1,1	0,91	1728	10461	6,98	6,38	0,94	1,05	plongeant
4	20	0,8	1,25	503	2213	1,56	1,19	1,26	1,5	-
8	35	0,8	1,25	880	3873	3,04	2,59	1,27	1,52	glissant / plongeant
12	50	0,8	1,25	1257	5533	4,39	4,17	1,27	1,52	plongeant
18	35	0,6	1,67	660	2179	1,87	1,59	1,65	2,04	glissant
19	50	0,6	1,67	942	3112	3,05	2,77	1,65	2,04	glissant

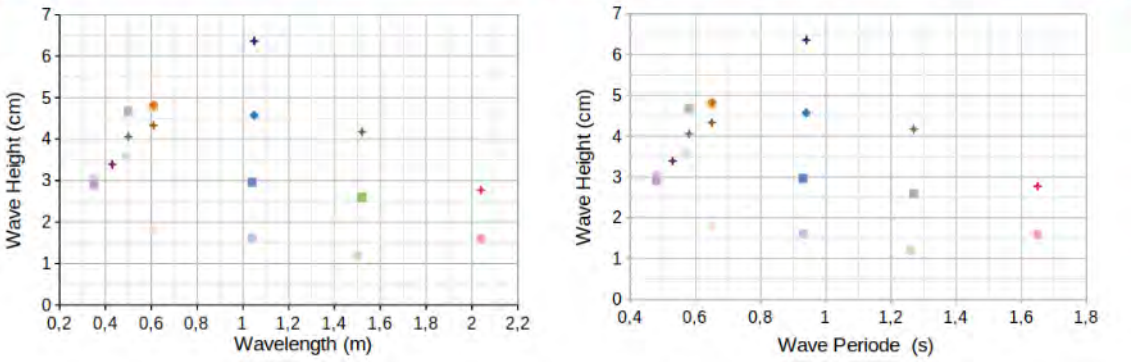

Figure 3.10: The top table links the software inputs controlling the flap wave generators with the wave characteristics extracted at water gauge 1 and 2. The two plots below depict all the waves generated, illustrated by their wave height vs. wavelength (on the left) and the wave period (on the right). These data corresponds to a water level of $h = 16$cm.

The various waves that the wave generator is capable of producing for a constant depth fixed at 16 cm offshore (h), corresponding to a water depth of 4 cm on the terrace (h_t), are summarized in Figure 3.10. The wave generator is controlled through the software Vectron Inverter Manager, and the table shown in Figure 3.10 links the software's internal inputs with the wave characteristics extracted from the two water gauges—the first ($S1$) located near the wave generator and the second ($S2$) before the sloping bottom (refer to Figure 3.2). The two bottom plots on Figure 3.10 map the waves generated by plotting the wave height against its wave length (left plot) and wave period (right plot); each color represents a fixed frequency of the wave generator, and the range of that color corresponds to different amplitudes of oscillation of the wave generator. All waves studied are monochromatic waves. In the present set-up, the wave structure is highly influenced by the water depth. The water depth is a critical parameter that can significantly alter the hydraulic regime of the model. Therefore, we need to consider the influence of the water depth (h and ht) on the wave forcing.

Wave evolution on the terrace: influence of the water depth

We present the results of a study on the influence of water depth on the wave forcings and examine the hydraulic limitations of the model. We focus on four wave regimes labelled WrA, WrB, WrC, and WrD, covering a wide range of different monochromatic waves. WrA represents the wave with the biggest wave height and the shortest wavelength, while WrD represents the wave with the smallest wave height and longest wavelength, while WrB and WrC are intermediate waves between these two extremes. These four scenarios are illustrated in Figure 3.11, where the table links the wave generator inputs with the wave characteristics at the water gauge just before the rigid slope. The four plots show the free surface evolution for each wave regime. These values correspond to a water level of $h = 16$cm and on the terrace of $h_t = 4$ cm. Having fixed these parameters allows us to establish a baseline to vary the water height (h and h_t) to observe how it modifies the wave characteristics.

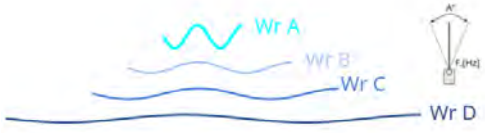

Wave Regime	Wave Generator		Wave characteristics		
	A [°]	F. [Hz]	H_o [m]	T_o [s]	λ_o [m]
A	30	1.4	4.7	0.74	0.75
B	30	0.8	2.5	1.28	1.50
C	40	0.6	2.3	1.69	2.00
D	50	0.4	2.1	2.50	3.10

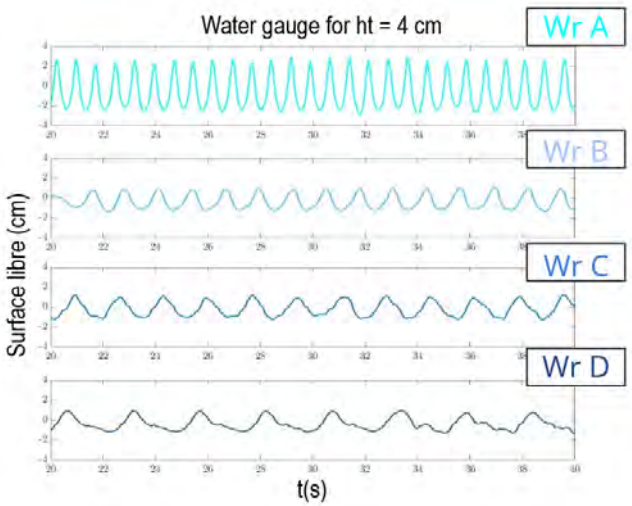

Figure 3.11: Table presenting the wave generator inputs and the extracted wave characteristics from water gauge 2 (just before the rigid bottom slope). The four plots depict the evolution of the free surface for the four wave regimes.

For each wave regime presented in Figure 3.11, we examine its spatio-temporal evolution on the sloping bottom and flat platform, as well as the wave height before and after breaking, considering six different water depths ranging from $h_t = 1$ cm to $h_t = 6$ cm at 1 cm intervals. Figure 3.12 presents the spatio-temporal evolution of the wave height for WrC entering the flat platform (starting at $x = 0$; moving away from the wave generator, we have negative values of x, and towards the wave generator, we have positive values of x). The position along the horizontal axis (spatial parameter x) is normalised by the wavelength, and the time by the wave period. In these plots, the red dashed line represents the wave speed under shallow water conditions, which is the regime we expect to observe on the flat platform.

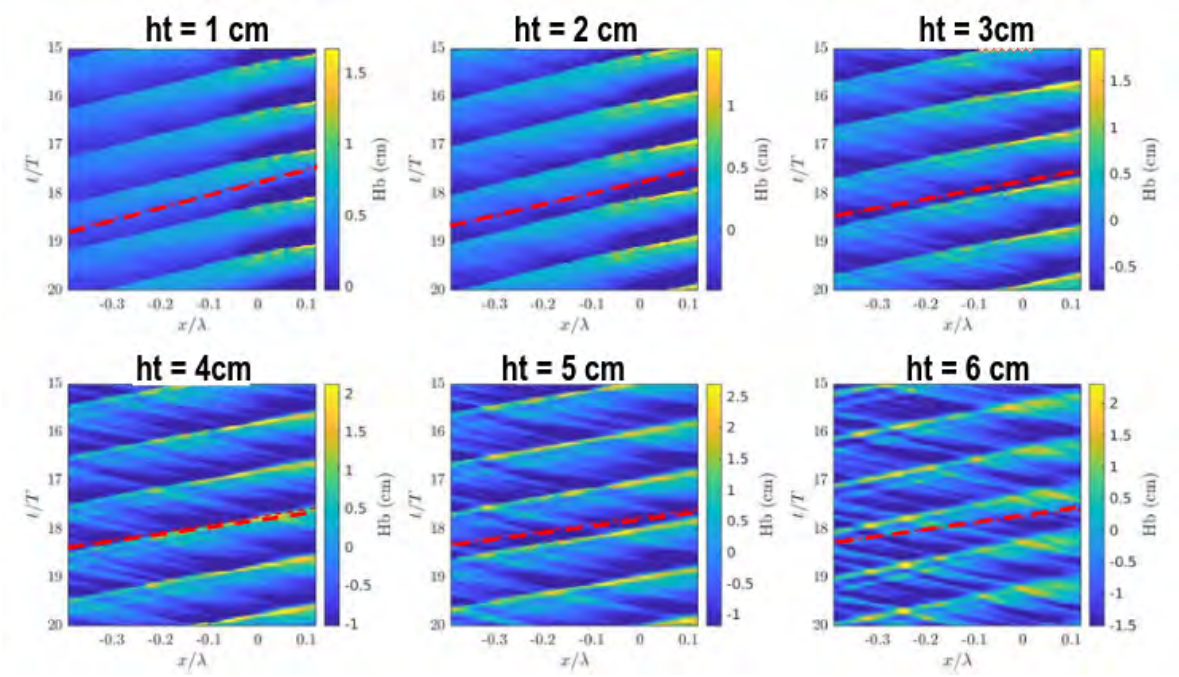

Figure 3.12: 6 plots of Spatio-temporal evolution of the wave height in the flat platform (H_b) for waver regime C (WrC) for water depth on the terrace going from water level on the terrace from $ht = 1$ to $ht = 4$cm

The observed trend in Figure 3.12 indicates that, as the water depth on the terrace increases, we deviate from the weakly dispersive shallow water theory. This transition allows us to discern when the waves entering the flat platform after breaking transform into bores. In other words, for lower water depths, we align well with the shallow water regime, but for water depths of $h_t = 5$ and 6 cm (the highest water depths tested), we deviate from this theory, resulting in more dispersive waves. These situations are undesirable, and therefore, we exclude water depths of 5 cm and 6 cm from further analysis.

Another important remark is that, even though an increase in water height leads to more pronounced reflections due to the closed system, we consistently observe propagative waves, and no basin waves are observed. Therefore, it can be expected that even when placing a reflective beach (steep beachface slope) due to the long extent of the water flume,

unwanted basin waves are avoided. This is more evident, especially for lower water level heights. However, at very low heights, the energy of waves significantly diminishes after breaking, making them too weak to impact the beach. Consequently, for the remainder of the study, we focus on waves generated at a water height on the terrace of 4 cm. This represents a good compromise between staying within the shallow water theory and having more energetic waves in the surf zone.

While Figure 3.12 specifically illustrates wave regime C, it's important to note that the trends and observations depicted are representative of the other three wave regimes (WrA, WrB, and WrD). Our analysis across all four wave regimes consistently revealed similar patterns, reinforcing the validity of the observed phenomena.

Wave evolution on the terrace: bore dynamics

In addition, we performed an analysis comparing the wave height before the shoaling processes, captured before the rigid slope H_0, and the maximum wave height after breaking H_b (representing the bore entering the surf zone) for the four wave regimes and water depths ranging from 1 cm to 4 cm. This comparison is illustrated in Figure 3.13, where each symbol represents a wave regime. This symbolism will be maintained throughout the manuscript: circles for WrA, squares for WrB, triangles for WrC, and diamonds for WrD. The smallest symbols represent the lowest water height. An important observation is that, for each given water height (e.g., $h_t = 4$ cm represented by the red line on the right), we notice that the amplitude of the bore generated after breaking is controlled by the water height on the terrace. Regardless of the forcing characteristics before breaking, H_b remains consistent.

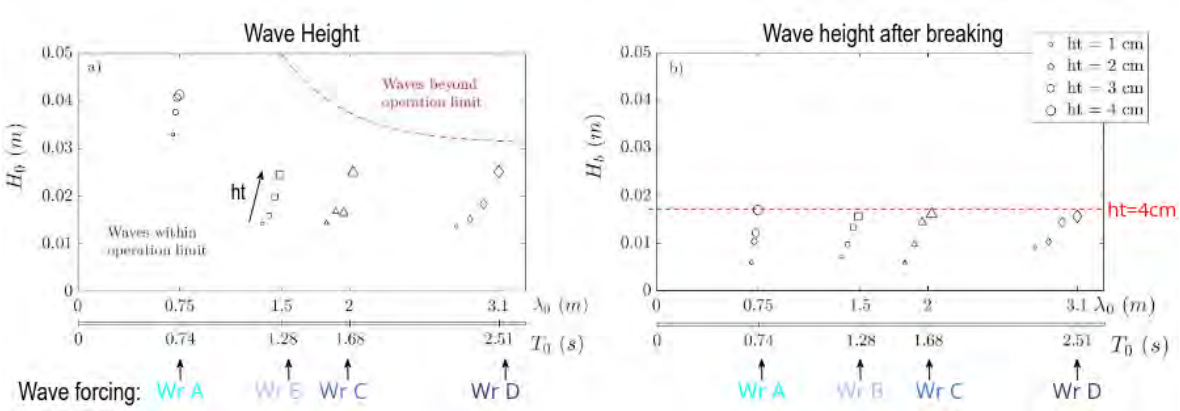

Figure 3.13: Characterization of the four wave regimes defined by their period or wavelength (x-axis) versus the wave height (H_0) at the beginning of the rigid slope (left plot) and the maximum bore height (H_b) entering the flat platform (right plot). Each symbol represents a specific wave regime, and the size of the symbol corresponds to the water depth where that wave regime was tested

Now, our focus shifts to quantifying how the bore dissipates within the flat platform and the influence of water height on this dissipation. We tracked the maximum bore height evolution on the terrace for each wave forcing performed at the four water levels ($h_t = 1 - 4$

cm), as represented in Figure 3.14. To facilitate comparisons between different cases, we normalized the bore height (H_b) and position on the terrace (x) by the water depth (h_t). The attenuation for the different wave regimes appears to follow a uniform pattern. Therefore, we propose introducing an exponential attenuation law for the bore on a flat platform expressed as $\frac{H_b}{h_t} = \gamma[1 + \frac{1}{\gamma}e^{\sigma(\frac{x-x_0}{h_t})}]$. Here, γ represents the bore height normalized by the water level on the terrace far away from the breaking point, and σ is an attenuation coefficient characterizing the extent of the attenuation length after breaking. Both fit coefficients depend on the water level on the terrace.

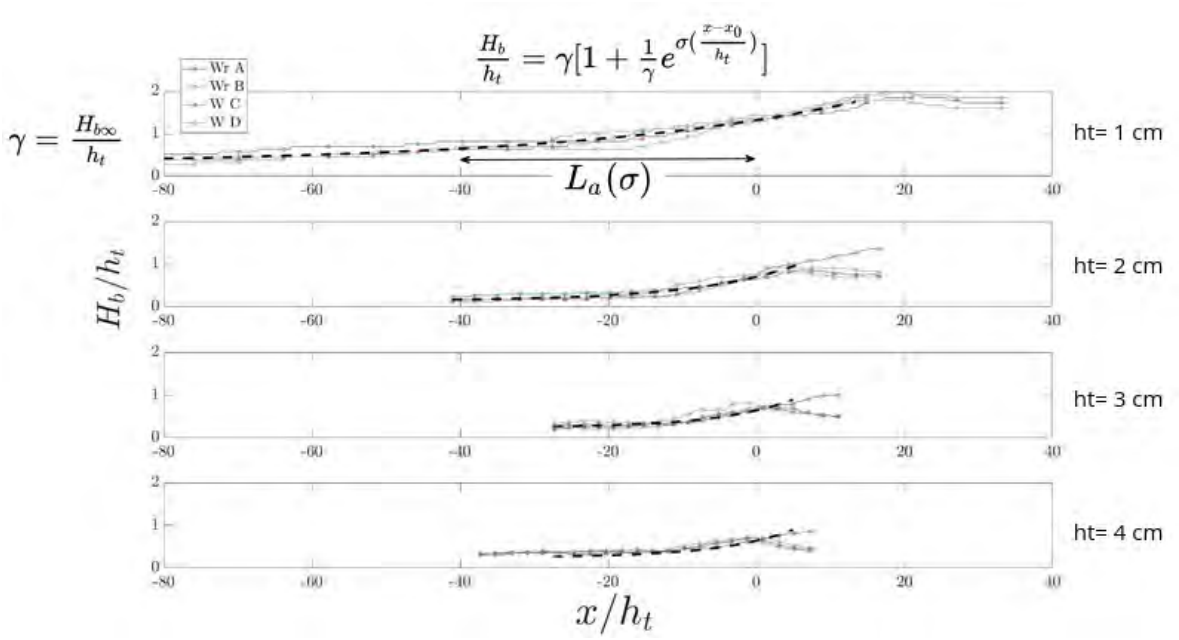

Figure 3.14: Evolution of the maximum bore height on the terrace, normalized by the water level on the terrace, for each wave regime. Each plot corresponds to a different water level on the terrace. The dashed black lines represent the proposed exponential fit, illustrating the bore dissipation law on the flat platform.

Figure 3.15 presents the fit coefficients of the attenuation law (γ and σ) for the four water depths. Although we only have four data points, and therefore extracting a trend is not possible, we observe that if gamma remains relatively constant, the height away from the terrace is proportional to the water height on the terrace. For sigma, we notice a slight increasing trend, suggesting that sigma increases with water height. However, as we only have four points, it is difficult to determine a trend, further investigation is needed. Nevertheless, this attenuation law will be used in the following section when analyzing the impact of the wave on the upper beachface to represent the dissipation of the bore on a flat platform.

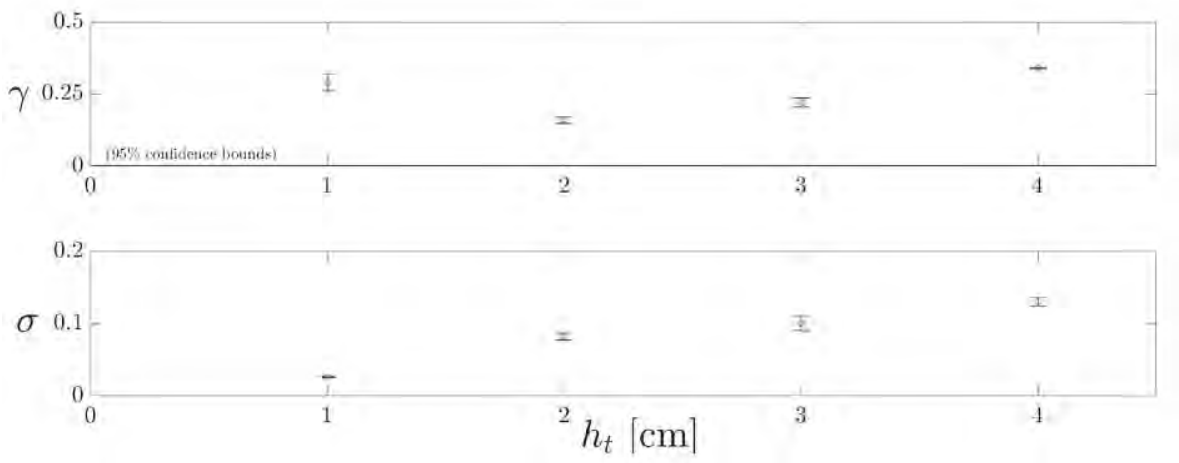

Figure 3.15: Evolution of fit coefficients for the different water depths: upper plot shows the variation of γ (bore height normalized by the water level on the terrace far away from the breaking point), while the lower plot displays the variation of σ (attenuation coefficient characterizing the extent of the attenuation length after breaking).

3.1.4 Dimensionless analysis for Scaling the LTT model

Having delved into the hydrodynamic behaviour of our LTT model in the preceding section, we can now explore the scaling of the model. This involves a comparison of dimensionless physical number between out model an the available field data from the two LTT terrace beaches presented in Chapter 3 (Nha Trang and Grand Popo). Inspired by Grasso et al. (2009), we calculated various dimensionless physical numbers and compared them with field values. These physical number include the Froude number, which is written a

$$F = \frac{H_0 \omega_p}{2\sqrt{gh}} \quad \text{with} \quad \omega_p = \frac{1}{T_0}; \tag{3.1}$$

where H_0 and ω_p are the offshore wave height and angular frequency, respectively. These values were extracted from the water gauge placed at the bottom of the rigid slope (S2). For the computation of the water depth h, in the laboratory, we used $h = 0.16$ cm, representing the closure depth in our experiment. In the field data, we used the following expression: Depth $h = 4H_s$, where H_s is the significant wave height.

For the Reynolds number we used the following formulation

$$Re = \frac{A\omega_p h}{\nu} \quad \text{with} \quad A = \frac{H_{rsm}}{2\sinh kh}; \tag{3.2}$$

where ν is the fluid viscosity, A is the particle excursion at the bottom, with k corresponding to the wave number and H_{rms} the root mean square wave height. In the laboratory, we

considered H_0 for H_{rms}, and for the field, we simplified and used the significant wave height. The water depth is calculated in the same way as for the Froude number. Additionally, the Particle Reynolds number is calculated using the following formula

$$Re_p = \frac{A\omega_p D_{50}}{\nu} = Re\frac{D_{50}}{h}. \tag{3.3}$$

To analyze the transport similitude, we used the Shields and Rouse numbers, applying the same method as in Grasso et al. (2009). The Shields number is defined by

$$\theta = 0.5 f_w \frac{(A\omega_p)^2}{g\left(\left(\frac{\rho_s}{\rho} - 1\right) D_{50}\right)} \quad \text{with} \quad f_w = \exp\left[5.213\left(\frac{2.5D_{50}}{A}\right)^{0.194} - 5.977\right]; \tag{3.4}$$

where f_w is a wave friction factor, approximated with the formula proposed by Swart (1975) as detailed above. ρ_s represents the sediment density, and ρ is the fluid density. On the other hand, for the Rouse number, the following formula was employed:

$$R_{\text{ou}} = \frac{W_s}{u'} \quad \text{with} \quad u' = \kappa\sqrt{\frac{f_w}{2}} A\omega_p; \tag{3.5}$$

where W_s is the sediment fall velocity, measured in the laboratory and for the field calculated with the Van Rijn (1993) formulation. u' is the turbulent intensity of the flow field, with κ being the von Karman constant (0.4) (Soulsby, 1997). The Dean number is also included in the scaling analysis, and the equation is given in Equation 2.1.

It is essential to note that maintaining complete similarity for all dimensionless numbers between the field and our small-scale physical model is not possible. Nonetheless, we prioritise the crucial physical numbers of the system, and those not entirely matched are considered for result interpretation. The comparison of these physical numbers between the laboratory model and the field data is given in Table 3.1.

Table 3.1: Table representing the physical dimensionless numbers for the scaling of the LTT model

Experiment	D_{50} [mm]	Wave Climate	H_0 [m]	T_0 [s]	W_s [cm/s]	Froude F	Reynolds Re (x $10^4)	Particle Reynolds Re_p	Dean Ω	Shields θ	Rouse Rou
Laboratory	0.120	Wc A	0.040	0.74	0.74	0.150	1.77	13.32	8.58	0.097	0.47
		Wc B	0.025	1.28		0.049	1.34	30.93	2.63	0.049	0.76
		Wc C	0.023	1.69		0.034	1.29	28.79	1.83	0.040	0.85
		Wc D	0.022	2.51		0.022	1.32	28.79	1.13	0.035	0.91
	0.260	Wc A	0.047	0.74	3.40	0.150	1.77	107.46	1.86	0.067	1.85
		Wc D	0.025	2.51		0.022	1.32	62.38	0.25	0.023	3.66
Nha Trang	0.60	Wc NT	0.920	4.09	8.4	0.110	307.01	1462	1.5 - 5.0	0.39	1.22
Grand Popo	0.60	Wc GP	1.470	8.89	8.4	0.068	102.67	3384	1.5 - 2.5	1.32	0.63

Analyzing the dimensionless numbers involving hydrodynamic parameters, we find accuracy in the Froude number, while for the Reynolds number, there are discrepancies. However, we still maintain a turbulent regime in our model. Regarding the Dean number, we intentionally ensured its coincidence with field values to maintain consistency and tried to vary it as much as possible in our model, using it as a control parameter for the upper beach response to changing waves. Subsequently, examining dimensionless numbers representing the transport regimes of the system, we calculated the Shields and Rouse numbers. We observe good similarity for the Rouse number, which in our model varies more than in the field, allowing us to analyze its influence on the system. On the other hand, the Shield number calculated for our model would indicate lower energy and less suspended material compared to the field. Nevertheless, we verified that in our model, we had intense suspended sediment transport. Both the Shield and Rouse numbers provide information about the transport regimes. Since the Shield number is calculated using an empirical relationship that might not be representative of our model due to simplifications made, we will not include it in our analysis, but we will consider this difference for the interpretation of our results.

3.1.5 Preliminary Results of the LTT Model

To validate our model, a series of long-term tests were conducted to observe the dynamics of the beachface and extract characteristic timescales from the physical model. These tests involved subjecting the beachface to a constant monochromatic wave (selected based on the previous analysis) impacting the beachface at various positions on the flat platform for duration ranging from 1 to 150 hours. Several wave forcings were tested for different initial beachface positions. The tests revealed two distinct temporal scales in the beachface slope dynamics, as illustrated in Figure 3.16.

Firstly, a rapid evolution of the slope to a quasi-equilibrium value was observed, fluctuating around $tan\beta_{eq} \sim 0.2$. Secondly, a slow evolution of the slope was identified, related to a sediment deficit regime due to the absence of sediment input into the system. The rapid evolution of the beachface slope to the quasi-equilibrium value was consistently achieved within the initial two hours of each run. An illustrative example of a 12-hour experiment is presented in Figure 3.16.

It is important to note that our model, as explained in the previous sections, was designed to characterize the rapid response of the beachface slope to changing waves. Consequently, the slow morphological evolution associated with sediment deficit is not considered, given our strong assumption that the only erodible part of the model is the upper beachface. Therefore, the model is validated for the analysis of rapid beachface slope adjustments to changing waves. For the application of the model, we will concentrate on runs that are not longer than 2 hours, and the interpretation of this timescale will be discussed in the following sections.

The primary application of the model is to investigate how the beachface slope responds to changing waves. To achieve this, we will systematically vary the initial beachface position to the breaking point and initial slope (L_{t_i} and β_i) and subject it to constant wave forc-

ing. By doing so, we aim to observe the rapid evolution of the beachface slope towards an equilibrium state within the initial two hours. Therefore, when we alter the initial state of the beachface and apply a specific forcing, what we are changing is the initial distance from equilibrium. These manipulations will effectively represent the transition from one out-of-equilibrium system to another. The entire system will never be in equilibrium as there are no sediment inputs. Nevertheless, we will focus on q quasi-equilibrium state which we refer to a rapid equilibrium state of the beachface slope. The results of this study is presented in the next two sections of this Chapter in the form of two articles. One of the articles has been submitted for review in the Coastal Engineering Journal, while the other is currently in preparation for publication. The sections that follow correspond to these articles.

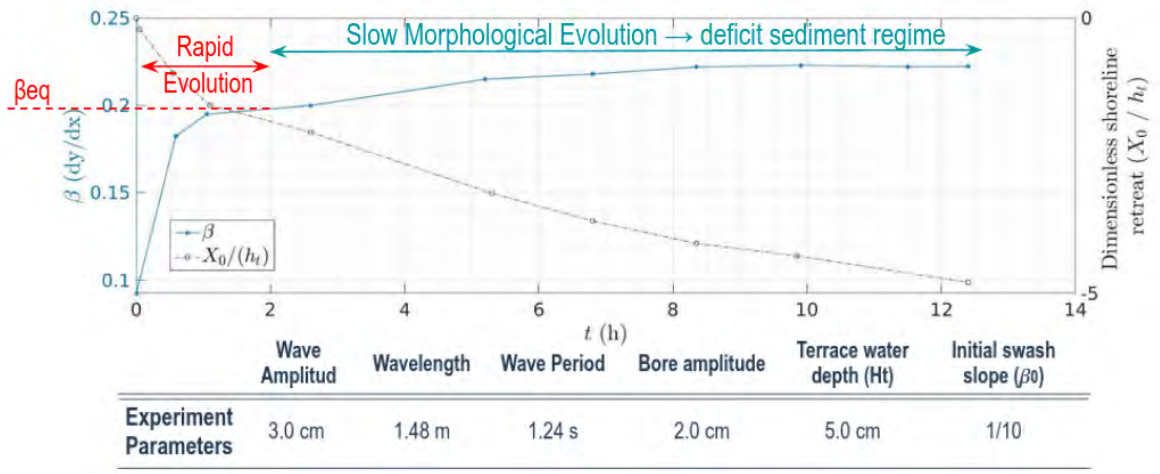

Figure 3.16: Example of a long-term experiment curried out with a monochromatic wave forcing conducted for 12 houres. The experiment parameters are shown at the bottom of the Figure. The evolution of the beachface slope ($\tan\beta$) is represented by the blue line and represented by the dashed black line is the shoreline retreat normalized by the water depth on the terrace (X_0/H_t).

3.2 Control of a Flat Lower Platform on the Upper Beach Slope

3.2.1 Abstract

The beach slope β is a key component characterizing the coastal response to wave forcing. Here we investigate the rapid adaptation of the upper beach slope to a given wave forcing, for the case of a lower flat platform. Such types of morphology are found on coral and rocky reef beaches and low tide terrace environments. The influence of the lower platform on this equilibrium beach state is shown to be significant depending on the breaking wave regime. In particular, the width of the platform and its water level can affect the wave dissipation along the inner surf and thus the wave structure entering the swash. This paper provides a classification of the beach slope equilibrium values as a function of the Dean number on a short time scale, based on both offshore and swash wave conditions. A decreasing trend of the beach slope with increasing offshore Dean number (Ω_0) is found for $\Omega_0 \gtrsim 2.08$. For $\Omega_0 \gtrsim 2.08$ it is observed that the beach slope gradient is strongly controlled by the surf zone dissipation and it becomes necessary to define the swash Dean number (Ω_{sw}) to classify the slope. Finally, a semi-empirical formula for the beach slope evolution in the case of a low tide platform is introduced and tested on two natural low-tide terrace beaches.

Keywords: Beach slope, hydro-morphodynamics, physical modelling, Dean number, swash zone, resilience, low tide terrace beach

3.2.2 Introduction

The swash zone is considered the most dynamic region of the coastal zone, characterized by highly unsteady and turbulent currents, large sediment transport rates and rapid morphological changes (Puleo, 2009; Kikkert et al., 2013). Understanding the dynamics of wave action therefore remains a challenge for coastal scientists, although much effort and progress has been made in recent years. Unfortunately, useful and classical models such as the Bruun rule (Bruun, 1954, 1962), the Dean equilibrium profile (Dean, 1977, 1991) or more complex cross-shore equilibrium models (Yates et al., 2009; Castelle et al., 2014b; Lemos et al., 2018) are not designed to predict rapid morphological changes such as those observed in the swash zone. To improve the prediction of swash evolution, numerical models have been developed to capture the swash dynamics with different levels of complexity (Larson et al., 2004; Pritchard and Hogg, 2005; Steenhauer et al., 2012; Briganti et al., 2016, see for example). These models have been obtained and/or validated from extensive series of experimental and field measurements and are used to aid in the understanding of swash morphodynamic systems. Despite these recent advances in swash modelling, the prediction of the correct net sediment transport rates and morphological changes in the swash zone are still lacking specific details and need to be improved (Chardón-Maldonado et al., 2016; Bakhtyar et al., 2009). In addition, high quality field measurements are needed to validate and develop all these numerical models. This is a concern because field measurements of sediment transport and fluid motions in the swash

zone are very difficult to obtain and analyze due to the complexity of the highly nonlinear and unsteady processes occurring simultaneously in this zone (Guza and Thornton, 1982; Puleo et al., 2003; Miles and Russell, 2004; Masselink et al., 2005; Masselink and Puleo, 2006; Turner et al., 2008). The improvements in swash knowledge will come from the development of numerical, analytical, and experimental data that will require both field and laboratory studies. This work seeks to improve the knowledge and understanding of swash dynamics by using a simplified laboratory model designed to identify, isolate, and control the specific processes that occur when approaching the swash region.

The morphology of the swash zone is characterized in part by the local beach slope (β), defined as the portion of the beach profile below the berm exposed to individual wave excursion and tidal cycles (Masselink and Li, 2001)). This slope (β) is considered a key morphological parameter of swash dynamics as it affects the relative influence of wave energy dissipation and reflection at the shore, the excursion of wave run-up at the shore, and thus the direction of net sediment flux, i.e. accretion vs. erosion as sediment exchange between land and ocean (Almar et al., 2017a, 2019a,b; Martins et al., 2017). The beach slope (β) continuously adapts to changes in hydrodynamic forcing, leading to a wide range of complex feedback mechanisms between morphology and hydrodynamics (Bernabeu et al., 2003). These mechanisms are the drivers of hydro-sedimentary system evolution, and the complexity is given as these feedback processes are highly non-linear and scale dependent, both temporally and spatially. It is known that β responds very quickly to wave forcing from seconds, hours to days (Hughes et al., 1997; Butt and Russell, 1999; Puleo et al., 2003; Masselink and Puleo, 2006; Almeida et al., 2020), consequently the response of the beach slope to wave forcing will have an important role on the local swash dynamics and on the hydro-morphological interactions between different inner-shore zones. In order to capture the rapid fluctuations of the beach slope to changing waves, the physical model used in this study is coupled to a short time scale (several tidal cycles).

Since early research, it has been attributed by many authors that beach slope increases with increasing average sediment size (Bagnold, 1940; Masselink et al., 2016; Bascom, 1951; Turner, 1995; Reis and Gama, 2010; Bujan et al., 2019). Much effort has been invested in the relationship between beach slope and sediment size, providing a significant amount of empirical relationships for predicting the slope. Most of these expressions show a power law dependence of slope on mean sediment size, D_{50} (Sunamura, 1984; Soares, 2003; Reis and Gama, 2010). In a recent paper, Bujan et al. (2019) extracted over 2000 measurements of beach slope with associated grain sizes from available data in the literature and tested several empirical and numerical equations on this large data set. They proved that even the most representative of these equations cannot describe the full distribution of the data set. These data show a large variability of the slope (β), probably due to the wide range of data sources and therefore beach specificities, such as their instantaneous state compared to the equilibrium profile to wave forcing. The empirical relations (β-D_{50}) can therefore be used to predict the beach slope in a highly generalized form, but they still lack the physical basis to provide a clear link to swash dynamics. In particular, the strong influence of the grain diameter D_{50} on the beach slope is probably due to the sediment fall velocity, which is known to influence the transport regime relative to the wave dynamics. Following recent field results provided by

Mingo et al. (2021), the present study therefore focuses on the relationship between the beach slope and the dimensionless sediment fall velocity, also known as the Dean number (β-Ω_0), based on the incoming wave characteristics.

The Dean number allows one to anticipate suspended sediment transport and direction by relating the offshore wave height (H_0) and peak period (T_0) to the sediment fall velocity (W_s). It is defined as $\Omega_0 = H_0/W_s T_0$ and can be interpreted as a dimensionless fall velocity or as a length scale ratio, since $\Omega_0 = H_0/H_g$ is the ratio of wave height to a typical height over which sediment settles during a wave period ($H_g = W_s T_o$) Dally and Dean (1984). Then, if $\Omega_0 = H_0/H_g >> 1$ sediments in suspension fall to a short height compared to the spatial dimension of the wave, meaning that sediment may remain in suspension and therefore be more subject to transport between different zones of the inner beach by mean flow currents over the water depth. This is usually the case for offshore sediment transport due to return flow across the water column. On the other hand, if $\Omega_0 = H_0/H_g << 1$, the sediment will settle before the arrival of the next wave, so sediment transfer between zones will be limited and local morphological changes can be expected. In this case, grains remain close to the bottom, which is usually the case for onshore transport. The Dean number is more conveniently used in microtidal beaches, where the environment is wave-dominated, to classify beaches into different morphological states. Because of its link to the direction of sediment transport, global cross-shore beach profiles can be described by this dimensionless number and classified into dissipative ($\Omega_0 > 5$), intermediate ($1 < \Omega_0 < 5$), and reflective ($\Omega_0 < 1$) states. Dissipative beaches are usually characterized by a small slope β, while reflective beaches are the opposite with a steep slope (Wright et al., 1984; Short, 1996). Note that the Dean number is an important dimensionless number used in the coastal literature to classify equilibrium beach profiles on annual or seasonal time scales. The focus of this paper is to determine whether this number remains relevant for analyzing swash morphology on short timescales.

Recent results obtained by analyzing field data from two low tide terraces (LTT) have shown interesting correlations between the beach slope (β) and the Dean number (Mingo et al., 2021). Although these two LTT beaches have similar sediment sizes, two contrasting behaviours have been observed that stand as sub-classes of the main group of low-tide terrace beaches of Wright et al. (1984). One is a swash regulated beach (SwRB) operating in a more reflective regime where the terrace is not active and energy dissipation is mainly produced in the swash zone. An active swash is observed, characterized by rapid and localized morphological changes of the beach face, the terrace becoming a consequence of the high dynamics in the swash zone. In this case, the Dean number remains lower than 2.5 ($\Omega_0 < 2.5$) and β is shown to decrease with increasing Ω_0 up to $\Omega_0 \approx 2.5$. On the other hand, the second subclass of low tide terrace beach is a surf regulated beach (SRB), where the swash zone is strongly controlled by the wave energy dissipation on the surf zone (low tide terrace). In this case, the beach was strongly affected by seasonal variations with a Dean number varying in a wide range from 1 to 6. This results in an active beach that fluctuates from a LTT dominated beach to a swash beach. When $\Omega_0 > 2.5$, the presence of LTT and its length are correlated with Ω_0, clearly highlighting SRB behaviour. When $\Omega_0 < 2.5$, the LTT disappears, suggesting a SwRB transition. Along this type of LTT beach, strongly affected by the surf, a correlation between the upper beach slope β and Ω_0, even if obtained, remains less obvious. The role of

the LTT length is probably of influence here.

Following this recent relationship between the beach slope β and the Dean number Ω_0, a laboratory-scale physical model is proposed to focus on two open questions related to previous observations. 1) Is the correlation between β and Ω_0 for SwRB ($\Omega_0 < 2.5$) a universal concept associated with a direct wave-by-wave forcing on the upper part of the beach? 2) How does LTT affect the upper beach response for SRB ($\Omega_0 > 2.5$) where the swash zone may be regulated by surf zone processes?.

The physical model proposed below is therefore designed to detail the response of the beach slope to single wave forcing on a short time scale. For this purpose, different initial geometric conditions are considered by varying the initial beach slope and the initial terrace length to highlight the relationship between β and Ω_0 depending on the influence of the terrace. A new beach slope predictor is then introduced for beaches with flat lower platforms. The results are discussed in relation to the aforementioned field observations of two LTT beaches, one at Nha Trang Vietnam (NT), the SRB case, and the other at Grand Popo Benin (GP), the SwRB case (Mingo et al., 2021).

3.2.3 Laboratory-scale physical model

A nearshore model is built into a laboratory wave flume. The specific aspect of this physical model is to focus only on the swash zone and its beach slope, keeping the breaking point fixed and the surf zone non-erodible, i.e. disregarding morphological changes beyond the swash zone. This allows a simple connection between the zone of interest and its associated morphological response to the offshore wave forcing, ignoring the morphological evolution of the entire coastal zone. Since this model is mainly concerned with the evolution of the beach slope due to wave forcing, only the short time scale period is considered. According to the initial geometric position of the beach face with respect to the breaking point and the initial slope β, initial dissipative to reflective conditions can be reproduced.

Experimental set-up

The nearshore physical model is designed to illustrate the dynamics of the beach slope under single wave action. This model is built into a unidirectional wave flume (12.65 m long, 0.3 m high, and 0.15 m wide) with an oscillating flap paddle wave generator at one end of the flume. A sketch of the experimental setup is shown in Figure 3.27.

The nearshore is modelled with a rigid wave breaking mechanism to keep the breaker position fixed around $x = 0$ (x is aligned with the wave propagation along the channel). This mechanism consists of a rigid gentle slope $\tan(\alpha) = 0.06$ from $x = 2$ m to $x = 0$ then reaching a rigid horizontal platform (not erodible) for $x \leq 0$. The characteristics of the offshore wave, amplitude and period, are determined at the bottom of this fixed slope ($x = 2$) using a tide gauge (see figure 3.27); the associated wavelength is calculated using linear wave theory. The amplitude of the wave increases along the slope. For the range of offshore forcing considered along the paper, this system keeps the breaking point fixed around $x = 0$. For $x < 0$, the

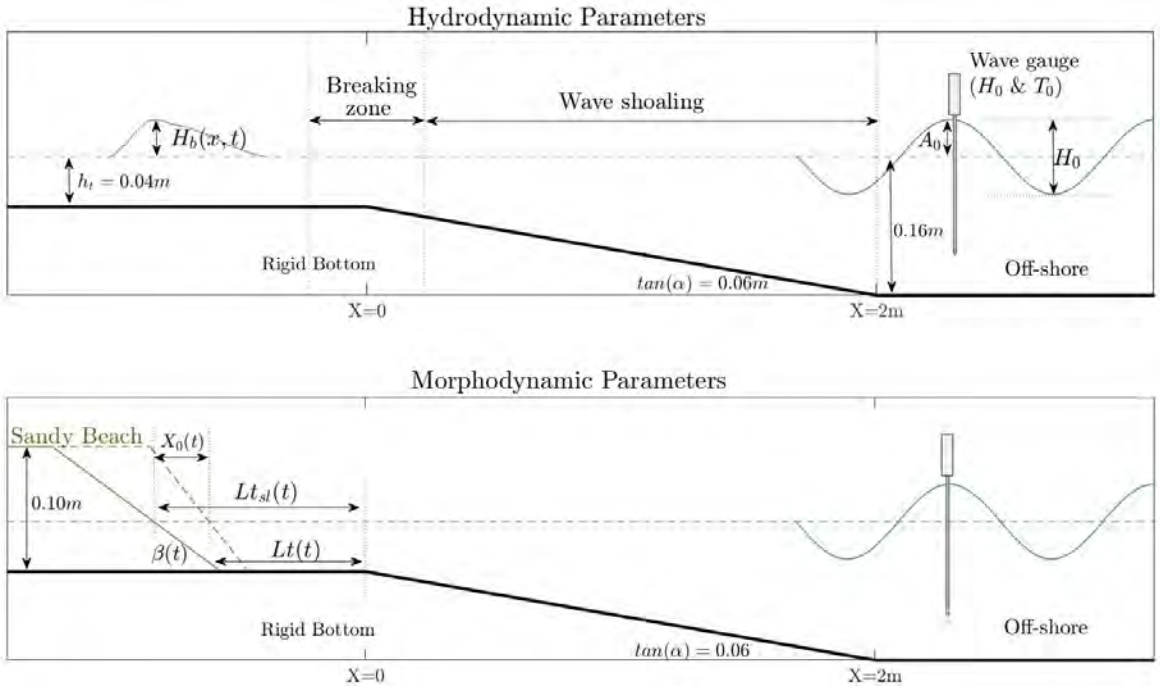

Figure 3.17: Sketch of the experimental setup. (a) Hydrodynamic parameters: $H_b(x,t)$ is the maximum wave amplitude after the breaking processes, H_0 & T_0 wave amplitude and period at the bottom of the fixed gentle slope using a wave gauge. (b) Morphodynamic parameters: $\beta(t)$ is the slope of the beach face, $Lt_{sl}(t)$ is the distance from the breaking point to the shoreline, $Lt(t)$ is the distance from the breaking point to the bottom of the beach face, and $X_0(t)$ is the shoreline retreat.

horizontal platform models the inner surf zone of a terraced beach. At the end of this terrace, a sloping sandy beach models the erodible beach face. The surf zone is characterized by a dissipation length, L_t, between the breaking point and the beach face. The erodible beach face, or equivalently the swash zone, consists of sand with mean size $D_{50} = 0.12$mm and relative density $s = 2.65$. The mean sediment size (D_{50}) chosen here allows to scale the range of Dean numbers obtained in the experimental setup similarly to the field. Furthermore, the mean water depth on the terrace $H_t = 4\,$cm is fixed for all experiments.

An experiment then consists of generating a monochromatic wave force, characterized by its amplitude H_0 and period T_0, for two hours starting at $t = 0$. After breaking at $x = 0$, the wave bore develop along the surf zone, of initial length $Lt(t = 0) \equiv Lt_i$ and constant depth H_t, before hitting the erodible beach surface of initial slope $\beta(t = 0) \equiv \beta_i$ (see figure 3.27). Note that the initial terrace length is also characterized by the initial distance of the shoreline position from the breaking point $Lt_{sl}(t = 0) \equiv Li_{sl}$, which is related to Li_{sl} as $Lt_{sl}(t = 0) = Lt_i + H_t/\beta_i$. Inner-surf dynamics and beach-surface morphodynamics are monitored using an optical attenuation light method, as explained later. The two hours of wave forcing correspond to about 3000 individual waves, depending on the wave period, hitting the beach face. In the field, this is in the range of a tidal cycle for wave periods around 10 s. This is therefore considered a rapid response of the beach face to a given wave forcing

compared to seasonal or annual morphological changes. The specificity of the proposed model is that, depending on the initial condition of the inner-surf morphology (β_i, Lt_i) and the wave conditions (H_0, T_0), different swash and beach states, close or not to equilibrium, in either dissipative or reflective conditions, can be easily considered.

The evolution of the beach face and the dynamics of the inner surf are then characterized as a function of time and cross-shore direction by the distances of the beach face to the breaking point $Lt_{sl}(t)$ and $L_t(t)$ and the associated shoreline motion $X_0(t) = Lt_{sl}(t) - Li_{sl}$, the beach slope $\beta(t)$ and the bore height $H_b(t, x)$. High resolution sCMOS-Lavision cameras are used to extract the spatio-temporal evolving interfaces of the free surface and the sand bed. A light attenuation technique, shadowgraphy, is used for this purpose. A uniform LED backlight is placed behind the experiment, from the camera point of view, allowing to extract side views of the experiments. This allows to obtain high quality time series images of the evolution of the beach face profile and the wave evolution on the sloping fixed bottom, the terrace and the beach face. Using the optical shadowgraph technique, the evolution of the free surface $H_b(x, t)$ in the inner-surf, the beach slope $\beta(t)$ and the shoreline position $Lt_{sl}(t)$ (as defined in the sketch of figure 3.27) are extracted from the collected images. Note that the acquisition frequency for the morphological analysis of the beach slope evolution ($\beta(t)$ & $Lt_{sl}(t)$) is 2 Hz, while it is 40 Hz for the free surface extraction $h_b(x, t)$.

Wave forcing: from the wave paddle to the breaking point

When waves arrive at the nearshore, they are strongly influenced by the seabed through shoaling, resulting in a variation of the local linear velocity leading to wave breaking, with subsequent influence on sediment transport (formation of shoals and sandbars). Changes in the bottom topography due to wave forcing produce variations in the structure of the incoming wave. These non-linear feedback interactions between waves and the seabed introduce additional space and time scale perturbations to the physical problem, affecting wave steepness, wave breaking, and consequently sediment transport at the nearshore.

In order to control this wave dynamic process in the laboratory and to maintain a constant wave forcing throughout the experiment, a non-erodible bottom with a gentle slope is introduced at a fixed distance from the wave paddle mechanism. This bottom morphology reproduces wave shoaling and keeps the breaking point fixed. The slope chosen for this rigid bottom is the result of a meticulous study carried out on the water channel, where the transformation and energy dissipation of the wave were analyzed for different wave structures and rigid slopes; resulting in $tan\alpha = 0.06$ (see Figure 3.27). This slope value allows to reproduce the wave shoaling in a suitable form and to reproduce different wave breaking mechanisms without losing all the wave energy during the wave shoaling, as shown in Figure 3.18.

Table 3.2: Wave characteristics generated by the Wave Paddle. All parameters are extracted from wave gauge measurements at $x = 2\,\mathrm{m}$, i.e. before the rigid slope.

	H_0 [m]	T_0 [m]	λ_0 [m]	Dean number Ω_0	Wave steepness s
Wave regime A	0.047	0.74	0.75	8.58	0.062
Wave regime B	0.025	1.28	1.50	2.63	0.016
Wave regime C	0.023	1.69	2.00	2.83	0.011
Wave regime D	0.021	2.51	3.10	1.13	0.006

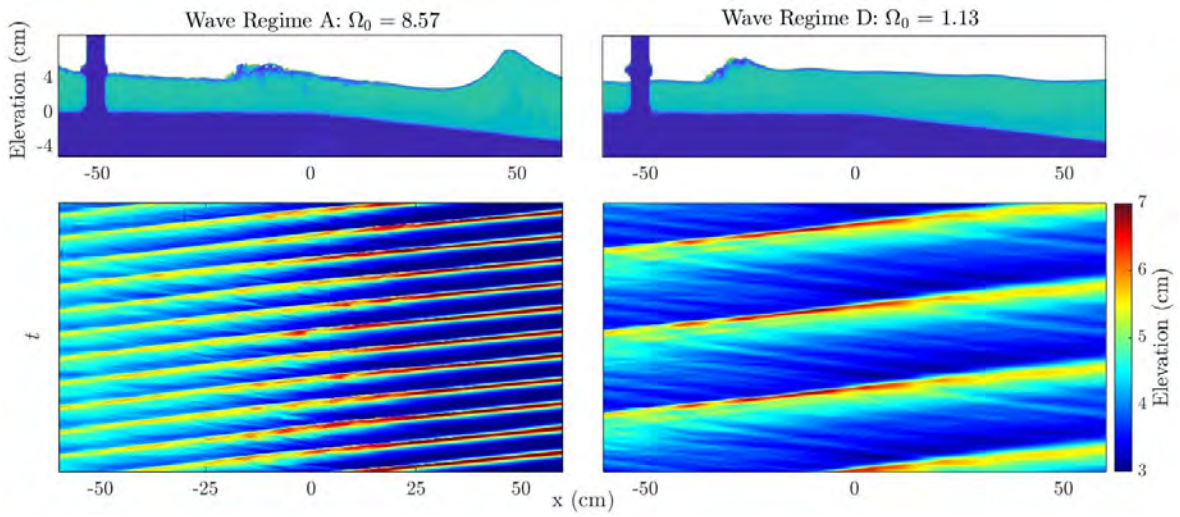

Figure 3.18: The left column shows wave regime A, while the right column shows wave regime D, representing the extreme wave regimes tested. The top row shows the free surface position and elevation at a given time, highlighting two different wave breaking mechanisms. The bottom row shows the spatio-temporal diagram of the wave regime.

Accordingly, the wave forcing becomes one of the parameters that we can control by changing the amplitude and period of the flap paddle wave generator, leading to a well controlled propagating sinusoidal wave of amplitude H_0, period T_0 and wavelength λ_0. The four wave regimes (A-D) that have been considered along this study are given in the table 3.2. As mentioned above, wave amplitude (H_0) and period (T_0) are measured with a wave gauge at the bottom of the rigid slope (see Figure 3.27). The wavelength (λ_0) is calculated using the mean depth dispersion relation according to Airy wave theory. Note that the waves generated by the wave paddle are limited by the geometric size of the water channel, the type of wave generator, the rigidly sloping bottom, and the water level. The region of possible wave generation in the parameter space (H_0, λ_0) or equivalently (H_0, T_0) is shown in Figure 3.19(a) together with the wave regimes considered here (symbols). As this work aims to highlight the influence of individual waves on the slope dynamics of the beach face, the wave forcing is represented by monochromatic waves. Each of the four regimes (A-D) of Table 3.2 and Figure 3.19(a) is also characterized by its offshore wave steepness (s) and Dean number (Ω_0).

Finally, Figure 3.19b shows the wave amplitude after the breaking process, i.e. at the

beginning of the terrace ($H_b(x = 0)$). It is clear that the wave heights after breaking are similar for the four wave regimes tested. This means that the wave height in the inner surf zone, i.e. over the terrace, is mostly controlled by the constant water depth H_t over the terrace. This observation is consistent with the field observations reported in Almeida et al. (2020).

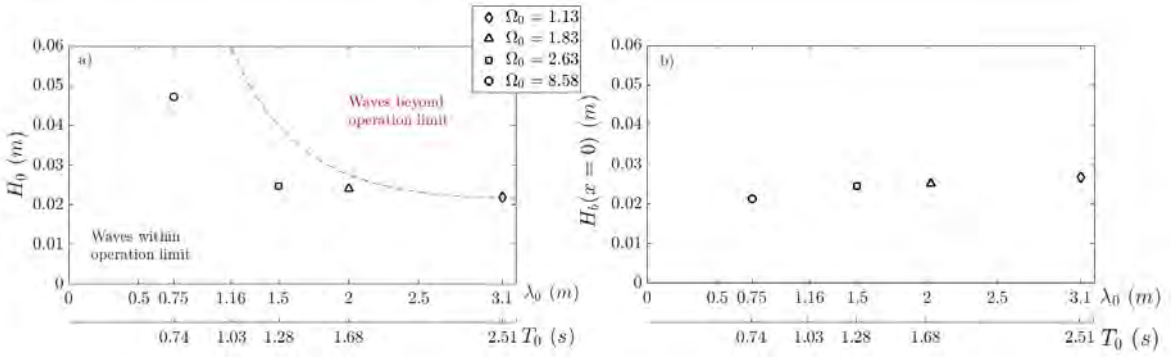

Figure 3.19: (a) Operating limits of the wave generator in the parameter space of the sinusoidally propagating wave (H_0, λ_0) and (H_0, T_0). Four types of wave regimes are used in the following experiments. The wave regimes are represented by the symbols: circle, triangle, square, and diamond. Each wave regime is associated with a monochromatic wave forcing characterized by its wave amplitude (H_0), period (T_0), and wavelength (λ_0) measured with a wave gauge at the bottom of the fixed slope (see table 3.2). (b) Amplitude plot Hb of the wave after breaking at $x \approx 0$ vs $T0$ and λ_0, for the same wave forcing as in figure (a).

Inner-surf and beach slope: initial conditions and typical observations

One experiment run consists to submit an initial beach face profile, characterised by its initial slope β_i and position Lt_i, to a constant wave regime for 2 hours. The flattest initial slope β_i used is 1/20 and the steepest 1/2.5, intermediate slope of 1/7, 1/5, 1/4 where also tested. The initial position of the beach-face Li_{sl} was varied from the wave breaking point $x = 0$ up to $x = -1.3$ m by intervals of around 30 cm. A summary of the initial morphology states, wave regimes and number of experiment runs is given in Table 3.3. The number of runs corresponds to the number of experiments undertaken for each wave regime (A,B,C and D) varying the initial morphological conditions.

Table 3.3: Set of of experimental runs and initial morphological characteristics performed for each wave regime (A, B, C and D).

Wave Regime			Morphological initial conditions			Number
Type	$s = H_0/\lambda_0$	Ω_0	$\tan\beta_i$	Li_{sl} (m)	Li_{sl}/H_t	of Runs
Wave Regime A	0.063	8.58	[0.06 : 0.40]	[0.10 : 1.15]	[2.50 : 28.75]	17
Wave Regime B	0.017	2.63	[0.06 : 0.40]	[0.10 : 1.30]	[2.50 : 33.75]	16
Wave Regime C	0.011	1.83	[0.05 : 0.40]	[0.10 : 1.00]	[2.50 : 25.00]	7
Wave Regime D	0.006	1.13	[0.05 : 0.40]	[0.10 : 1.30]	[2.50 : 32.50]	8

Water levels and wave forcing remain constant throughout the experiment. There is no sediment input during the experiments, i.e. the sediment available for transport corresponds only to the initial beach-face configuration. Therefore, the initial beach slope (β_i) will control whether there is more or less sediment available for transport. The beach slope can either decrease ($\beta_i > \beta_f$) or increase ($\beta_i < \beta_f$), but since there is no sediment input, the beach face position $Lt_{sl}(t)$ is mainly seen to remain unchanged or move away from the breaking point, beach erosion. Only one accretion case is observed, where the shoreline migrated towards the breaking point and was associated with a markedly flat initial beach slope ($tan\beta_i = 1/20$). This shoreline erosion or accretion is much slower than the adjustment of the beach slope and introduces a different time scale into the study.

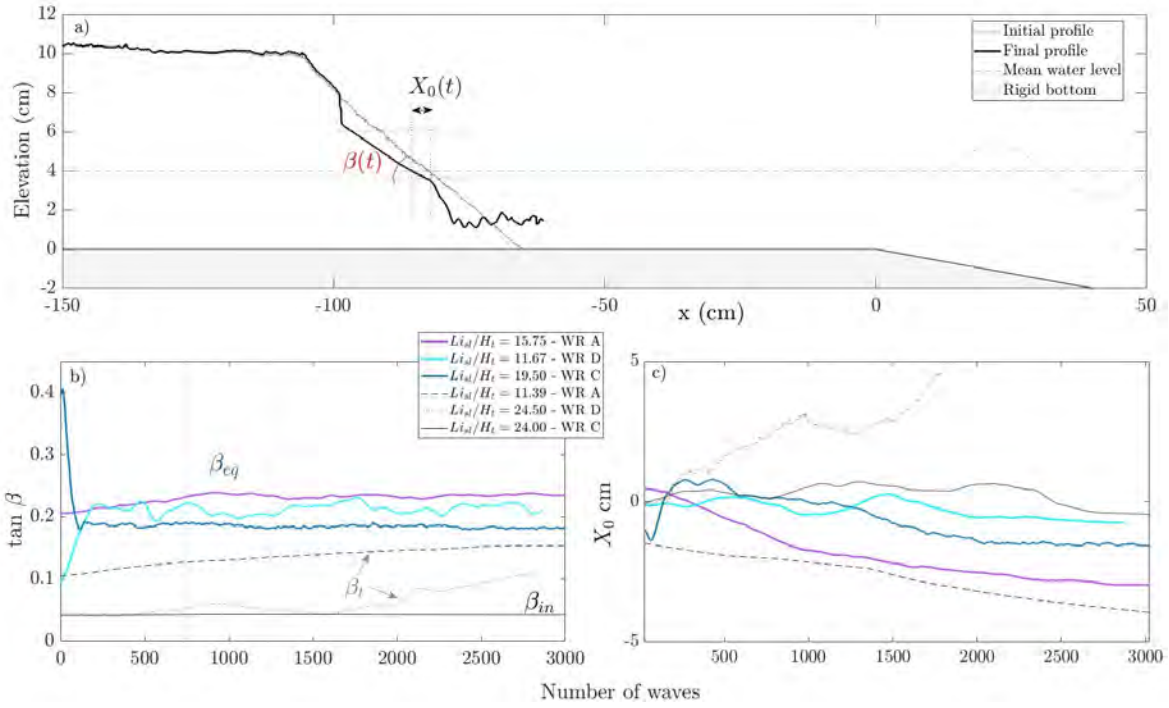

Figure 3.20: (a) Initial and final position of the beach-face profile. The beach slope $\beta(t)$ defined between excursion limits of the wave (red dashed lines) surrounding the shoreline and $X_0(t)$ refers to the local shoreline position evolution. (b) 6 examples of the beach slope evolution plotted against the numbers of waves impacting the beach face: 3 cases of rapid equilibrium beach slope evolution represented by the solid blue, cyan and violet lines (β_{eq}), 2 cases of transitional beach slope states represented by dashed and dotted black lines (β_t) and 1 case of an inactive beach slope (β_{in}) represented by black line. (c) Local evolution of the beach slope position represented by the parameter X_0 associated to each beach slope rapid equilibrium experiment in Figure (b).

The beach slope (β) is defined in this experiment as the linear part of the beach-face profile around the mean water level on the terrace. This linear part is shaped by the wave run-up and back-rush. By identifying the limits of the wave excursion, the evolution of the beach slope can be extracted (see Figure 3.20a). Three different situations can be identified

for typical slope evolution in the present experiments. First, a fast equilibrium beach slope (β_{eq}) can be observed. In this case the slope converges to a stable value below 3000 wave impact on the beach face. This equilibrium slope corresponds to a mean value of 500 waves after convergence. Three examples of rapid equilibrium regimes for the beach slope are shown in Figure 3.20b (blue, cyan, and purple solid lines). At the other end, an inactive beach slope β_{in} regime can also be observed. Here the beach face does not respond to wave forcing. An example is shown in Figure 3.20b (black solid line).

Finally, an intermediate state of the beach slope between the two previously described was obtained. For these cases, the slope slowly converges to its equilibrium slope, without the prior 3000 wave impact on the beach face converging. This transient state is represented by the dashed and dotted black lines in Figure 3.20b. The latter case is considered inactive in this study, as it evolves on a time scale that becomes significantly important compared to other processes observed in the field, such as seasonal variation or even intertidal water level evolution. Figure 3.20c illustrates the associated local shoreline evolution, $X_0(t)$, as defined previously. Both accretive and erosive conditions are obtained on relatively long time scales compared to the rapid slope adjustment discussed here. Note that the intermediate regime mentioned earlier is more clearly highlighted as a long time scale evolution of both slope and shoreline position, which are thus coupled. The specific analysis of this long time evolution is left to a future work, while we discuss below the rapid evolution of the slope and the associated equilibrium state. It is interesting to note that the equilibrium beach slope β_{eq}, as defined here, is reached in less than 1000 waves hitting the beach. This time scale could correspond to one or more tidal cycles in nature, depending on the tidal range.

Scaling consideration from field observations

The scaling of this experimental device is done by a geometric and physical comparison between the physical model and available field data from two low tide terrace (LTT) beaches, one at Nha Trang Vietnam and the other at Grand Popo Benin. The hydro-mophodynamics of these two LTT beaches are well described in the following papers: Lefebvre et al. (2014); Almar et al. (2014); Abessolo Ondoa et al. (2016); Almar et al. (2017b); Thuan et al. (2019); Almeida et al. (2020). The authors classified these beaches as LTT environments with similar sediment size but very different wave climate. Nha Trang (NT) is a sandy beach located in a semi-enclosed bay in southern Vietnam with a microtidal ranging from 0.4 m to 1.7 m. This beach is exposed to a low to medium energy wave climate with seasonal variability. The annual significant wave height is 0.95 m with an associated mean peak period of 6.2 s. Sediment size at NT is medium to coarse with an average grain size of 0.6 mm. Grand Popo (GP) is an open microtidal coastline forming a 500 km long mild embayment in the Gulf of Guinea. This coast is exposed to a medium to high energy wave (mean significant wave height 1.36 m; mean peak period 9.4 s), which is mostly constant over the year. Sediment size is also medium to coarse with a mean grain size of 0.6 mm.

Table 3.4: Geometrical dimensionless relations for the physical model and field data.

	Off-shore wave H_0/λ_0	Terrace (inner-surf) Li_{sl}/H_t	beach slope $tan\beta_i$	Hydro-morphological parameters H_t/λ_0	H_t/H_0
Laboratory Model					
Wave regime A	0.063	[1.06 : 33.75]	[0.05 : 0.4]	0.055	0.86
Wave regime B	0.017			0.027	1.64
Wave regime C	0.011			0.020	1.82
Wave regime D	0.0069			0.013	1.90
Nha Trang	[0.039 : 0.048]	15.5	[0.05 : 0.18]	[0.010 : 0.10]	[0.38 : 2.38]
Grand Popo	[0.011 : 0.012]	32.0	[0.10 : 0.35]	[0.0039 : 0.0140]	[0.30 : 1.44]

The geometric design of the physical model used here is based on maintaining the same geometric dimensionless numbers that relate the morphology of the system to the structure of the wave. First, three dimensionless parameters are used in this scaling strategy to independently characterize the offshore wave forcing, the surf zone, and the beach face morphology. These parameters are: the ratio of offshore wave amplitude to offshore wavelength H_0/λ_0 (offshore wave forcing), the ratio of terrace length to water depth on the terrace H_t/Li_{sl} (surf zone) and the beach slope β_i (swash zone). Then, two dimensionless numbers, also based on length ratio, are defined to relate the off-shore wave structure and inner-surf morphology. They are the ratio between terrace water depth with offshore wavelength H_t/λ_0 and terrace water depth with offshore wave amplitude H_t/H_0. All these five dimensionless numbers are summarized in Table 3.4. As shown here, the laboratory physical model mostly preserves the geometric hydro-morphological dimensionless numbers observed at NT and GP.

Table 3.5: Laboratory and field physical parameters

	D_{50} [mm]	Sediment Fall velocity W_s [cm/s]	Dean $\Omega = H_0/(T_0 W_s)$	Rouse $Ro = W_s/\sqrt{gH_t}$
Laboratory model	0.12	0.74 (measured)	Wave Regime A: 8.58 Wave Regime B: 2.63 Wave Regime C: 1.83 Wave Regime D: 1.13	0.0118
NT	0.60	8.4 (Van Rijn (1993))	[1.5 : 5.0]	0.0258
GP	0.60	8.4 (Van Rijn (1993))	[1.5 : 2.5]	0.0237

A set of scaling relationships governing the physical processes of the hydro-sedimentary system is also required to increase confidence in laboratory results. However, as is often the case with complex systems, a choice has to be made on the most relevant physical process and associated dimensionless numbers to be scaled to represent field observations. In particular, a perfect similarity between laboratory and field is unattainable, since the use of the same fluid in the same gravity fields does not allow for independent variation of all physical parameters,

leading to incompatibility in the scaling of all dimensionless numbers.

The physical dimensionless number used here as the most relevant to characterize beach shape is the Dean number Ω_0 discussed earlier. The range that Dean covers here is summarized in Table 3.5. Another relevant dimensionless number associated with sand transport under turbulent flow is the Rouse number *Ro*. An estimate of the magnitude of this number, both at the laboratory scale and in the field, is also given in Table 3.5. It is found to be slightly smaller than in the field. However, this value is indicative of suspended transport, which means that the transport regime remains similar in both cases. Finally, not discussed here is the Reynolds number characterizing the flow regime, which here is high enough to suggest a turbulent regime as in the field.

3.2.4 beach slope equilibrium state

Influence of the off-shore wave forcing

We first discuss the influence of the offshore wave forcing, here characterized by the Dean number Ω_0, on the final slope β_{eq} as defined above, independent of the initial geometric conditions of the beach face (β_i & Lt_i). Both the initial slope $\tan\beta_i$ and the final slope $\tan\beta_f$ are plotted against the offshore Dean number in Figure 3.21. Each symbol in Figure 3.21 corresponds to an experiment. These symbols correspond to the 4 wave regimes tested (circle, square, triangle, and diamond for wave regimes A, B, C, and D, respectively). The color map of the symbols represents their corresponding initial terrace length scaled by the terrace water depth H_t. As mentioned in section 3.2.3, the intermediate state β_t is considered inactive for this analysis because it operates on a much slower time scale than the equilibrium beach slope values (β_{eq}). Then the final values of the beach slope (β_f) are either equilibrium values (β_{eq}) or inactive values (β_{in}).

In the figure 3.21 two different zones of the final beach slope are identified: the equilibrium zone (β_{eq}) and the inactive zone (β_{in}). The equilibrium zone is mostly localized around $\tan\beta = 0.2$. The inactive zone is strongly associated with the morphological time scale analyzed, the initial conditions of the beach face (low initial slope and beach face position far from the breaking point) and the wave forcing (wave energy injected into the system). Here it is found that it is mostly obtained for $\tan\beta < 0.1$. Then, if β_i is not in these two zones, the beach slope will rapidly evolve towards the equilibrium zone highlighted in Figure 3.21(b).

Two contrasting behaviours of the beach slope are observed when classifying the equilibrium slopes (β_{eq}) using the offshore Dean number (Ω_0), as shown in Figure 3.21(b). For $\Omega_0 < 3$ there is an inverse relationship between β_{eq} and Ω_0, i.e. β_{eq} decreases with increasing Ω_0. In this case, a stable beach slope can be associated with the offshore wave forcing, here the Dean number Ω_0, has only a small scatter around a given $\beta_{eq}(\Omega_0)$. In particular, the terrace length does not affect the equilibrium state as defined here. These cases are observed for $\Omega_0 < 3$ and $\lambda_0 >> L_t$. On the contrary, for $\Omega_0 > 3$ the dispersion on β_{eq} increases with increasing Dean number. This is clearly observed for wave regime A (short wavelength and high Dean number). Nevertheless, this variation of β_{eq} at a given Ω_0, even if small, is not

a random dispersion, but can be related to the terrace length. In particular, as the terrace length increases, $Lt_i/H_t \nearrow$, $\beta_{eq} \searrow$ decreases. Then, for $\Omega_0 > 3$, Ω_0 is not the only control parameter of the beach slope equilibrium, the surf zone dissipation now influences the final state.

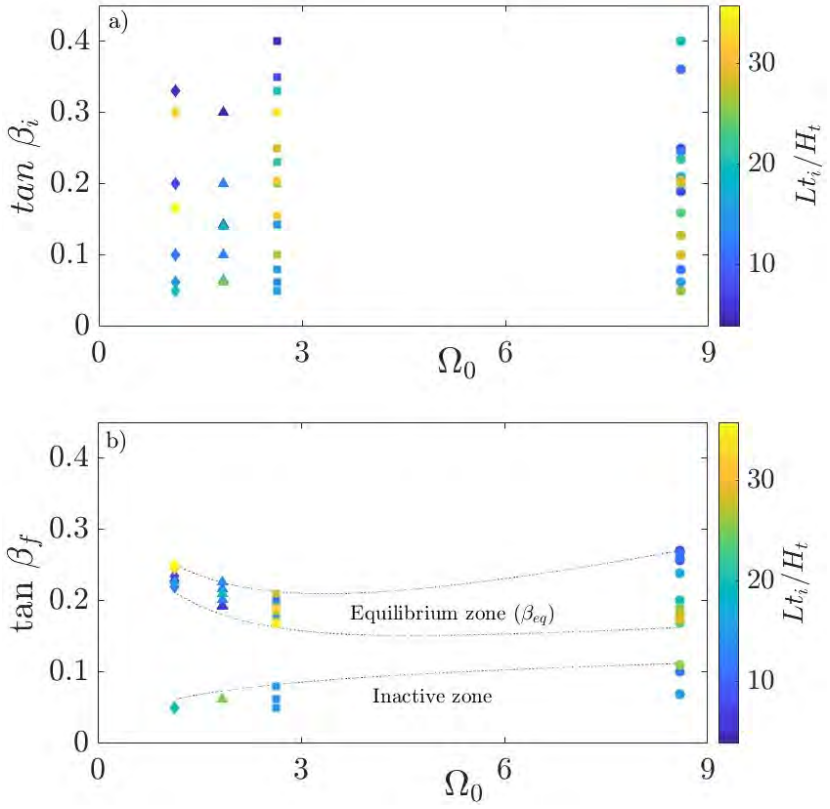

Figure 3.21: (a) Initial beach slope values plotted against their associated Dean number, calculated with off-shore parameters Ω_0. Figure (b) Final values of the beach slope also plotted against their associated Dean number. Each symbol corresponds to one experiment run and the type of symbol (circle, squares, triangle and diamond) is associated to each wave regime A, B, C or D summarised in Table 3.3. The color map corresponds to the initial terrace length (Lt_i/H_t).

To highlight the latter observation, we show the influence of the initial geometric beach face conditions (β_i & Lt_i) on the beach face dynamics for the wave regime A, i.e. $\Omega_0 = 10.7$, for which the maximum dispersion of the equilibrium beach state is obtained. The beach slope β as a function of the number of waves hitting the beach is shown in Figure 3.22. In particular, each panel of Figure 3.22 (a,b and c, respectively) shows the slope evolution for different initial slopes $\tan\beta_i = 0.35$, $\tan\beta_i = 0.2$ and $\tan\beta_i = 0.1$, respectively. Moreover, for each initial condition, two different initial beach face positions Lt_i, i.e. initial terrace length or equivalently surf length, are considered for each initial slope. In particular, the black lines correspond to experiments with $Lt_i = 0$, while the dashed black lines correspond to $Lt_i = 65cm$. These lengths are given in dimensionless form in figure 3.22, using h_t as

the characteristic length scale. The initial shoreline position Li_{sl}/H_t is also given for each case. Note again that Li_{sl} varies slightly with β_i as explained in section 3.2.3. On the right side of each panel (a, b and c), the corresponding initial and final beach face profiles are also shown for both initial terrace lengths (gray lines correspond to the initial state and black lines correspond to the final state).

We can see that when the beach face is active (Figure 3.22(a-b)), the slope $\tan\beta$ evolves to an equilibrium value that depends mostly on Li_{sl}/H_t. Then, as expected, the evolution of the beach slope depends on the terrace length. In the following, we will show that this is simply due to the wave dissipation along the inner surf zone.

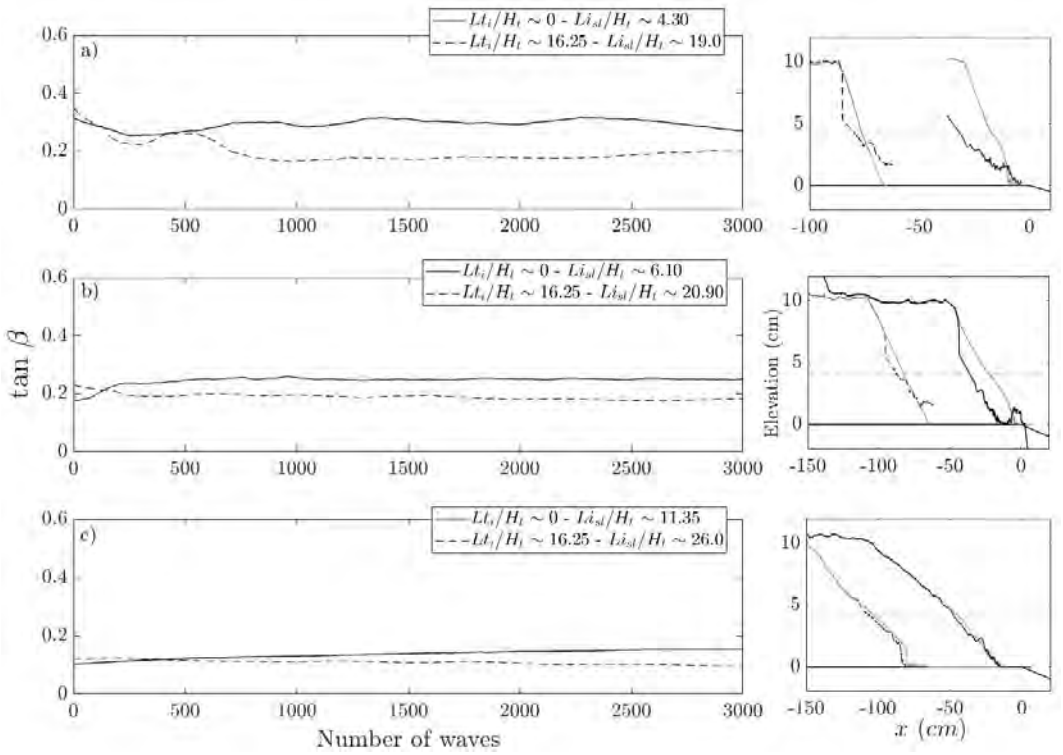

Figure 3.22: Panel a, b and c show two experiments with the same initial beach slope but at two different positions from the breaking point for wave regime A. The beach slope initial positions are scaled with the water level on the terrace. The solid black lines represents the beach slope evolution for experiments starting at $Lt_i/H_t = 0$, and the dashed black line at $= Lt_i/H_t = 16.25$. Left figures show the beach slope evolution as a function of the number of waves impacting the beach-face. Right figures illustrate the initial and final beach-face profile.

Influence of the inner-surf dissipation

In order to characterize the influence of the terrace length on the wave dissipation, experiments were performed without the sandy beach. The aim of these experiments is to extract the wave transformation law after the breaking point, which is characterized by the decrease

of the wave height on the flat platform (surf zone).

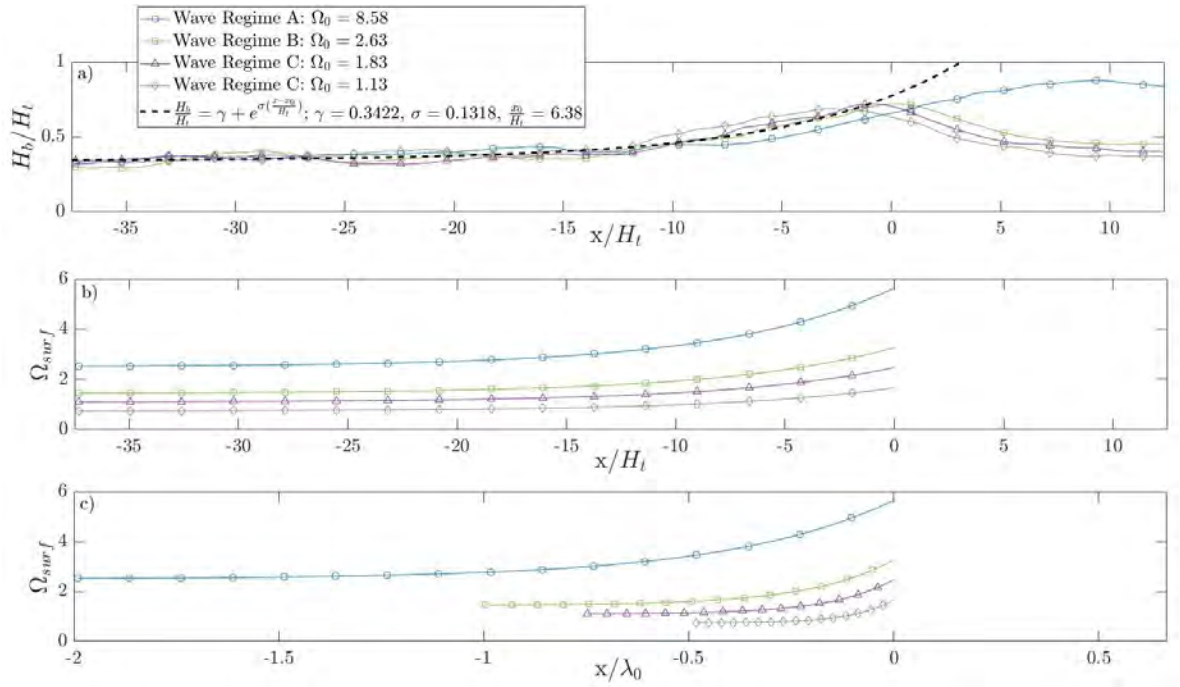

Figure 3.23: (a) Wave amplitude and position on the terrace (H_b and x) are normalized by the water level on the terrace (H_t). (b) Surf Dean number evolution on the flat platform, where the position on the terrace is scaled by the water level at that point (x/H_t). (c) Surf Dean number evolution on the flat platform, where the position is scaled by the off-shore wavelength (x/λ_0).

Figure 3.23a illustrates the evolution of the maximum wave height ($H_b(x)$) on the terrace scaled by the water level on the terrace (H_t) for the 4 wave regimes. This parameter is known in the literature as the breaker index $\gamma = H_b/H_t$. At the shallow water boundary, the breaker index indicates that the breaking process begins when the wave height becomes greater than a fraction of the water depth. Accordingly, the estimation of γ at breaking can be found around $\gamma_{br} = 0.8 - -1$ in the literature (Miche, 1944; McCowan, 1891).The breaking point for the 4 wave regimes is located around $x = 0$ in the present experiments, meaning that $\gamma_{br} \equiv \gamma(x = 0)$. It is found here that γ is independent of the wave regime and has a value of $\gamma_{br} \approx 0.7$ (see Figure 3.23a). Note that for wave regime A, the breaking processes occur slightly before the beginning of the terrace, i.e. for $x > 0$. However, it is observed that 4 wave regimes behave similarly for $x < 0$. In particular, the decrease of the bore height H_b/H_t along the terrace, $x < 0$, remains the same for all wave regimes. In addition, the dissipation of wave energy occurs mostly for $-15 < x/H_t < 0$. After this dissipation zone, the bore remains rather constant for the 4 wave forcings. Consequently, the height of the bores generated at the breaking point $x = 0$ and their decrease due to dissipation for $x < 0$ does not depend on the offshore wavelength and amplitude, but only on the water depth above the terrace, i.e. in the inner surf zone. From these observations, a single law of wave dissipation in the surf

zone can be extracted for all wave regimes. It is found to follow an exponential decrease with distance from the breaking point, as shown by the dashed black line in Figure 3.23a. It can be written as

$$\frac{H_b}{H_t} = \gamma_\infty + \exp\left[\sigma(x - x_0)/H_t\right] \quad \text{with} \quad \gamma_\infty = 0.3422; \quad \sigma = 0.1318; \quad x_0/H_t = 6.38. \quad (3.6)$$

Coefficients γ_0, x_0/H_t and σ are obtained using best fit of experimental data. The coefficient σ corresponds to the spatial damping rate of the bore height due to friction. The amplitude of the exponential term is assumed here to be order one as it represent the order of magnitude of the breaker criterion γ_{br}. However, an offset of the breaking point x_0/H_t is allowed as to recover the relevant γ_{br} obtained for our set of experiments. We can thus compare this solution with the breaker index (γ_{br}) at the breaking point $x = 0$. We obtain $H_b(x = 0)/Ht(x = 0) = 0.77$, which is in accordance with our previous estimation and close to values found in the literature. On the other hand, the inshore-limit of solution (3.15) is γ_∞, found to be 0.3422. This corresponds to the ratio of the bore height far away from the breaking point and the water height ($\gamma_\infty = H_{b\infty}/H_t$). Based on this analysis, i.e. accounting for this exponential dissipation of bore height along the inner-surf zone, a Surf Dean number can be determined, based on the local position of the bore with respect to the breaking point. It is thus defined as

$$\Omega_{surf} = \frac{H_b(x/H_t)}{T_0 W_s}. \quad (3.7)$$

This Surf Dean number (Ω_{surf}) accounts for the effect of wave energy dissipation through the reduction of wave amplitude on a flat platform (3.15). As noted in equation 3.7, the surf dean number depends on the bore height, the water level on the terrace, the offshore wave period, and the sediment fall velocity. The evolution of the Surf Dean number for the four wave regimes is shown in Figure 3.23b.

Characterization of the equilibrium state based on inner-surf dissipation model

To emphasize the impact of wave dissipation due to a flat platform on the equilibrium state of the beach slope, we estimate a Swash Dean number Ω_{sw} at the bottom of the beachface Lt_i, as being the evaluation of the Surf Dean number Ω_{surf} defined in Equation 3.7 at $x/H_T = -Lt_i/H_t$, i.e.

$$\Omega_{sw} = \frac{H_b(x/H_t = -Lt_i/H_t)}{T_0 W_s}, \quad (3.8)$$

with $H_b(x/H_t = -Lt_i/H_t)$ obtained from (3.15). The equilibrium slopes (β_{eq}) are thus plotted against its associated Swash Dean number Ω_{sw} in Figure 3.24.

Figure 3.24 shows a parabolic correlation between β_{eq} and Ω_{sw}. However, $\Omega_{sw} > 2.08$ mostly corresponds to wave regime A and $\Omega_{sw} < 2.08$ to wave regimes B, C and D. Therefore, a transition between these wave regimes is obtained at $\Omega_{sw} \approx 2.08$, which corresponds to the minimum value of β_{eq} obtained here. For $\Omega_{sw} < 2.08$, the swash mostly control the dynamics of the equilibrium beach slope. Then, even if the definition of Ω_{sw} allows a slightly better correlation with β_{eq}, it is somehow similar to Ω_0 (see figures 3.21 and 3.24 at small dean). However, for $\Omega_{sw} > 2.08$, the surf clearly controls the beach slope. The Swash Dean Ω_{sw} allows to explain the dispersion of β_{eq} obtained when using the Offshore Dean Ω_0. Here a unique law is obtained to classify the equilibrium beach slopes for surf and swash control cases through the transition point obtained around $\Omega_{sw} = 2.08$ or equivalently $\Omega_0 \approx 3$.

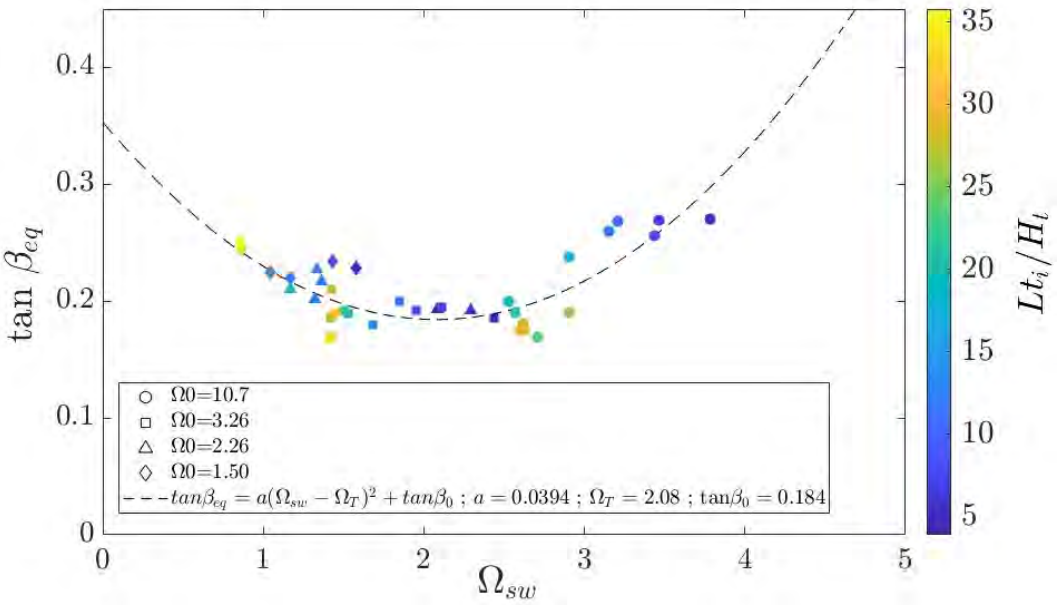

Figure 3.24: Beach slope equilibrium value (β_{eq}) plotted against their associated Swash Dean number (Ω_{sw}) calculated at the bottom of the beach-face. Each symbol corresponds to one experiment and the colormap corresponds to the initial beach slope position scaled by the water level on the terrace (Lt_i/H_t)

Application to field case

Based on the previous observations from the physical model, we propose a quadratic law of $\beta_{eq}(\Omega_{sw})$ as

$$\tan\beta_{eq} = \alpha(\Omega_{sw} - \Omega_T)^2 + \tan\beta_0 \quad \text{with} \quad \alpha = 0.0394; \quad \Omega_T = 2.08; \quad \tan\beta_0 = 0.184 \quad (3.9)$$

The fitting coefficients of this equation are α, Ω_T and $\tan\beta_0$. Ω_T corresponds to a Dean transition from a swash-dominated to a surf-dominated beach system and β_0 is the associated beach face angle. A combination with equations 3.15 and 3.8 leads to a simple model that

allows to predict the rapid beach slope equilibrium induced by local wave action. This model reads :

$$\tan\beta_{eq} = \alpha\left(\left(\gamma_\infty + \exp\left[\sigma(x-x_0)/H_t\right]\right)\frac{H_t}{T_0 W_s} - \Omega_T\right)^2 + \tan\beta_0. \tag{3.10}$$

To make the model suitable for use with field data, a few simplifications and approximations are required. First, the transition $(\Omega_T, \tan\beta_0)$ is likely to be system and scale dependent. However, a transition between swash-dominated and surf-dominated has been found in field situations around a similar value of Dean number, $\Omega_0 \approx 2.5$, as recalled in section 3.2.2. Then $\Omega_T = 2.08$ can be expected to remain relevant for field application. On the other hand, $tan\beta_0$, which corresponds to the minimum value of the beach slope obtained at the transition, is likely to be different between laboratory and field observations. This value depends strongly on the hydraulic regime of each system (wave sediment transport capacity). Adjustment of this parameter is therefore necessary for field data. In addition, the exact break location and dissipation law must be simplified to be useful for field application. It is suggested to simply combine $x_{sl} - x_0 = Lt$ regardless of the detailed role of x_0 in relation to 3.10. If the terrace length $L_t(t)$ is not available from field data, the relation $Lt \sim 0.4\lambda_0(t)$ suggested by Mingo et al. (2021) can be used instead.

This approach leads to the derivation of a simplified model that can be tested on field data to predict the rapid evolution of beach slope. This can be written as :

$$\tan\beta_{eq} = \alpha\left(\left(\gamma_\infty + \exp\left[\sigma L_t/H_t\right]\right)\frac{H_t}{T_0 W_s} - \Omega_T\right)^2 + tan\beta_0, \tag{3.11a}$$

$$\tan\beta_{eq} = \alpha\left(\left(\gamma_\infty + \exp\left[0.4\lambda_0\sigma/H_t\right]\right)\frac{H_t}{T_0 W_s} - \Omega_T\right)^2 + tan\beta_0, \tag{3.11b}$$

with $\alpha = 0.0394$, $\sigma = 0.1318$, $\gamma_\infty = 0.3422$ and $\Omega_T = 2.08$, all fixed from the best fit of the physical model. The inputs from field measurements are thus the offshore wavelength and period (λ_0, T_0) and the sediment fall velocity W_s. For the model (3.11a), L_t is also an input from field measurements. Finally, two parameters remain adjustable for the (3.11a) and (3.11b) models. The first is the slope at the transition $\tan\beta_0$ as explained above. The second is the water depth above the terrace H_t. The latter parameter could be measured in the field. However, it mostly implies the dissipation law over the terrace, which could be strongly case dependent. Since this is the couple (σ, H_t), we propose here to adjust H_t, which varies strongly in the field due to tidal evolution and seasonal variations. Its evaluation can then be discussed with respect to the expected range of values from the field.

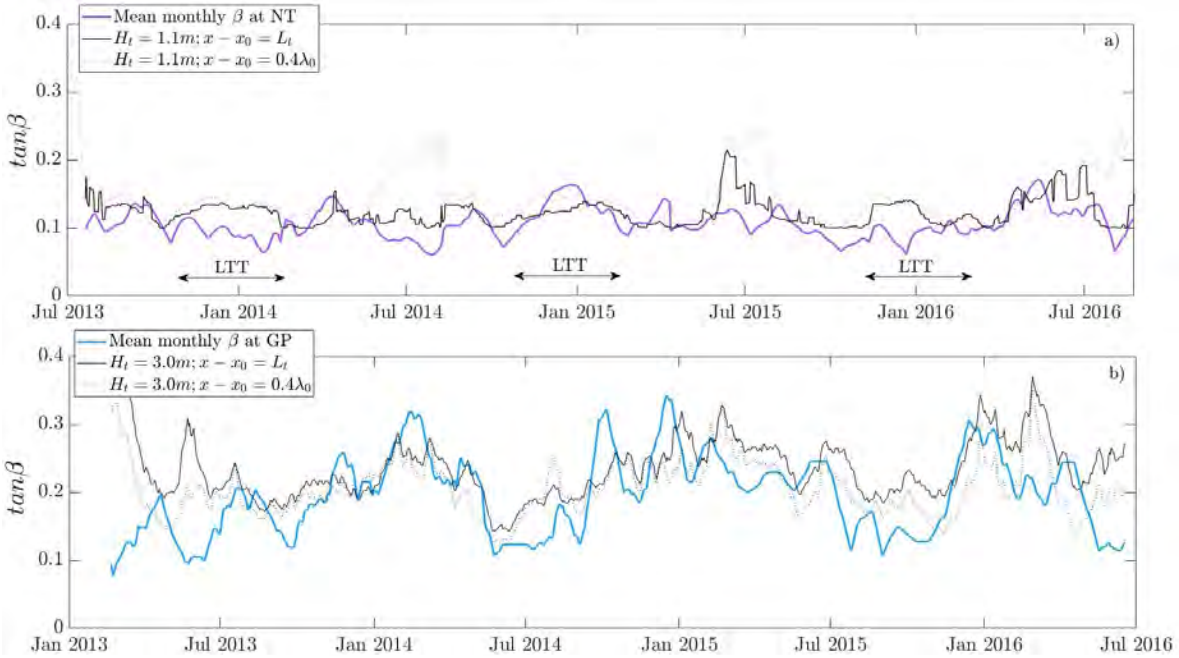

Figure 3.25: a) Beach slope evolution at Nha Trang. The thick solid violet line corresponds to field observations, solid black line corresponds to the model results using the terrace length as in an input and doted line corresponds to the model results using the relation 0.4λ instead of the terrace length as input. b) Same comparison than figure a but for Grand Popo, where field observation are represented with a thick solid blue line.

In the following, the models (3.11a) and (3.11b) are tested using the field data from Nha Trang and Grand Popo discussed in sections 3.2.2 and Mingo et al. (2021). These data include monthly mean measurements of beach slope β, terrace length L_t, and wave parameters (H_0, T_0, λ_0) over a period of 3.5 years. It was observed that for NT and GP the minimum slope is about 1/10. We therefore suggest $tan\beta_0 = 0.10$ as a first guess for the slope value at the transition. γ and σ correspond to the coefficients obtained from dissipation law on a flat platform (3.15). It should also be noted that several levels of H_t were tested to identify the optimal value of H_t that best described the field observations, as explained earlier. For Nha Trang, this value is $H_t = 1.1m$, which corresponds to the tidal range. For Grand Popo, the optimal mean water level on the terrace is $H_t = 3m$, which is almost twice as high as the maximum water depth during high tide. This difference could be attributed to the attenuation law used in the model, which is probably case-dependent, as the dissipation mechanism could be more complex than that obtained in the physical laboratory model.

The comparison of field data with the results obtained from the simplified models (3.11a)) and (3.11b) are shown in Figure 3.25(a) for NT and in Figure 3.25(b) for GP. In particular, field measurements are shown with blue solid lines, black solid lines and black dashed lines corresponding to model (3.11a) and model (3.11b) respectively. The models show good agreement with both data sets (NT and GP). Although, the model performance may vary its ability to accurately predict the beach slope dynamics within each scenario, surf or swash control

cases. In swash control cases, the model reproduces most of the beach slope to changes in offshore wave forcing through significant and rapid fluctuations of the slope, as observed at GPP on the whole data set and at NT mostly during the summer seasons. In these cases, the role of the terrace remains small. However, the ability of the models to predict the evolution of the beach surface slope from a swash dominated to a surf dominated situation is quite good (see for example the decrease of the slope from July 2015 to January 2016 at NT, for which the beach system evolves towards a terrace dominated regime).

Figure 3.25 also highlights an important result regarding the influence of the distance from the breaking point to the beachface, as modelled by either the terrace length $L_t(t)$ (black solid line) or the relation $L_t \sim 0.4\lambda(t)$ (dotted line). Only a small difference between the models used for NT and GP is obtained, regardless of whether the distance is represented using $L_t(t)$ or $L_t \sim 0.4\lambda(t)$.

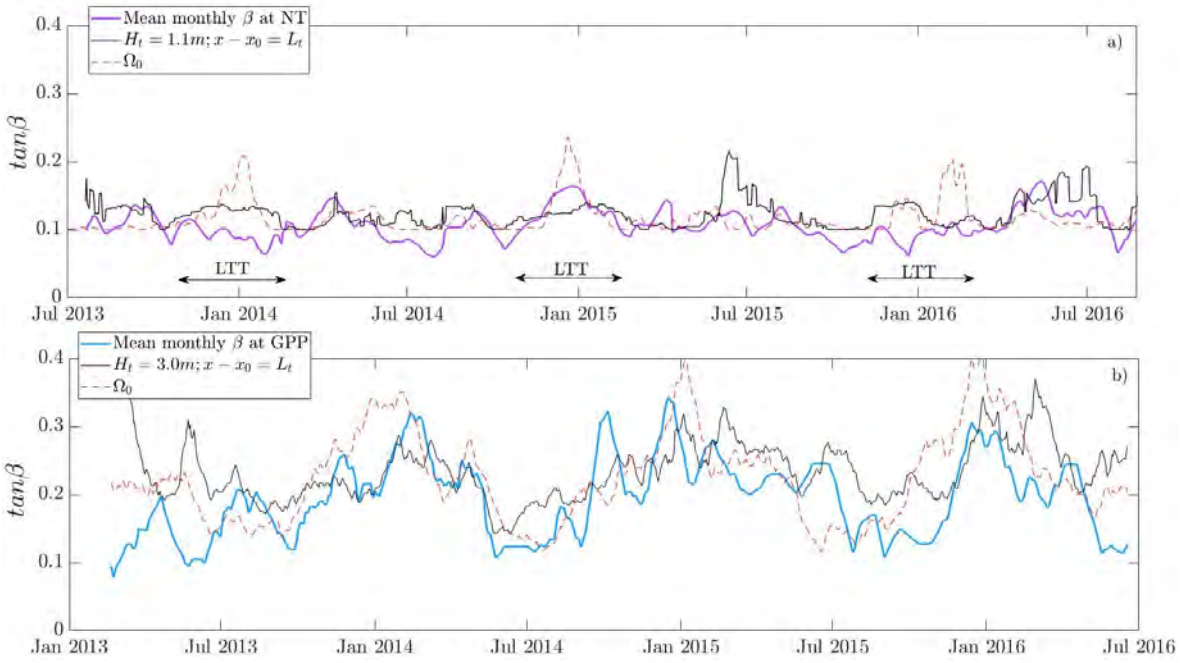

Figure 3.26: a) Beach slope evolution at Nha Trang. The thick solid violet line corresponds to field observations, solid black line corresponds to the model results using the Swash Dean number and the red dashed line corresponds to the model results using the off-shore Dean number instead of the Swash Dean number. b) Same comparison than figure a but for Grand Popo, where field observation are represented with a thick solid blue line.

Note that for H_t additional studies are needed to fully evaluate the behaviour of the attenuation law under different water level conditions. However, as it was concluded that for swash control cases the beach slope responds directly to the offshore wave forcing, the wave height attenuation on the terrace could be neglected and the model could be tested directly with the offshore Dean number evolution Ω_0. This is shown in Figure 3.26, where the dashed red line represents the evolution of the beach slope using the off-shore Dean number

(Ω_0) instead of the swash Dean number (Ω_{sw}). This is advantageous because it simplifies the model and allows the evolution of the beach slope to be predicted using only offshore parameters such as wave height and period. However, it can be seen that some of the beach slope dynamics are lost when terrace dissipation is not taken into account. As an example of this, one can observe the difference in the prediction from July 2015 to January 2016 at NT (mentioned above). Obviously, the role of the terrace dissipation in the evolution of the beach slope at this stage of the morphological evolution, i.e. the increase of the terrace influence, is necessary to recover the observed decrease of the beach slope. A more accurate and dedicated evaluation of the models with field observations would deserve specific studies in the future.

3.2.5 Discussion

The laboratory-scale physical model described in this paper had three main objectives: (i) to highlight the rapid adjustment of the beach slope under wave action by quantifying the relationship between the offshore Dean number Ω_0 and the beach slope equilibrium β_{eq} on a short time scale, (ii) to understand and model the influence of inner-surf zone dissipation on this short time scale equilibrium state, using an idealized flat platform as a model of a terrace beach, an inner-surf zone influences the beach slope dynamics, and (iii) to compare obtained laboratory scale models with field data from two LTT environments. To this end, the inner-surf physical model was designed to highlight the specific influence of (Li_{sl} & β_i) to mimic either reflective, dissipative, or LTT environments. Depending on this initial geometry (Li_{sl} & β_i) and on the offshore wave forcing, it has been shown that the beach slope can either converge to an equilibrium value β_{eq}, referred to as the short time scale equilibrium state, or remain inactive. This rapid response must be seen as the beach slope equilibrium depending on both Li_{sl} and Ω_0, i.e. $\beta_{eq}(Li_{sl}, \Omega_0)$. Such an approach therefore allows to evaluate the slope of the beach face independent of the global erosion or accretion of the system.

Dean number interpretation

Our results from the inner-shore physical model show a relationship between β_{eq}, Li_{sl}, and Ω_0 that distinguishes two contrasting behaviours:

- For $\Omega_0 < 2.5$, β_{eq} is only weakly dependent on Li_{sl}, i.e. $\beta_{eq}(\Omega_0)$. This is referred to as an active swash system for which β_{eq} decreases for increasing Ω_0.
- For $\Omega_0 > 2.5$, the systems becomes surf-dominated, i.e. $\beta_{eq}(\Omega_0, Li_{sl})$, and the inner-surf length can not be disregarded.

These results allow to distinguish swash dynamics in a swash control or surf control environment, for $\Omega_0 < 2.08$ and $\Omega_0 > 2.08$ respectively. For the swash control beach ($\Omega_0 < 2.5$), the observed pattern of beach slope evolution suggests an inshore sediment flux, while for the surf control cases ($\Omega_0 > 2.08$) a constant beach face erosion was observed with constant sediment transport in offshore directions beyond the breaking point. This behaviour of the

hydro-sedimentary systems is consistent with the Dean number interpretation, where small Ω_0 facilitates accretion while large Ω_0 leads to erosive morphodynamics.

The classification of swash and surf control beaches using the offshore Dean number was proposed by Mingo et al. (2021) for two LTT beaches. Laboratory results support this classification, as the transition between these two states was found to be $\Omega_0 \approx 2.5$ both in the laboratory and in the field. However, it is worth mentioning an important limitation of this laboratory work and the field study conducted by Mingo et al. (2021) on the Dean number interpretation. In both laboratory and field, Ω_0 varies due to the steepness of the wave type H_0/λ_0 and not due to the variation in sediment fall velocity. Therefore, further laboratory scale investigations are needed to clarify the role of Ω_0 and its interpretation as a control parameter of the swash dynamics.

Influence of a flat platform on beach slope dynamics

Low tide terrace environments are known to be tide-modified beaches that exhibit characteristics of both dissipative and reflective sites (Miles and Russell, 2004; Almar et al., 2016). At low tide, the terrace can be exposed to the surface and therefore there is no wave action on the upper beach face. As the water level on the terrace rises, lower levels favour wave breaking on the terrace, creating very dissipative conditions of the surf zone. On the contrary, it is suggested that during high tide, waves can pass unbroken over the terrace and act directly on the beach face, creating very reflective conditions (Lemos et al., 2018; Miles and Russell, 2004). Consequently, the water depth on the terrace, and consequently the wave dissipation along the inner surf, is a key parameter in LTT environments.

The innovative aspect of the inner-beach physical model used in this study is that it allows the simplification of these very complex hydro-sedimentary systems to a few key parameters. In particular, it allows to isolate and distinguish processes that are mostly coupled, such as β and Li_{sl}, and both with the offshore forcing. Here, the initial conditions (β_i, Li_{sl}) are varied independently of the off-shore forcing, leading to several states of the beach, from reflective to dissipative, with or without a significant influence of wave dissipation in the inner surf.

In order to quantify the influence of the terrace on the slope dynamics of the beach face, wave dissipation was modelled using the laboratory model. A dissipation law was found to be an exponential decay depending on the distance to the breaking point and the water depth above the terrace (see model (3.15)). Interestingly, it has been shown that the maximum bore amplitude along the terrace is only controlled by the water depth. This dissipation law has been incorporated into the definition of the Dean number to extract a local swash Dean number Ω (see equation 3.8). This new definition allowed to rationalize the obtained beach slope equilibrium β_{eq}, which was thus shown to be a unique function of Ω_{sw} in the range of experimental parameters considered here. In particular, it shows a quadratic relationship between β_{eq} and Ω_{sw}, where $\Omega_{sw} = 2.08$ corresponds to a minimum slope. This critical value of $\Omega_{sw} = 2.08$ distinguishes distinguishes the two different mechanisms of beach slope response, i.e., swash-controlled and surf-controlled.

- For $\Omega_{sw} < 2.08$, i.e. in the swash control case, $\beta_{eq}(\Omega_0 \approx \Omega_{sw})$ decreases with increasing Ω_0, i.e. Ω_{sw}.
- For $\Omega_{sw} > 2.08$, i.e. in the surf control situation, $\beta_{eq}(\Omega_0, Li_{sl} \rightarrow \Omega_{sw})$ increases with increasing Ω_{sw}.

Comparison of field observations of two LTT environments with physical model results

Finally, the results obtained from the physical model were compared with those obtained from field experiments carried out at two LTT beaches, Nha Trang and Grand Popo (Almeida et al., 2020; Thuan et al., 2019).

Grand Popo was classified as a swash control beach, with a good correlation between the monthly mean offshore Dean number Ω_0 and the monthly mean upper beach slope β. The Dean number at Grand Popo varied between 1.5 and 2.5 and the slope between $tan\beta = 0.1 - 0.3$, there was an inverse correlation between these two parameters (see figure 6 in paper Mingo et al. (2021)). These field results agree well with the laboratory results for swash control cases, which have similar orders of magnitude as well as an inverse correlation between Ω_0 and β_{eq}. The physical laboratory experiments and GP show comparable morphodynamics, characterized by local morphological changes with no cross-shore sediment exchange beyond the inner-shore zone. This finding emphasizes the importance of individual wave action in regulating the dynamics of the upper beach slope over short time scales for swash control scenarios.

On the other hand, Nha Trang has been classified as a surf control beach by Mingo et al. (2021). Nha Trang shows a strong seasonal fluctuation where the beach continuously adapts to summer and winter wave conditions, distinguishing two clear phases: a LTT environment in winter and a more reflective state in summer. A robust correlation was found between the dynamics of the terrace length Lt (which appears and disappears according to the seasonal fluctuation) and the mean monthly Offshore Dean number Ω_0. However, the mean monthly dynamics of the beach surface slope β did not follow the monthly fluctuations of the offshore Dean number Ω_0. This suggests that the flat terrace acted as a filter to dissipate gravity waves, so that the beach slope did not respond directly to offshore wave action. The beach slope at Nha Trang varied around $tan\beta = 0.1$. In the laboratory, the lowest value of active beach slope generated by single waves on a short time scale was $tan\beta = 0.15$. This minimum value was reached when $\Omega_0 = 8.58$ (surf control) and a significant initial terrace length $Li_{sl}/H_t = 28$.

However, despite the quantitative differences between the results of the physical model and the field experiments at NT, two similar behaviours are observed. One is that the terrace acts as a low-pass filter. This has important consequences for the shortest waves (e.g. during storms) that might dissipate over the terrace, resulting in limited action on the beach face. The other similarity has to do with sediment transport, it is observed from the physical model that for surf control cases (high Dean numbers) the sediment was transported beyond the breaking zone in offshore directions, highlighting a strong cross-shore sediment exchange. While at NT, the morphological changes were observed mainly due to cross-shore sediment

exchange transport beyond the inner-shore zones (Almeida et al., 2020).

The local Dean number, defined as the swash Dean number Ω_{sw}, is shown to be a relevant dimensionless parameter to refine the quantitative situation of the equilibrium beach slope β_{eq}. A parabolic relation between β_{eq} and Ω_{sw} (see Figure 3.15) allows to describe swash and surf control cases with a unique law (see Equation 3.9). From this laboratory relationship between β_{eq} and Ω_{sw}, a model is proposed to predict the evolution of the beach slope as a function of simple parameters, such as offshore wave period and wavelength (T_0 and λ_0), water depth on the terrace (H_t), and sediment fall velocity W_s (see equations (3.11a) and (3.11b)). This beach slope model was tested using data from Nha Trang (NT) and Grand Popo (GPP) beaches. The 3.5 year evolution of the monthly beach slope was reconstructed for both beaches using the model, and the results were compared with beach slope values obtained from field experiments (see Figure 3.25 and 3.26). The comparison shows good agreement between the modelled and observed beach slope, indicating that the model is able to capture the dynamics of beach slope evolution at both NT and GP and to distinguish between surf and swash control situations.

3.2.6 Conclusion

This study presents a physical model for understanding the dynamics of beach slope evolution in reflective and LTT environments using a simplified approach of inner-shore hydro-sedimentary systems. The physical model is designed to capture an equilibrium beach slope β_{eq} on a short recovery time scale for different monochromatic wave forcings. This is done by imposing a variety of initial beach morphology conditions, characterized by the inner surf zone length or terrace length Lt_i and the initial upper beach slope β_i. The results of this physical model allowed to classify the equilibrium beach slope as a function of the Dean number, based on either the offshore wave forcing or the local swash resulting flow characteristics, Ω_0 and Ω_{sw}, respectively. The results show that two situations can be distinguished: a surf control or a swash control morphodynamics for $\Omega_0 > 2.08$ and $\Omega_0 < 2.08$, respectively. This definition is shown to be in agreement with field experiments carried out at two LTT beaches (Mingo et al., 2021).

The distinction between the off-shore and swash dean Ω_0 and Ω_{sw} was possible thanks to a hydrodynamic study carried out to study the transformation of the waves on the flat platform, i.e. the modeled terrace, in order to quantify the wave energy dissipation. The main objective was to study the influence of the flat platform on the morphodynamics of the beach slope. In particular, it was observed that the wave breaking process when approaching the platform is depth controlled, i.e. the water level in the inner surf controls the maximum wave height and the dissipation after the breaking point. This process can be modeled by an exponential attenuation of the wave height away from the breaking point (see equation (3.15)). Such an evaluation allowed to propose a simple definition of the local swash Dean number, Ω_{sw}. It was shown to be a more relevant dimensionless number to characterize the morphodynamics in the surf control situation, i.e. $\Omega_0 > 2.08$, than the offshore Dean Ω_0. Thus, a simplified model is proposed to predict the rapid evolution of the beach slope as a function of the swash Dean

number Ω_{sw}. The proposed model effectively describes the overall evolution of the beach slope on a short time scale, and highlights the distinction between swash and surf control scenarios. Further investigation is needed to improve our understanding of this phenomenon, including exploring the interpretation of the Dean number and investigating transient states that could lead to more refined out-of-equilibrium modelling.

Finally, the beach slope model together with the wave dissipation law into the inner-surf have proven relevance in describing swash and surf control for two LTT field situations, Gran-Popo and Nha Trang, given some parameter adjustments from physical models as explained along the paper. However, it remains unclear whether the law can be applied to other LTT environments. In particular, since water level is a critical parameter in the system, it is essential to investigate how the attenuation coefficients from the dissipation law change with varying water levels. Further studies are needed to clarify this aspect and to improve our understanding of wave dissipation on a flat platform. Nevertheless, this work is a starting point for explaining the variability of beach slopes observed in the field and has the potential to improve our understanding of coastal morphodynamics.

3.3 Beach adaptation to rapid wave changes

Building upon the previous results presented in Section 3.2, this section investigates the relationship between the equilibrium beach face slope and the Dean number (β_{eq} and Ω) using the same physical model. The objective is to clarify the role of the Dean number as a control parameter of swash dynamics in beaches with a surf zone recreated by a flat platform. Furthermore, we also study the out-of-equilibrium zone of the beachface slope observed between the inactive and equilibrium zones defined in Section 3.2. The results of this investigation are presented in the form of an article. This is a separate and independent article from Section 3.2, nevertheless the description of the model and methods used to extract the studied parameters are the same, so readers may skip that section if desired.

3.3.1 abstract

This study explores the parameters within the Dean number that affect the dynamics of the beach face slope for double-sloped beaches. A new interpretation of the Dean number is proposed as the relationship between wave steepness and the Rouse number. These findings suggest using local swash wave steepness to classify beach systems as either surf or swash dominated. A positive correlation between β_{eq} and s_{sw} is observed for surf-dominated environments while an inverse correlation is observed for swash-dominated beaches states. The equilibrium values of the beachface slope fluctuate around a constant value, with lower slope values observed only for inactive or transitory states. These low slope values may be associated with out-of-equilibrium states and warrant further investigation. Our study provides a framework for future research to explore the interactions between the Rouse number and other physical processes in out-of-equilibrium states.

3.3.2 Introduction

The swash zone is defined as the interface between land and sea, known to be a highly dynamic region in the nearshore (Puleo, 2009; Kikkert et al., 2013). The morphology of the swash zone is partly characterized by the local beach-face slope, defined by Masselink as the portion of the beach profile below the berm exposed to wave action (Masselink and Puleo, 2006). The rapid evolution of the beach-face slope is an important phenomenon to study due to its significant impact on the coastal zone. The beach-face slope plays a crucial role in determining the stability of the shoreline and the dynamics of the hydro-sedimentary system. Changes in the beach-face slope can lead to changes in wave energy dissipation or reflection, wave run-up excursion, and sediment exchange between land and sea (accretion or erosion). In continuation of the previous study (Section 3.2), this article aims to deepen our understanding of the rapid response of beach-face slope to single wave forcing by using a physical model based on a simplified approach of the inner-shore hydro-sedimentary system for double-slope beaches.

Understanding the factors that control the rapid evolution of beach face slope is critical as coastal areas are under increasing pressure from climate change and human activities, resulting in significant changes to the coastline. In recent decades, an increase in the frequency of storm events has been observed, leading to more severe episodic coastal erosion (Callaghan et al., 2008; Masselink et al., 2016), coastal retreat due to mean sea level rise (Bruun, 1962; Dean and Houston, 2016), and among other effects mainly related to climate change, there is an increase in wave energy that directly impacts the coastline and affects storm wave characteristics (Sterl et al., 2009; Hemer et al., 2013). All these factors strongly influence the inner coast and how these systems will adapt and evolve to new equilibrium states is an essential research priority to reach better management and protection strategies of these valuable environments.

The objective of this paper is to investigate the primary parameters that govern the rapid dynamics of the beach-face slope and to assess their influence on the ability of the system to recover after storms or severe events, and ultimately to reach a new equilibrium state. To achieve this goal, we extended previous work based on a simplified physical model that captures the rapid response of the beach-face slope (β) to individual wave actions, while taking into account the initial geometric conditions of the beach-face. This model was designed to replicate the shoaling process of incoming waves with a gentle rigid slope (fixing the breaking point) followed by a surf zone that can be replicated by a rigid flat platform, thus replicating double-slope beaches.

This physical model was used to investigate the influence of a flat platform on swash dynamics and its correlation with the Dean number, also known as sediment fall velocity (Dean, 1973), for short time scales (several tidal cycles depending on tidal range and wave period) calculated with offshore or local wave conditions (Ω_0 or Ω_{sw}). The laboratory results were compared with field experiments conducted at two different locations: Nha Trang, Vietnam (Almeida et al., 2016) and Grand Popo, Benin (Ondoa et al., 2016; Almar et al., 2019b). Results from previous work (Mingo et al. (2021) and Section 3.2) showed that swash dynamics in LTT environments can exhibit two opposite behaviours - swash or surf control - depending on the Dean number. Dean number, also known as dimensionless fall velocity, is commonly used to classify microtidal beaches by relating offshore wave height (H_0) and peak period (T_0) to sediment fall velocity (W_s). However, changes in these parameters can affect the hydro-sedimentary system in different ways. For example, changes in wave amplitude or peak period can alter the wave structure, while changes in sediment fall velocity can affect the hydrodynamic regime by affecting the relative energy required for sediment transport.

Overall, this study focuses on the importance of carefully considering the specific parameters being manipulated when interpreting the results of Dean number experiments. By doing so, we can gain a deeper understanding of the Dean number as a control parameter for beach slope dynamics and identify the main factors that differentiate surf control from swash control cases. Building on previous work where the Dean number was strongly varied by changing the wave period, we will conduct two additional laboratory experimental campaigns to test the effects of sediment size and changes in the different offshore wave amplitudes. Through these investigations, we aim to improve our understanding of rapid beach slope dynamics in order to develop more robust, yet simple, beach slope models.

3.3.3 Laboratory Model

We use a nearshore experimental model previously developed to characterise the slope response of the beach-face to a given wave forcing, for an out-of-equilibrium initial state. The model consists of a simplified bottom topography over which monochromatic surface evolves prior impacting the upper erodible beach-face. From the wave-forcing paddle to the beach, the topography is made of a rigid, gentle slope followed by a flat platform, which keeps the breaking point fixed near the beginning of the platform. The sandy beach, placed on the flat platform, replicates the upper beach-face and is the only erodible part of the model (see Set-up 3.3.3 and Figure 3.27 for details). It can be noted that, accordingly, the physical model does not consider any morphological changes of the seabed beyond the swash zone.

By adjusting the initial slope and the position of this erodible beach-face relative to the breaking point, the physical model is able to mimic a range of initial beach face states, from reflective to dissipative, as well as those with lower flat platforms. This type of morphology can be seen in nature in coral and rocky reef environments and low tide terrace beaches. These beaches are known as double-slope beaches, which are characterised by two distinct slopes - one representing the slope of the beach face and the other representing the slope of the surf zone.

Subjected to a given wave forcing, the system is set out-of-equilibrium. It has been shown previously that a rapid adjustment of the only beachface slope is first obtained on a short time scale disregarding longtime evolution of the shore line. In particular, previous experiments have indeed shown that the model captures a rapid equilibrium value of the beach-face slope (β_{eq}) in response to constant individual wave action, typically before the first 1000 waves impact the beach-face. Not surprisingly, the specific number of waves depend on the initial state of the beach-face relative to the rapid-equilibrium state.

Laboratory model set-up

A sketch of the experimental setup is shown in Figure 3.27. For a more detailed description of the experimental setup and the hydrodynamics behind the model, we refer the reader to our previous paper (Section 3.2.3).

The physical model of the inner shore region is built into a unidirectional water flume measuring 12.65 m in length, 0.3 m in height, and 0.15 m in width. Monochromatic waves are generated with an oscillating flat paddle located at one end of the flume. The gentle rigid slope ($\tan\alpha = 0.06$) is set between $x = 2$m and $x = 0$m and the flat platform for $x \leq 0$, where x is opposite to the wave propagation along the channel, and $x = 0$ corresponds to the transition from the rigid slope to the flat platform (see figure 3.27). Our model keeps the breaking point fixed around $x = 0$ for the range of offshore forcing considered in this study. The swash zone is represented by a sandy beach characterized by the beach face slope (β). The surf zone is characterized by a dissipation length, L_t, between the breaking point and the beach face position.

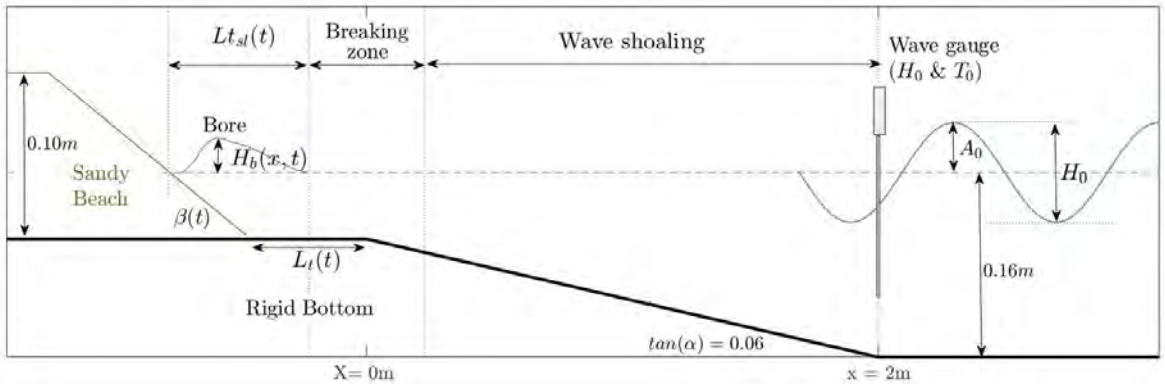

Figure 3.27: Sketch of swash physical model showing primary model parameters.

The characteristics of off-shore waves are measured at $x = 2$ m, i.e. at the entrance of the rigid slope, by using a water gauge. Wave characteristics include amplitude (H_0) and period (T_0). Wavelength (λ_0) is obtained by the relation of dispersion of linear gravity wave at finite depth according to Airy wave theory. The main hydro-morphological evolution at the nearshore zone of the model is captured by the use of high-resolution sCMOS cameras. These cameras enable the acquisition of high-quality time-series images (see Figure 3.28a) of the beach-face profile and wave evolution on the sloping bottom and flat platform. Optical shadow-graph techniques are then employed to extract key variables such as the free surface evolution $H_b(x,t)$, beach-face slope $\beta(t)$, and shoreline position $Lt_{sl}(t)$ from the collected images (see Figure 3.28b). In particular, the image acquisition frequency for the morphological analysis of the beach slope evolution ($\beta(t)$ and $Lt_{sl}(t)$) is 2Hz, while for the hydrodynamic analysis of the free surface ($H_b(x,t)$) it is 40Hz. Finally, the beach-face slope is automatically identified between the limits of wave excursions using a post-processing program developed for this purpose.

Three typical states of slope evolution have been identified. These states include a rapid equilibrium slope regime, an inactive slope, and an intermediate state of slow convergence to the equilibrium slope. The intermediate state, which involves long timescale evolution of both slope and shoreline position, is referred to as a transient state. However, it is not analyzed here and is reserved for future investigation. Therefore, in this work, this state is considered inactive as it evolves on a time scale that becomes significantly important compared to other observed processes. An example of the evolution of each beach face regime is shown in Figure 3.28(c) and (d), where the equilibrium state is represented by the blue line, the transient state by the dashed black line, and the inactive state by the solid black line.

This study specifically examines the rapid evolution of the beach-face slope and its corresponding equilibrium state. The equilibrium slope (β_{eq}) is reached in less than 1000 waves hitting the beach face, ranging from 200-1000 waves. Depending on the tidal range, this timescale may correspond to one or more tidal cycles in nature. Once the equilibrium slope settles before 1000 waves hit the beach-face, we extract its value by calculating the average slope over a range of 500 waves.

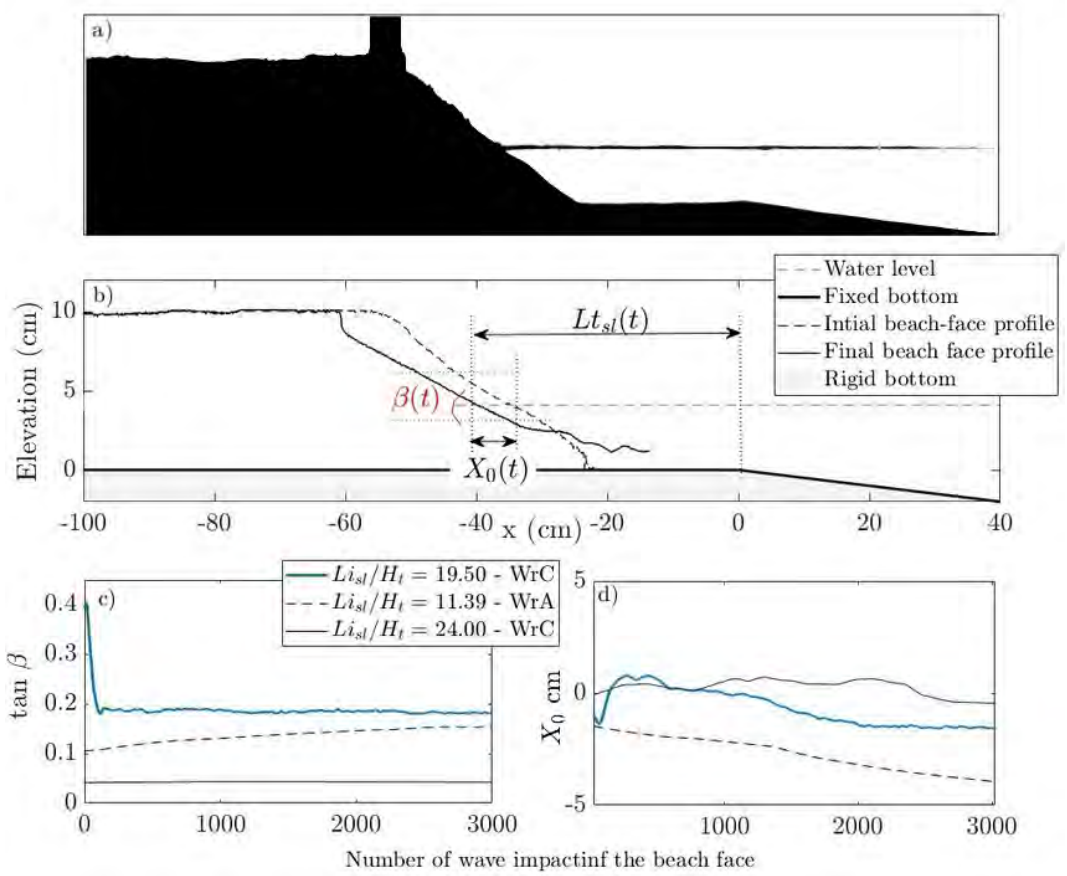

Figure 3.28: a) Example of an initial state profile image obtained with high-resolution sCMOS camera. b) Initial and final position of the beach-face profile. The beach-face slope β is defined between excursion limits of the wave ((red dashed lines) surrounding the shoreline. $X_0(t)$ refers to the local shoreline position evolution. c) 3 examples of the beach-face slope evolution characterizing the equilibrium, inactive and transitory regime, represented by a blue line, black dashes line and solid black line respectively. d) The local shore line evolution, X_0 associate to the three examples from Figure (c).

Range of parameters: exploring the influence of the Dean number as a control parameter of the beachface slope

Our previous studies have identified the Dean number (defined as $\Omega_0 = H_0/(T_0 W_s)$) as a key control parameter of beach face dynamics in response to changing waves. This conclusion was based on field experiments at two LTT beaches and a laboratory physical model (described above) designed to build on these field observations. These studies suggested that the Dean number could be used to classify double-slope beaches as swash or surf dominated, but in both cases (field and laboratory) the main parameter that varied within the Dean number was the wave period. Therefore, to better understand the role of Dean number as a control parameter, it is crucial to test all parameters that could affect it, including wave height and sediment fall velocity. To this end, the same physical model from previous work is used and an extended laboratory test program is developed.

Previously, experiments were conducted using an inland physical model by varying the Dean number in the range $\Omega_0 = 1.13 - 8.58$, mainly by varying the wave period using four different wave regimes (WrA–D). The same sediment sand was used for all experiments. In particular, the beach face was modelled using sand with an average grain size of $D_{50} = 0.12mm$, resulting in a constant sediment fall velocity of $W_s = 0.74cm/s$. A total of 48 experiments were performed by varying the initial geometric conditions of the beach face (Lt_i & β_i). The selection of these wave regimes and initial geometric conditions was based on a careful study that scaled the physical model to field observations of two LTT beaches, one at Nha Trang Vietnam and the other at Grand Popo Benin. The details of this scaling process are described in Section3.2, and the hydro-morphodynamics of these two LTT beaches are described in Lefebvre et al. (2014); Almar et al. (2014); Abessolo Ondoa et al. (2016); Almar et al. (2017b); Thuan et al. (2019); Almeida et al. (2020).

To build on this earlier research, we have designed two additional types of experiments. The first type involves varying the Dean number within the same range as in the previous work, but by manipulating only the offshore wave height while keeping the wave period constant. For these experiments the same sand as in previous work is maintained ($W_s = 0.74cm/s$) and experiments are carried-out for only one initial geometrical state of the beach face. The second type of experiment involves changing the sediment fall velocity (W_s) by modifying the mean grain size (D_{50}). Therefore to analyze the impact of sediment fall velocity, we replicate the same initial states (Lt_i & β_i) and wave forcing used in the previous work.

We can divide our test program into two campaigns: (1) where the sandy beach is made of sand with a mean grain size of $D_{50} = 0.27mm$ and wave regimes are varied by acting either on wave period or wave height. (2) where the sandy beach is made of sand with a mean grain size of $D_{50} = 0.26mm$ and two extreme wave forcing from Campaign 1 are tested. For both cases (campaigns 1 and 2), the initial geometrical conditions of the beach face are varied. The main hydro-morphological parameters of this test program are summarized in Table 3.6. The annual mean parameters of both LTT beaches used previously to design and compare laboratory results are also summarized in Table 3.6. The initial geometrical conditions varied and the number of experiments run for each phase are shown in Table 3.7.

In the following Campaign 1A will be referred to as C_{1A}, Campaign 1B as C_{1B} and Campaign 2A as C_{2A}.

Table 3.6: Test program main hydro-morphological parameters. Wave parameters are measured at the bottom of the rigid slope.

Experiment		D_{50}	W_s	Wave parameters						Dean	Rouse
		[mm]	[cm/s]	Wave Regime	Symbol	H_0 [cm]	T_0 [s]	λ_0[m]	$s = H_0/\lambda_0$	$\Omega_0 = H_0/(T_0 W_s)$	$Rouse = W_s/\sqrt{gH_t}$
Campaign 1	A	0.120	0.74	WrA	○	4.7	0.74	0.75	0.063	8.58	0.0118
				WrB	□	2.5	1.28	1.50	0.017	2.63	
				WrC	△	2.3	1.69	2.00	0.011	1.83	
				WrD	◊	2.1	2.51	3.10	0.006	1.13	
	B				∗	[1.0 - 5.93]	1.03	1.16	[0.01 - 0.05]	[1.31 - 7.78]	
Campaign 2	A	0.260	3.4	WrA	◯	4.7	0.74	0.75	0.063	1.86	0.0542
				WrD	◊	2.1	2.51	3.10	0.006	0.25	

Table 3.7: Test program initial geometrical conditions and number of experiments runs for each phase.

Experiment		Morphological Initial Conditions			Numbers
		β_i	Li_{sl} [m]	Li_{sl}/H_t	of Runs
Campaign 1	A	[0.06 : 0.40]	[0.10 : 1.15]	[2.50 : 28.75]	17
		[0.06 : 0.40]	[0.10 : 1.30]	[2.50 : 33.75]	16
		[0.05 : 0.40]	[0.10 : 1.00]	[2.50 : 25.00]	7
		[0.05 : 0.40]	[0.10 : 1.30]	[2.50 : 32.50]	8
	B	0.140	0.40	10	9
Campaign 2	A	[0.05 : 0.40]	[0.10 : 1.15]	[2.50 : 28.75]	6
		[0.05 : 0.40]	[0.10 : 1.30]	[2.50 : 32.50]	6

Note that by varying the sediment size, we manage to obtain the same Dean number for different wave forcing. This is particularly the case for Campaign 1 - WrC and for Campaign 2 - WrA, for which the Dean number is $\Omega_0 \approx 1.85$ in both cases.

3.3.4 Beach Face slope rapid equilibrium state: Influence of sediment size

Typical evolution of the beach face slope

We first compare the results of two experiments from C_1A for wave regimes WrA and WrD (WrA correspond to the shortest wave length and WrD to the longest) with two experiments from C_{2D} with the same wave regimes and initial conditions. The experiments chosen start close to the equilibrium state found in C_{1A} to isolate the impact of changing the sediment size and thus avoid influence of other parameters when starting far away from its equilibrium state. In particular, all experiments start from $\beta_i = 0.2$ and $Lt_i \sim 0$. Comparisons are shown in Figure 3.29, where the upper panel (a,c) illustrate both experiments using WrA for both sand (C_{1A} and C_{2A}) and the lower (b,d) for WrD. Experiments from C_{1A} are represented with a dashed blue line and those from C_{2A} with a violet full line.

These results reveal a slight increase in the equilibrium beach face slope β_{eq} due to the use of larger sediment sizes. This observation is consistent with existing literature that have proven a positive correlation between sediment size and beach slope (Sous et al. (2013); Bujan et al. (2019)). This increase in β_{eq} is observed before 1000 waves impacting the beach face, which aligns with the time scale used in previous analyses to determine the equilibrium slopes and could be comparable to several tidal cycles in nature. Notably, the increase in β_{eq} is more pronounced for WrD, indicating that sediment size may exert a greater influence on beach face slope dynamics under certain wave conditions.

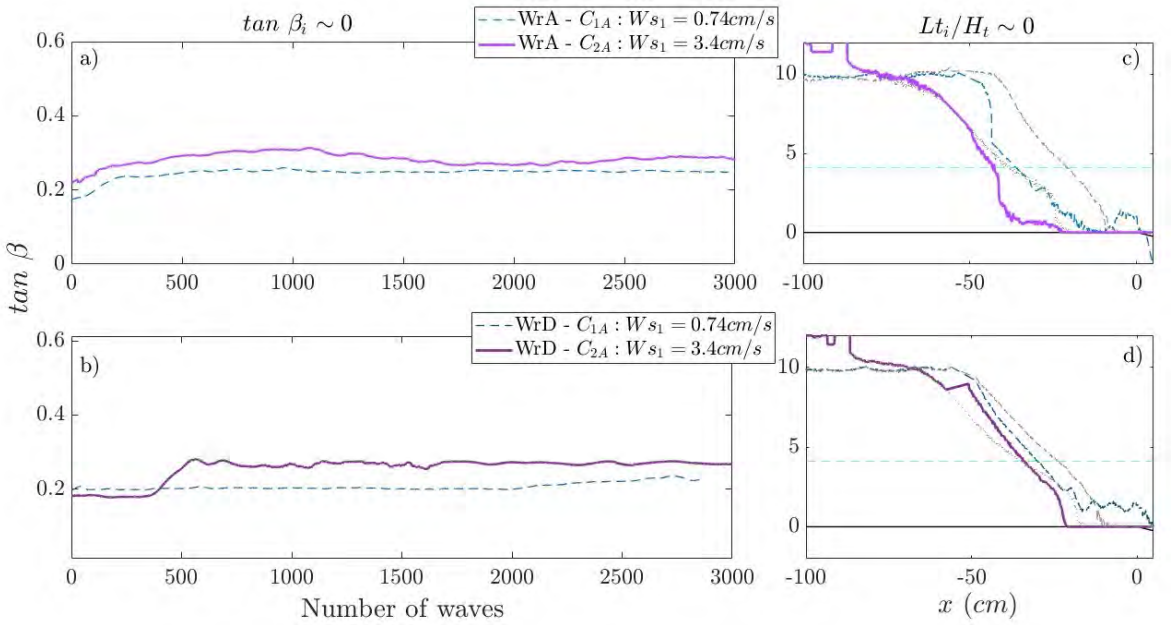

Figure 3.29: Left figures (a and b) show the beach face slope evolution as a function of the number of waves impacting the beach face. 4 Experiments are illustrated, two for WrA represented in Figure (a) and two for WrD in Figure (b). Violets solid line correspond to experiments with grains size of $D_{50} = 0.26mm$ (Campaign C_{2A}) and blue dashed lines of $D_{50} = 0.12mm$ (Campaign C_{1A}). The 4 experiments have the same initial conditions, $Lt_i/H_t \sim 0$ and $\beta_i \sim 0.2$. Right figures (c and d) show both beach profiles at 3000 wave impact associated to both experiments plotted in the left figures. The initial beach profile is shown with a dashed gray line for C_{1A} and gray dotted line for C_{2A}(in Figure c and d).

On the relevance of the Dean number to predict the quasi-equilibrium state

To investigate whether the Dean number can capture the observed increase in β_{eq} when changing the sediment size, we examine whether the equilibrium slopes (β_{eq}) from all experiments with the larger sediment sand (C_2A) agree with the conclusions drawn from the analysis of C_{1A}. Increasing the sediment size reduces the Dean number directly through W_s, with this effect being more pronounced for WrA (reduction from $\Omega_0 = 8.58$ to 1.86) than for WrD (reduction from $\Omega_0 = 1.13$ to 0.25). Previous work on C_{1A} revealed three distinct zones when plotting the final beach face slope against the offshore Dean number: an equilibrium zone around $\tan\beta = 0.2$, an inactive zone strongly influenced by beach face initial conditions and wave forcing, and a transition zone between the equilibrium and inactive zones where the beach face slope evolves rapidly toward the equilibrium zone. This transition zone can also be considered as a non-equilibrium zone. In addition, for $\Omega_0 < 3$, swash-dominated environments were observed, where the beach-face slope responds directly to the offshore wave action and the flat platform weakly influences the swash dynamics. In contrast, for WrA, where the Dean number exceeds 3, a large dispersion of β_{eq} was observed, indicating a surf-dominated system where the flat platform cannot be neglected.

Figure 3.30 presents the final beach-face slope values for both experimental campaigns (C_{1A} and C_{2A}) plotted against their corresponding offshore or swash Dean number. These results illustrate the influence of varying the Dean number across its parameters: C_{1A} varies mainly through wave period T_0, C_{1B} through wave amplitude H_0, and C_{2A} through sediment fall velocity W_s. The analysis also takes into consideration the initial beach morphology, which is represented by a color map showing the initial terrace length scaled by the terrace water depth H_t. Each symbol in Figure 3.30 represents one experiment and is identified by a specific type of symbol corresponding to the wave regime used in that experiment (as described in Table 3.6).

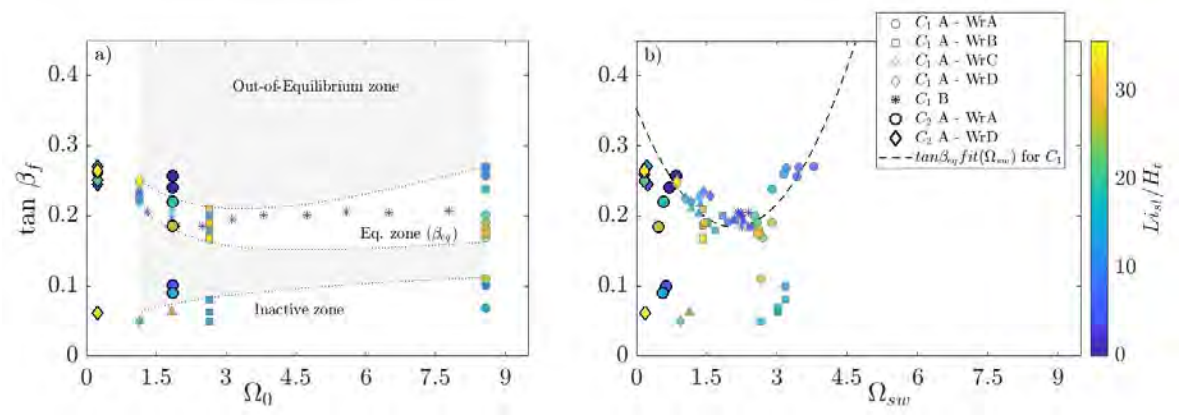

Figure 3.30: (a) and (b) Final values of the beach face slope plotted against their associated offshore and swash Dean number respectively (Ω_0 Ω_{sw}). Each symbol corresponds to one experiment and the type of symbol is associated to the wave regime summarised in Table 3.6. The gray and white zone reffed to equilibrium, inactive and out-of-equilibrium zones extracted from experiments C_{1A}. The color map illustrates the initial position of the shoreline to the breaking point, representing the terrace length Li_{sl}.

Note from Figure 3.30(a) when comparing results from different sediment size, C_{1A} with C_{2A}, represented by the bigger and smaller symbols certain ambiguities arises that require further investigation. Specifically, when $\Omega_0 = 1.8$, there is an overlap of the results for experiments from C_{1A} WrC (represented by triangles in Figure 3.30) and C_{2A} WrA (bigger circles represented by the bigger circles in Figure 3.30). The ambiguity arises as it is unclear whether we are in surf or swash-dominated cases within this overlap. Although experiments from C_{1A} WrC ($\Omega_0 = 1.8$) were classified as swash-dominated states, experiments corresponding to other grain sizes and wave forcing (C_{2A} WrA) exhibit a clear larger dispersion of β_{eq}. Within this dispersion, it is observed that β_{eq} decreases when the terrace width increases (as shown in the color map in Figure 3.30). This behaviour is associated with surf-dominated cases observed in C_{1A} WrA. Furthermore, if we focus on the results of all experiments from the second campaign (C_{2A}), we observe that increasing the sediment size decreases Ω_0 and shifts the results found for C_{1A} (equilibrium and inactives) to the left. As a result, the distinction between surf and swash-dominated beaches is not maintained.

In previous work, a swash Dean number was defined to capture the influence of the

terrace on wave-dominated cases. The local swash Dean number incorporated an exponential borehole height dissipation law on a flat platform and achieved a unique parabolic relationship between β_{eq} and Ω_{sw}, plotted in Figure 3.30(b) and represented by the dashed black line. However, when the results from the second campaign (C_{2A}), where the sediment sand size was varied, were superimposed on the previous results, it was found that the relationship was not maintained for the larger sediment size. In particular, the results from C_{2A} WrA, represented by the larger circles, appear to have the same surf-dominated behavior as observed for the smallest sediment size in C_{1A}.

The fact that the results of the second campaign (C_{2A}) do not agree with the trend of the beach face slope found for the experiments with the smaller sand size (C_{1A}) makes sense because changing the sediment size directly affects the transport regime relative to the wave dynamics. This could lead to the shift observed in the results for both cases when using Ω_0 and Ω_{sw} as control parameters. These ambiguities raise the question whether the Dean number as a control parameter can classify the equilibrium beach face slopes and distinguish between swash and surf dominated cases. Therefore, in the following section, we discuss the physical interpretation of the Dean number.

In Figure 3.30, the results for C_{1B} using the same sediment size as in C_{1A} show an interesting observation. The Dean number was varied in C_{1B} by changing only the offshore wave height, resulting in a Dean number range from nearly 1.5 to 8, while keeping the same initial conditions for C_{1B} ($tan\beta_i \sim 0.14$ & $Li_{sl}/H_t \sim 10$). When classifying the equilibrium slopes with Ω_0, all values migrated to the equilibrium zone. And when the Swash Dean number was used as a control parameter, these β_{eq} values clustered around the same Ω_{sw}. These results are illustrated in Figure 3.30 by the asterisks. These observations are consistent with the previous studies (Section 3.2) that have shown that flat-platform inner-shore morphologies are depth-controlled processes, where the water level on the terrace controls the maximum wave height and dissipation after breaking. Since the position of the beach face to the breaking point (Lt_i), the water level on the terrace (H_t), the wave period (T_0), and the sediment size (D_{50}) remained constant for all experiments in C_{1B}, it was expected that a single value of β_{eq} would be obtained for a unique Ω_{sw}. These results emphasize the depth-controlled nature of such inner-shore morphologies with a flat platform.

3.3.5 Swash and Surf-Dominated Beaches: beyond the Dean Number

The Dean number is a dimensionless parameter that characterizes the efficiency of sediment transport by waves, defined as the ratio of offshore wave height and peak period to sediment fall velocity. A high Dean number would usually suggests a more efficient off shore sediment transport, as preventing deposition on the beachface, while a low Dean number would limit transport due to a stronger effect of sand deposition. However, the interpretation of the Dean number is not straightforward, as its variation can have different effects on the dynamics of the hydro-sedimentary system. This is probably the reason for the inconsistencies found in the previous section for different experimental campaigns.

The Dean number can be varied based on two factors: wave forcing (H_0 and T_0) or the relative transport regime with respect to wave dynamics, i.e. the relationship between wave forcing and sediment fall velocity. The experimental campaigns were specifically designed to distinguish the parameters varied within the Dean number in order to understand their physical significance and their impact on the hydro-sedimentary system. However, the results showed that the Dean number could not distinguish between these two physical processes at least based on the local slope of the beachface (see Figure 3.30). In order to better understand the physical meaning of the Dean number and its impact on the hydro-sedimentary system, we propose to redefine it as a product of two dimensionless parameters that can characterize each of these processes: the wave steepness and the Rouse number.

The Rouse number allows to characterise the vertical distribution of suspended sediment in a turbulent fluid flow. It is calculated as the ratio of the sediment fall velocity (W_s) to the product of the von Karman constant (k) and the shear velocity (u_*) for a turbulent shear flow, i.e. $Rouse = W_s/(ku_*)$ (Rouse, 1937). This number relates the sediment fall velocity to the turbulence in the fluid, which is responsible for mobilizing and suspending the sediment. In our experiments, turbulence is induced by the waves which induce shear flows over the flat platform. It is thus an unknown fraction of the fluid flow induced by wave propagation over the terrace. To simplify our analysis, we thus define the Rouse number as the ratio of the sediment fall velocity to an hydrodynamic velocity on the terrace, based on wave celerity over a shallow fluid layer as defined in equation 3.12.

$$Ro = \frac{W_s}{U_t} \quad \text{with} \quad U_t = \sqrt{g(H_t + A_0)} \tag{3.12}$$

Here Ro is the simplified Rouse number characterizing the system entering the surf zone (flat platform), where W_s is the sediment fall velocity, U_t is the wave velocity, g is the acceleration due to gravity, H_t is the water level on the terrace, and A_0 is the offshore wave amplitude. Note that U_t corresponds to the wave speed in shallow limit for a wave amplitude A_0 over a constant depth H_t. This simplified Rouse number gives an insight of the expected mode of transport of sediment at the beginning of the terrace (surf zone). Note that by simplifying the Rouse number, the transport mode limits established in the literature (Rouse, 1937) may change . However, the physical meaning remains the same: as the Rouse number increases, less sediment is in suspension and more sediment is transported as bedload, while the opposite is true as the Rouse number decreases. In this paper we will refer to the simplified Rouse number directly as the Rouse number (Ro).

Under shallow water theory, waves are not frequency-dispersive, and therefore wavelength can be calculated as a product of wave period and wave celerity. Then, under this assumption, the offshore Dean number can be expressed as the product of the wave steepness (s_0) and the inverse of the Rouse number (Ro), which can be represented as follows:

$$\Omega_0 = \frac{H_0}{T_0 W_s} \quad \rightarrow \quad \Omega_0 = s_0\, Ro^{-1} \quad \text{with} \quad s_0 = \frac{H_0}{T_0\sqrt{g(H_t + A_0)}} \tag{3.13}$$

The obtained dimensionless number s_0 defined a wave steepness based on off-shore wave period T_0 and wave height A_0, and the wave celerity over the flat platform U_t. Then $T_0 U_t$ is an estimation of the wave length over the flat platform based on the characteristics of the wave off-shore. Based on Equation 3.13, we can thus separate the physical processes related to hydrodynamic wave shape and relative transport regime induced by the wave, allowing us to highlight their individual impact on swash dynamics. Then, varying wave period or wave height in experiments C_{1A} and C_{1B}, allows to highlight the influence of wave steepness. Moreover, comparing experiments from C_{1A} and C_{2A}, where the sediment fall velocity is strongly varied, allows to show the influence of the Rouse number (Ro). Wave regime of each campaign can now be represented by the Rouse number (Ro) and wave steepness (s_0) composing together the off-shore Dean number (Ω_0). This relation of control parameters (Ro and s_0) for each experimental campaign is presented in Figure 3.31, which also includes NT and GP data as a reference for our laboratory experiments positioning relative to natural data.

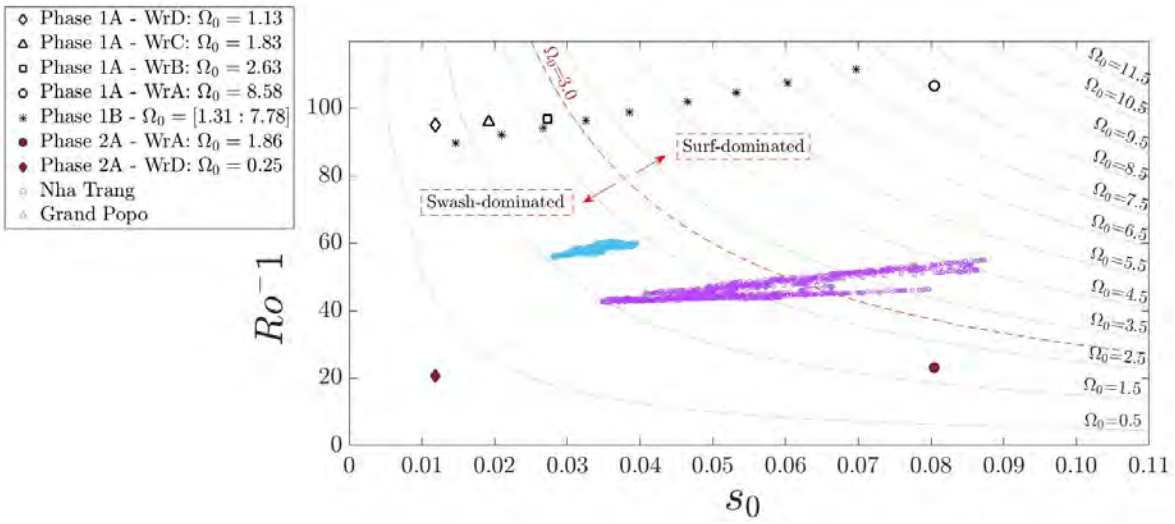

Figure 3.31: Wave steepness at the entry of the flat platforms (s_0) plotted against the inverse Rouse number for each phase of the test program and for nature data (NT & GP), represented by the black or colored symbols. Solid gray and red lines correspond to Dean isoline ($\Omega_0 = s_0\, Ro^{-1}$).

From Figure 3.31 it can be seen that our laboratory experiments cover a wide range of control parameters (Ro and s_0) and include field data (NT and GP). The plot shows that a constant offshore Dean number (Ω_0) (lines) can correspond to a wide range of wave steepness (s_0) and different transport regimes (controlled by the Ro). This effect is particularly noticeable for lower values of Ω_0, such as the Dean isoline for $\Omega_0 = 1.5$. Previous results from the study of C_{1A} indicated that $\Omega_0 = 3$ (red dash line in Figure 3.31) represents a transition between surf and swash dominated beach states, for $\Omega_0 > 3$ and $\Omega_0 < 3$, respectively. This definition was found for $Ro^{-1} \sim 100$, but as the Rouse number increased, experiments with the highest wave steepness (C_{2A}-WrA, represented by the burgundy circle in Figure 3.31) did not behave as a swash-dominated beach, as would be expected based on such Dean transition.

Therefore, the transition between these two types of states, surf or swash dominated, is likely to be a more complicated relationship between Ro and S_0 than described by the Dean number ($\Omega_0 = S_0, Ro^{-1}$).

3.3.6 Equilibrium Beach face slope

In the previous section, we concluded that the Dean number was not sufficient to fully describe the rapid dynamics of the beach face slope. Therefore, we redefined the Dean number as the product of the wave steepness and the Rouse number to highlight the influence of varying either the wave forcing or the relative transport regime on the wave dynamics. In this section, we will separately study the influence of these two dimensionless parameters (s_0 and Ro) on the rapid response of the beach face slope. By understanding how the system responds to these parameters, we intend to develop a physical definition of swash and surf dominated beaches.

Influence of Wave Steepness

To better understand the effect of wave steepness on the equilibrium beach slope, we first consider the dimensionless parameter s_0, which represents the wave steepness. To account for the dissipation of wave height in the surf zone, we introduce a surf wave steepness (s_{sf}) analogous to the surf Dean number. This surf wave steepness takes into account the effect of wave height dissipation on a flat platform, as defined in the previous paper (Section 3.2). Specifically, equation 3.14 defines s_{sf}, where the dissipation law on a flat platform is defined in equation 3.15.

$$s_{sf} = \frac{H_b(x/H_t)}{T_0\sqrt{gH_t}} \tag{3.14}$$

$$\frac{H_b}{H_t} = \gamma_\infty + \exp\left[\sigma(x - x_0)/H_t\right] \quad \text{with} \quad \gamma_\infty = 0.3422; \quad \sigma = 0.1318; \quad x_0/H_t = 6.38. \tag{3.15}$$

Therefore to emphasize the impact of wave dissipation due to the terrace on the equilibrium state of the beach slope, we estimate a swash wave steepness (s_{sw}) at the shoreline Lt_{sl}. This dimensionless number is the evolution of the surf wave steepness, defined in Equation 3.16

$$s_{sw} = \frac{H_b(x/H_t = -Lt_{sl}/H_t)}{T_0\sqrt{gH_t}}, \tag{3.16}$$

Figure 3.32 compares the results of using wave steepness to classify the response of the beach face slope dynamics. This figure shows the equilibrium beach face slope as a function of either s_0 or s_{sw} for all experiments. The same symbol code as in Figure 3.30 is used to

distinguish between the experimental campaign and the wave regimes. The color map also represents the shoreline position to the breaking point for each experiment.

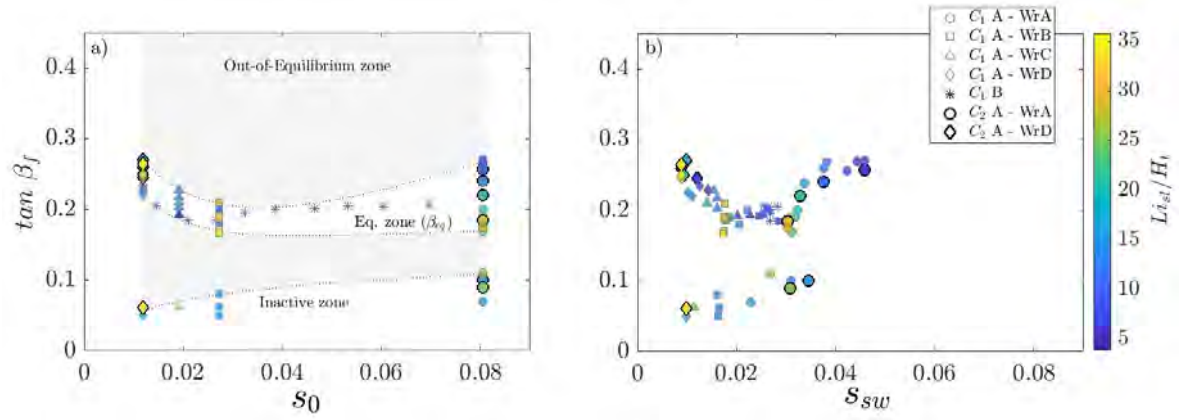

Figure 3.32: (a) an (b) Equilibrium beach face slope (β_{eq}) vs their associated off shore or swash wave steepens (s_0 or s_{sw}, respectively). The color map represents the initial distance from the shore-line to the breaking point Li_{sl}. Each wave regime is represented by a different symbol and experiments from the second campaign are represented with a bigger size symbol associated to the wave regime.

Based on Figure 3.32, it is clear that the offshore wave steepness can be used to identify the equilibrium, out-of-equilibrium, and inactive zones for all sediment sizes. By incorporating the local swash wave steepness, a clear parabolic relationship between β_{eq} and s_{sw} was observed for both sediment sizes. This suggests that the behavior associated with the Dean number in experiments with the same sediment size (C_{1A}) can be attributed to the type of wave forcing hitting the beach face. Across all experiments with different terrace lengths, initial beach face slopes, wave regimes and sediment sizes, the equilibrium zone was observed to be around $tan\beta = 0.2$, with fluctuations due to dissipation on the terrace (right branch of the parabolic relationship between s_{sw} and β_{eq}) or different wave regimes when $s_0 < 0.03$ (left branch of the parabolic relationship).

In addition, the morphologies observed in these experiments are highly depth-induced systems, indicating that the water level on the terrace controls the height of the bore and its dissipation after breaking. As a result, wave period plays a critical role in the dynamics of the beach face slope, since changes in swash wave steepness are primarily driven by variations in the wave period of the wave forcing. Figure 3.32(b) shows not only a parabolic relationship, but also a linear trend between the inactive values of the beach face slope and s_{sw}. The linear trend suggests that for the lowest wave steepness generated by an increase in period, lower initial beach face slope values can be activated by this wave forcing and evolve towards the equilibrium zone. Conversely, for the shortest waves generated with low wave periods, this type of wave forcing has more difficulty activating low initial beach face slopes, possibly due to the high dissipation of wave energy in the surf zone.

Influence of Rouse Number

Our observations indicate that wave steepness serves as an effective classifier of the rapid adjustment of the beach face slope. However, when using the Dean number as a control parameter, it became clear that sediment size plays a critical role in influencing the hydro-sedimentary system by directly affecting the sediment fall velocity, which is reflected in the Rouse number. In this section we aim to investigate the significance of the Rouse number in this context. To this end, we present a plot of the final values of the beach face slope against the Rouse number in Figure 3.33.

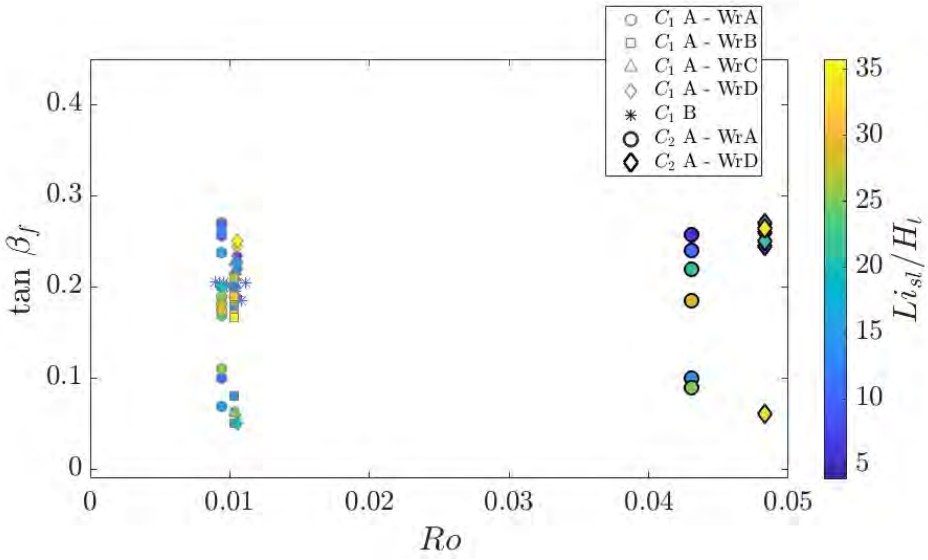

Figure 3.33: Beach face slope final values vs Rouse number. Each experiment is represented by one symbol and the type of symbol differentiates the wave regime and experimental campaign. The color map illustrates the initial shoreline position to the breaking point for each experiment.

As shown in Figure 3.33, there is no direct relationship between the equilibrium beach face slope and the Rouse number. This lack of correlation can be attributed to the fact that changes in sediment size strongly affect the relative transport regime, which does not affect the final equilibrium values of the beach face slope, but the way the beach face evolves towards the equilibrium zone associated with the wave steepness. Although an equilibrium zone can be associated with a particular type of wave forcing, changes in sediment size can lead to variations in the energy required to mobilize and transport sediment, resulting in differences in suspended sediment concentration in the water column on the terrace. Therefore, the time scale required to reach the equilibrium zone associated with wave steepness may vary. The Rouse number reflects this variability as this dimensionless number defines the concentration profile of suspended sediment in a flowing fluid.

To better understand the influence of the Rouse number on the rapid dynamics of the beach face slope, we need to study the hydro-sedimentary systems in non-equilibrium states. This involves determining the characteristic capture time of the hydro-sedimentary system

(t_c) towards the equilibrium zone. In Figure 3.34, we present the characteristic time of four experiments from C_{1A} and C_{2A} for WrA and WrD, and initial beach face conditions that start far from the equilibrium zone, to illustrate the effect of the Rouse number.

Figure 3.34(a) shows two experiments with each sediment size (C_{1A} and C_{2A}) for WrA (represented by circles) and two experiments with each sediment size but for WrD (represented by diamonds). The smaller symbols represent the experiments from the first campaign (C_{1A}) associated with the smallest sediment size, while the larger symbols with a thick black outline represent the experiments from the second campaign (C_{2A}). The figure shows the relationship between the wave steepness (s_0) and the inverse of the Rouse number (Ro) for the four experiments. Subfigures (b) and (c) show the evolution of the beach face slope for the two experiments (C_{1A} and C_{2A}) using WrD and WrA, respectively. In both cases, the initial beach face slope starts near the breaking point ($Li_{sl} \sim 0$), but for WrA the initial slope is higher than the equilibrium zone ($\beta_i = 0.3$), while for WrD it is lower ($\beta_i = 0.1$).

The color map in Figure 3.34(a) represents the characteristic capture time (Tc) of the beach face slope to reach its rapid equilibrium value (β_{eq}), which is associated with the number of waves hitting the beach face. Comparing the four experiments, it can be seen that the characteristic time for the experiments with the smallest sediment size (C_{1A}) is shorter than that of the experiments with the largest sand size (C_{2A}). This is due to the fact that the smaller sediment size has a higher concentration of sediment in suspension, making it more likely to be transported and resulting in a faster evolution of the system. Accordingly the time scale T_c decreases with decreasing Ro.

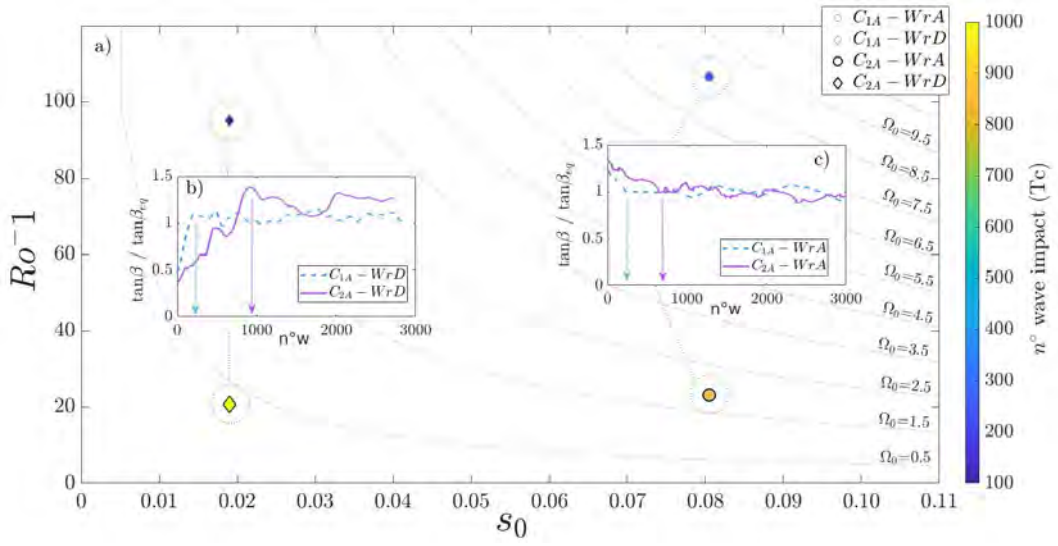

Figure 3.34: Beach face slope final values vs Rouse number. Each experiment is represented by one symbol and the type of symbol differentiates the wave regime and experimental campaign. The color map illustrates the initial shoreline position to the breaking point for each experiment.

In summary, the hydro-sedimentary dynamics of the swash zone are complex and strongly influenced by changes in Rouse number and wave steepness. Nevertheless, results obtain here

suggest that the influence of s_0 and Ro can be distinguished leading to some simplified view of the hydro-sedimentary dynamics, with in particular: s_0 mostly affects the quasi-equilibrium state through β_{eq} while the Ro mostly affect the evolution time scale T_c. Due to the non-linear hydro-morphological interactions within this zone, the sediment transport mechanisms and associated characteristic capture time scales to reach equilibrium can vary significantly. Understanding the characteristic capture time scale (Tc) of the swash hydro-sedimentary is critical to understanding the dynamics of this zone. Since the swash zone is inherently highly dynamic, constantly undergoing different physical processes on different time scales, a complete understanding of the rapid dynamics of the beach face slope to individual wave action is necessary to see how it interacts with other physical processes. Therefore, further investigation of how the beach face slope evolves towards the equilibrium zone should be continued, especially under non-equilibrium conditions, as natural systems are likely to be continuously in such a state. Investigating how the Rouse number and wave steepness control this out-of-equilibrium zone (gray shaded zone in Figure 3.32(a)) is the focus of ongoing research, and initial results are discussed in the following.

Distinction of swash and surf dominated beach states

The behaviour of the equilibrium beach face slope (β_{eq}) with respect to the swash wave steepness (s_{sw}) is parabolic, as seen in Figure 3.32(b). However, each branch of this parabola represents different processes related to swash dynamics. The right branch is associated with surf-dominated states, where wave energy is dissipated during breaking and on the flat terrace, with the surf zone controlling the energy reaching the swash zone. The left branch, on the other hand, is associated with swash-dominated states, where even in shallow water conditions and with the same bottom topography, incoming waves dissipate directly on the beach face, making the dynamics of the swash zone dominant over the surf zone. For these two physical processes, the behavior of β_{eq} with respect to wave steepness is opposite: for surf-dominated states, β_{eq} increases with increasing s_{sw}, while for swash-dominated states it decreases. In this section, we propose a physical approach to understand the dynamics of beach slope with respect to wave steepness.

Surf dominated states are associated with the shortest waves and the largest wave steepness (WrA) and on the contrary, swash dominated states are associated with the longest waves and the smallest wave steepness (WrD). Wave breaking can be characterized by the Iribarren number (Battjes, 1974), defined as $\xi = \frac{tan\alpha}{\sqrt{(s_0)}}$. The braking process of the 4 wave forcings (WrA–D) and the resulting bore associated with their Iribarren number are shown in Figure 3.35. As the wave steepness decreases (WrA $\rightarrow$ WrD), the breaking process changes from plunging to surging, and the bore characteristics in the surf zone are not the same. Wave regime A, associated with the largest wave steepness, produces a violent plugging breaking where a large part of the offshore wave energy is dissipated, the resulting bore is not as energetic and the bore continues to dissipate over the surf zone. Conversely, for the lowest wave steepness as a result of long periods (WrD), the wave may not break at all (surging breaker), resulting in an energetic bore reaching the swash zone. The energy reaching the swash zone from these non-breaking situations can be approximately equal to the offshore

wave forcing. A collapsing breaker is between a plunging and a surging breaker and therefore between breaking and non-breaking, this is observed for WrB and WrC.

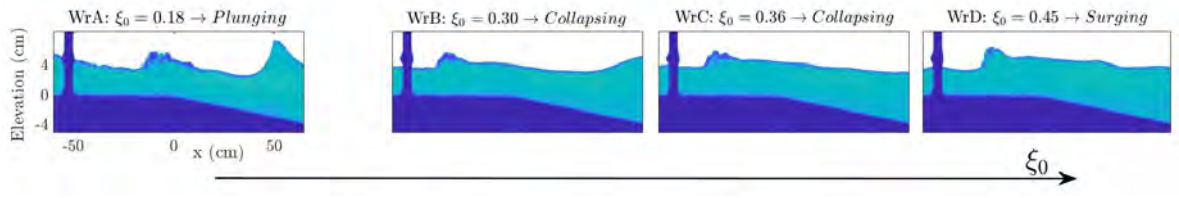

Figure 3.35: Wave breaking process for wave regime A, B, C and D

For surf dominated states (WrA: $s_{sw} > 0.025$), we believe that the reason why the equilibrium beach face slope increases with wave steepness is purely geometric. Here, the beach-face slope adapts itself to reduce the asymmetry between wave run-up and wave run-down until an equilibrium is reached. This hypothesis is explained in Figure 3.23 and equation 3.17 and 3.18.

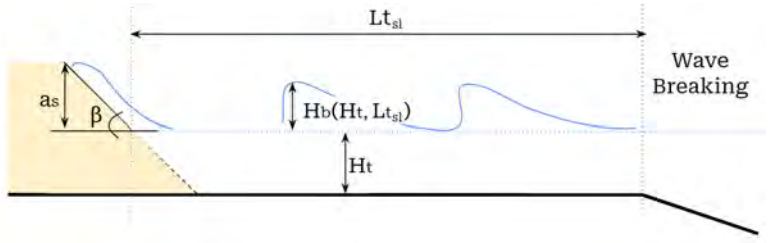

$$
\begin{aligned}
T_s &= \frac{Ls}{\sqrt{g\,Ht}} \\
T_s &= \frac{a_s}{tan\beta\,\sqrt{g\,Ht}} \\
T_s &\equiv T_0 \\
tan\beta_{eq} &= \frac{a_s}{T_0\,\sqrt{g\,Ht}}
\end{aligned}
\tag{3.17}
$$

Figure 3.36: sketch of surf dominated dynamics.

In (3.17), L_s is horizontal projection of the wave excursion at the beach face, a_s is the maximum vertical wave run-up, and T_s is thus the wave period associated with one cycle of up and down surge of the incoming wave, assuming the velocity during the swash being $\sqrt{gH_t}$. Since the wave energy has already been dissipated in the breaking and surf zone, the physics of the beach face could then be based on an equilibrium between Ts and T_0. And since the maximum wave excursion is proportional to the hole amplitude H_b, we can write

$$
tan\beta_{eq} \propto \frac{H_b(H_t, Lt_{sl})}{T_0\sqrt{gH_t}} \quad \rightarrow \quad tan\beta_{eq} \propto s_{sw}, \tag{3.18}
$$

i.e. the slope of the beach face would be proportional to the wave steepness. This could explain the positive correlation found between s_{sw} and β_{eq}, where a decrease in wave height due to dissipation in the terrace would lead to a decrease in s_{sw}, resulting in a decrease in β_{eq}.

The previous model only suggest an adjustment of the slope to reach a phase adjustment

between incoming wave and swash oscillation. However, such mechanism reaches a limit when s_{sw} decreases below 0.03. In this case, i.e. swash dominated cases, we assume that the negative correlation between s_{sw} or s_0 with β_{eq} is related to a slope efficiency for dissipating wave energy reaching the swash zone, which where not dissipated along the surf. This is a non-breaking wave system in the inner-shore and perhaps the beach-face response to the incoming path is to maintain this system in such a way that as s_{sw} increases the system reduces the beach-face slope to avoid wave breaking. This remains a strong assumption which would require further investigation.

In this way, the parabolic relationship between β_{eq} and s_{sw} can be explained by the interaction of two physical processes that distinguish surf from swash dominated states. We observed that the intersection of these processes corresponds to the minimum value of the parabola. We can conclude that for this type of morphology (double-sloped beach), the rapid response of the beach face slope to individual wave action fluctuates around $tan\beta_{eq} = 0.2$, and as a function of wave steepness, the equilibrium beach face slope will follow the surf dominated positive correlation between β_{eq} and s_{sw} or the swash dominated inverse correlation. These relationships are plotted in Figure 3.37, represented by the red and green solid thick lines. We can see from this figure that for surf-dominated cases, β_{eq} decreases towards the inactive zone β_{in} as the length of the terrace increases (reflected by a decrease in s_{sw}). This means that for long terrace lengths, the bore that reaches the beach face has no energy to affect the beach face morphology. For swash-dominated cases, we see that as the wave forcing varies (s_{sw} varies), the beach face is active and fluctuates between different equilibrium values; the equilibrium and inactive zones are well separated despite the terrace length. Finally, in both cases it was not possible to reach equilibrium values greater than $tan\beta > 0.3$. It seems that steeper values of β are unstable regardless of the wave forcing.

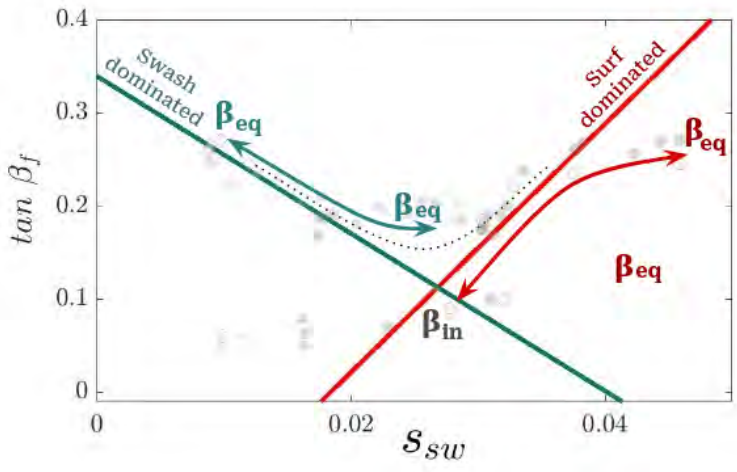

Figure 3.37: Final values of the Beachface slope vs the Swash wave steepness (β_f vs s_{sw}). Each rung is represented by gray symbol associated to their respective wave regime: circle for WrA, square for WrB, triangles for WrC, diamonds for WrD and asterisk for Wr from C_{1B}. The red solid line represents the equilibrium trend of β_{eq} for surf dominated cases and the green solid line the equilibrium trend of swash dominated cases.

The proposed scenario seem consistent with the obtained results at the laboratory scale. However, critical assumptions have been proposed here, which still require deeper validation, from both laboratory experiments and field observations.

3.3.7 Discussion on out-of-equilibrium beach evolution

The analysis of the equilibrium beach face slope on a short time scale demonstrated the importance of wave steepness in the response of the beach face slope. The use of the offshore wave steepness s_0 allowed the categorization of the beach face slope response into three zones: equilibrium, inactive, and an out-of-equilibrium zone between these zones (as shown in Figure 3.32(b)). To approach this out-of-equilibrium zone (represented by the gray shaded area in Figure 3.32(b)), the first step is to identify the slope adaptation mechanisms of the beach face for each experiment to derive a pattern associated with wave forcing.

For all experiments, it was observed that the beach face slope could migrate to the equilibrium zone in three different ways, which we classified into two groups based on the local exchange of sediment in the beach face. The first group corresponds to sediment exchange from the lower to the upper part of the beach face, leading to an increase of the beach face slope (green profile in Figure 3.38(a)). The second group corresponds to sediment exchange from the upper to the lower part of the beach face, resulting in either a decrease of the beach face slope (red profiles in Figure 3.38(b)) or an increase of the slope (yellow profiles in Figure 3.38(c)). Since there is no sediment input in these experiments, the sediment available in the system is strongly controlled by the initial beach face slope (β_i). Therefore, for the first case (sediment exchange from lower to upper beach face), the shoreline can either remain in place or retreat with respect to the breaking point ($\Delta SL \leq 0$). For the second case (sediment exchange from upper to lower beach face), if there is a decrease in beach face slope (red profiles), the shoreline can either remain in place or retreat ($\Delta SL \leq 0$). If there is an increase in beach face slope (yellow profiles), then the shoreline will always retreat ($\Delta SL < 0$).

The previous classification focused on the rapid slope adaptation mechanism, which was found to occur before about 1000 waves hit the beach face. However, another classification can be made based on the direction of sediment flux in the inner-shore zone. In these experiments, two situations were observed: one where the mean sediment flux transport was onshore and the sediment remained close to the beach face, resulting in only local adaptation of the beach face. This situation was associated with swash control cases. The second situation involved sediment transport in an off-shore direction, resulting in constant erosion of the beach face. This constant erosion occurs on a much larger time scale than the rapid adaptation of the beach face slope and was observed in the surf control state associated with WrA. In the latter case (surf dominated), sediment is transported offshore beyond the breaking point.

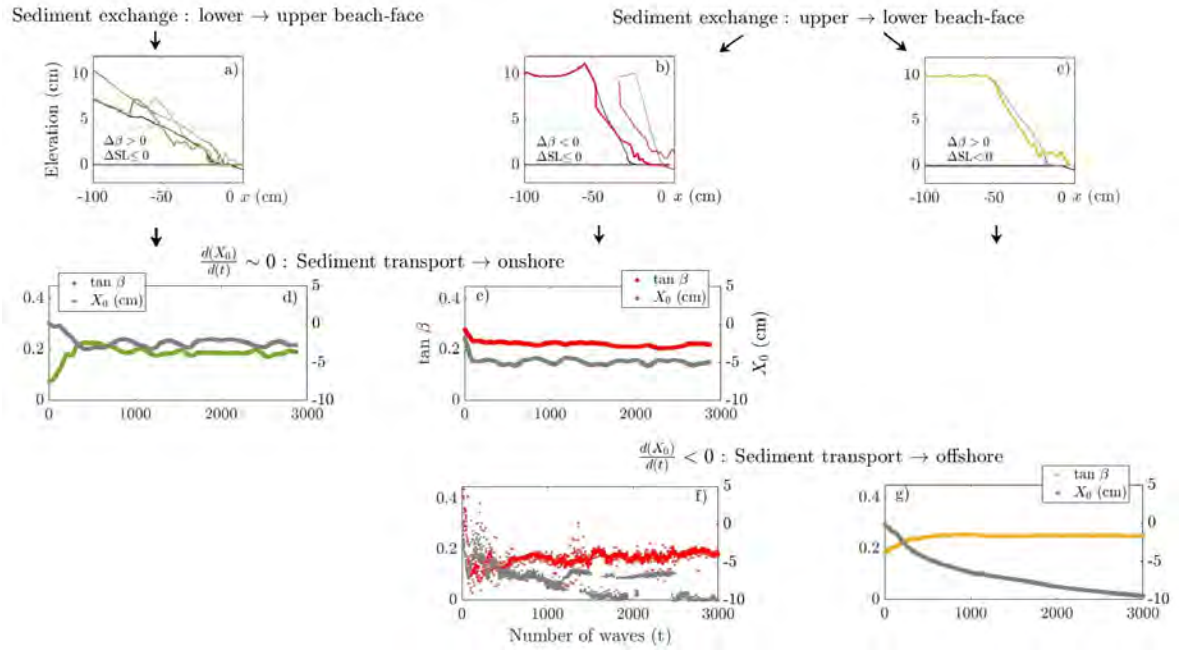

Figure 3.38: Upper panels (a, b and c) show initial and final beach profiles for distinct situations, which classify the rapid slope mechanism to evolve to the equilibrium zone. Three cases are identified: Figure (a) is associated with an increase of the beach face slope by an exchange of sediment from the lower to the upper part of the beach face. Here two examples are shown of the initial (represented in gray) and final (represented in green) position of the beach face profile. One example correspond to a situation where the adjustment of the beachface includes a retreat of the shoreline ($\Delta SL < 0$) and another where the shoreline remained in the same place ($\Delta SL = 0$). In figure (b), the slope decreases due to an exchange from the upper part of the beach face to the lower part (again both situation $\Delta SL < 0$ and $\Delta SL = 0$ are shown). Figure (c) represents also an adjustment of the beach face slope due to a sediment change from the upper to the lower part of the beach face, increasing the beach face slope value. This last case was observed to be always associated with an retreat of the shoreline ($\Delta SL < 0$). The lower panels (Figure d–g) illustrate the evolution of the beach face slope represented in the color of the slope mechanism to migrate to the equilibrium zone and the local evolution of the shorelines (X_0) represented in gray.

The experimental cases classified on the basis of the adaptation mechanism of the beach face slope can be further subclassified on the basis of the mean sediment net flux directions in the inner-shore zone. This is obtained through the evolution of the shoreline, represented by the local evolution of the shoreline position X_0 in figure 3.38(d–g) (again, $X_0$is defined in Figure 3.28). Two situations have been identified: onshore transport and off-shore transport beyond the breaking point. These two cases are highlighted by the behaviour of X_0 and its associated shoreline position evolution.

When sediment is transported in the onshore direction, there is a rapid adjustment of the shoreline due to the rapid adaptation of the beach face slope, followed by stability in the absence of further sediment input or variations in other physical parameters. This situation

is associated with the case where the beach face slope increases due to sediment transport from the lower to the upper part of the beach face for low enough initial slope (green case in Figure 3.38(a)) and when the slope decreases due to sediment transport from the upper to the lower part of the beach face for high initial slope (red case in Figure 3.38(b)). In both cases, after the rapid adjustment of the beach face slope, the sediment remains stable in the inner shore zone, as shown in Figure 3.38(d) and (e).

On the other hand, it has been observed that sediment can also be transported in offshore directions beyond the breaking point. In these cases, after the rapid adjustment of the slope of the beach face, there is a constant erosion of the beach face with a much lower erosion rate ($\frac{dX_0}{dt}$) than the slope adjustment. These situations are associated with slope adjustment due to sediment exchange from the upper to the lower part of the beach face, as shown in Figure 3.38(f) and (g).

The classification presented in Figure 3.38 can be further summarized by defining different zones within the out-of-equilibrium area that are identified for different wave steepness (β vs. s_0). This leads to the distinction of different zones within the out-of-equilibrium region based on how rapidly the beach face slope adapts to the wave forcing. The resulting zones are shown in Figure 3.39, where the color coding reflects the rapid adaptation mechanisms of the beach face slope, as shown in Figure 3.38 (a), (b), or (c). In addition, the net sediment transport in the coastal zone is taken into account and represented by either a hatched zone (with oblique dotted lines) or an unhatched zone.

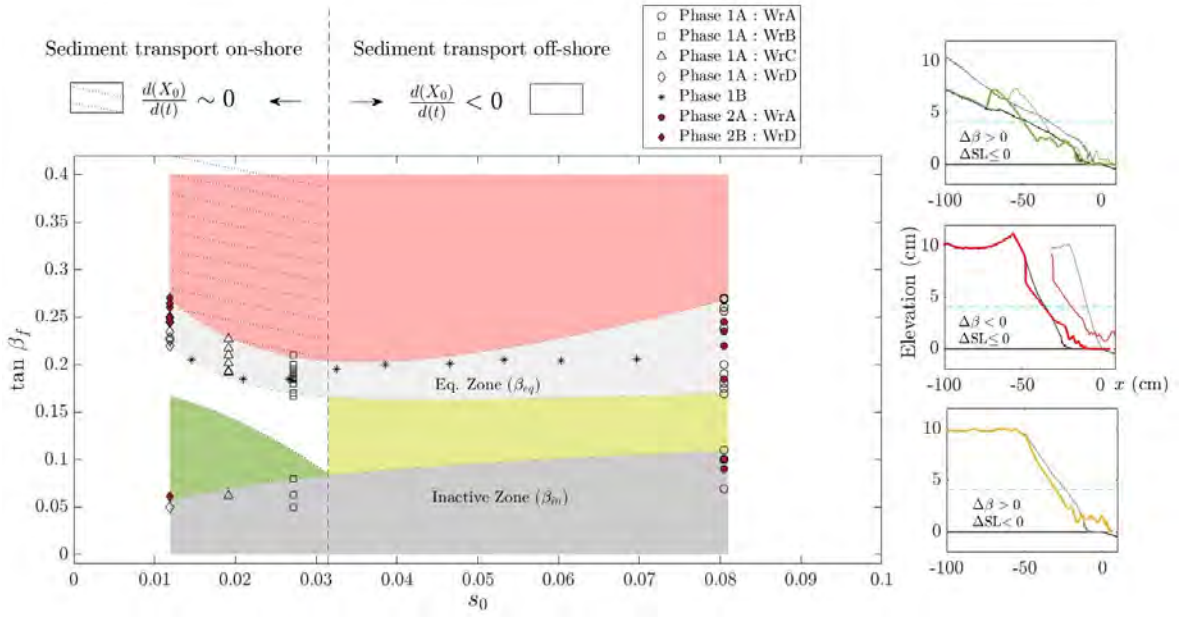

Figure 3.39: Main Figure shows the final beachface slope vs offshore wave steepness (s_0). The colored area represents the slope adaptation mechanisms towards the equilibrium zone, detailed in Figure 3.38 and associated to the small 3 plots in the right of the Figure. The hatched and un-hatched zone represent of the main Figure represents the net flux sediment transport direction also detailed in Figure 3.38.

3.3.8 conclusion

In order to understand the physical influence of wave dynamics on the swash zone, previous studies have usually examined the relationship between beach face slope and Dean number. The present work actually provides clarification of the influence of the Dean number. In particular, we have provided a new interpretation of the Dean number as the relationship between two main parameters, wave steepness and Rouse number, which affect swash dynamics in different ways.

Wave steepness allowed us to classify a beach as either surf or swash dominated, indicating where wave energy is dissipated. For surf dominated beaches $s_{sw} > 0.025$, wave energy is dissipated during the breaking process and along the flat platform (surf zone). Consequently, the energy reaching the beach is limited. Here, the quasi-equilibrium slope β_{eq} increases with increasing s_{sw}. It was suggested that this trend can be explained by a phase adjustment between swash oscillation and wave period. In contrast, in swash-dominated conditions, energy is dissipated directly at the beach face. Swash dominated cases are obtained for $s_{sw} < 0.025$. In this case, another mechanism allows to reach higher value of the beachface slope. In particular, β_{eq} increases with decreasing s_{sw} in this regime. This could probably be attributed to a wave dissipation mechanism within the swash which still requires to be investigated. Finally, note that in Figure 3.31, wave steepness against the inverse Rouse number (s_0 vs Ro^{-1}) also includes field data from NT and GP. According to our classification, surf dominated beaches are those with $s_0 > 0.03$ or equivalent $s_{sw} > 0.025$, and both NT and GP would therefore be classified as surf dominated beaches. However, this is not the case for GP. Here, observations from GP and NT would suggest a transition around $s_0 \approx 0.04$. This is close but slightly higher. This discrepancy could be due to uncertainties in evaluating parameter

We found that the Rouse number had little effect on the equilibrium values of beach face slope, which were primarily controlled by wave steepness. However, the Rouse number did affect the characteristic capture time (Tc) required to reach equilibrium values. This time is critical to understanding swash behaviour because these systems are highly dynamic, and Tc indicates whether equilibrium has been reached or if the system will remain in a constant out-of-equilibrium state, requiring more consideration of other physical processes acting simultaneously. Therefore, an out-of-equilibrium approach is necessary to incorporate the influence of the Rouse number.

We have classified the equilibrium values of beach face slope associated with a short time scale and identified different zones within the out-of-equilibrium region associated with sediment transport. This provides a first framework for future studies using an out-of-equilibrium approach to explore the interactions with other physical processes and how the Rouse number influences each of these zones. In summary, our work provides valuable insights into the rapid dynamics of the beach face slope and lays the groundwork for further research in this area.

Chapter 4

Perspectives and overall conclusions

Contents

4.1 Perspectives

4.1.1 Revisiting field data with insights from laboratory experiments

After conducting an extensive laboratory study, we revisited the field analysis to validate and restructure our hypotheses, draw new conclusions, and outline the future directions of this research. One of the key findings from this study is the identification and quantification of swash- and surf-dominated beach states, which we initially observed at two low tide terrace environments (NT and GP) that had similar sediment sizes but vastly different wave climates (see Chapter 2). In the laboratory, we further investigated this phenomenon and concluded that for these types of morphologies, which are characterized by a double-slope condition at the foreshore and considered as a depth-induced system, the dynamics of the beachface respond differently to wave forcing.

In our initial findings, we observed that the Dean number can effectively distinguish between swash-dominated and surf-dominated beach states, with $\Omega_0 < 2.5$ indicating a surf-dominated state and $\Omega_0 > 2.5$ indicating a swash-dominated state. However, we recognized that this dimensionless number is multifaceted and by manipulating its parameters, various physical processes are influenced, such as wave structure and the relative energy required for sediment transport. These variations can have distinct impacts on the net sediment transport within the studied region.

To address this complexity, we proposed a conceptual framework in Chapter 3, where the Dean number can be understood as the product of two dimensionless numbers: wave steepness and the Rouse number, that each represents different physical aspects of the system. Wave steepness (s) characterizes the wave structure, while the Rouse number controls the mode and rate of sediment transport. By analyzing the Dean number in this manner, we were able to disentangle the contributions of wave structure and sediment dynamics to the overall behaviour of the coastal system.

Through our simplified approach that lead to develop a physical laboratory model, we made significant progress in understanding the differentiation between surf-dominated and swash-dominated environments. Our findings suggest that the classification of these environments (swash-and surf-dominated) is largely associated to the wave structure, with wave steepness playing a critical role in the direction of sediment transport. Furthermore, we have identified the Rouse number as a key factor influencing the system's response time, which is a crucial parameter in coastal systems, as it controls the interactions between different physical processes occurring simultaneously.

Swash-dominated states: Grand Popo LTT beach

Based on our previous findings (Chapter 2 – field study), Grand Popo beach can be classified as swash-dominated by observations of its physical behaviour. However, if we want to classify it using laboratory conclusions, we can use either the offshore wave steepness (s_0)

or the local wave steepness (s_{sw}). The limit was found to be around 0.03, where $s < 0.03$ corresponds to swash-dominated and $s > 0.03$ corresponds to surf-dominated. Figure 3.31 in Section 3.3 show the range of wave steepness for Grand Popo and laboratory data. We can observe that Grand Popo is located around $s_0 = 0.03$ which is in the transition zone. Although the comparison between laboratory and field data is challenging due to the scaling procedure, we can conclude that the orders of magnitude are reasonable, and the main physical tendencies observed in the laboratory can be applied to the field.

One of the defining features of swash-dominated environments is their rapid response to offshore wave action, particularly in the beachface slope. As discussed in Chapter 3, the majority of offshore wave energy is transferred to the swash zone and dissipated directly on the beachface, leading to a quick adjustment of its slope. Consequently, a rapid equilibrium slope can be associated with individual offshore wave forcing, as demonstrated by the classification model based on the Dean number developed in Section 3.2, which was later refined to include wave steepness in Section 3.3. Due to the fast timescale of the beachface slope adjustments, the Rouse number has little influence on swash-dominated systems, making the use of the Dean number as a control parameter a reasonable choice.

Given the fact that the beachface slope can be then predicted with offshore wave parameters in swash-dominated environments disregarding the effects of the surf zone, empirical formulations based on the only offshore wave characteristics may then be relevant to predict the rapid evolution of the beachface slope at Grand Popo. Therefore, formulations extracted from the literature are going to be tested and their performance is going to be compared with the models proposed in this work, including a data-driven model proposed in Chapter 2 and a semi-empirical model proposed in Chapter 3.

In total, four data-driven and semi-empirical formulations extracted from the literature are chosen to predict the beachface slope evolution at Grand Popo. Two of them proposed by Rector (1954) and Kim et al. (2014) that are based on the fact that the beachface slope is strongly related to wave skewness and the median grain size. Specifically, the formulation proposed by Rector (1954) based on laboratory tests highlights the importance of wave steepness and wave period, which is consistent with our observations on sediment transport in the foreshore. Therefore, the empirical formulation proposed by Rector (1954) is a good choice to compare with our models. On the other hand, the other two empirical formulations that we are going to test are not dependent on wave steepness or wave period, but rather on offshore wave height and mean sediment size (Reis and Gama, 2010; Uda and Hashimoto, 1982). We believe these relations will be less affected, as we have observed that this type of morphology are depth-induced system, meaning that the water level on the terrace highly controls the wave height on the foreshore and therefore variations in wave height will not necessarily be reflected after the wave breaking. The results are presented in Figure 4.1, where the beachface slope evolution at Grand Popo, extracted from measured data, is compared with different empirical or semi-empirical formulations. Table 4.1 presents the specific equations of these empirical models and their root mean square error (RMSE) between the measured beachface slope evolution and the predicted values.

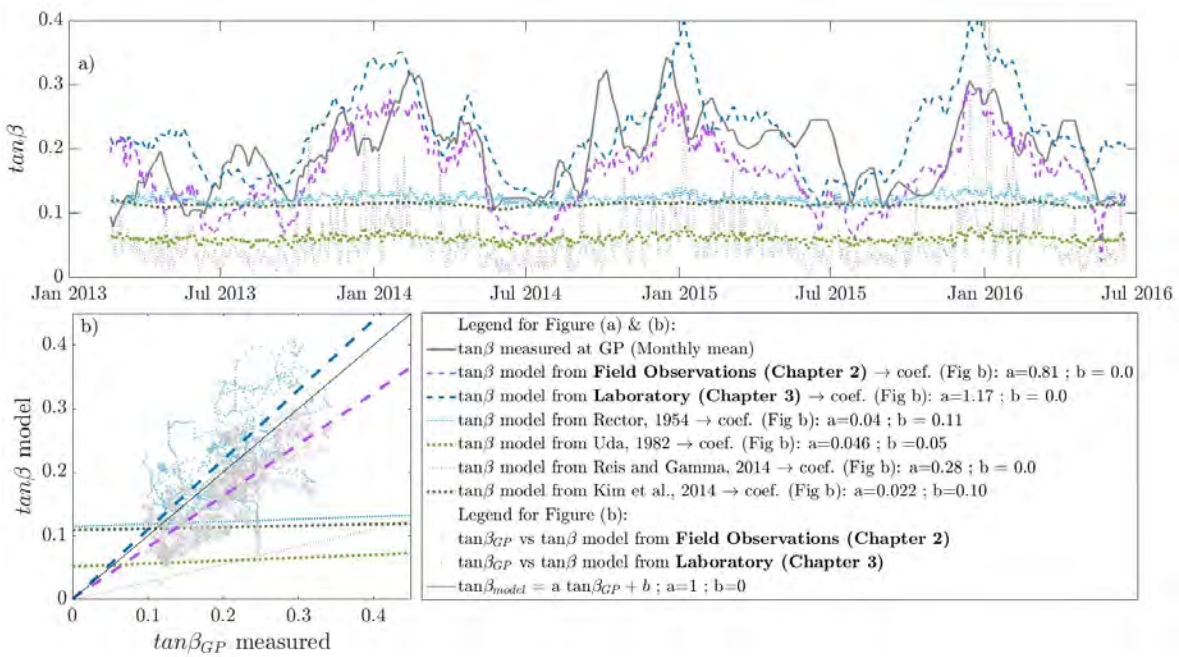

Figure 4.1: (a) Monthly mean beachface slope evolution at Grand Popo, where the measured data is plotted with the thick grey line. The dashed lines corresponds to the beachfaces slope evolution calculated from model proposed in this work while the dotted lines correspond to models from literature (Rector (1954); Uda and Hashimoto (1982); Reis and Gama (2010); Kim et al. (2014)). Figure (b) Plots the best linear fit between the daily beachface slope measured at GP ($tan\beta$measured) vs the one calculated from the different models. This linear relations are shown with the same legend than Figure (a).

Table 4.1: Beachface slope data-driven or semi-empirical models that are tested to predict Grand Popo beachface slope evolution.

Source	Equation	RMSE ($tan\beta_{GP}$ & $tan\beta_{model}$)	Comments
Field Observation Model (Chapter 2)	$y(x) = F(\Omega_0)(x-\hat{x})^3 + G(\Omega_0)(x-\hat{x}) + \hat{y}$	0.05	Data-driven model
Laboratory Model (Chapter 3)	$tan\beta = \alpha(\Omega_0 - \Omega_T)^2 + tan\beta_0$ $\alpha = 0.0394$; $\Omega_T = 2.08$; $tan\beta_0 = 0.1$	0.06	Semi-empirical model
Rector, 1954	$tan\beta = 0.07(D_{50}/(1000L))^{0.1}/(H_s/L)^{0.42}$	0.10	Semi-empirical model
Uda, 1982	$tan\beta = 4.5(D_{50}/(1000H_s))^{0.5}$	0.14	Data-driven model
Reis and Gamma, 2010	$tan\beta = 0.9H_s^{(-10/3)}D_{50}^{(4/3)}$	0.15	Semi-empirical model
Kim et al., 2014	$tan\beta = 0.332T^{-0.416}D_{50}^{0.122}$	0.10	Data-driven model

Figure 4.1(a) displays the measured beachface slope evolution at GP (grey thick line) and the predicted slopes evolution from the different data-driven and semi-empirical models (dotted lines corresponding to models extracted from literature, dashed blue and violet lines corresponding to models proposed in this work). Figure 4.1(b) presents a scatter plot of the daily tangent beachface slope measured at GP versus the values obtained from both models proposed in this work, represented by the dots and crosses, where the linear fit of these scatter

plots are represent with the dashed lines (violet for the field model and blue for the laboratory model). For the values obtained from the literature models only the linear fit is represented by the dotted line following the same legend than Figure 4.1(a).

The results from Figure 4.1 show that none of the empirical formulations extracted from literature accurately described the beachface slope evolution at GP. Three of them exhibit a rather constant evolution of the slope around a certain value, which is not even the mean beachface slope value observed at GP (Rector, 1954; Uda and Hashimoto, 1982; Kim et al., 2014). Meanwhile, the last model proposed by Reis and Gama (2010) shows a rapid daily fluctuation of the slope, but fails to represent the evolution observed at GP. We believe that equations that depend on offshore wave height are not suitable for this type of topography that is highly controlled by the water level on the terrace. Similarly, equations based on wave steepness and period may need better calibration of their free parameters to be used at Grand Popo.

While the two models proposed in this study show promising results in predicting the overall trend evolution related to seasonal fluctuations, this could be attributed to the fact that these models were specifically developed for the LTT topography and are based on swash-dominated situations. Nevertheless, they fall short to capture the rapid fluctuations of the beachface slope observed on shorter timescales ranging from weekly to monthly. Other physical processes such as infragravity wave actions, tidal effects, sediment input, or transitional states like storms that put the system out-of-equilibrium could cause these beachface slope rapid fluctuations. It was observed at GP that the shape of the beach profile does not change throughout the year, indicating that global it is a stable profile thus, transitory states associated with large sediment transport are not dominant. This suggests that the monthly rapid fluctuations of the beachface slope may be due to tidal effects or infragravity waves actions, that should be further more investigated.

Although the simplified approach used at GP was successful in extracting two simple models for swash-dominated environments based on individual gravity waves, further testing is necessary to validate the models in other LTT swash-dominated environments and why not other morphologies. This will help determine the generality of the approach. In particular, the parameter of water depth on the terrace should be carefully examined as it was found to be crucial for LTT topographies. Even in microtidal environments, this parameter controls the system's behaviour, and its effect should be investigated. Calibrating the model with this parameter may improve its accuracy and applicability in different environments.

Surf dominated states: Nha Trang LTT beach

Nha Trang beach is classified as a surf-dominated environment based on field observations and the laboratory model ($s_0 > 0.03$). As discussed in Chapter 3, the surf zone and its associated physical processes cannot be disregarded when analysing swash dynamics. While the simplified approach presented in this work provided valuable insights on the foreshore dynamics of LTT surf-dominated environments, such as the strong correlation between offshore wave forcing and terrace dynamics (discussed in Chapter 2), or the quantification of wave

dissipation on a flat platform (discussed in Section 3.2), it was not possible to fully capture the complexity of swash dynamics in surf-dominated cases using a single model parameter (based only on the Dean number). Thus, it is necessary to consider other physical processes to accurately predict the dynamics of these systems. Furthermore, Nha Trang beach is a highly dynamic beach, exhibiting clear seasonal fluctuations (see Figure 2.2), with a LTT winter profile associated with energetic wave conditions and a unique slope profile observed in the foreshore during summer wave climate. The transition between summer and winter is characterized by an erosive phase and an accretive phase marked by high cross-shore sediment transport rates. Therefore, due to all of these characteristics, it is necessary to study Nha Trang beach dynamics with an out-of-equilibrium approach for a better understanding of these complex systems and more accurate predictions.

Both Figure 4.2 and Figure 4.3 reveal that the dynamics of the system exhibit two different temporal scales of fluctuations: one associated with a seasonal fluctuation where the beach profile changes its morphology to a winter or summer beach state, and the other associated with weekly or monthly fluctuations where the global profile is maintained, and there can be local changes or translations but maintaining the shape associated with that wave climate. Thus, The transitional state is related to a shape changing of the beach profiles, while the summer or winter profiles experience local variations but maintaining the shape of the beach profile associated with that specific wave climate, fluctuating around a mean profile. This is represented in the left part of the Figures 4.2 and Figure 4.3, where the gray lines represent the daily profiles, and the thick colored line represents the mean seasonal profile.

Figures 4.2 and 4.3 illustrate the mean summer and winter profiles in panels (a) and (b), respectively. The transition between winter 2014 and summer 2015 is shown in panel (c) of Figure 4.2, and the transition between summer 2015 and winter 2016 is shown in panel (c) of Figure 4.3. The top panels of each transition profile present the evolution of the beachface slope ($\tan\beta$), the offshore wave period (T_0), and the offshore wave steepness (s_0). The winter and summer transitions conditions are indicated by blue and violet colors respectively and the transitions is indicate in green when it is in an accretive phase and in red when it is in an erosive phase.

During winter conditions in LTT environments, the beachface slope exhibits fluctuations with a time scale of approximately a week (see Figures 4.3 and 4.2(C_3) - blue part). However, laboratory studies have shown that individual gravity waves have a relatively low impact on the beachface due to high dissipation in the surf zone (see Section 3.2). This was also confirmed by field experiments (Almeida et al., 2020). Therefore, these rapid fluctuations could be associated with the actions of IG waves, as these long free waves do not dissipate in the surf zone and their energy dissipates directly on the beachface. Alternatively, tidal fluctuations can also cause rapid fluctuations, leading to over-swash and affecting the beachface slope. As mentioned above for GP, further investigation is needed to understand the role of IG waves and tidal effects. In contrast, the summer profile exhibits less local and rapid fluctuations of the beach face slope, likely due to less energetic waves impacting the beachface. As shown in laboratory experiments, waves with steepness greater than 0.03 and low energy ($H_0 \searrow$) will not have a significant impact on low slopes ($tan\beta$ 0.1), resulting in an inactive beachface

slope. Therefore, the fluctuations for these low beachface slope values (around $tan\beta \sim 0.1$) may be attributed to sediment flux balance in the global beach shape.

Finally, the seasonal fluctuations occurring between winter and summer states are characterized by changes in the global beach profile, transitioning from a single slope foreshore to a double slope LTT foreshore, or vice versa. This physical process is induced by the interactions of wave forcing on the beach system and the sediment flux balance within the system, resulting in global modifications of the foreshore morphology. The deposition of sediment on the bottom of the beachface produces a decrease in the mean beachface slope value during the transition from winter to summer (Figure 4.2(c)), while erosion of the beachface generates a flat platform, increasing the mean beachface slope during the transition from summer to winter (Figure 4.3(c)). It should be noted that the sediment transport direction controlled by the wave forcing and the interactions with sediment flux in the system play an important role in determining the dynamics of these surf-dominated environments. In the last part of this research work, we began to approach these questions by using the same simplified approach but now focusing on the out-of-equilibrium profiles dynamics.

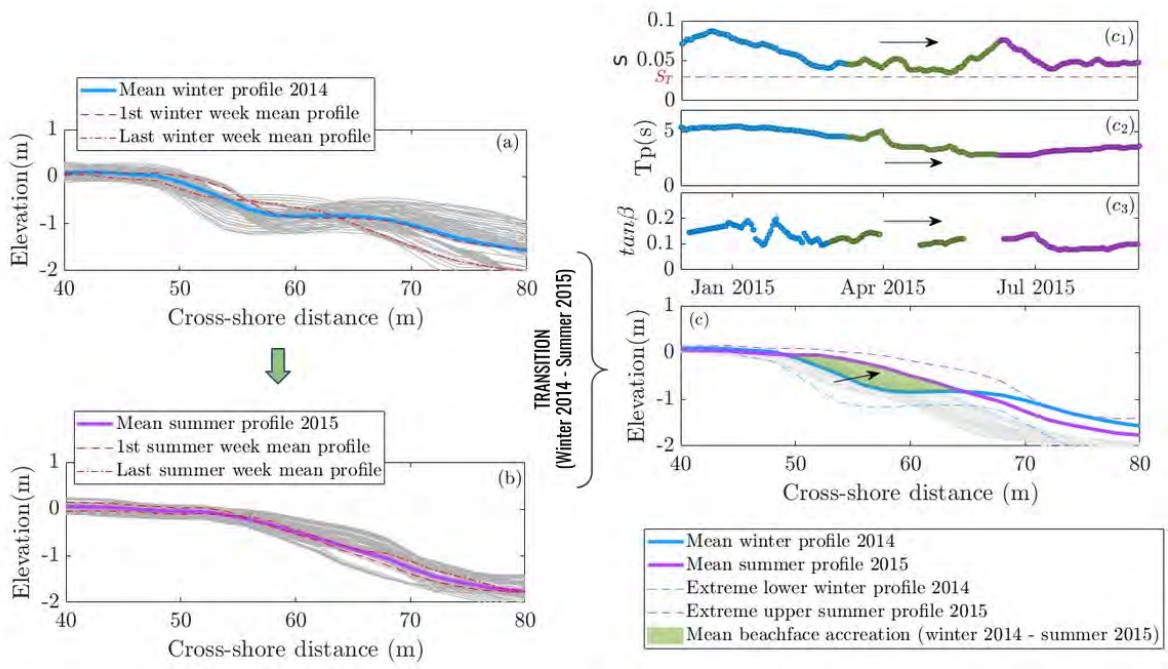

Figure 4.2: Illustrates Nha Trang beach state transition between winter 2014 and summer 2015.(a) and (b) plot the daily beach profiles represented in gray and mean seasonal mean beach profiles represented with blue thick line for winter 2014 and violet line for summer 2015. Figure (c) shows the daily a mean profiles for the transition between winter 2014 to summer 2015. For this transition period Figure c_1, c_2 and c_3 present the evolution of wave steepness (s), ave peak period (T_p) and the beachface slope profile (β), respectively.

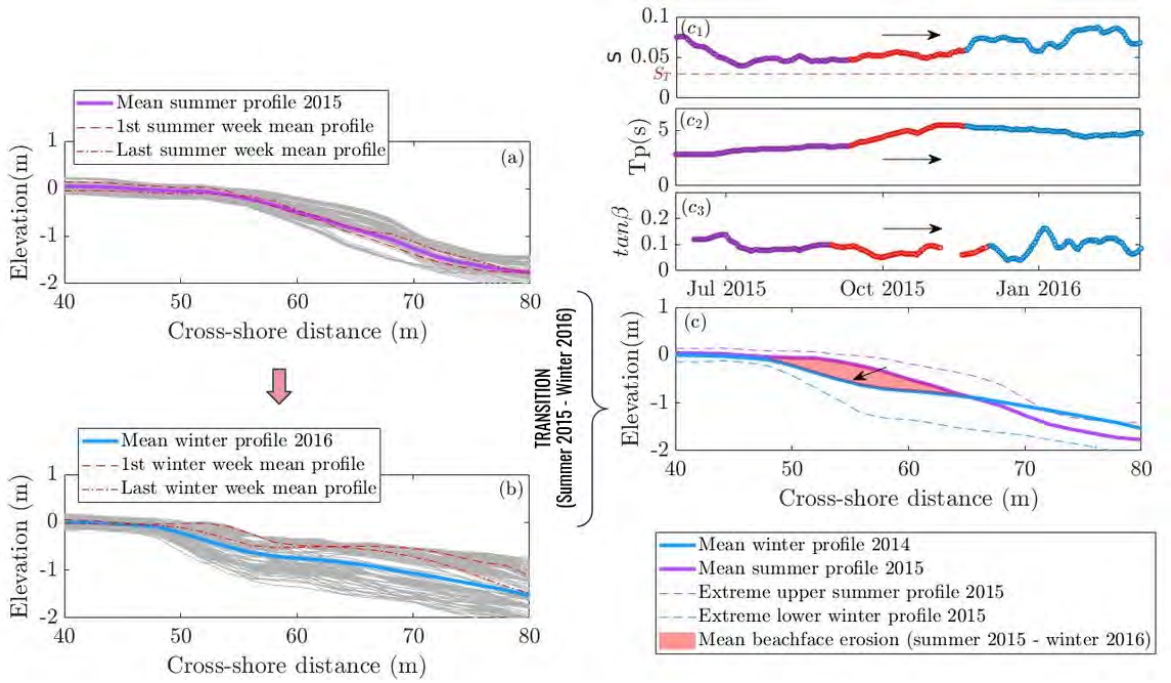

Figure 4.3: Illustrates Nha Trang beach state transition between summer 2015 and winter 2016.(a) and (b) plot the daily beach profiles represented in gray and mean seasonal mean beach profiles represented with violet thick line for summer 2015 and blue line for winter 2016. Figure (c) shows the daily a mean profiles for the transition between summer 2015 to winter 2016. For this transition period Figure c_1, c_2 and c_3 present the evolution of wave steepness (s), ave peak period (T_p) and the beachface slope profile (β), respectively.

4.1.2 Incorporating a sediment input device to enhance the physical model for studying transitional states of beach profiles

Equilibrium states are rarely observed on natural beaches, regardless of the timescale considered, due to the complex phenomena we have described. As a result, it is necessary to understand the transient dynamics from one state to another. In these hydro-sedimentary systems with high temporal and spatial variability, accurately describing and modeling coastal field observations will depend on characterizing these transient dynamics. Beach state transitions from out-of-equilibrium to equilibrium can occur through various factors and can be broadly categorized in: (i) transitions from one hydrodynamic forcing state to another (e.g., due to storms or seasonal changes) and (ii) evolution of the equilibrium state due to sediment transport along the coast (e.g., longshore current). These two situations can occur under a global budget sediment deficit or a sediment excess. It is an open question how these factors will impact the new equilibrium state, the time characteristics of these states and the transitional beach dynamics.

The laboratory model used in the previous sections was designed and used to classify rapid equilibrium beachface slope and its transitory zones. During those experiments the system did

not have any sediment input, which resulted in a sediment deficit regime where the amount of available sediment for transport was only dependent on the initial beachface slope value (β_i). Nevertheless an disequilibrium of the beachface can be generated not only by variations of the wave forcing but also to an disequilibrium in the systems sediment budget generating either an erosive or accresive situation (as seen in NT, Figure 4.2(c) and Figure 4.3(c)). Therefore to incorporate this disequilibrium parameter, a sediment input device is developed and incorporate to the physical model to recreate sediment transport due to longshore current. Thus, the disequilibrium of the beach due to wave variation or sediment inputs can be studied together.

The sediment input device consists of a rechargeable sand reservoir on top and a vibrating support with adjustable frequency and inclination. The sand is introduced into the system by landing on the vibrating support and falling into the water flume as a fine curtain perpendicular to the flume direction. The flow rate and position of the sand can be regulated by adjusting various parameters. Figure 4.3 shows a schematic of the system.

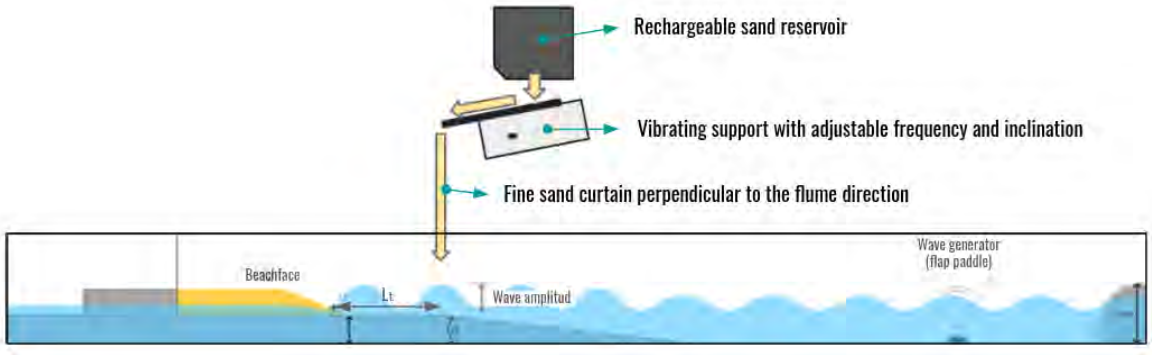

Figure 4.4: Schema of the sediment input device introduced to the laboratory model

The experimental device was first tested by carrying out experiments that built upon previous results detailed in Chapter 3. Following the same experimental set-up as described in Section 3.2, two experiments were performed. In both experiments, the initial beachface slope was steeper than its equilibrium position, and two different wave regimes were tested: WrD, which corresponds to swash-dominated states and sediment transport onshore directions, and WrA, which corresponds to surf-dominated states and sediment transport offshore directions. To these initial conditions during the hall experiment run a constant sediment flux of $0.6gr/s$ was incorporated. The initial conditions of these experiments are summarized in Table 4.2, and the results are shown in Figure 4.5.

Table 4.2

Morpho-initial conditions					Hydro-intial conditions				Sediment input	Sediment transport directions (without sediment input device)
D_{50} [mm]	W_s [cm/s]	Lt_i/H_t	$tan\beta_i$	H_t[cm]	T_0 [s]	H_0 [cm]	Ω_0	s	Q [gr/s]	
0.120	0.74	5	0.3	4	0.74	4.7	8.58 (WrA)	0.063	0.6	transport off-shore
					2.51	2.1	1.13 (WrD)	0.006		transport on-shore

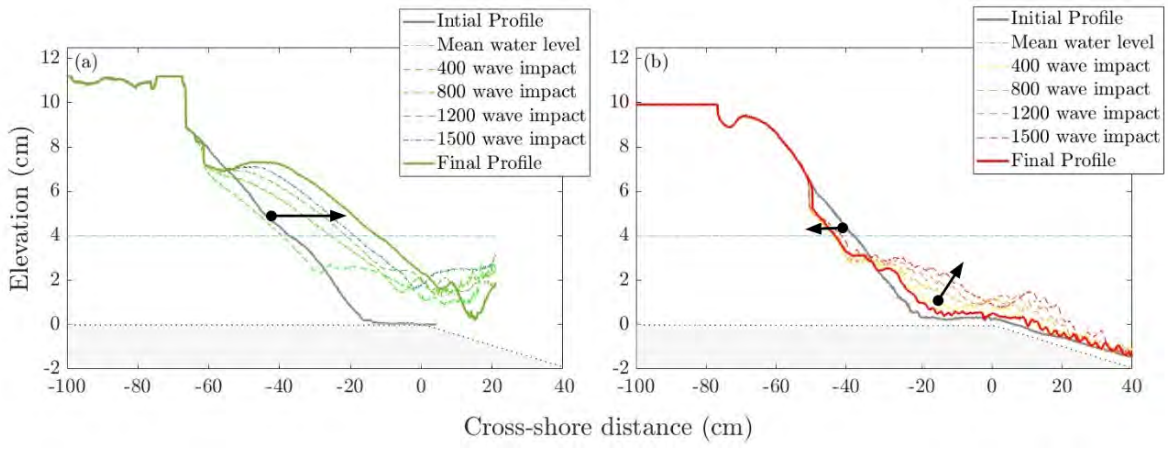

Figure 4.5: (a) Beachface profile evolution for experiment curried out with WrD and (b) for WrA. Both experiments were done with an sediment input of 0.6gr/s, an initial beachface slope equal to $tan\beta_i = 0.3$ and the initial position to the breaking point at 20cm.

Figure 4.5 shows the beach profiles for both experiments at different instants. The initial and final profiles are plotted with a continuous line, while the intermediate profiles are plotted with a dashed line. Figure 4.5(a) represents the experiment carried out with WrD, while Figure 4.5(b) represents the experiment carried out with WrA.

For WrD, a clear accretion phase is observed for the entire beachface, with a unique and rather constant slope during the transition to a new equilibrium state. The accretion mechanism is due to individual wave action moving the sediment onshore and upshore directions, resulting in a unique accretion beachface front moving offshore directions. This was expected to happen, as a similar mechanism of beachface slope adaptation for cases without sediment input was highlighted during previous experiments. On the other hand, under WrA, a more complex mechanism is observed, generating a mixed erosion-accretion profile. The shoreline erodes with a constant beachface slope, associated with the equilibrium value observed in the previous analysis, while the bottom of the beachface accretes. The accretion phase is observed in the lower part of the profile, where it seems to be due to an accumulation of sediment. This is because the wave forcing cannot move it upwards, and the offshore return flux moves the sediment offshore directions slower than the sediment input flux. This generates accretion at the bottom, with a different mechanism observed for WrD.

These initial results obtained with the sediment input device have provided us with valuable insights consistent with the laboratory conclusions presented in Chapter 3. Moreover, the findings demonstrate promising prospects for studying the intricate transitional states of beach profiles. The proposed model could potentially be used to investigate the dynamics of the beachface under sediment deficiency or excess conditions, as well as to characterize the transitional states of the system when it is out-of-equilibrium due to changes in wave forcing or sediment inputs. However, the model requires further parameterization to ensure its accuracy, and ongoing efforts are being made to optimize its performance.

4.2 Overall conclusions

This thesis proposed a simplified approach to study nearshore hydro-morphological systems, specifically focusing on the dynamics of the swash zone and its interactions with other sub-regions of the nearshore. To simplify the coastal systems, the first step was to identify a specific surf zone morphology amidst the existing diversity. We focused on LTT environments, which are a common type of beaches seen in nature in coral and rocky reef zones, composite beaches and low tide terrace sandy beaches. This choice allowed us to define a specific surf zone topography, which in turn enabled us to reduce the complexity of the nearshore system by identifying a few key hydro-morphological parameters that best described the dynamics of each sub-region. By applying this simplification of the nearshore systems in a combined laboratory and field observation study, we were able to gain interesting insights and understanding, particularly in LTT environments.

4.2.1 Main Contributions

The main contributions of this thesis will be presented in association with the three objectives of the study. For each highlight, we propose a graphical synthesis of the obtained results.

- **Coastal hydro-sedimentary systems simplified approach**

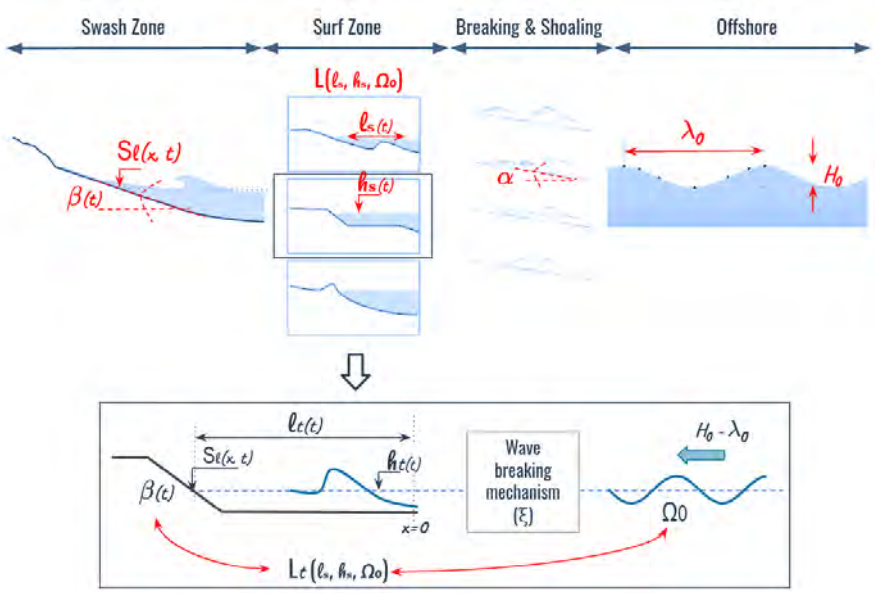

Figure 4.6: Simplification of coastal system by highlighting the main coastal parameters of each sub-region of the nearshore.

This thesis presents a physically-based approach to simplify complex nearshore dynamics by defining dimensionless hydro-morphological parameters that capture the essential

physics of the system. Although the approach can simplify coastal systems to a great extent, potentially losing beach-specific details, it is still based on fundamental principles of coastal physics. The approach proved to successfully characterizes LTT environments and provided a clear understanding of the intricate interactions among the swash zone, surf zone, and offshore regions. By understanding the nearshore as four sub-regions based on wave transformation, and linking the swash zone with offshore dimensionless parameters (Dean number, waves steepness, Rouse number) through a surf dissipation law, the proposed framework offers a powerful tool for studying coastal processes. An important future research direction is to explore the extension of this approach to other surf morphologies by adapting the surf dissipation law. Furthermore, the extension of this approach to incorporate sediment transport by longshore currents is a promising direction for future investigation, as it would enable 3D modeling and a more comprehensive understanding of coastal dynamics, particularly the interplay between longshore and cross-shore interactions. Lastly, this small-scale physical model can also facilitate the study of infragravity waves by adjusting the wave generator settings accordingly. Moreover, it could be also possible to incorporate the influence of the variation of water levels into the physical model to study tidal effects.

- **Characterizing the role of swash dynamics within the coastal hydro-sedimentary systems**

  Based on field observations and laboratory experiments using the simplified approach, LTT environments were sub-classified into either swash-dominated or surf-dominated states. This classification was achieved by analyzing the response of the beachface slope (β) to offshore wave forcing characterized by the Dean number (Ω_0) using field data of two LTT environments (Nha Trang and Grand Popo). When $\Omega_0 < 2.5$, an inverse correlation between β and Ω_0 was observed, defining swash-dominated states. In contrast, when $\Omega_0 > 2.5$, β remained relatively constant, indicating surf-dominated environments where the terrace dissipates the incoming waves, having little impact on the beachface, and on the contrary the terrace length was highly correlated with the Dean number. To deepen our understanding of this relationship (β-Ω_0), we developed a laboratory physical model that highlighted the rapid response of the beachface slope to changing waves.

  In the laboratory, we were able to extract equilibrium values for short times scales of the beachface slope (β_{eq}) to individual wave actions, accounting for the initial geometrical position of the beachface (β_i and lt_i). In addition, we provided a clarification of the Dean number by a new interpretation of it through the relation between two main dimensionless parameters: wave steepness (s) and the Rouse number (Ro) which affects the swash zone in the different ways. It was concluded that the Rouse number had little effect on the equilibrium values of the beachface slope which were primarily controlled by the wave steepness. Therefore these equilibrium values were classified using either offshore or local swash wave steepness (s_0 or s_{sw}, respectively), resulting in a parabolic trend between β_{eq} and s_{sw}, as shown in Figure 4.7. The two branches of the parabola describe two different physical mechanisms that described the equilibrium beachface slope (β_{eq}) response to changing waves, where the intersection of theses processes cor-

respond to the minimum value of the parabola ($tan\beta_{min} \sim 0.2$). These two different mechanism resulted in the definition of surf-and swash-dominated environments that agrees with field observations using the Dean number.

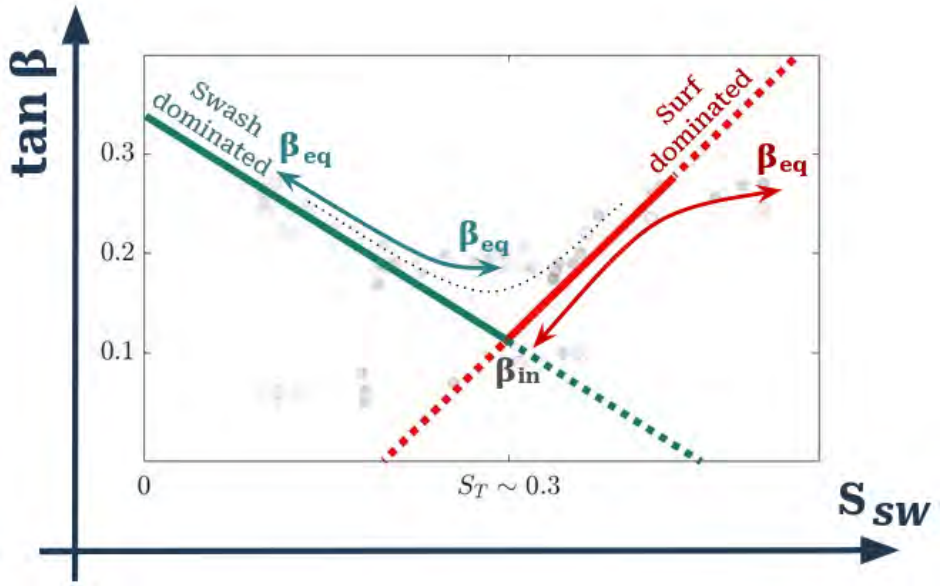

Figure 4.7: Equilibrium beachface slope values (β) plotted as a function of local swash wave steepness (s_{sw}) defining two different physical process associated to swash and surf dominated states.

Our analysis revealed that surf-dominated environments are characterized by significant wave dissipation in the surf zone, which controls the amount of energy that reaches the swash zone. It was observed that as the length of the terrace increases, the rapid equilibrium beachface slope ((β_{eq}) gradually decreases towards an inactive value (β_{in}). In contrast, swash-dominated environments are primarily influenced by wave forcing, where the beachface adjusts rapidly to fluctuations in wave characteristics, resulting in different equilibrium values (β_{eq}). We observed an inverse correlation between β_{eq} and s_{sw} in these situations. Swash-dominated environments were generated by long waves that have low dissipation in the surf zone thus, the majority of the offshore wave energy directly dissipating on the beachface. Therefore swash dynamics are directly related to offshore wave forcing, and the surf zone dynamics can be disregarded when analyzing swash zone dynamics.

- **Rapid evolution of the beach face slope**

  We used wave steepness to identify three zones of beachface slope behaviour: equilibrium (β_{eq}), inactive (β_{in}), and an out-of-equilibrium zone in between. To better understand the physical mechanism in the out-of-equilibrium zone, we classified it into three different types based on how the beachface slope migrated to the equilibrium zone. Three situations were observed and classified into two groups based on the local exchange of sediment along the beachface associated to a short time scale (adjustments occur before about 1000 waves hit the beach face), as shown in the right plots of Figure 4.8.

The green profile corresponds to an increase of the beachface slope due to sediment transported from the lower to the upper part of beachface (groupe 1), while the yellow and red profiles correspond to sediment exchange from the upper to the lower part of the beachface, inducing an increase or decrease in slope, respectively (groupe 2). Further more another classification was proposed based on the wave capacity of sediment transport in the nearshore associated to longer time scale than the rapid adaptation of the beachface slope. Where two situations were identified: (i) one for which sediment flux was transported onshore and the sand remained close to the beachface, resulting in only local adaptation of the beachface, this was associated with swash-dominated states. And the second (ii) involved sediment transport in an off-shore direction, resulting in constant erosion of the beach face observed after the rapid adaptation of the slope. This situation was associated with surf-dominated states. The transition between these zones was observed at $s_0 \sim= 0.03$.

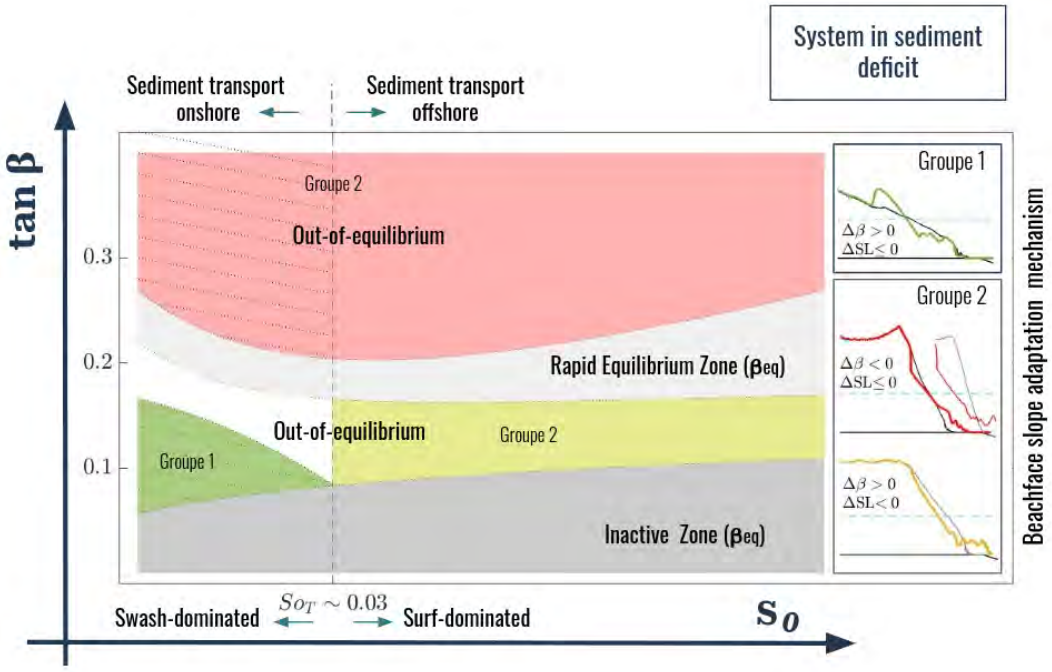

Figure 4.8: Beachface slope rapid adaptation mechanism under sediment deficit regime.

While we previously concluded that the Rouse number had little influence on the rapid equilibrium values of the beachface slope, we observed that the Rouse number affected the characteristic capture time required to reach the equilibrium values. This time is important to understand the highly dynamic nature of coastal systems and to determine whether equilibrium can be reached or if the system will remain in a constantly out-of-equilibrium state. Out-of-equilibrium states require consideration of other physical processes acting simultaneously, and therefore quantifying the influence of the Rouse number and characteristic time is crucial for correctly understanding the system.

The laboratory study provided valuable insights that were used to revisit the field data obtained from Nha Trang and Grand Popo beaches for a better understanding. It was confirmed that Nha Trang is a surf-dominated beach, while Grand Popo is a swash-dominated beach. The study concluded that the models proposed in both the laboratory and field studies, which used the offshore Dean number as a control parameter to predict the beachface slope evolution, could be effective in swash-dominated states (i.e., Grand Popo) due to the little influence of the Rouse number on the rapid equilibrium values of the beach slope to wave forcing. However, we observed that at Nha Trang, a very dynamic beach, an equilibrium model is not suitable for describing the dynamics of the swash zone due to the physical processes occurring in the surf zone. These processes directly influence the swash zone, such as wave dissipation or large sediment exchange between different regions of the nearshore, which affects the entire foreshore profile. Furthermore, we observed a beachface slope dynamics associated with the sediment budget, generating erosive and accretive phases of the foreshore.

Overall, this thesis provides new insights into the concept of rapid equilibrium and transitional states of beach profiles, providing a simplified approach that has proven to be a powerful tool for describing complex coastal systems. The last section of this work presents a sediment input device that incorporates the influence of sediment input into the simplified physical model. This device allows studying different regime associated with disequilibrium in the initial system, and then quantifying the evolution towards new equilibrium states. The physical model can be used to study the disequilibrium generated by changes in wave forcing or sediment inputs. This work lays the groundwork for future research in this area, in particular for the study of beach evolution towards new states of equilibrium based on available sediment inputs or deficits, using an out-of-equilibrium simplified approach.

Publications and Presentations

Publications

- **Mingo, I. M.; Lacaze, L.; Almar, R. "Beach adaptation to rapid wave changes".** In preparation for submission 2023.
- **Mingo, I. M.; Lacaze, L.; Almar, R. "A Semi-Empirical Formula of Beach Slope on Flat Lower Platforms".** Paper submitted to Coastal Engineering (revision).
- **Mingo, I. M.; Lacaze, L.; Almar, R. "Surf and Swash Dynamics on Low Tide Terrace Beaches,"** Coasts, Vol. 1, No. 1, 2021, pp.73–89. doi:10.3390/coasts1010005.

Presentations

- **Equilibrium of the Upper Beach Slope with a Flat Lower Platform - AGU Fall Meeting (Chicago, USA)**. Oral Presentation, December 2022.
- **Swash Zone Rapid Adapatation to Changing Waves: a Laboratory Study - Journées Nationales Génie Côtier – Génie Civil (Chatou, France)**. Oral Presentation, October 2022. Conference Paper DOI: 10.5150/jngcgc.2022.090 (Winner of Jean Crepey Award for young researchers in the field of applied oceanology).
- **Coupled Behaviour of Surf-Swash on Low Tide Terrace Beaches - Coastal Dynamics 2021 (Delft, Netherlands).** Poster, July 2021.

Bibliography

Abessolo Ondoa, G., Almar, R., Kestenare, E., Bahini, A., Houngue, G., Jouanno, J., Du Penhoat, Y., Castelle, B., Melet, A., Meyssignac, B., et al., 2016. Potential of video cameras in assessing event and seasonal coastline behaviour: Grand popo, benin (gulf of guinea). Journal of Coastal Research , 442–446.

Allan, J.C., Gabel, L., O'Brien, F., 2023. Monitoring the response and efficacy of a dynamic revetment constructed adjacent to the columbia river south jetty, clatsop county, oregon: 2013-2022, in: Coastal Sediments 2023: The Proceedings of the Coastal Sediments 2023. World Scientific, pp. 933–947.

Almar, R., Almeida, P., Blenkinsopp, C., Catalan, P., 2016. Surf-swash interactions on a low-tide terraced beach. Journal of Coastal Research , 348–352.

Almar, R., Blenkinsopp, C., Almeida, L.P., Bergsma, E.W., Catalan, P.A., Cienfuegos, R., Viet, N.T., 2019a. Intertidal beach profile estimation from reflected wave measurements. Coastal Engineering 151, 58–63.

Almar, R., Blenkinsopp, C., Almeida, L.P., Catalán, P.A., Bergsma, E., Cienfuegos, R., Viet, N.T., 2019b. A new remote predictor of wave reflection based on runup asymmetry. Estuarine, Coastal and Shelf Science 217, 1–8.

Almar, R., Blenkinsopp, C., Almeida, L.P., Cienfuegos, R., Catalan, P.A., 2017a. Wave runup video motion detection using the radon transform. Coastal Engineering 130, 46–51.

Almar, R., Hounkonnou, N., Anthony, E.J., Castelle, B., Senechal, N., Laibi, R., Mensah-Senoo, T., Degbe, G., Quenum, M., Dorel, M., et al., 2014. The grand popo beach 2013 experiment, benin, west africa: From short timescale processes to their integrated impact over long-term coastal evolution. Journal of Coastal Research , 651–656.

Almar, R., Kestenare, E., Reyns, J., Jouanno, J., Anthony, E., Laibi, R., Hemer, M., Du Penhoat, Y., Ranasinghe, R., 2015. Response of the bight of benin (gulf of guinea, west africa) coastline to anthropogenic and natural forcing, part1: Wave climate variability and impacts on the longshore sediment transport. Continental Shelf Research 110, 48–59.

Almar, R., Marchesiello, P., Almeida, L.P., Thuan, D.H., Tanaka, H., Viet, N.T., 2017b. Shoreline response to a sequence of typhoon and monsoon events. Water 9, 364.

Almar, R., Nicolae Lerma, A., Castelle, B., Scott, T., 2018. On the influence of reflection over a rhythmic swash zone on surf zone dynamics. Ocean Dynamics 68, 899–909.

Almar, R., Ranasinghe, R., Snchal, N., Bonneton, P., Roelvink, D., Bryan, K.R., Marieu, V., Parisot, J.P., 2012. Video-Based detection of shorelines at complex MesoMacro tidal beaches. J. Coast. Res. 28, 1040–1048. doi:10.2112/JCOASTRES-D-10-00149.1.

Almeida, L.P., Almar, R., Blenkinsopp, C., Senechal, N., Bergsma, E., Floc'h, F., Caulet, C., Biausque, M., Marchesiello, P., Grandjean, P., et al., 2020. Lidar observations of the swash zone of a low-tide terraced tropical beach under variable wave conditions: The nha trang (vietnam) coastvar experiment. Journal of Marine Science and Engineering 8, 302.

Almeida, L.P., Almar, R., Marchesiello, P., Benshila, R., Martins, K., Blenkinsopp, C., Floc'h, F., Ammann, J., Grandjean, P., Viet, N.T., Thuan, D.H., Binh, L.T., Senechal, N., Detandt, G., Biausque, M., Garlan, T., Bergsma, E., Caulet, C., Tran, H.Y., 2016. Swash zone dynamics of a sandy beach with low tide terrace during variable wave and tide conditions. Proc. Journées Natl. Génie Côtier-Génie Civ. .

Anfuso, G., Ruiz, N., 2004. Morfodinámica de una playa mesomareal expuesta con terraza de bejamar (Faro, Sur de Portugal). Ciencias Mar. 30, 575–584. doi:10.7773/cm.v30i4.341.

Anthony, E.J., 1998. Sediment-wave parametric characterization of beaches. Journal of Coastal Research , 347–352.

Astier, J., 2014. Morphodynamique de la zone de" swash": étude en canal à houle par une méthode de stéréoscopie optique. Ph.D. thesis.

Bagnold, R., 1940. Beach formation by waves: Some model experiments in a wave tank.(includes photographs). Journal of the Institution of Civil Engineers 15, 27–52.

Bakhtyar, R., Barry, D.A., Li, L., Jeng, D.S., Yeganeh-Bakhtiary, A., 2009. Modeling sediment transport in the swash zone: A review. Ocean Engineering 36, 767–783.

Baldock, T., Manoonvoravong, P., Pham, K.S., 2010. Sediment transport and beach morphodynamics induced by free long waves, bound long waves and wave groups. Coastal Engineering 57, 898–916.

Banner, M., Peregrine, D., 1993. Wave breaking in deep water. Annual Review of Fluid Mechanics 25, 373–397.

Barlas, B., Beji, S., 2016. Rip current fatalities on the black sea beaches of istanbul and effects of cultural aspects in shaping the incidents. Natural Hazards 80, 811–821.

Bascom, W.N., 1951. The relationship between sand size and beach-face slope. Eos, Transactions American Geophysical Union 32, 866–874.

Battjes, J., 1988. Surf-zone dynamics. Annual Review of Fluid Mechanics 20, 257–291.

Battjes, J.A., 1974. Surf similarity, in: Coastal Engineering 1974, pp. 466–480.

Bayle, P.M., Blenkinsopp, C.E., Conley, D., Masselink, G., Beuzen, T., Almar, R., 2020. Performance of a dynamic cobble berm revetment for coastal protection, under increasing water level. Coastal Engineering 159, 103712.

Bayle, P.M., Kaminsky, G.M., Blenkinsopp, C.E., Weiner, H.M., Cottrell, D., 2021. Behaviour and performance of a dynamic cobble berm revetment during a spring tidal cycle in north cove, washington state, usa. Coastal Engineering 167, 103898.

Benoit, M., Raoult, C., Yates, M., . Fully nonlinear and dispersive modeling of surf zone waves: Non-breaking tests. Coastal Engineering Proceedings , 15–15.

Bergsma, E.W.J., Almar, R., 2018. Video-based depth inversion techniques, a method comparison with synthetic cases. Coast. Eng. 138, pp. 199–209.

Bernabeu, A., Medina, R., Vidal, C., 2003. A morphological model of the beach profile integrating wave and tidal influences. Marine Geology 197, 95–116.

Bertin, X., de Bakker, A., Van Dongeren, A., Coco, G., André, G., Ardhuin, F., Bonneton, P., Bouchette, F., Castelle, B., Crawford, W.C., et al., 2018. Infragravity waves: From driving mechanisms to impacts. Earth-Science Reviews 177, 774–799.

Biausque, M., 2018. Approche multi-proxys de la réponse des plages sableuses ouvertes aux événements de tempêtes, en incluant les phases de récupération. Ph.D. thesis. Université de Bordeaux.

Bird, E.C., 2011. Coastal geomorphology: an introduction. John Wiley & Sons.

Bodge, K.R., 1992. Representing equilibrium beach profiles with an exponential expression. Journal of coastal research , 47–55.

Boon, J.D., Green, M.O., 1988. Caribbean beach-face slopes and beach equilibrium profiles, in: Coastal Engineering 1988, pp. 1618–1630.

Briganti, R., Torres-Freyermuth, A., Baldock, T.E., Brocchini, M., Dodd, N., Hsu, T.J., Jiang, Z., Kim, Y., Pintado-Patiño, J.C., Postacchini, M., 2016. Advances in numerical modelling of swash zone dynamics. Coastal Engineering 115, 26–41.

Brocchini, M., Baldock, T., 2008. Recent advances in modeling swash zone dynamics: Influence of surf-swash interaction on nearshore hydrodynamics and morphodynamics. Reviews of Geophysics 46.

Brunel, C., Certain, R., Sabatier, F., Robin, N., Barusseau, J., Aleman, N., Raynal, O., 2014. 20th century sediment budget trends on the western gulf of lions shoreface (france): An application of an integrated method for the study of sediment coastal reservoirs. Geomorphology 204, 625–637.

Bruun, P., 1954. Coast erosion and the development of beach profiles. volume 44. US Beach Erosion Board.

Bruun, P., 1962. Sea-level rise as a cause of shore erosion. Journal of the Waterways and Harbors division 88, 117–130.

Bruun, P., 1988. The bruun rule of erosion by sea-level rise: a discussion on large-scale two-and three-dimensional usages. Journal of coastal Research , 627–648.

Bujan, N., Cox, R., Masselink, G., 2019. From fine sand to boulders: Examining the relationship between beach-face slope and sediment size. Marine Geology 417, 106012.

Butt, T., Russell, P., 1999. Suspended sediment transport mechanisms in high-energy swash. Marine Geology 161, 361–375.

Butt, T., Russell, P., 2000. Hydrodynamics and cross-shore sediment transport in the swash-zone of natural beaches: a review. Journal of coastal research , 255–268.

Callaghan, D., Nielsen, P., Short, A., Ranasinghe, R., 2008. Statistical simulation of wave climate and extreme beach erosion. Coastal Engineering 55, 375–390.

Callaghan, J., Helman, P., 2008. Severe storms on the east coast of australia.

Carter, R.W.G., 2013. Coastal environments: an introduction to the physical, ecological, and cultural systems of coastlines. Elsevier.

Castelle, B., Almar, R., Dorel, M., Lefebvre, J.P., Senechal, N., Anthony, E.J., Laibi, R., Chuchla, R., Penhoat, Y.D., 2014a. Rip currents and circulation on a high-energy low-tide-terraced beach (Grand Popo, Benin, West Africa). J. Coast. Res. 70, 633–638. doi:10.2112/SI70-107.1.

Castelle, B., Bujan, S., Ferreira, S., Dodet, G., 2017. Foredune morphological changes and beach recovery from the extreme 2013/2014 winter at a high-energy sandy coast. Marine Geology 385, 41–55.

Castelle, B., Marieu, V., Bujan, S., Ferreira, S., Parisot, J.P., Capo, S., Sénéchal, N., Chouzenoux, T., 2014b. Equilibrium shoreline modelling of a high-energy meso-macrotidal multiple-barred beach. Marine Geology 347, 85–94.

Castelle, B., Masselink, G., Scott, T., Stokes, C., Konstantinou, A., Marieu, V., Bujan, S., 2021. Satellite-derived shoreline detection at a high-energy meso-macrotidal beach. Geomorphology 383, 107707.

Castelle, B., Scott, T., Brander, R., McCarroll, R., 2016. Rip current types, circulation and hazard. Earth-Science Reviews 163, 1–21.

Chardón-Maldonado, P., Pintado-Patiño, J.C., Puleo, J.A., 2016. Advances in swash-zone research: Small-scale hydrodynamic and sediment transport processes. Coastal Engineering 115, 8–25.

Chella, M.A., Bihs, H., Myrhaug, D., 2015. Characteristics and profile asymmetry properties of waves breaking over an impermeable submerged reef. Coastal Engineering 100, 26–36.

Cienfuegos, R., Barthélemy, E., Bonneton, P., 2010. Wave-breaking model for boussinesq-type equations including roller effects in the mass conservation equation. Journal of waterway, port, coastal, and ocean engineering 136, 10–26.

Cowell, P.J., Thom, B.G., 1994. Morphodynamics of coastal evolution. Coastal evolution: Late Quaternary shoreline morphodynamics , 33–86.

Dally, W.R., Dean, R.G., 1984. Suspended sediment transport and beach profile evolution. Journal of waterway, port, coastal, and ocean engineering 110, 15–33.

Davidson, M., Splinter, K., Turner, I., 2013. A simple equilibrium model for predicting shoreline change. Coastal Engineering 73, 191–202.

Davidson, M., Turner, I., 2009. A behavioral template beach profile model for predicting seasonal to interannual shoreline evolution. Journal of Geophysical Research: Earth Surface 114.

Dean, R.G., 1973. Heuristic models of sand transport in the surf zone, in: First Australian Conference on Coastal Engineering, 1973: Engineering Dynamics of the Coastal Zone, Institution of Engineers, Australia Sydney, NSW. pp. 215–221.

Dean, R.G., 1977. Equilibrium beach profiles: Us atlantic and gulf coasts .

Dean, R.G., 1991. Equilibrium beach profiles: characteristics and applications. Journal of coastal research , 53–84.

Dean, R.G., Houston, J.R., 2016. Determining shoreline response to sea level rise. Coastal Engineering 114, 1–8.

Dee, D., Uppala, S., Simmons, A., Berrisford, P., Poli, P., Kobayashi, S., Andrae, U., Balmaseda, M., Balsamo, G., Bauer, d.P., et al., 2011. The era-interim reanalysis: configuration and performance of the data assimilation system, qj roy. meteor. soc., 137, 553–597.

Dohmen-Janssen, C.M., Hanes, D.M., 2002. Sheet flow dynamics under monochromatic nonbreaking waves. Journal of geophysical research: Oceans 107, 13–1.

Dohmen-Janssen, C.M., Hanes, D.M., 2005. Sheet flow and suspended sediment due to wave groups in a large wave flume. Continental Shelf Research 25, 333–347.

Drazen, D.A., Melville, W.K., Lenain, L., 2008. Inertial scaling of dissipation in unsteady breaking waves. Journal of fluid mechanics 611, 307–332.

Elfrink, B., Baldock, T., 2002. Hydrodynamics and sediment transport in the swash zone: a review and perspectives. Coastal Engineering 45, 149–167.

Foster, D., Bowen, A., Holman, R.A., Natoo, P., 2006. Field evidence of pressure gradient induced incipient motion. Journal of Geophysical Research: Oceans 111.

Gallop, S.L., Bryan, K.R., Coco, G., Stephens, S., 2011. Storm-driven changes in rip channel patterns on an embayed beach. Geomorphology 127, 179–188.

Gallop, S.L., Kennedy, D.M., Loureiro, C., Naylor, L.A., Muñoz-Pérez, J.J., Jackson, D.W., Fellowes, T.E., 2020. Geologically controlled sandy beaches: Their geomorphology, morphodynamics and classification. Sci. Total Environ. 731, 139123. URL: https://doi.org/10.1016/j.scitotenv.2020.139123, doi:10.1016/j.scitotenv.2020.139123.

Gourlay, M.R., 1981. Beaches, profiles, processes and permeability. Proc. Seventeenth Coast. Engng. Conf., (Sydney, Aust. Mar.23-28, 1980) 2 , New York, U.S.A., Am. Soc. Civ. Engrs., 1981, Part 2, Chapter 80, 1320–1339. doi:doi.org/10.9753/icce.v17.79.

Grasso, F., Michallet, H., Barthélemy, E., 2011. Sediment transport associated with morphological beach changes forced by irregular asymmetric, skewed waves. Journal of Geophysical Research: Oceans 116.

Grasso, F., Michallet, H., Barthélemy, E., Certain, R., 2009. Physical modeling of intermediate cross-shore beach morphology: Transients and equilibrium states. Journal of Geophysical Research: Oceans 114.

Guedes, R.M., Bryan, K.R., Coco, G., 2013. Observations of wave energy fluxes and swash motions on a low-sloping, dissipative beach. Journal of geophysical research: Oceans 118, 3651–3669.

Guza, R., Thornton, E.B., 1985. Observations of surf beat. Journal of Geophysical Research: Oceans 90, 3161–3172.

Guza, R.T., Thornton, E.B., 1982. Swash oscillations on a natural beach. Journal of Geophysical Research: Oceans 87, 483–491.

Hemer, M.A., Yalin, F., Mori, N., Semedo, A., Xiaolan, W.L., 2013. Projected changes in wave climate from a multi-model ensemble. Nat. Clim. Chang. 3, 471–476.

Herbers, T., Elgar, S., Guza, R., 1995. Generation and propagation of infragravity waves. Journal of Geophysical Research: Oceans 100, 24863–24872.

Hibberd, S., Peregrine, D., 1979. Surf and run-up on a beach: a uniform bore. Journal of Fluid Mechanics 95, 323–345.

Holland, K., Holman, R.A., 1999. Wavenumber-frequency structure of infragravity swash motions. Journal of Geophysical Research: Oceans 104, 13479–13488.

Holland, K., Puleo, J., 2001. Variable swash motions associated with foreshore profile change. Journal of Geophysical Research: Oceans 106, 4613–4623.

Holman, R., Bowen, A., 1984. Longshore structure of infragravity wave motions. Journal of Geophysical Research: Oceans 89, 6446–6452.

Holman, R.A., Jr, A.H.S., Lippmann, T.C., John, W., Holman, B.R.A., Sallenger, A.H., 1993. Linked references are available on JSTOR for this article : The Application of Video Image Processing to the Study of Nearshore Processes 6, 78–85.

Holthuijsen, L.H., 2010. Waves in oceanic and coastal waters. Cambridge university press.

Hsu, T.J., Hanes, D.M., 2004. Effects of wave shape on sheet flow sediment transport. Journal of Geophysical Research: Oceans 109.

Hsu, T.W., 1998. Geometric characteristics of storm-beach profiles caused by inclined waves. Ocean Engineering 25, 69–84.

Hsu, T.W., Lin, T.Y., Tseng, I.F., 2007. Human impact on coastal erosion in taiwan. Journal of Coastal Research 23, 961–973.

Hsu, T.W., Ou, S.H., Wang, S.K., 1994. On the prediction of beach changes by a new 2-d empirical eigenfunction model. Coastal Engineering 23, 255–270.

Hughes, M.G., 1992. Application of a non-linear shallow water theory to swash following bore collapse on a sandy beach. Journal of Coastal Research , 562–578.

Hughes, M.G., Baldock, T.E., 2004. Eulerian flow velocities in the swash zone: field data and model predictions. Journal of Geophysical Research: Oceans 109.

Hughes, M.G., Masselink, G., Brander, R.W., 1997. Flow velocity and sediment transport in the swash zone of a steep beach. Marine Geology 138, 91–103.

Hunt, E., Davidson, M., Steele, E.C., Amies, J.D., Scott, T., Russell, P., 2023. Shoreline modelling on timescales of days to decades. Cambridge Prisms: Coastal Futures 1, e17.

IPCC Working Group 1, I., Stocker, T., Qin, D., Plattner, G.K., Tignor, M., Allen, S., Boschung, J., Nauels, A., Xia, Y., Bex, V., Midgley, P., 2013. IPCC, 2013: Climate Change 2013: The Physical Science Basis. Contribution of Working Group I to the Fifth Assessment Report of the Intergovernmental Panel on Climate Change. Ipcc AR5, 1535.

Jensen, A., Pedersen, G.K., Wood, D.J., 2003. An experimental study of wave run-up at a steep beach. Journal of Fluid Mechanics 486, 161–188.

Kalligeris, N., Smit, P., Ludka, B., Guza, R., Gallien, T., 2020. Calibration and assessment of process-based numerical models for beach profile evolution in southern california. Coastal Engineering 158, 103650.

Kemp, P., 1975. Wave asymmetry in the nearshore zone and breaker area. Nearshore sediment dynamics and sedimentation , 47–67.

Kikkert, G.A., Pokrajac, D., O'Donoghue, T., Steenhauer, K., 2013. Experimental study of bore-driven swash hydrodynamics on permeable rough slopes. Coastal engineering 79, 42–56.

Kim, H., Hall, K., Jin, J.Y., Park, G.S., Lee, J., 2014. Empirical estimation of beach-face slope and its use for warning of berm erosion. Journal of Measurements in Engineering 2, 29–42.

King, C., 1972. Beaches and Coasts. E. Arnold. URL: `https://books.google.fr/books?id=yG9SwgEACAAJ`.

Komar, P.D., 1977. Beach processes and sedimentation. .

Komar, P.D., Inman, D.L., 1970. Longshore sand transport on beaches. Journal of geophysical research 75, 5914–5927.

Kriebel, D.L., Kraus, N.C., Larson, M., 1991. Engineering methods for predicting beach profile response, in: Coastal Sediments, ASCE. pp. 557–571.

Kroon, A., Davidson, M., Aarninkhof, S., Archetti, R., Armaroli, C., Gonzalez, M., Medri, S., Osorio, A., Aagaard, T., Holman, R., et al., 2007. Application of remote sensing video systems to coastline management problems. Coastal Engineering 54, 493–505.

Larson, M., 1991. Equilibrium profile of a beach with varying grain size, in: Coastal Sediments, ASCE. pp. 905–919.

Larson, M., Kraus, N.C., 1995. Prediction of cross-shore sediment transport at different spatial and temporal scales. Marine geology 126, 111–127.

Larson, M., Kubota, S., Erikson, L., 2004. Swash-zone sediment transport and foreshore evolution: field experiments and mathematical modeling. Marine geology 212, 61–79.

Leckler, F., Dubardier, B., 2010. Laboratory experiment on rip current circulations over a moveable bed: Drifter measurements. Journal of Geophysical Research: Oceans 115.

Lee, G.h., Nicholls, R.J., Birkemeier, W.A., 1998. Storm-driven variability of the beach-nearshore profile at duck, north carolina, usa, 1981–1991. Marine geology 148, 163–177.

Lefebvre, J.P., Almar, R., Viet, N.T., Thuan, D.H., Binh, L.T., Ibaceta, R., Duc, N.V., 2014. Contribution of swash processes generated by low energy wind waves in the recovery of a beach impacted by extreme events: Nha trang, vietnam. Journal of Coastal Research , 663–668.

Lemos, C., Floc'h, F., Yates, M., Le Dantec, N., Marieu, V., Hamon, K., Cuq, V., Suanez, S., Delacourt, C., 2018. Equilibrium modeling of the beach profile on a macrotidal embayed low tide terrace beach. Ocean Dynamics 68, 1207–1220.

Lipiec, E., Ruggiero, P., Mills, A., Serafin, K.A., Bolte, J., Corcoran, P., Stevenson, J., Zanocco, C., Lach, D., 2018. Mapping out climate change: assessing how coastal communities adapt using alternative future scenarios. Journal of Coastal Research 34, 1196–1208.

Lippmann, T.C., Holman, R.A., 1989. Quantification of sand bar morphology: A video technique based on wave dissipation. J. Geophys. Res. Ocean. 94, 995–1011.

Longuet-Higgins, M.S., 1970. Longshore currents generated by obliquely incident sea waves: 1. Journal of geophysical research 75, 6778–6789.

Longuet-Higgins, M.S., Stewart, R., 1962. Radiation stress and mass transport in gravity waves, with application to 'surf beats'. Journal of Fluid Mechanics 13, 481–504.

Ludka, B., Guza, R., O'Reilly, W., Yates, M., 2015. Field evidence of beach profile evolution toward equilibrium. Journal of Geophysical Research: Oceans 120, 7574–7597.

Luijendijk, A., Hagenaars, G., Ranasinghe, R., Baart, F., Donchyts, G., Aarninkhof, S., 2018. The state of the world's beaches. Scientific reports 8, 1–11.

Madsen, P.A., Sørensen, O., Schäffer, H., 1997. Surf zone dynamics simulated by a boussinesq type model. part i. model description and cross-shore motion of regular waves. Coastal Engineering 32, 255–287.

Martins, K., Blenkinsopp, C.E., Almar, R., Zang, J., 2017. The influence of swash-based reflection on surf zone hydrodynamics: A wave-by-wave approach. Coastal Engineering 122, 27–43.

Mason, T., Coates, T., 2001. Sediment transport processes on mixed beaches: a review for shoreline management. Journal of Coastal Research , 645–657.

Masselink, G., Castelle, B., Scott, T., Dodet, G., Suanez, S., Jackson, D., Floc'h, F., 2016. Extreme wave activity during 2013/2014 winter and morphological impacts along the atlantic coast of europe. Geophysical Research Letters 43, 2135–2143.

Masselink, G., Evans, D., Hughes, M.G., Russell, P., 2005. Suspended sediment transport in the swash zone of a dissipative beach. Marine geology 216, 169–189.

Masselink, G., Hughes, M., 1998. Field investigation of sediment transport in the swash zone. Continental Shelf Research 18, 1179–1199.

Masselink, G., Li, L., 2001. The role of swash infiltration in determining the beachface gradient: a numerical study. Marine Geology 176, 139–156.

Masselink, G., Puleo, J.A., 2006. Swash-zone morphodynamics. Continental Shelf Research 26, 661–680.

Masselink, G., Short, A.D., 1993. The effect of tide range on beach morphodynamics and morphology: a conceptual beach model. J. Coast. Res. 9, 785–800.

McCowan, J., 1891. Vii. on the solitary wave. The London, Edinburgh, and Dublin Philosophical Magazine and Journal of Science 32, 45–58.

Mentaschi, L., Vousdoukas, M.I., Pekel, J.F., Voukouvalas, E., Feyen, L., 2018. Global long-term observations of coastal erosion and accretion. Scientific reports 8, 12876.

Merkens, J.L., Reimann, L., Hinkel, J., Vafeidis, A.T., 2016. Gridded population projections for the coastal zone under the shared socioeconomic pathways. Global and Planetary Change 145, 57–66.

Miche, M., 1944. Mouvements ondulatoires de la mer en profondeur constante ou décroissante. Annales de Ponts et Chaussées, 1944, pp (1) 26-78,(2) 270-292,(3) 369-406 .

Miles, J., Russell, P., 2004. Dynamics of a reflective beach with a low tide terrace. Continental Shelf Research 24, 1219–1247.

Miller, J.K., Dean, R.G., 2004. A simple new shoreline change model. Coastal Engineering 51, 531–556.

Milliman, J.D., Farnsworth, K.L., 2013. River discharge to the coastal ocean: a global synthesis. Cambridge University Press.

Mingo, I.M., Almar, R., Lacaze, L., 2021. Surf and Swash Dynamics on Low Tide Terrace Beaches. Coasts 1, 73–89. doi:10.3390/coasts1010005.

Moore, B., 1982. Beach profile evolution in response to changes in water level and wave height. MS Thesis, Dept. of Civil Eng., Univ. of Delaware .

Morim, J., Trenham, C., Hemer, M., Wang, X.L., Mori, N., Casas-Prat, M., Semedo, A., Shimura, T., Timmermans, B., Camus, P., et al., 2020. A global ensemble of ocean wave climate projections from cmip5-driven models. Scientific data 7, 105.

Morton, R.A., Gibeaut, J.C., Paine, J.G., 1995. Meso-scale transfer of sand during and after storms: implications for prediction of shoreline movement. Marine geology 126, 161–179.

Oerlemans, S.C., Nijland, W., Ellenson, A.N., Price, T.D., 2022. Image-based classification of double-barred beach states using a convolutional neural network and transfer learning. Remote Sensing 14, 4686.

Oltman-Shay, J.M., Hathaway, K.K., 1989. Infragravity energy and its implications in nearshore sediment transport and sandbar dynamics .

Ondoa, G.A., 2020. Response of sandy beaches in West Africa, gulf of Guinea, to multi-scale forcing. Ph.D. thesis. Université Paul Sabatier-Toulouse III.

Ondoa, G.A., Almar, R., Kestenare, E., Bahini, A., Houngue, G.H., Jouanno, J., Du Penhoat, Y., Castelle, B., Melet, A., Meyssignac, B., Anthony, E.J., Laibi, R., Alory, G., Ranasinghe, R., 2016. Potential of video cameras in assessing event and seasonal coastline behaviour: Grand Popo, Benin (Gulf of Guinea). J. Coast. Res. 1, 442–446. doi:10.2112/SI75-089.1.

Ondoa, G.A., Bonou, F., Tomety, F.S., du Penhoat, Y., Perret, C., Degbe, C.G.E., Almar, R., 2017. Beach response to wave forcing from event to inter-annual time scales at grand popo, benin (Gulf of Guinea). Water (Switzerland) 9. doi:10.3390/w9060447.

Pachauri, R.K., Allen, M.R., Barros, V.R., Broome, J., Cramer, W., Christ, R., Church, J.A., Clarke, L., Dahe, Q., Dasgupta, P., et al., 2014. Climate change 2014: synthesis report. Contribution of Working Groups I, II and III to the fifth assessment report of the Intergovernmental Panel on Climate Change. Ipcc.

Phillips, J.D., 1992. Nonlinear dynamical systems in geomorphology: revolution or evolution? Geomorphology 5, 219–229.

Pilkey, O.H., Young, R.S., Rîggs, S.R., Smith, A.S., Wu, H., Pilkey, W.D., 1993. The concept of shoreface profile of equilibrium: a critical review. Journal of coastal research , 255–278.

Pitman, S.J., 2014. Methods for field measurement and remote sensing of the swash zone .

Power, H., Hughes, M., 2008. Wave behaviour in the inner surf zone .

Power, H.E., Baldock, T.E., Callaghan, D.P., Nielsen, P., 2013. Surf zone states and energy dissipation regimes-a similarity model. Coast. Eng. J. 55. doi:10.1142/S0578563413500034.

Pritchard, D., Hogg, A.J., 2005. On the transport of suspended sediment by a swash event on a plane beach. Coastal Engineering 52, 1–23.

Puleo, J., Beach, R., Holman, R.A., Allen, J., 2000. Swash zone sediment suspension and transport and the importance of bore-generated turbulence. Journal of Geophysical Research: Oceans 105, 17021–17044.

Puleo, J., Holland, K., Plant, N., Slinn, D., Hanes, D., 2003. Fluid acceleration effects on suspended sediment transport in the swash zone. Journal of Geophysical Research: Oceans 108.

Puleo, J.A., 2009. Tidal variability of swash-zone sediment suspension and transport. Journal of Coastal Research 25, 937–948.

Rector, R.L., 1954. Laboratory study of equilibrium profiles of beaches. 41, US Beach Erosion Board.

Reis, A.H., Gama, C., 2010. Sand size versus beachface slope—an explanation based on the constructal law. Geomorphology 114, 276–283.

Robertson, B., Hall, K., Zytner, R., Nistor, I., 2013. Breaking waves: Review of characteristic relationships. Coastal Engineering Journal 55, 1350002.

Rocha, M., Michallet, H., Silva, P.A., 2017. Improving the parameterization of wave nonlinearities–the importance of wave steepness, spectral bandwidth and beach slope. Coastal Engineering 121, 77–89.

Rouse, H., 1937. Modern conceptions of the mechanics of fluid turbulence. Transactions of the American Society of Civil Engineers 102, 463–505.

Ruessink, B., 1998. Bound and free infragravity waves in the nearshore zone under breaking and nonbreaking conditions. Journal of Geophysical Research: Oceans 103, 12795–12805.

Ruggiero, P., Kaminsky, G.M., Gelfenbaum, G., Cohn, N., 2016. Morphodynamics of prograding beaches: A synthesis of seasonal-to century-scale observations of the columbia river littoral cell. Marine Geology 376, 51–68.

Ruggiero, P., Kaminsky, G.M., Gelfenbaum, G., Voigt, B., 2005. Seasonal to interannual morphodynamics along a high-energy dissipative littoral cell. Journal of Coastal Research 21, 553–578.

Sabatier, F., 2001. Fonctionnement et dynamiques morpho-sédimentaires du littoral du delta du Rhône. Ph.D. thesis. URL: `http://www.theses.fr/2001AIX30103`. thèse de doctorat dirigée par Lippmann-Provansal, Mireille Géosciences de l'environnement. Géographie Aix-Marseille 3 2001.

Short, A., Jackson, D., 2013. Beach morphodynamics (chapter). Treatise Geomorphol. 10, 106–129.

Short, A.D., 1996. The role of wave height, period, slope, tide range and embaymentisation in beach classifications: a review. Revista chilena de historia natural 69, 589–604.

Siegle, E., Huntley, D.A., Davidson, M.A., 2007. Coupling video imaging and numerical modelling for the study of inlet morphodynamics. Marine Geology 236, 143–163.

Smit, M., Aarninkhof, S., Wijnberg, K.M., González, M., Kingston, K., Southgate, H., Ruessink, B., Holman, R., Siegle, E., Davidson, M., et al., 2007. The role of video imagery in predicting daily to monthly coastal evolution. Coastal engineering 54, 539–553.

Soares, A.G., 2003. Sandy beach morphodynamics and macrobenthic communities in temperate, subtropical and tropical regions: a macroecological approach. Ph.D. thesis. University of Port Elizabeth.

Soulsby, R., 1997. Dynamics of marine sands .

Soulsby, R., Humphery, J., 1990. Field observations of wave-current interaction at the sea bed. Springer.

Sous, D., Lambert, A., Rey, V., Michallet, H., 2013. Swash–groundwater dynamics in a sandy beach laboratory experiment. Coastal engineering 80, 122–136.

Southgate, H.N., Wijnberg, K.M., Larson, M., Capobianco, M., Jansen, H., 2003. Analysis of field data of coastal morphological evolution over yearly and decadal timescales. part 2: Non-linear techniques. Journal of Coastal Research , 776–789.

Souza, A.J., Burchard, H., Eden, C., Pattiaratchi, C., van Haren, H., Craig, P., Huang, N., 1997. Coastal ocean turbulence and mixing. Coupled Coastal Wind, Wave and Current Dynamics .

Splinter, K.D., Turner, I.L., Davidson, M.A., Barnard, P., Castelle, B., Oltman-Shay, J., 2014. A generalized equilibrium model for predicting daily to interannual shoreline response. Journal of Geophysical Research: Earth Surface 119, 1936–1958.

Steenhauer, K., Pokrajac, D., O'Donoghue, T., 2012. Numerical model of swash motion and air entrapment within coarse-grained beaches. Coastal Engineering 64, 113–126.

Stépanian, A., 2002. Evolution morphodynamique d'une plage macrotidale à barres: Omaha beach (Normandie). Ph.D. thesis. Université de Caen.

Sterl, A., Van Den Brink, H., De Vries, H., Haarsma, R., Van Meijgaard, E., 2009. An ensemble study of extreme storm surge related water levels in the North Sea in a changing climate. Ocean Sci. 5, 369–378. doi:10.5194/os-5-369-2009.

Stive, M.J., Roelvink, D.J.A., de Vriend, H.J., 1991. Large-scastivele coastal evolution concept: the dutch coast: paper no. 9, in: Coastal Engineering 1990, pp. 1962–1974.

Stringari, C.E., Power, H.E., 2019. The Fraction of Broken Waves in Natural Surf Zones. J. Geophys. Res. Ocean. 124, 9114–9140. doi:10.1029/2019JC015213, arXiv:1904.06821.

Sunamura, T., 1984. Quantitative predictions of beach-face slopes. Geological Society of America Bulletin 95, 242–245.

Svendsen, I.A., 1984. Wave heights and set-up in a surf zone. Coastal engineering 8, 303–329.

Svendsen, I.A., Putrevu, U., 1996. Surf-zone hydrodynamics, in: Advances in coastal and ocean engineering. World Scientific, pp. 1–78.

Swart, D.H., 1975. A schematization of onshore-offshore transport, in: Coastal Engineering 1974, pp. 884–900.

Thomson, J., Elgar, S., Raubenheimer, B., Herbers, T., Guza, R., 2006. Tidal modulation of infragravity waves via nonlinear energy losses in the surfzone. Geophysical Research Letters 33.

Thorn, C.E., Welford, M.R., 1994. The equilibrium concept in geomorphology. Annals of the Association of American Geographers 84, 666–696.

Thornton, E., Dalrymple, T., Drake, T., Elgar, S., Gallagher, E., Guza, B., Hay, A., Holman, R., Kaihatu, J., Lippmann, T., et al., 2000. State of nearshore processes research: Ii .

Thornton, E.B., Guza, R., 1982. Energy saturation and phase speeds measured on a natural beach. Journal of Geophysical Research: Oceans 87, 9499–9508.

Thuan, D.H., Almar, R., Marchesiello, P., Viet, N.T., 2019. Video sensing of nearshore bathymetry evolution with error estimate. Journal of Marine Science and Engineering 7, 233.

Toffoli, A., Bitner-Gregersen, E.M., 2017. Types of ocean surface waves, wave classification. Encyclopedia of maritime and offshore engineering , 1–8.

Tucker, M., 1950. Surf beats: Sea waves of 1 to 5 min. period. Proceedings of the Royal Society of London. Series A. Mathematical and Physical Sciences 202, 565–573.

Turner, I.L., 1995. Simulating the influence of groundwater seepage on sediment transported by the sweep of the swash zone across macro-tidal beaches. Marine Geology 125, 153–174.

Turner, I.L., Russell, P.E., Butt, T., 2008. Measurement of wave-by-wave bed-levels in the swash zone. Coastal Engineering 55, 1237–1242.

Uda, T., Hashimoto, H., 1982. Description of beach changes using an empirical predictive model of beach profile changes, in: Coastal Engineering 1982, pp. 1405–1418.

Valiela, I., 2009. Global coastal change. John Wiley & Sons.

Van Rijn, L.C., 1993. Principles of sediment transport in rivers, estuaries and coastal seas.

Vos, K., Harley, M.D., Splinter, K.D., Simmons, J.A., Turner, I.L., 2019. Sub-annual to multi-decadal shoreline variability from publicly available satellite imagery. Coastal Engineering 150, 160–174.

Wang, X., Pinardi, N., Malacic, V., 2007. Sediment transport and resuspension due to combined motion of wave and current in the northern adriatic sea during a bora event in january 2001: A numerical modelling study. Continental Shelf Research 27, 613–633.

Waters, C., 1939. Equilibrium Slopes of Sea Beaches, unpublished. Ph.D. thesis. MS Thesis, University of California, Berkeley.

Wentworth, C.K., 1922. A Scale of Grade and Class Terms for Clastic Sediments Author (s): Chester K . Wentworth Published by : The University of Chicago Press Stable URL : http://www.jstor.org/stable/30063207 . J. Geol. 30, 377–392.

Wright, L., May, S., Short, A., Green, M., 1984. Beach and surf zone equilibria and response times, in: Coastal Engineering 1984, pp. 2150–2164.

Wright, L., Nielsen, P., Short, A., Green, M., 1982a. Morphodynamics of a macrotidal beach. Marine geology 50, 97–127.

Wright, L.D., Guza, R.T., Short, A.D., 1982b. Dynamics of a high-energy dissipative surf zone. Marine geology 45, 41–62.

Wright, L.D., Short, A.D., Green, M., 1985. Short-term changes in the morphodynamic states of beaches and surf zones: an empirical predictive model. Marine geology 62, 339–364.

Wunk, W., 1949. Surf beats. EOS, Transactions American Geophysical Union 30, 849–854.

Yang, H., Yang, S., Xu, K., Wu, H., Shi, B., Zhu, Q., Zhang, W., Yang, Z., 2017. Erosion potential of the yangtze delta under sediment starvation and climate change. Scientific reports 7, 10535.

Yates, M.L., Guza, R., O'reilly, W., 2009. Equilibrium shoreline response: Observations and modeling. Journal of Geophysical Research: Oceans 114.